Modelling Entrainment in Debris Flow Analysis for Dry Granular Material

by

Chao Kang

A thesis submitted in partial fulfillment of the requirements for the degree of

Doctor of Philosophy

in

Geotechnical Engineering

Department of Civil and Environmental Engineering

University of Alberta

Abstract

Debris flow entrainment refers to the increase in mass by way of erosion of the channel beds or undermining the channel banks. Entrainment makes the calculation of travel distance and velocities of debris flow much more complex and difficult. Shear failure of the material in the channel bed is usually considered to be the dominant mechanism in entrainment analysis. However in granular flow, material at the surface of the channel bed can be eroded by progressive scouring under the base of the debris. This may result in more material being eroded and entrained than just considering the shear failure mechanism.

A new analytical model is proposed to calculate entrainment in debris flow analysis by considering both rolling and shearing motion. Newton's Law of Motion is used to calculate accelerations, velocities, and displacements of granular particles. To study the entrainment process inside granular flow and to verify the new entrainment model, numerical experiments have been carried out using the Discrete Element Method (DEM). Velocities, including translational velocity, rotational velocity and average velocity, total volume, shear stresses are monitored using measurement circles in the numerical experiment. Variations of the depth of erosion at specific locations along the debris flow channel are monitored and the average entrainment rates are calculated. By comparing the numerical experimental results with the analytical solutions, it is found that results from the analytical model agree well with that from the numerical experiments.

In order to use the new entrainment model into debris flow runout calculation, the new entrainment model has been incorporated in a runout model based on an energy approach. Entrainment calculation governed by a second order partial differential equation is solved using the finite difference method. The total mass and profile of the channel bed are adjusted during

the entrainment calculation. Sensitivity analyses have been carried out on the new model by varying the model parameters including internal friction angle, basal friction angle, turbulent coefficient and mean of Probability Density Function (PDF) etc.

Back analysis of historical cases is carried out using the new model. Several case histories have been studied which include the Tsingshan debris flow, Niumian Rock Avalanche, Fjærland debris flow, Faucon debris flow and Zymoetz River rock avalanche. An extremely large rock avalanche occurred on April 9, 2000 at Yigong is also studied in the thesis. Measurements obtained from site investigation, including flow velocity, flow height, entrainment depth at specific locations, run-out distance and total volume at deposition fan, have been used to evaluate the model. The results are encouraging based on comparisons of the run-out distance, front velocity and total volume of the debris. Improvements are required on the entrainment depth and total volume in some cases when lateral spreading of the debris is significant.

Acknowledgement

First and foremost, the author would like to express my appreciation to Professor D.H. Chan for his continuous support and encouragement through this study. He spent an enormous amount of time discussing this topic and helping the author to solve the problems in equation development and numerical simulation. He also gave the author great support for author's living and research, and strived for the opportunities to broaden author's perspective. His enthusiasm and concern for his students' research is second to none.

Special thanks would like to be given to supervisor committee member and final examination committee member including Dr. Dr.Charles Ng, Dr. Ali Bayat, Dr.Derek Apel, Dr. Lijun Deng, Dr. David Zhu and Dr. Raj Rajaratnam, for their kind suggestion on the revision and polish of the thesis.

The author is thankful to Professor X.M. Meng and Professor W.W. Chen at Lanzhou University for their generous assistance during field investigation in China. The author is also indebted to Dr. F.Y. Zhang and Dr. P. B. Yuan for their kind help and suggestion in field study.

The author would like to acknowledge Professor P. Cui for supervising the author on selecting data on case studies and giving support during visiting study at Chengdu, China. Thanks are extended to all colleagues from the Institute of Mountain Hazards and Environment, Chinese Academy of Sciences. Special thanks are addressed to Dr. F.H. Su, Dr. G.G. Zhou, Prof X.Q. Chen and Dr. C.J. Ouyang.

The author is also thankful to F.X. Zhang, Y. Li, Y. Tang, C. Lu, Y. F. Cui for their sincere help involving the discussion with them on developing the model and conducting numerical

experiment. Other fellow graduate students at University of Alberta also gave me some useful advice towards my research.

I would like to give my thanks to Geotechnical Engineering Group of the University of Alberta for providing a supportive and homelike environment for the author.

During developing the computer program, I was helped by L.J. Huang and H.Q. Wang. It is difficult for me to complete my study without their help.

The author would like to give my thanks for all my family members for their understanding, kind help and encouragement.

Last but not least, the author would like to thank my fiancee Yuan Lu for her love and understanding.

Table of Contents

List of Tables

List of Figures

1. INTRODUCTION

1.1. Introduction to debris flow

Debris flows are rapid mass movement in steep hilly terrains where earthly materials flow down in a valley or channel usually triggered by a landslide. Debris flow poses significant geologic hazards worldwide resulting in fatalities, property damage, and limiting the use of land in populated urban areas. Also referred to mudslides, mudflows, or debris torrents, these events tend to occur in association with heavy rainfall, tropical storms, earthquakes, volcanic activity, snowmelt, glacial melt, and after land disruption such as wildfire, mining, logging, or vegetation removal. Debris flows can be defined as rapidly flowing mass, predominantly coarse granular material and mud mixtures that may consist of large unsorted materials such as boulders, trees, and other debris (Hungr et al. 2014). It can be usually fast-moving with variable solid concentration and large runout distance.

Due to the fast moving characteristics, debris flow is one of the most hazardous and unpredictable surface process that results in many losses of lives and property damages (Schürch et al. 2011). Human activities and increase in rainfall intensity in mountainous regions, cause the increase of the number of cases of debris flow over recent years. This leads to an increase in the number of casualties caused by debris flow because there are still many people living in hazardous areas such as the base and valleys of mountains.

Considering the percentage of human casualties caused by debris flow and the occurrences of debris flow in all natural hazards, it is revealed that debris flow results in more casualties than any other events. It means that once a debris flow is initiated, the element of surprise and the destructive power of the debris usually cause more casualties than other natural hazards.

1.2. Introduction to debris flow entrainment

In many debris flow events, flow channels are typically covered by surficial deposits, sometimes several meters thick of loose granular material. Rapid moving debris could mobilize these materials that could significantly change the total volume of the debris during the flow process (Table 1-1). The inclusion of solid and fluid from the boundary of the flowing debris is called entrainment (Iverson 2012). The rate of this process is affected by the shear stress applied on the bed sediment, the internal friction between the particles, the velocity of the flowing debris, the slope angle of the channel, the cohesion of the bedding material and the pore water pressure generated by shearing of fine grained materials in the bed (Iverson 2012; Mangeney et al. 2010; Egashira et al. 2001). Field observations following debris flow events in many cases indicate that large volumes of sediment are often entrained by debris flows from the channel bed and banks (McCoy et al. 2013).

One of the mechanisms causing material entrainment in debris flows is bed destabilization and erosion. Destabilization of bed material is the result of drag forces acting at the base of the flow channel which may be aided by strength loss due to rapid undrained loading, impact loading and liquefaction of the saturated channel fill. Another important mechanism of material entrainment results from instability of stream banks undercut by bed erosion. It is important to consider that steep stream and gully channels are often being actively incised. Thus, their banks may exist in a state of marginal equilibrium that is easily disturbed by lowering of the bed, such as often occurs during passage of a debris flow surge. The bank may respond immediately and release a shallow landslide directly into the body of the surge, or may release with a delay, to provide material available for incorporation into the next surge (Jakob et al. 2005). Such entrainment mechanisms

are able to change the mobility of the material through changes of the flow volume and its rheological behavior (Luna et al. 2012).

Table 1-1: Summary of rock avalanche and debris flow involving entrainment

Case	Initial volume (m^3)	Entrained volume (m^3)	Average slope angle of entrainment zone	Final volume (m^3)	Entrainment material	References
Huascaran, Peru, 1970 Rock and ice avalanche	1.4×10^7	3.9×10^7	20º ~ 45º	5.2×10^7	Glacial till and ice	Evans and Clague (1994)
Mt. Ontake, Japan, 1984 Volcanic rock avalanche	3.4×10^7	2.2×10^7	20º ~ 45º	56×10^6	Colluvium and alluvium	Voight and Sousa (1994)
Nomash River, Canada, 1999 Rock slide-debris avalanche	3.0×10^5	3.0×10^5	20º ~ 45º	600×10^3	Till-derived colluvium	Hungr and Evans (2004)
Tsingshan, Hong Kong, 1990 Debris flow	4.0×10^2	196×10^2	23º ~ 35º	20×10^3	Colluvium, residual soil	Lo and Chau (2003)
Faucon, French,2003 Debris flow	8.5×10^3	36.5×10^3	3º ~ 50º	45×10^3	Tills, kame terraces and moraines	Remaître et al. (2009)
Fjærland, Norway, 2004 Debris flow	2.5×10^4	21.5×10^4	4º ~ 60º	240×10^3	Quaternary till and older debris-flow material	Breien et al. (2008)
Wenjiagou, China, 2010, Debris flow	---	3.1×10^6	12º ~ 32º	6×10^3	Colluvium	Tang et al. (2012)
Niumian, China, 2008, Rock Avalanche	3.7×10^6	3.8×10^6	30º ~ 70º	7.5×10^6	Colluvium	Xing et al. (2014a)
Yigong, China, 2000, Rock Avalanche	90×10^6	70×10^6	30º ~ 35º	160×10^6	Colluvium	Xu et al. (2012)
Zymoetz river rock avalanche	9×10^5	5×10^5	35º ~ 78º	14×10^5	Glacial sediment	Boultbee et al. (2006)
Guanling, Guizhou	12.3×10^5	4.7×10^5	25º ~ 35º	17×10^5	Quaternary sediments	Xing et al. (2014b)
Dolomites, Italy, 1997 Debris flows	6×10^2	54×10^2	7º ~ 30º	60×10^2	Postglacial sediments	Berti et al. (1999)

1.3. Introduction to entrainment rate

Although bed material entrainment and basal erosion rate are similar and have the same unit, their definitions are quite different and it can be easily confused. Basal erosion rate is defined as the rate of change of the channel elevation (m/s) which is a local scale definition. Instead, bed material entrainment rate is the volumetric flux of material per unit area that enters the flowing mass. It is the average rate of the change of channel elevation which also has a unit of $(m^3/s)/m^2$ (Iverson and Ouyang 2015). The unit of bed material entrainment rate can be simplified into m/s. Since the mechanism is different, it is critical to distinguish them. In this thesis, entrainment rate is defined as the rate of change of the channel elevation.

1.4. Scope of study

Entrainment is an important part of debris flow analysis. Many debris flow cases involve significant changes in mass during the flow process. Therefore it is necessary to study the entrainment process and to develop a method of analysis and a numerical model to be incorporated into debris flow analysis using the continuum approach.

Entrainment analysis often adopts a static approach by calculating the shear stresses in the soil under the channel bed and comparing with the shear strength of the material. The Mohr Coulomb criterion is often used to determine failure in the soil which will enable the calculation of the depth of erosion. However in granular flow, material at the surface of the bed can be eroded by a different mechanism. Granular soil can be eroded by progressive scouring at the base of the debris. The progressive scouring mechanism requires less shear stress to mobilize the material under a rolling motion and this may result in more material being eroded and entrained than the shear failure mechanism. Presently, there is no model that can incorporate the progressive

scouring mechanism. In consideration of the issues discussed above regarding entrainment in debris flow simulation, the purposes of this research are focused on the following area:

(1) Review of debris flow runout models, entrainment experiments and models;

(2) Understand the progressive souring mechanism of erosion;

(3) Develop a numerical model that can calculate the amount of entrainment;

(4) Incorporate the model into debris flow runout analysis;

(5) Calibrate the model through numerical experiments;

(6) Perform sensitivity analysis of parameters in the new model;

(7) Verify the model with case histories;

(8) Apply the new model to simulate debris flow;

1.5. Outline of thesis

The above work is presented in the thesis in a paper format. In this format, each chapter is a self-contained discussion of an issue or presentation of the model. The papers have been published, submitted or in preparation for journal publication.

Chapter 2 reviews the existing entrainment models including empirical models and analytical models. Analytical models will be introduced in detail. Besides, experiments and field measurements involving entrainments, including river bed erosion, are briefly summarized in this chapter.

The main ideas and mathematical formulation of the new entrainment model are presented in Chapter 3. Assumptions and analytical interpretation of the terms in the model are presented.

Chapter 3 is taken from the paper that has been submitted to the International Journal of Geomechanics. The paper is currently under review.

Chapter 4 presents a numerical experiment that is used to verify the new entrainment model. The numerical experiment is carried out using the Discrete Element Method. The DEM model provides a deeper insight into the erosion mechanism and it can estimate the entrainment rate and erosional depth during the simulation. Entrainment rates at specific locations are used in model verification.

Chapter 5 provides the implementation of the new entrainment model into an energy based runout model. The mathematical formulation and numerical scheme are provided in this chapter. Sensitivity analysis of the key model parameters have been carried out. The model is also used to study Tsing Shan debris flow case (1990) that has been observed to have significant amount of entrainment.

The Yigong rock avalanche is one of largest non-seismic mass movement in recent years. Since this case is a very specific one with huge amount of entrainment, it is exclusively studied in this research and presented in Chapter 6. This chapter has been accepted by the Journal of Landslides and it is now available online on the journal website.

The new entrainment model is also used to back analyze four debris flow cases in Chapter 7. Simulation results from the new model and that from case histories are compared. The results from the proposed entrainment model are also compared with that using the dynamic entrainment model.

Chapter 8 concludes the work and discusses the problems encountered in model testing and validation. Suggestions for model improvements are also provided.

Reference

Berti, M., Genevois, R., Simoni, A., and Tecca, P. R. (1999). Field observations of a debris flow event in the Dolomites. Geomorphology, 29(3), 265-274.

Boultbee, N., Stead, D., Schwab, J., and Geertsema, M. (2006). The Zymoetz River Rock Avalanche, June 2002, British Columbia, Canada. Engineering Geology, 83(1), 76-93.

Breien, H., De Blasio, F. V., Elverhøi, A., and Høeg, K. (2008). Erosion and morphology of a debris flow caused by a glacial lake outburst flood, Western Norway. Landslides, 5(3), 271-280.

Egashira, S., Honda, N., and Itoh, T. (2001). Experimental study on the entrainment of bed material into debris flow. Physics and Chemistry of the Earth, Part C: Solar, Terrestrial & Planetary Science, 26(9), 645-650.

Evans, S. G., and Clague, J. J. (1994). Recent climatic change and catastrophic geomorphic processes in mountain environments. Geomorphology, 10(1), 107-128.

Hungr, O., and Evans, S. G. (2004). Entrainment of debris in rock avalanches: an analysis of a long run-out mechanism. Geological Society of America Bulletin, 116, 1240-1252.

Hungr, O., Leroueil, S., and Picarelli, L. (2014). The Varnes classification of landslide types, an update. Landslides, 11(2), 167-194.

Iverson, R. M., Reid, M. E., Logan, M., LaHusen, R. G., Godt, J. W., and Griswold, J. P. (2011). Positive feedback and momentum growth during debris-flow entrainment of wet bed sediment. Nature Geoscience, 4(2), 116-121.

Iverson, R. M. (2012). Elementary theory of bed-sediment entrainment by debris flows and avalanches. Journal of Geophysical Research, 117, F03006, doi:10.1029/2011JF002189.

Iverson, R. M., and Ouyang C. J. (2015), Entrainment of bed material by Earth-surface mass flows: Review and reformulation of depth-integrated theory. Reviews of Geophysics, 53, doi:10.1002/2013RG000447.

Jakob, M., Bovis, M., and Oden, M. (2005). The significance of channel recharge rates for estimating debris-flow magnitude and frequency. Earth Surface Processes and Landforms, 30(6), 755-766.

Lo, K. H., and Chau, K. T. (2003). Debris-flow simulations for Tsing Shan in Hong Kong. Proceedings of the Third International Debris-Flow Hazards Mitigation: Mechanics, Prediction, and Assessment (DFHM) Conference, Editors: Rickenmann, D., and Chen, C.L., Savos, Switzerland, September 10-12, 2003, Millpress, Rotterdam, 577–588.

Luna, B. Q., Remaître, A., Van Asch, T. W., Malet, J. P., and Van Westen, C. J. (2012). Analysis of debris flow behavior with a one dimensional run-out model incorporating entrainment. Engineering geology, 128, 63-75.

Mangeney, A., Roche, O., Hungr, O., Mangold, N., Faccanoni, G., and Lucas, A. (2010). Erosion and mobility in granular collapse over sloping beds. Journal of Geophysical Research, 115, F03040, doi:10.1029/2009JF001462.

McCoy, S. W., Tucker, G. E., Kean, J. W., and Coe, J. A. (2013). Field measurement of basal forces generated by erosive debris flows. Journal of Geophysical Research: Earth Surface, 118(2), 589-602.

Remaître, A., Malet, J. P., and Maquaire, O. (2009). Sediment budget and morphology of the 2003 Faucon debris flow (South French Alps): scouring and channel-shaping processes. Proceedings of the International Conference ‘Landslide Processes’: from

geomorphological mapping to dynamic modelling, Editors: Malet, J.P., Remaître, A., and Bogaard, T., Strasbourg, France, February, 6-7, 2009, CERG Editions, Strasbourg, 75-80.

Schürch, P., Densmore, A. L., Rosser, N. J., and McArdell, B. W. (2011). Dynamic controls on erosion and deposition on debris-flow fans. Geology, 39(9), 827-830.

Tang, C., van Asch, T. W., Chang, M., Chen, G. Q., Zhao, X. H., and Huang, X. C. (2012). Catastrophic debris flows on 13 August 2010 in the Qingping area, southwestern China: the combined effects of a strong earthquake and subsequent rainstorms. Geomorphology, 139, 559-576.

Voight, B., and Sousa, J. (1994). Lessons from Ontake-san: a comparative analysis of debris avalanche dynamics. Engineering Geology, 38(3), 261-297.

Xing, A. G., Xu, Q., and Gan, J. J. (2014a). On characteristics and dynamic analysis of the Niumian valley rock avalanche triggered by the 2008 Wenchuan earthquake, Sichuan, China. Environmental Earth Sciences, 1-15.

Xing, A., Wang, G., Li, B., Jiang, Y., Feng, Z., and Kamai, T. (2014b). Long-runout mechanism and landsliding behavior of a large catastrophic landslide triggered by a heavy rainfall in Guanling, Guizhou, China. Canadian Geotechnical Journal, (ja).

Xu, Q., Shang, Y., van Asch, T., Wang, S., Zhang, Z., and Dong, X. (2012). Observations from the large, rapid Yigong rock slide–debris avalanche, southeast Tibet. Canadian Geotechnical Journal, 49(5), 589-606.

2. LITERATURE REVIEW

Erosion and deposition are important processes of a debris flow event but they are usually poorly understood due to many uncertainties associated with debris flow characteristics. In analyzing debris flow, traditional approaches are inadequate if the debris flow is susceptible to erosion and deposition (Coe et al. 2008). Most debris flows have some sort of entrainment during the flow process and the incorporation of erosion and deposition makes the analysis much more complicated. Mathematical models have been developed to calculate the amount of entrainment. The parameters for the model can be determined from laboratory or field tests. This chapter will briefly discuss various approaches in debris flow modelling and different constitutive models for analyzing the debris material. Various entrainment models are also mentioned in this chapter. Flume experiments and field tests used to understand debris flow entrainment are also summarized here. For comparison with debris flow entrainment models, models used in estimating the amount of river erosion are also discussed.

2.1. Debris flow runout models

To assess the extent of damages caused by a debris flow event, numerical modelling and debris flow analysis are often conducted. There are several approaches in debris flow modelling including the empirical approach, the discontinuum approach and the continuum approach.

2.1.1. Empirical approach

In empirical approach, calculations of the volume, speed, runout distance and the extent of a debris flow are based on historical observations of a large number of events (Fannin et al. 2012; Moffat et al. 2011). Depending on the classification and the characteristics of a debris flow,

predictions are made for a future event or back analysis is carried out to understand a current event (Fannin and Wise 2001; Miller and Burnett 2008). This approach requires large amount of data which can only be applied on a regional scale.

2.1.2. Discontinuum approach

In the second approach using the discontinuum method, debris flow is modelled using many small elements that interact with each other, see Cundall and Strack (1979). The discrete element method (DEM) has been used in simulating many large movements of granular assemblies. However, DEM is limited by the size of the problem that can be practically analyzed and it is difficult to determine the material parameters in the DEM model that will simulate the real material response. Although DEM gives realistic simulation, it is not very accurate in predicting debris flow characteristics.

2.1.3. Continuum approach

The third approach is based on continuum models in which the body of the debris is considered to be a continuum. The formulation of the model is based on physical laws such as Newton's Law of Motion, the Laws of the Conservation of Mass and the Law of the Conservation of Energy. The equations governing the motion of the debris are derived to calculate the flow characteristics, such as velocity, depth, runout distance etc., see Wang et al. (2010). Numerical techniques, such as the finite element method, finite different method or the block continuum method, are often used to provide the numerical solution for debris flow analysis. This approach is one of the most common approaches and it is one of the most effective ways of analyzing practical debris flow problems. The continuum approach is adopted in this research.

2.2. Constitutive modelling of debris flow

It is essential to adopt an appropriate constitutive law in modelling and predicting debris flow behavior. Many constitutive models have been proposed to describe the rheological properties of debris flow using an equivalent fluid. According to the properties of debris, the following constitutive models for debris have been proposed: Newtonian fluid model, non-Newtonian fluid model, dilatant fluid model, Coulomb friction model, Coulomb friction model and Voellmy fluid model (Table 2-1). These models shows the relationship between shear rate and shear stress exerting on channel bed and are applied to different flow condition. Normally, the relationship between shear rate and shear stress for Newtonian model is linear instead of that for Non Newtonian fluid models are non-linear. The shear stress exerted by coarse particles on channel bed is normally estimated using Coulomb friction model or Voellmy fluid model. Correlations between shear rate and shear stress indicated by some typical models are plotted in Figure 2-1. It is seen from the figure that yield strength must be exceeded before debris flow occurs if Bingham flow model is used. If the slope of the curve increases with the increase of shear rate, shear-thickening will be detected. Inversely, if the slope decrease, shear thinning can be detected.

Table 2-1: Summary of constitutive models for debris flow analysis

Models		Equation	Application
Newtonian model		$\tau = \mu \frac{du}{dz}$	Solid concentration below a certain limit
Non Newtonian fluid model	Bingham model	$\frac{du}{dz} = 0$ for $\tau < \tau_0$ $\tau = \tau_0 + \mu \frac{du}{dz}$ for $\tau > \tau_0$	Mudflows and fine-grained slurries.
	Herschel-Bulkley Model	$\frac{du}{dz} = 0$ for $\tau < \tau_0$ $\tau = \tau_0 + \mu_\eta (\frac{du}{dz})^\eta$ for $\tau > \tau_0$	Fines fraction higher than 10%.

Models		Equation	Application
Dilatant fluid model	Quadratic model	$\frac{du}{dz}=0$ for $\tau<\tau_0$ $\tau=\tau_0+\mu\frac{du}{dz}+\xi(\frac{du}{dz})^2$ for $\tau>\tau_0$	Hyperconcentrated sediment flows
	Bagnold	$\tau=\alpha_i\rho_s\lambda^2d^2(\frac{du}{dz})^2\sin\phi_d$	Dispersive stress
	The generalized viscoplastic model	$\tau=c\cos\phi+p\sin\phi+\mu_1(\frac{du}{dz})^\eta$	General debris flow
Coulomb friction model		$\tau=\sigma\tan\phi$	Granular flow
Coulomb viscous model		$\frac{du}{dz}=0$ for $\tau<\tau_c+\sigma\tan\theta$ $\tau=\tau_c+\sigma\tan\phi+\mu\frac{du}{dz}$ for $\tau>\tau_c+\sigma\tan\theta$	Transport of large clasts
Voellmy fluid model		$\tau=\sigma\tan\phi+\gamma\frac{u^2}{\zeta}$	Snow avalanche

Notes: τ is the shear stress, μ is effective viscosity and du/dz is shear rate; τ_0 is the yield strength; μ_η is the consistency index, η is the flow-behavior index; ξ is a turbulent-dispersive parameter; α_i is a numerical constant; ρ_s is the grain density; $\lambda=((C_m/C)^{1/3}-1)^{-1}$ is the linear concentration; C and C_m are solid volumetric concentration and maximum possible volume concentration (0.74 for uniform spheres), respectively, d is grain diameter, ϕ_d is the dynamic angle of internal friction; p is mean normal pressure which is rate-independent; μ_1 are consistency index; σ is normal stress; τ_c is cohesive strength; γ is the unit weight of material and ζ is a turbulence coefficient with the dimension of acceleration. (Modified from Wang (2008))

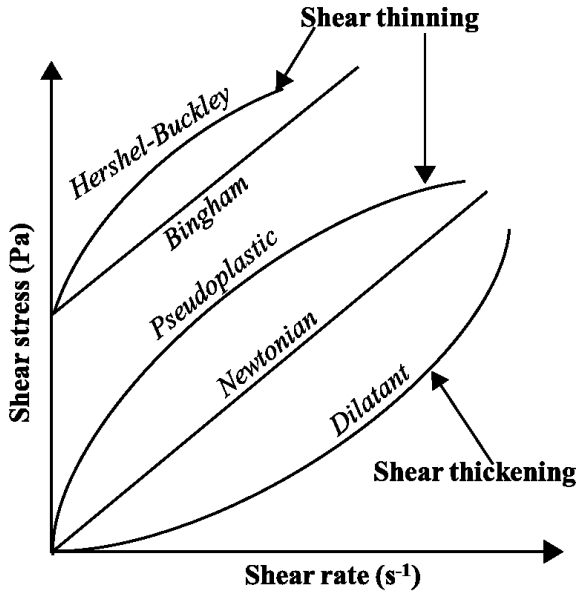

Figure 2-1: Shear stress against shear rate for different fluid models

2.3. Numerical modelling of debris flow entrainment

Some efforts have been made in the past to estimate the volume of erosion and incorporate basal entrainment. The models for estimating the amount of material incorporated from channel bed can be roughly summarized as analytical models and empirical models. In the analytical approach, Newton's Law of Motion or force equilibrium are used to calculate the entrainment rate or depth of erosion of the channel base. Shear stress and shear resistance are the most important factors in calculating entrainment. Diffusion process caused by the difference of sediment concentration between erodible channel bed and the main body of the debris is also considered as one possible mechanism of entrainment (Iverson and Ouyang 2015). On the other hand, in the empirical approach the entrainment rate is empirically related to flow velocity or shear stress exerting on the erodible bed. The coefficient of correlation between entrainment rate and flow velocity or shear stress is often determined by model calibration based on a large number of case histories.

2.3.1. The analytical approach

Although it is difficult to use the analytical approach to predict entrainment, and some scholars said that analytical techniques are unlikely to be useful in the foreseeable future (Jakob et al. 2005), it is still possible to calculate entrainment analytically by considering stresses and resistances in the debris flow channel.

2.3.1.1 Static analysis

In the static approach, static shear stresses in the channel bed under the debris are calculated and failure is considered when the static shear stress exceeds the shear strength of the material. The depth in which failure occurs is determined and the amount of material is calculated which will

be added to the main body of the debris. Limitation of the static analysis is that it can only estimate the upper bound of the depth of erosion since rate effect is not taken into account.

Medina et al. (2008a) developed a static equation of entrainment by considering static equilibrium between the flow frictional stresses and the basal resistance stresses (Figure 2-2). The upper layer represents the debris which the lower layer shows the erodible material. The dash line in the Figure 2-2 is the new channel surface after the channel bed is eroded by h_{ent} in depth. Shear resistance is estimated using Mohr-Coulomb law. Therefore, entrainment depth can be estimated using

$$h_{ent} = \frac{\tau_b - \tau_{res}}{\rho_f g(\cos\theta \tan\phi_{bed} - \sin\theta)} \qquad [2\text{-}1]$$

where τ_{res} is the resistance stress of the material due to internal friction of the particles, τ_b is the active force, g is the gravity acceleration, θ is the slope angle, ϕ_{bed} is the friction angle of sediment particles and ρ_f is density of debris.

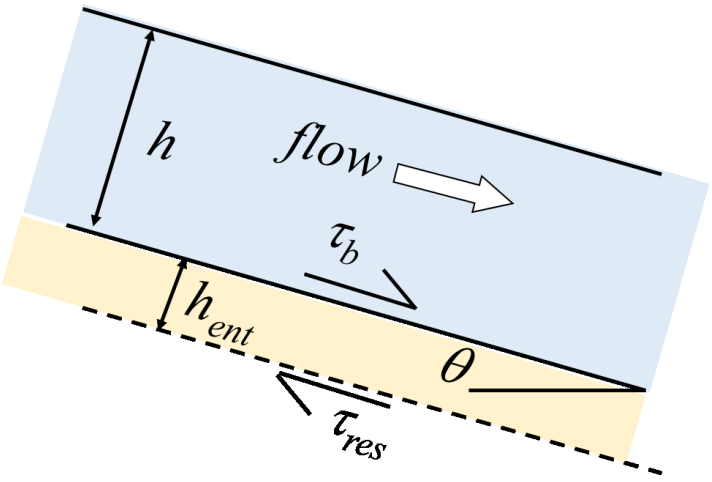

Figure 2-2: Schematic graph of analytical entrainment models-static approach

Sovilla et al. (2006) proposed a formula to calculate bed erosion of snow avalanche. The entrainment process has three modes: ploughing, step entrainment and basal erosion modes. The snow pack is divided into several layers in the entrainment calculation. In the model, driving force for entrainment is calculated from the shear component of the normal force acting on the layer. The frictional force comes from the cohesion of the snow depending on the snow texture. Based on mass and momentum conservation of each layer, the speed of the snow entering the avalanche is calculated from:

$$W(x,t) = \sqrt{\frac{p(x,t) - p^*(x)}{\rho_a(1 - \frac{\rho_s(x)}{\rho_a})}} \qquad [2\text{-}2]$$

where W(x,t) is the entrainment velocity (m / s), p(x,t) is the normal stress the avalanche applies on the layer, p*(x) is the layer strength, ρ_a is the mean flowing density of the avalanche, $\rho_s(x)$ is density of the layer. This formulation can be used to calculate the rate of erosion for the three entrainment mechanisms.

The mass entrainment rate is estimated from:

$$\dot{M}_{e}(x,t) = \sum_{i=1}^{n} \rho_{si} W_i(x,t) \qquad [2\text{-}3]$$

where $\dot{M}_{e}(x,t)$ is entrainment rate (kg / (m^2s)) of unit area, ρ_{si} is density of i^{th} layer and n refers the number of layers in the calculation. For more detailed information, see Sovilla et al. (2006).

2.3.1.2 Dynamic analysis

In the dynamic approach, the rate of entrainment is calculated based on the rate of erosion of the material in the channel bed. The rate of erosion is determined based on shear failure at the

surface and the material is removed from the surface based on the velocity of flow of the main body of the debris (Medina et al. 2008a). It is assumed in this approach that the velocity of newly eroded material is the same as the average velocity of the debris. Entrainment occurs when the bed shear stress is greater than the shear resistance (Figure 2-3). Therefore the quantity of the new incorporated mass is dependent on the availability of momentum which is given by:

$$\frac{\partial z}{\partial t} = \frac{(\tau_b - c - h\rho_f g \cos\theta \tan\phi_{bed})}{\rho v} \qquad [2\text{-}4]$$

in which $\partial z/\partial t$ is the rate of entrainment (m/s), and v is mean velocity of the debris (m/s).

The difference between static and dynamic entrainment model is that the static model calculates the entrainment depth according to the stress equilibrium/failure of the erodible layer, while the dynamic model calculates the rate of erosion based on the net driving stress exerting at the interface between the debris and erodible layer.

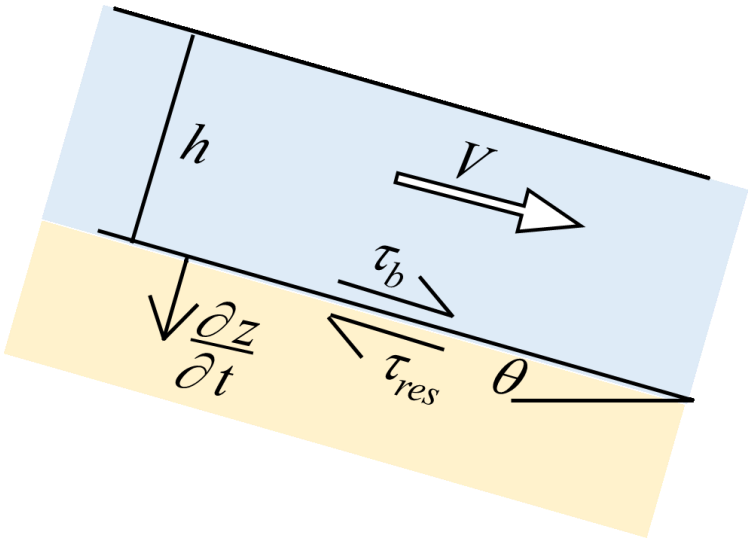

Figure 2-3: Schematic graph of analytical entrainment models-dynamic approach

The entrainment model proposed by van Asch et al. in 2004 (Luna et al. 2012) is a dynamic one dimensional debris flow model that takes into account the entrainment concept based on the

shear stress and shearing resistance which is affected by the generation of excess pore water pressure under undrained loading on the in-situ material. The increase in pore water pressure is calculated by using Skempton (1954) equation. Flow is treated as a laminar, single phase and incompressible continuum process. Debris flow and channel bed are divided into three layers from top to bottom: top layer (flowing debris), erodible layer (erodible bed) and substrate layer (stable bed). Due to the moving mass overlays the erodible bed, a loading on the bed deposits is generated. The model calculates this load on the in-situ soil through changes in the vertical normal stress and shear strength caused by the debris flow. Then, factors of safety at the bottom and top of the erodible bed are calculated as follows:

$$F_{bot} = \frac{c_{bot} + (\sigma_{bot} - P_{bot}) \tan \delta_{bot}}{\tau_{bot}} \quad [2\text{-}5]$$

$$F_{top} = \frac{c_{bot} + (\Delta\sigma - \Delta P) \tan \delta_{bot}}{\Delta\tau} \quad [2\text{-}6]$$

where c_{bot} is the cohesion and δ_{bot} is the friction angle of the in-situ soil, $\Delta\sigma$, ΔP and $\Delta\tau$ are the changes in normal and shear stress caused by the variation characteristics of debris above the channel bed, and pore water pressure respectively, σ_{bot} and P_{bot} are the normal stress and pore water pressure at the bottom of the erodible bed respectively.

The depth of erosion can be calculated by analyzing the factors of safety at the top and bottom of the erodible layer. In the case when $F_{top} < 1$ and $F_{bot} < 1$, then d_{sc}, thickness of eroded layer, equals the total thickness of the erodible layer d; In the case where $F_{top} > 1$ and $F_{bot} < 1$, then d_{sc} is again equal to the total thickness of in-situ material d; In the case, where $F_{top} < 1$ and $F_{bot} > 1$, it is showed that only a portion of d will fail and it can be calculated as follows.

$$d_{sc} = \frac{1 - F_{top}}{F_{bot} - F_{top}} d \qquad [2\text{-}7]$$

This model is similar to the dynamic model except that it involves the FOS for erodible layer. Although the interaction between debris flow and in-situ soil is considered here, entrainment rate is not taken into account. The influence of debris flow velocity on entrainment is omitted (Luna et al. 2012). Besides, the effect of grain size is not considered in the entrainment calculation process.

Iverson (2012) considered the behavior of a slide block descending on an erodible slope with the ability of incorporating soil from the static bed, see Figure 2-4. Newton's Second Law is applied on the sliding material. Coulomb friction rule is employed to estimate basal frictional resistance which also takes into account the shear rate. The entrainment rate based on the change in the weight of the sliding block is calculated from:

$$\frac{dm}{dt} = \frac{m}{v}[G - \Gamma v - (\frac{dv}{dt})] \qquad [2\text{-}8]$$

where $G = g (\sin\theta - \mu_0 \cos\theta)$, $\Gamma = g \mu_v \cos\theta / V$, g is gravitational acceleration, θ is the uniform angle of inclined plane, t is time, v is its velocity, m is the slide-block mass, μ_0 is basal frictional coefficient, μ_v and V are constants.

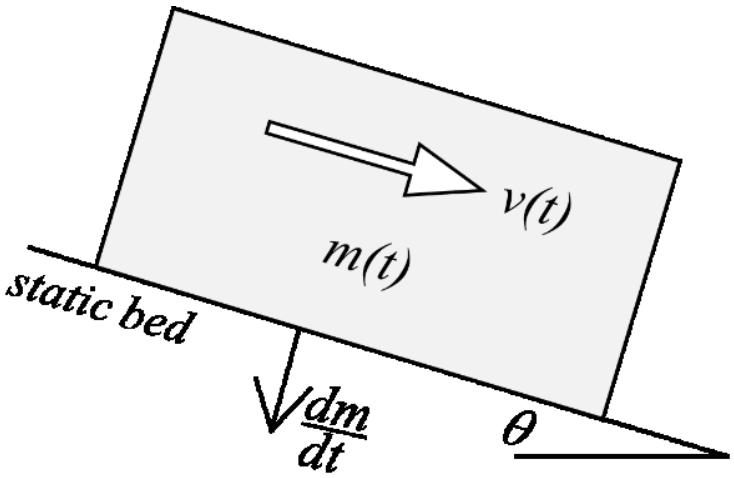

Figure 2-4: Schematic illustration of slide block model in entrainment analysis

If an ideal case is considered in which frictional resistance is zero ($G = G_0 = g \sin\theta$, $\Gamma = 0$) and v is constant, then:

$$\left[\frac{dm}{dt}\right]_{\max} = G_0 \frac{m}{v_0} \qquad [2\text{-}9]$$

The equation above is an upper-bound condition for sustainable entrainment. Therefore, it is postulated that:

$$\frac{dm}{dt} = \alpha G \frac{m}{v} \qquad [2\text{-}10]$$

in which α is an entrainment-efficiency parameter. The value of α must satisfy $0 \leqslant \alpha \leq 1$, but it needs not be a constant. If the value of α changes, it always satisfies $\alpha = 1 - [(dv / dt + \Gamma v) / G]$, but this will lead in indeterminate value. Therefore, a continuum mechanical analysis is needed to determine the parameter α.

After analyzing the slide-block problem, Iverson (2012) considered mass and momentum exchange between three continuous layers, a flow layer with a free upper surface, an erodible

bed sediment layer, and a deeper substrate that cannot be entrained owing to high strength, respectively, see Figure 2-5.

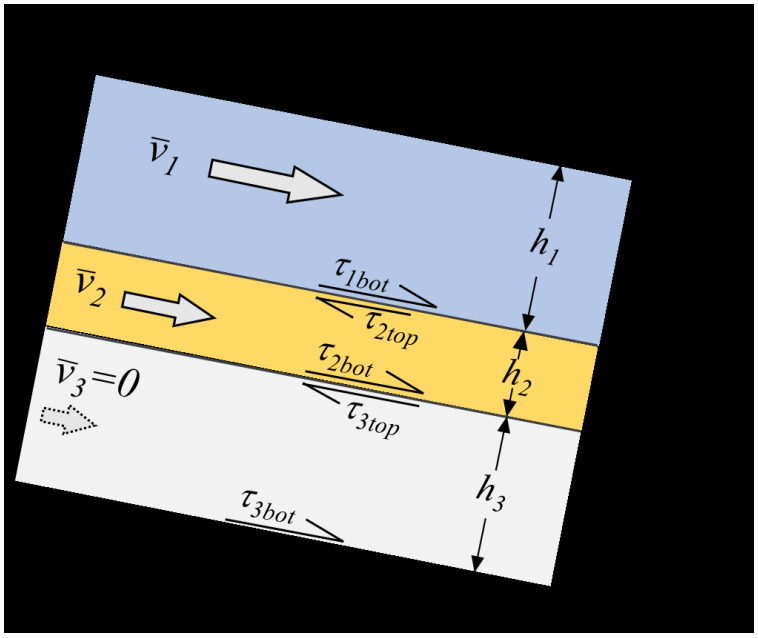

Figure 2-5: Schematic illustration of velocity profiles (Iverson 2012)

Based on the assumption that the variations of all quantities in the transverse direction are negligible, mass balance and translational momentum balance equations in a continuous material are integrated using kinematic boundary conditions that relates velocities at the top and bottom of the erodible layer to the other velocity components at the same location. After the momentum equations for those three layers are obtained, it is considered that the flow and erodible bed layers can exchange momentum and momentum must be conserved during such an exchange. By adding the equations for flow layer and erodible layer, it is found that the bed sediment entrainment rate can be calculated from:

$$E = \frac{(\tau_{1bot} - \tau_{2bot})}{\rho(v_{1bot} - v_{2top})} \qquad [2\text{-}11]$$

where τ_{1bot} is the shear stress at the bottom of the first layer, τ_{2bot} is the shear stress at the bottom of the second layer, v_{1bot} is the velocity at the bottom of first layer, v_{2bot} is the velocity at the bottom of first layer, ρ is the bulk density of flow and bed material. The numerator of this equation can be interpreted as an excess boundary shear stress, which expresses the difference between the basal shear stress exerted by the flow and the boundary shear resistance exerted by the channel bed. The threshold for entrainment in this equation is consistent with the dynamic equation proposed by Medina et al. (2008a).

If basal slip is considered and bed-sediment layer is stable prior to entrainment, equation [2-12] can be used to estimate the entrainment rate using the Coulomb friction rule to calculate the shear stress.

$$E = \frac{\rho g h_1 (\mu_1 - \mu_2)\cos\theta + \mu_2 p_{2top} - \mu_1 p_{1bot}}{(1 - s_1)\rho \overline{v_1}} \qquad [2\text{-}12]$$

where μ_1 and μ_2 are Coulomb friction coefficients for layers 1 and 2, p_{1bot} and p_{2top} are boundary pore fluid pressures for layers 1 and 2, s_1 is a fitting parameter ranging from s_1=0 if there is no simple shear to s_1=1 if there is no basal slip, $\bar{v}_1$ is depth-averaged velocity in first layer, h_1 is height of layer 1 in the z direction, and ρ is bulk density.

On the other hand, the equation above indicates that E will decrease as the basal slip velocity v_{1bot} increases. This contradicts conventional understanding but proves the results of the slide-block analysis to be correct when:

$$\alpha = \frac{\rho g h (\mu_1 - \mu_2)\cos\theta - (\mu_1 p_{1bot} - \mu_2 p_{2top})}{\rho g h_1 \sin\theta - \mu_2 \rho g h_1 \cos\theta} \qquad [2\text{-}13]$$

Iverson and Ouyang (2015) updated the equation for estimating basal erosion rate. Jump conditions at the interfaces between each layer, which descripts the sudden change of shear stress

and horizontal velocity in the debris, were considered in the derivation. The general bed erosion formula can be expressed as:

$$-\frac{\partial z}{\partial t}=\frac{\tau_{1bot}-\tau_{2top}}{\bar{\rho}_1 u_1(z_b)}-u_1(z_b)\left[\frac{\sigma_{2top}-\sigma_{1bot}}{\tau_{1bot}-\tau_{2top}}\right] \qquad [2\text{-}14]$$

where $\bar{\rho}_1$ is the depth averaged density of the first layer, $u_1(z_b)$ is the velocity at the interface between first and second layer, σ_{2top} is normal stress at the top of second layer, σ_{1bot} is the normal stress at the bottom of second layer.

In this model, the difference in density between each layer is considered. The first term on the right side of [2-14] accounts for excess shear stress that causes erosion. The second term represents the effects of dilatancy. If no dilatancy exists, it will reduce to the model proposed by Medina (2008b).

2.3.1.3 Diffusion process

Diffusion is also being considered as one of the mechanisms of entrainment of bed sediment. It is noticed that difference in the solid concentration is the main trigger for particles to be eroded. Takahashi et al. (1991) proposed a formular for estimating the entrainment and depostion of debris flow based on this mechanism. Sediment concentration is considered as the main factor in the estimation. Flow height and particle size are also taken into account.

$$E=\begin{cases}\alpha v\dfrac{c_e-c}{c_*-c_e}\dfrac{h}{d} & \text{for } E\geq 0\\[2ex] \beta v(c_e-c)\dfrac{h}{d} & \text{for } E<0\end{cases} \qquad [2\text{-}15]$$

in which α and β are the experimental coefficients, c_e is the equilibrium sediment concentration of debris flow by volume, c is the ediment concentration of debris flow by volume, c_* is the

sediment concentration by volume of bed sediment (non-moving layer), h is the flow depth, d is the grain size of debris flow.

Egashira et al. (2001) proposed a formula to calculate erosion rate assuming that the slope of the channel bed is always adjusted to the angle corresponding to limiting equilibrium conditions. The material in the channel left behind by an unsaturated debris will approach the limiting equilibrium slope angle. Using mass conservation for the eroded material yields

$$E\Delta x = Ev\Delta t = c_* v\Delta z \qquad [2\text{-}16]$$

where E is the erosion rate, v is the average velocity of the debris flow, Δx is the distance increment, Δt is the time increment, c_* is the sediment concentration by volume of bed sediment (non-moving layer) and Δz is the erosion depth during Δt.

Geometrical relationship between the initial bed slope and equilibrium slope angle, $\theta - \theta_e = \arctan(\Delta z / \Delta x)$, is incorporated into the mass conservation law of eroded material in order to obtain the entrainment rate E (m/s).

$$E = c_* v \tan(\theta - \theta_e) \qquad [2\text{-}17]$$

in which θ is the bed slope and θ_e is the equilibrium bed slope.

As an important property, the size of sediment could influence the entrainment rate greatly. Papa et al. (2004) analyzed the influence of sediment size on bed erosion. It is found that when the sediment size of debris flow body is the same as bed sediment, the velocity profile is in the equilibrium flow condition. However, when the bed sediment size increases, the velocity distribution becomes similar to a velocity profile in flow over the rigid bed.

2.3.2. Empirical models

Empirical models are primarily developed based on the analysis of statistical data from field cases and laboratory experiments. Flow velocity, shear stress and solid concentration are generally used in the development of empirical entrainment model.

De Blasio et al. (2011) suggested a semi-empirical model to calculate the rate of erosion. In the model, the rate of erosion depends solely on the tangent component of the weight at the base of the flow channel and on the average velocity of the debris. Critical shear stress is used as the thereshold to determine the occurance of entrainment. Measurements from Fjæland debris flow is utilized to calibrate the model. This model seems promising since it relates debris flow velocity and basal shear stress to entrainment.

$$\frac{dh}{dt} = c\left|U\right|^{y}(\tau_{xy} - \overline{\tau}) \text{ for } \tau_{xy} > \overline{\tau} \quad [2\text{-}18]$$

$$\frac{dh}{dt} = 0 \text{ for } \tau_{xy} < \overline{\tau} \quad [2\text{-}19]$$

where dh/dt is the rate of bed erosion (m/s), U is the velocity of the debris flow, $\overline{\tau}$ is the critical shear rate for erosion, c and y are constants. In principle these constants should be determined experimentally.

McDougall and Hungr (2005) incorporated a simple material entrainment algorithm, based on the assumption of natural exponential growth with displacement, into a new computer model designed to simulate rapid landslide motion across 3D terrain. The bed erosion velocity (m/s) and the volume growth rate (s^{-1}), defined as bed-normal depth eroded per unit flow depth and unit displacement, can be related by:

$$\frac{\partial z}{\partial t} = E\ h\ v \qquad [2\text{-}20]$$

where E is volume growth rate (m^{-1}), h is flow depth and v is flow velocity.

The growth rate, E, is determined by trial and error. Therefore average volume growth rate, $\bar{E}$, is suggested to be used to replace E which can be preliminary estimated from:

$$\bar{E} = \frac{\ln(V_f / V_0)}{\bar{S}} \qquad [2\text{-}21]$$

where V_0 is the estimated total volume entering the zone, V_f is the estimated total volume exiting the zone and $\bar{S}$ is the approximate average path length of the zone. Limitation of this equation is that it is assumed that material is eroded evenly along the channel.

Chen et al. (2006), for preliminary estimates, proposed a relationship to estimate the yield rate E (dimensionless):

$$E \cong \alpha \frac{V_{eroded}}{A_{affected} d_{com}} \qquad [2\text{-}22]$$

where V_{eroded} is the total eroded volume, $A_{affected}$ is the total erosion affected area, d_{com} is the travel distance of the centre of mass, and α is a correction coefficient to account for the system non-linearity. Before the application of the model, the correction coefficient should be determined by the calibration.

Pitman et al. (2003) proposed an empirical formula to estimate the entrainment rate e_s (m/s).

$$e_s = \begin{cases} \alpha\sqrt{u^2 + v^2} & \tau \geq \tau_0 \\ 0 & \tau \leq \tau_0 \end{cases} \qquad [2\text{-}23]$$

where α is proportionality constant to be fitted to experimental results, and u and v are horizontal and vertical components of velocity, respectively.

Hsu et al. (2008) considered different velocity profiles of granular flows for different basal behavior and divided the granular flows into four types: a flow with full slip, a flow with zero slip, partial slip with positive velocity at the base and plug flow with no slip. It is suggested that for all-slip case, erosion rate, $-\partial z/\partial t$ (m/s), based on Archard wear equation, can be written as:

$$-\frac{\partial z}{\partial t} = \frac{k p_n v}{H} \qquad [2\text{-}24]$$

In which, p_n is the normal pressure, v is the sliding velocity, H is the hardness of the surface being worn away, k is a nondimensional wear coefficient dependent on the materials in contact.

Stock and Dietrich (2006) noted that the valley slope is adjusted to the long-term frequency of debris flows. Valleys soured by debris flow should not be modelled using conventional bedrock river-incision laws. A new model is proposed in which the depleting rate of the channel bed is proportional to the integral of the solid inertial normal stresses from particle impacts along the flow and the number of upvalley debris-flow sources. The expression of model is found to be:

$$-\frac{\partial z}{\partial t} = \frac{K_0 K_1}{\frac{T_0^2}{E_{eff}}(F)} fL\left[\cos(\theta_b)\ \nu_s\ \rho_s\ D_e^2 \left(\frac{u_s}{h}\right)^w\right]^n \qquad [2\text{-}25]$$

where K_0 is a constant of proportionality that relates the bulk inertial normal stress to higher excursions of inertial normal stress, K_1 is the proportionality constant between rock resistance and incision rate that has dimensions that vary with w and n so that the right side of the expression with units of erosion rate, T_0 (Pa) is the tensile strength of the bedrock, E_{eff} (Pa) is the elastic modulus of the bedrock, F (m) is a function of the fracture spacing of bedrock and size of

eroding boulders, f (a^{-1}) is the is the frequency of flows over the bedrock per annum, D_e (m) is the effective grain size, u_s (m/s) is the surface velocity, h (m) is the flow height, L (m) is the length of eroding flow, and w and n are empirical exponents.

Wicklein and Papanicolaou (2000) suggested the equation for estimating the entrainment rate of material that could potentially be entrained into the flow. In the model, it is considered that bed shear stress fluctuation is the dominant mode of the sediment entrainment which had been discussed by Cao (1997) and Jain (1992).

$$E_i = 0.02\rho \times SG_j \times A \times d_i \times (1-p) \times p_{A_{ij}} \times \frac{F_i}{T_b} \times \frac{d_t}{T_b} \qquad [2\text{-}26]$$

where ρ is water density, SG is specific gravity, A is bed area, d_i is particle size, p is porosity, p_A is the percent active layer, F_i is the probability density function of excess shear stress and T_b is the bursting event period. In theory, all of this material can be entrained into the flow. Since the flow has a finite carrying capacity for material, excess material would redeposit on the bed.

Cao et al. (2004) presented a theoretical model upon the conservative laws of shall water hydrodynamics. Entrainment and deposition are considered in the model. Variation of bed channel elevation is defined as

$$\frac{\partial z}{\partial t} = \frac{D-E}{1-p} \qquad [2\text{-}27]$$

where E and D is sediment entrainment and deposition fluxes across the bottom boundary of flow, and p is bed sediment porosity. E and D are determined using following empirical relationships.

$$D = \omega_0 (1-C_a)^m C_a \qquad [2\text{-}28]$$

$$E = \frac{160}{R^{0.8}} \frac{1-p}{\theta_c} \frac{(\theta - \theta_c) d U_\infty}{h} \quad [2\text{-}29]$$

where ω_0 is settling velocity of a single particle in tranquil water, C_a is near-bed sediment concentration, m is exponent, R is particle Reynolds number, θ is Shields parameter, θ_c is critical Shields parameter for initiation of sediment movement, d is sediment particle diameter, h is flow depth and U_∞ is free surface velocity.

2.3.3. Incorporation of entrainment into debris flow simulation

Different frames of reference are used in the momentum equations in different debris flow models, which include the Lagrangian and Eulerian frame of reference. To incorporate entrainment term into these models, conservation of momentum should be considered carefully. In the Lagrangian framework, if eroded mass enters the debris flow body with a velocity that differs from the depth-average velocity, the equations for calculating the entrainment using Lagrangian frame is not easy to be conservative. Depth-integrated velocity of debris and velocity of entrained material can be distinguished if Eulerian frame is used (Iverson and Ouyang 2015).

2.4. Experiments and field tests in debris flow entrainment study

To verify the analytical equations for entrainment calculations and find the relationship between parameters referred in empirical equations, laboratory experiments and field tests have been carried out. Small-scale and large-scale flume experiments were conducted by Egashira (2001), Mangeney (2010) and Iverson (2011). Field tests were also carried out and devices for monitoring entrainment in real time have been developed (McCoy et al. 2010 and Berger et al. 2011).

2.4.1. Flume experiment

2.4.1.1 Flume Apparatus

To test the entrainment of debris flow, experiments have been conducted on inclined flumes. Different sizes of flume had been built and used (Iverson and Ouyang 2015). The experimental setup mainly consists of a tank, an erosional zone and a deposition pad (Figure 2-6). The tank is used for storing the source material. Source material generally consists of fines and coarse granular particles. The erosion zone is composed of erosional part and two transition parts, one is located in front of erosional zone and one behind. Some of apparatuses have only one transition zone or no transition zone. Deposition zone is also optional in some apparatus. Some of the apparatus use the tank to collect the debris instead of a runout pad. The geometrical properties of the flumes developed for testing the entrainment are summarized in

Table 2-2.

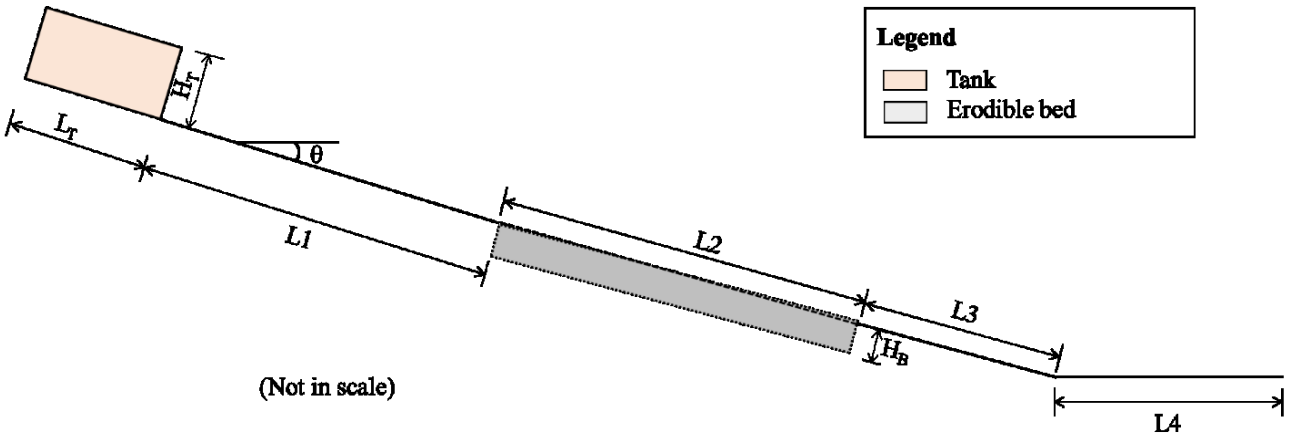

Figure 2-6: Schematic graph of the apparatus adopted for flume experiments

Table 2-2: Summary of size of the flumes in entrainment study

Properties	Tank			Transition length (m)		Erodible bed			Channel size		Deposition zone
	H_T (m)	L_T (m)	Material	L_1 (m)	L_3 (m)	H_B (m)	L_3 (m)	Material	Width (m)	θ (°)	L_4 (m)
Iverson (2011)	≈ 1.6	4.7	SGM[1]	6	42	≈ 0.12	47	SGM[1]	2.0	31	---
Mangeney (2010)	0.14	0.2	Glass beads	0	0	0 - 0.006	3	Glass beads	0.1	0 – 30	---
Egashira (2001)	---	---	Water&Sand	4	0	0.1	2	Water& Sand	0.1	12	---

[1] -56% gravel, 37% sand and 7% mud-sized grains

2.4.1.2 Material and variations in the test

In the flume tests, erodible material sometimes is the same as the source material, but sometimes not. Egashira et al. (2001) and Papa et al. (2004) built a small scale flume experiment to test the debris flow entrainment. A sand stopper was placed at the lower end of the flume to separate the flume into two parts. In the upstream part, a debris was produced by water and sediment supply. Sediment bed was formed using the same material as the supplied debris. In the test, grain size, channel slope and sediment discharge varied. When the bed sediment size increases, the velocity distribution becomes similar to a velocity profile in flow over the rigid bed. It is also found that the relative erosion rate, E/E_0, has an almost unique relation which decreases monotonically with increase in the relative grain size, d/d_0 , although it varies slightly with sediment flux concentration, where E is the mean erosion rate, d is sediment size, d_0 is grain size of debris, and E_0 is the erosion rate in the case that solid material of debris is the same as the bed sediment.

Mangeney et al. (2010) setup the flume experiment to test the effect of the channel slope and erodible depth on the runout distance. Glass beads that are subspherical, cohesionless and highly rigid were used as source and erodible material. Channel slope varies from 0 to around 25.2

degrees. The thickness of the erodible material ranges from 0 to 5 mm. Flow height, deposition height, deposition angle, front velocity and runout distance were used as the criteria to analyze the effect of channel slope and thickness of erodible bed on debris movement.

Scaling is a critical issue in the design of laboratory experiments (Iverson 2015). On the basis of employing miniature experiments with sand-air mixtures, Iverson et al. (2004) revealed that although miniature experiments are unlikely to mimic some avalanches behavior that is possible at geophysical scales, it can be applied to test models of ideal granular avalanches by neglecting the effects of intergranular fluid and cohesion. Rickenmann et al. (2003) found that the limited volume available for the surges is a major restriction during the laboratory experiments. It is then estimated that scaling effect could be an important factor contributing to the relatively large scatter when analyzing the erosion volumes and can also affect the surge properties in the test.

Therefore, Iverson et al. (2011) carried out a large scale entrainment experiment in which an erodible bed is formed by discharging SGM abruptly from a headgate (Figure 2-7). Then, same material is released from the tank to simulate the debris material. The key variable manipulated is the bed-sediment volumetric water content. The impact of bed-sediment water content on entrainment is analyzed by measuring flow-front speed, flow volume and momentum gains at specified locations. Normal stress, pore water pressure and height of debris material are monitored by electronic sensors during the test. The results show that pore pressure generated as wet bed sediment is overridden and progressively entrained by debris can reduce friction and lead to synergistic growth of debris mass and momentum.

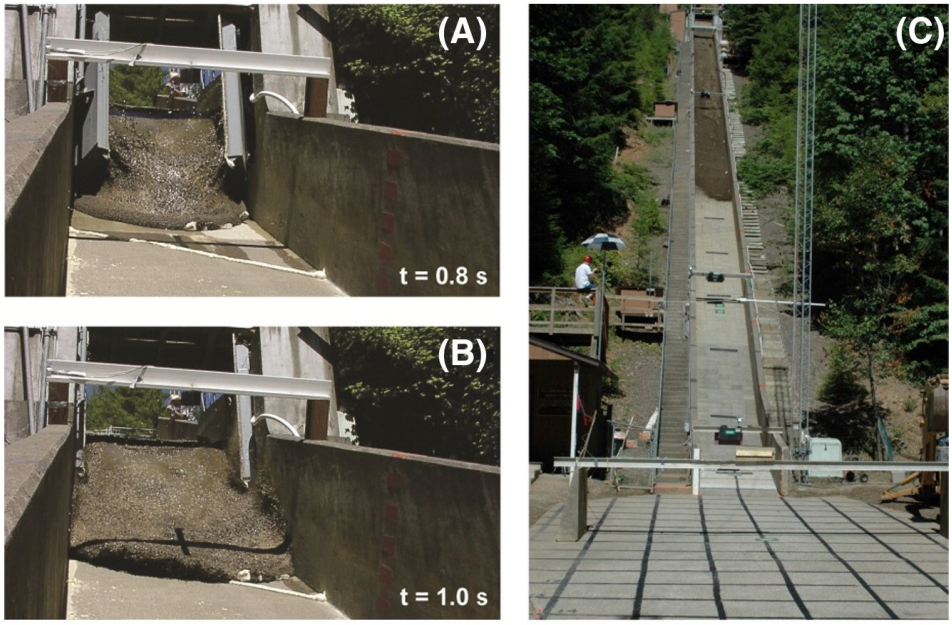

Figure 2-7: USGS debris-flow flume during an experiment. (A) and (B) show the flow state at t = 0.8 s and t = 1.0 s, respectively. (c) shows the debris is descending flume about 5 s. (Iverson et al. 2015)

2.4.1.3 Other entrainment study devices

Hsu et al. (2008) developed a new devise to test bed rock erosion caused by granular material. The drum is made from a section of PVC pipe with an inner diameter of 56 cm. Both sidewalls are composed of Plexiglas, bounding a 15 cm wide channel. In the test, erosion occurs between granular flow and erodible sample inserted in the drum bed. Magnitude of erosion is determined by weighting the erodible sample before and after the test. Average erosion rate can be estimated in the test, but variation of erosion rate with time cannot be obtained.

Bowman et al. (2010) creatively use a geotechnical centrifuge apparatus to study debris flow entrainment under undrain and drained conditions. Both fixed and erodible bases are used in the experiment. It is noted that using the centrifuge apparatus could produce a better approximation of real-scale physical process

2.4.2. Field observation

Berger et al (2011) designed an erosion sensor to monitor the entrainment process. It consists of a column of sensors, initially 1 m long, composed of 20 cylindrical aluminum tubes (50 mm tall and 25 mm in diameter). Electronic resistor inside of each tube is connected to the adjacent elements. As debris erodes one or more elements, shear force is exerted on each connection. If the shear resistance of the connection is smaller than shear force, it will be broken and a drop in the total resistance is recorded on a data logger. Therefore, the erosional rate can be obtained by dividing the erosional depth by the duration of erosion process. Due to the detection limit and presence of a sediment layer covering the sensors, the magnitude of erosion and the timing of erosion for small debris flow cannot be determined respectively (Berger et al. 2011). Although those drawbacks restrict the use of the sensor, this method at least offers a new thought to monitor the entrainment during the process of debris flows.

Subsequently McCoy et al (2013) designed an apparatus using sensors to measure changes in the height of the bed sediment after Berger et al. (2011). The resistor in each element is connected using small plugs easy to unplug. Variation of the length of the resistance chain is detected by measuring voltage at the bottom of the chain. During the test, rainfall, bed force, flow height, flow stage and pore water pressure are monitored at the same time. Besides, incision bolts had been used to measure the average incision rate by McCoy et al. (2013). The bolt essentially provides a record of the pre-flow channel surface. After the debris flow, the variation of covered length of the bolt can be measured, average incision rate in one debris flow event is therefore estimated.

2.4.3. Numerical experiments

Numerical simulation is a fast and convenient method to predict erosion during a debris flow. Normally, Discrete Element Model (DEM) is used to simulate the movement of debris. As a typical DEM in simulating granular flow, Particle Flow Code (PFC) is capable of describing the mechanical behaviours of assembles of discs and spheres by calculating the contact forces and subsequent displacements of each individual particle in response to its interaction with adjacent particles.

Banton (2009) tested channelized granular flows by considering the particle properties and basal surface properties. It was found that rebound coefficient between particles is important in the simulation when the flow is turbulent with a high velocity gradient. Three laboratory experiments in which granular materials released from a rough inclined slope, carried out by Savage and Hutter (1991) and Hutter et al. (1995) were simulated. The simulation results agree very well with the measurements in the test.

Iimura et al. (2009) studied the entrainment of agglomerates deposits on plate surface by shear flows using discrete element method. Effect of shear rate, structure of deposits and adhesion between particle and plate surface on the entrainment is examined by counting the particles remaining on the plates. It is concluded that there is a critical value for shear force beyond which entrainment will be observed. This study is of help to understand of entrainment for cohesive fine particle."

The dynamic response of colluvium accumulation slopes in Sichuan Province of China was studied by He et al. (2010). Horizontal shearing waveforms of Wenchuan earthquake were used to study the dynamic response of the colluvium. It is concluded that material properties and interface in the accumulation affected the velocity a lot. Effect of moving debris on retaining

wall and earthfills was tested using PFC2D by Li et al. (2010) and Salciarini et al. (2010). A slope with constant inclined angle was constructed and a retaining wall was placed away from the toe of the slope. By varying the size of the retaining wall and particle properties, influences of geometry and particles properties were examined by measuring the impact force acting on retaining wall. Though plenty of numerical flume experiments have been conducted, very few have taken entrainment rate into account in numerical flume experiment using PFC2D.

2.4.4. Summary

Using sensors to monitor the change of channel bed in large-scale flume or small-scale flume is also a good choice in studying entrainment. It can measure the variation of channel bed under field situation. However, it is really difficult to capture other kinematic characteristics of debris flow that is useful in verifying the new analytical entrainment model. Therefore, simplified numerical experiment, in which ideal particle shape and size are assumed, will be used to study entrainment in this thesis. Normal stress, shear stress and velocity at different time stage are monitored.

2.5. River erosion

2.5.1. Channel erosion

2.5.1.1 Analytical approach

Fukuda and Lick (1980) found that the entrainment rate and equilibrium concentration are closely related to the shear stress applied at the sediment-water interface and upon the water content of the sediment. Linear increases in sediment water content could cause linear increases in the entrainment rate:

$$E = \lim_{c \to 0} \int_0^h \frac{\partial C}{\partial t} dz = \lim_{c \to 0} h \frac{dC}{dt} \qquad [2\text{-}30]$$

where dC/dt is the slope of the concentration versus time curve and h is the depth of the overlying water.

Mehta and Partheniades (1982) related dC/dt to the time-rate of change, dz/dt, of the depth of erosion, z, below the initial bed surface according to:

$$\frac{dz}{dt} = \frac{h}{\rho} \frac{dC}{dt} \qquad [2\text{-}31]$$

where h is the depth of flow, dC/dt is the time rate of change of suspended sediment concentration, C, and ρ is depth varying dry density of the bed.

Shrestha and Orlob (1996) divided the basal erosion into two types, mass erosion and surface erosion. Mass erosion is defined as bulk erosion en masse, of the sediment from the topmost layer, downward to new deposits. Surface erosion is considered as particle-by-particle resuspension from the bed.

The mean rate of mass erosion per unit bed surface area over a time interval Δt is equal to the mass transferred to the water column as given by:

$$E = S_e h = \frac{T}{\Delta t} \rho_s \left(\frac{\rho_b - \rho_w}{\rho_s - \rho_w} \right) \qquad [2\text{-}32]$$

where S_e is the rate of change of sediment concentration in the water column due to erosion, T is thickness of erodible layer, h is average flow depth, ρ_s is density of sediment material, ρ_b is bulk density and ρ_w is density of the suspending medium, respectively.

The mean rate of surface erosion is estimated using properties of the sediment, fluid characteristics and hydrodynamic shearing stresses.

$$E = S_e h = M'\left(\frac{\tau_b}{\tau_{ce}} - 1\right) \text{ if } \tau_b > \tau_{ce} \qquad [2\text{-}33]$$

where M′ is erodibility constant determined empirically, τ_b is bed shear stress determined from the hydrodynamics of the fluid at bed level, and τ_{ce} is critical shear stress. Critical shear stresses and erodibility constants for specific cohesive materials can be determined in the laboratory using a rotating cylinder device.

2.5.1.2 Empirical approach

Maa and Lee (1997) and Maa et al. (1998) proposed empirical equations to estimate the entrainment rate based on in situ and laboratory experiments.

$$E = E_0\ e^{-\lambda t} \qquad [2\text{-}34]$$

where E_0 is an initial re-suspension coefficient in g/ cm^2 / s, λ is a rate constant in s^{-1} and t is time.

$$E = m\ \tau_{ex}^{n} \qquad [2\text{-}35]$$

where m and n are two dimensionless empirical constants and τ_{ex} is approximated excess bed shear stress.

Lee and Mehta (1994) related the rate of erosion to the applied bed shear stress after a review of laboratory data on the erosion of cohesion sediment beds.

$$\dot{\varepsilon} \qquad \left(\tau \quad -\tau_s\right) \qquad [2\text{-}36]$$

$$\left(\frac{\tau_b - \tau_s}{}\right)^{1/2} \qquad [2\text{-}37]$$

where τ_b is the erosion bed shear strength for a placed bed, τ_s is the bed shear strength as a function of depth z below the bed surface for a deposited bed and α_1, α_2 and α_3 are empirical coefficients. Equation 2-36 can be approximated by Equation 2-37 in certain cases.

2.5.2. Bank erosion

Besides the erosion of channel bed, erosion of material coming from channel banks is also an important part in river channel erosion. Duan (2001) developed a two dimensional numerical model to estimate the bank erosion rate by considering the mass balance within a control volume near the bank.

$$\omega = -\frac{\left(\frac{\partial q_1}{\partial l}\frac{dr}{2} + q_r - q_{br}\right)}{h_b} \qquad [2\text{-}38]$$

where ω is bank erosion rate (if bank advance, $\omega > 0$; if the bank retreats, $\omega < 0$; and if the bank is unchanged, $\omega = 0$); d_r is defined as the width of the control volume that is nearest to the edge of bank; h_b is flow depth at the near bank region; q_l and q_r are total sediment transport rates in the longitudinal and transversal directions, respectively; and q_{br} is transversal component of the sediment transport rate at the near bank region as a results of bank erosion.

2.5.3. The summary of river erosion

The model used to calculate the rate of erosion is mostly based on the diffusion process that means the rate of erosion is a function of the change of sediment concentration. Although some of the models consider the difference between shear stress at the base of the debris and shear resistance of bed material, at least one empirical constant is used in the equation which makes

the model difficult to be used in debris flow cases since the constant is mostly dependent on the slope of the channel, particles shapes and size (Egashira et al. 2001).

Reference

Banton, J., Villard, P., Jongmans, D., and Scavia, C. (2009). Two-dimensional discrete element models of debris avalanches: Parameterization and the reproducibility of experimental results. Journal of Geophysical Research, 114, F04013, doi:10.1029/2008JF001161.

Berger, C., McArdell, B. W., and Schlunegger, F. (2011). Direct measurement of channel erosion by debris flows, Illgraben, Switzerland. Journal of Geophysical Research, 116, F01002, doi:10.1029/2010JF001722, 2011b.

Bowman, E. T., Laue, J., Imre, B., and Springman, S. M. (2010). Experimental modelling of debris flow behaviour using a geotechnical centrifuge. Canadian geotechnical journal, 47(7), 742-762.

Cao, Z. (1997). Turbulent bursting-based sediment entrainment function. Journal of Hydraulic Engineering, 123(3), 233-236.

Cao, Z., Pender, G., Wallis, S., and Carling, P. (2004). Computational dam-break hydraulics over erodible sediment bed. Journal of hydraulic engineering, 130(7), 689-703.

Chen, H., Crosta, G. B., and Lee, C. F. (2006). Erosional effects on runout of fast landslides, debris flows and avalanches: a numerical investigation. Géotechnique, 56(5), 305-322.

Coe, J. A., Cannon, S. H., and Santi, P. M. (2008). Introduction to the special issue on debris flows initiated by runoff, erosion, and sediment entrainment in western North America. Geomorphology, 96(3), 247-249.

Cundall, P. A., and Strack, O. D. (1979). A discrete numerical model for granular assemblies. Géotechnique, 29(1), 47-65.

De Blasio, F. V., Breien, H., and Elverhøi, A. (2011). Modelling a cohesive-frictional debris flow: an experimental, theoretical, and field-based study. Earth Surface Processes and Landforms, 36(6), 753-766.

Duan, J. G. (2001). Numerical analysis of river channel processes with bank erosion. Journal of Hydraulic Engineering, 127(8), 702-703.

Egashira, S., Honda, N., and Itoh, T. (2001). Experimental study on the entrainment of bed material into debris flow. Physics and Chemistry of the Earth, Part C: Solar, Terrestrial & Planetary Science, 26(9), 645-650.

Fannin, R. J., and Wise, M. P. (2001). An empirical-statistical model for debris flow travel distance. Canadian Geotechnical Journal, 38(5), 982-994.

Fannin, R. J., Busslinger, M., and Jordan, P. (2012). Debris flow travel distance: Field traverse data and regional guidelines for terrain stability assessment. Proceeding of the 11th International and 2nd North American Symposium on Landslides, Editors: Eberhardt, E., Froese, C., Turner, K., and Leroueil, S., Banff, Canada, June 3-8, 2012, Balkema, Taylor and Francis Group, London, 1: 751-756.

Fukuda, M. K., and Lick, W. (1980). The entrainment of cohesive sediments in freshwater. Journal of Geophysical Research: Oceans, 85(C5), 2813-2824.

He, J., Li, X., Li, S., Yin, Y., and Qian, H. (2010). Study of seismic response of colluvium accumulation slope by particle flow code. Granular Matter, 12(5), 483-490.

Hsu, L., Dietrich, W. E., and Sklar, L. S. (2008). Experimental study of bedrock erosion by granular flows. Journal of Geophysical Research, 113, F02001, doi:10.1029/2007JF000778.

Hutter, K., Koch, T., Pluüss, C., and Savage, S. B. (1995). The dynamics of avalanches of granular materials from initiation to runout. Part II. Experiments. Acta Mechanica, 109, 127-165.

Iimura, K., Watanabe, S., Suzuki, M., Hirota, M., and Higashitani, K. (2009). Simulation of entrainment of agglomerates from plate surfaces by shear flows. Chemical Engineering Science, 64(7), 1455-1461.

Iverson, R. M., Logan, M., and Denlinger, R. P. (2004). Granular avalanches across irregular three-dimensional terrain: 2. Experimental tests. Journal of Geophysical Research, 109, F01015, doi:10.1029/2003JF000084.

Iverson, R. M., Reid, M. E., Logan, M., LaHusen, R. G., Godt, J. W., and Griswold, J. P. (2011). Positive feedback and momentum growth during debris-flow entrainment of wet bed sediment. Nature Geoscience, 4(2), 116-121.

Iverson, R. M. (2012). Elementary theory of bed-sediment entrainment by debris flows and avalanches. Journal of Geophysical Research, 117, F03006, doi:10.1029/2011JF002189.

Iverson, R. M., and Ouyang C.J (2015), Entrainment of bed material by Earth-surface mass flows: Review and reformulation of depth-integrated theory. Reviews of Geophysics, 53, doi:10.1002/2013RG000447.

Iverson, R. M. (2015). Scaling and design of landslide and debris-flow experiments. Geomorphology. doi:10.1016/j.geomorph.2015.02.033

Jain, S. C. (1992). Note on lag in bedload discharge. Journal of Hydraulic Engineering, 118(6), 904-917.

Jakob, M., Bovis, M., and Oden, M. (2005). The significance of channel recharge rates for estimating debris-flow magnitude and frequency. Earth Surface Processes and Landforms, 30(6), 755-766.

Lee, S. C., and Mehta, A. J. (1994). Cohesive sediment erosion. dredging research program, DRP 94-6, U.S. Army Corps of Engineers, Engineering Research Center, Vicksburg, Miss.

Li, X., He, S., Luo, Y., and Wu, Y. (2010). Discrete element modeling of debris avalanche impact on retaining walls. Journal of Mountain Science, 7(3), 276-281.

Luna, B. Q., Remaître, A., Van Asch, T. W., Malet, J. P., and Van Westen, C. J. (2012). Analysis of debris flow behavior with a one dimensional run-out model incorporating entrainment. Engineering geology, 128, 63-75.

Maa, J. P. Y., and Lee, C. H. (1997). Variation of the resuspension coefficients in the lower Chesapeake Bay. Journal of Coastal Research, 63-74.

Maa, J. P. Y., Sanford, L., and Halka, J. P. (1998). Sediment resuspension characteristics in Baltimore harbor, Maryland. Marine Geology, 146(1), 137-145.

Mangeney, A., Roche, O., Hungr, O., Mangold, N., Faccanoni, G., and Lucas, A. (2010). Erosion and mobility in granular collapse over sloping beds. Journal of Geophysical Research, 115, F03040, doi:10.1029/2009JF001462.

McCoy, S. W., Kean, J. W., Coe, J. A., Staley, D. M., Wasklewicz, T. A., and Tucker, G. E. (2010). Evolution of a natural debris flow: In situ measurements of flow dynamics, video imagery, and terrestrial laser scanning. Geology, 38(8), 735-738.

McCoy, S. W., Tucker, G. E., Kean, J. W., and Coe, J. A. (2013). Field measurement of basal forces generated by erosive debris flows. Journal of Geophysical Research: Earth Surface, 118(2), 589-602.

McDougall, S., and Hungr, O. (2005). Dynamic modelling of entrainment in rapid landslides. Canadian Geotechnical Journal, 42(5), 1437-1448.

Medina, V., Bateman, A., and Hürlimann, M. (2008a). A 2D finite volume model for debris flow and its application to events occurred in the Eastern Pyrenees. International Journal of Sediment Research, 23(4), 348-360.

Medina, V., Hürlimann, M., and Bateman, A. (2008b). Application of FLATModel, a 2D finite volume code, to debris flows in the northeastern part of the Iberian Peninsula. Landslides, 5(1), 127-142.

Mehta, A. J., and Partheniades, E. (1982). Resuspension of deposited cohesive sediment beds. Proceedings of the Eighteenth Coastal Engineering Conference, Editor: Edge, B. L., Cape Town, South Africa, November 14-19, 1982, ASCE, New York, 2: 1569-1588.

Miller, D. J., and Burnett, K. M. (2008). A probabilistic model of debris-flow delivery to stream channels, demonstrated for the Coast Range of Oregon, USA. Geomorphology, 94(1), 184-205.

Moffat, R., Fannin, R. J., and Garner, S. J. (2011). Spatial and temporal progression of internal erosion in cohesionless soil. Canadian Geotechnical Journal, 48(3), 399-412.

Papa, M., Egashira, S., and Itoh, T. (2004). Critical conditions of bed sediment entrainment due to debris flow. Natural Hazards and Earth System Science, 4(3), 469-474.

Pitman, E. B., Nichita, C. C., Patra, A. K., Bauer, A. C., Bursik, M., and Weber, A. (2003). A model of granular flows over an erodible surface. Discrete and Continuous Dynamical Systems Series B, 3(4), 589-600.

Rickenmann, D., Weber, D., and Stepanov, B. (2003), Erosion by debris flows in field and laboratory experiments. Proceedings of the Third International Debris-Flow Hazards Mitigation: Mechanics, Prediction, and Assessment (DFHM) Conference, Editors: Rickenmann, D., and Chen, C.L., Savos, Switzerland, September 10-12, 2003, Millpress, Rotterdam, 883–894.

Salciarini, D., Tamagnini, C., and Conversini, P. (2010). Discrete element modeling of debris-avalanche impact on earthfill barriers. Physics and Chemistry of the Earth, 35(3), 172-181.

Savage, S. B., and Hutter, K. (1991). The dynamics of avalanches of granular materials from initiation to runout. Part I: Analysis. Acta Mechanica, 86, 201-223.

Shrestha, P. L., and Orlob, G. T. (1996). Multiphase distribution of cohesive sediments and heavy metals in estuarine systems. Journal of Environmental Engineering, 122(8), 730-740.

Skempton, A. W. (1954). The pore-pressure coefficients A and B. Geotechnique, 4(4), 143-147.

Sovilla, B., Burlando, P., and Bartelt, P. (2006). Field experiments and numerical modeling of mass entrainment in snow avalanches. Journal of Geophysical Research, 111, F03007, doi:10.1029/2005JF000391.

Stock, J. D., and Dietrich, W. E. (2006). Erosion of steepland valleys by debris flows. Geological Society of America Bulletin, 118, 1125-1148.

Takahashi, T. (1991). Debris flow. Rotterdam: Balkema.

Wang, X. B. (2008). Geotechnical analysis of flow slides, debris flows, and related phenomena (Doctoral dissertation). University of Alberta, Edmonton, Canada.

Wang, X. B., Morgenstern, N. R., and Chan, D. H. (2010). A model for geotechnical analysis of flow slides and debris flows. Canadian Geotechnical Journal, 47(12), 1401-1414.

Wicklein, E., and Papanicolaou, A. N. (2000). Sediment transport modeling in mountain streams. Proceedings of the 2000 ASCE Water Resources Engineering and Water Resources Planning and Management Conference, Editors: Hotchkiss, R.H. and Glade, M., Minneapolis, United States, July 30-August 2, 2000, ASCE, New York, 1-10.

3. ENTRAINMENT MODEL FORMULATION FOR DEBRIS FLOW ANALYSIS[1]

3.1. Abstract

Debris that entrain sediment by undermining channel beds or scouring channel banks can become exceptionally mobile and destructive. Therefore, the calculation of entrainment plays an important role in debris flow runout analysis. An entrainment model is proposed that takes into account surface erosional effects by considering progressive scouring and shear failure on the channel surface. By considering simple geometry and particle configurations, the equations for the progressive scouring are developed. In deriving the equations for the progressive scouring mode of erosion, two types of motions are considered: rolling motion and sliding motion. Newton's Law of Motion is applied to calculate the acceleration, velocity, and displacement of the particles. A probability density function (PDF) is used in the calculation of the entrainment rate for different configurations of particle contact. Measurements from flume experiments are used for model verification. It is found that the entrainment rate can be calculated using a normal distribution PDF. The proposed entrainment model has been shown to be effective in calculating debris entrainment.

3.2. Introduction

Debris flows are rapid mass movement in steep hilly terrains where earthly materials flow down in a valley or channel usually triggered by a landslide or heavy rainfall. It is usually fast-moving with variable solid concentration and long runout distance. Due to its fast moving characteristics,

[1] This chapter has been submitted to the International Journal of Geomechanics in May 2016. The paper is currently under review.

debris flow is one of the most hazardous and unpredictable surface process that results in many losses of lives and property damages (Schurch et al. 2011). For example, between 2004 and 2010 there were 2,327 people killed by debris flow in China out of 6,910 who were killed by natural disasters. One recent example showing the destructive power of debris flow is the Zhouqu debris flow which occurred on August 7, 2010. It caught the residents of Zhouqu by surprise and 1,765 people were killed and more than 5,500 houses were destroyed.

In order to assess the extent of damages caused by a debris flow event, numerical modelling and debris flow analysis are often carried out. There are several approaches in debris flow modelling. This includes the empirical approach, the discontinuum approach and the continuum approach. In the empirical approach, calculations of the volume, speed, runout distance and the extent of a debris flow is based on historical observations of a large number of events, see Fannin et al. (2012) and Moffat et al. (2011). This approach requires the observation of a large number of events in different geological conditions. Moreover the result is only applicable in similar geological conditions. In the second approach using discontinuum model, debris flow is modelled using many small elements that interact with each other, see Cundall and Strack (1979). The advantage of this approach is that it can simulate large deformation and changes in mass can be accommodated easily. However it is difficult to determine the property for the debris and very difficult to incorporate the effect of water. The third approach is based on continuum models in which the body of the debris is considered to be a continuum. The formulation of the model is based on physical laws such as Newton's Law of Motion, the Laws of the Conservation of Mass and the Law of the Conservation of Energy. The equations governing the motion of the debris are derived to calculate the flow characteristics, such as velocity, depth, runout distance etc., see Wang et al. (2010). Numerical techniques, such as the

finite element method, finite different method or the block continuum method, are often used to provide the numerical solution for debris flow analysis. This approach is one of the most common approaches and it is one of the most effective ways of analyzing practical debris flow problems.

In many debris flow events, flow channels are typically covered by surficial deposits, sometimes several meters thick of loose granular material. A rapidly moving debris could mobilize these materials which could change the volume of the debris significantly during the flow process. The inclusion of material through erosion of the flow channel is called entrainment. Many debris flows have significant amount of entrainment resulting in a substantially larger final volume than its initial volume, see Table 3-1. In these cases, the final volume is much larger than the initial volume since the debris erodes and includes the material along its flow path. Tsingshan debris flow is a special case in which the entrained volume is about fifty times the initial volume. This can change the mechanics and characteristics of flow thus making prediction and back analysis of debris flow much more difficult. The rate of this process is affected by the shear stress applied on the bed sediment, the internal friction between the particles, the velocity of the flowing debris, the slope angle of the channel, the cohesion of the bedding material and the pore water pressure generated due to shearing of fine grained materials in the bed.

Table 3-1: Example of rock avalanche and debris flow involving entrainment

Case	Initial volume (m^3)	Entrained volume (m^3)	Average slope angle of entrainment zone (º)	Final volume (m^3)	Entrained volume / Final volume (%)	Entrainment material	Reference
Huascaran, Peru, 1970 Rock and ice avanlanche	13×10^6	39×10^6	20~45	52×10^6	75	Glacial till and ice	Hungr and Evans (2001)

Case	Initial volume (m^3)	Entrained volume (m^3)	Average slope angle of entrainment zone (º)	Final volume (m^3)	Entrained volume / Final volume (%)	Entrainment material	Reference
Mt. Ontake, Japan, 1984 Volcanic rock avalanche	34×10^6	22×10^6	20~45	56×10^6	39	Colluvium and alluvium	Hungr and Evans (2004)
Nomash River, Canada, 1999 Rock slide-debris avalanche	300×10^3	300×10^3	25~45	600×10^3	50	Till-derived colluvium	McDougall and Hungr (2005)
Tsingshan, Hong Kong, 1990 Debris flow	400	19600	23~35	20000	98	Colluvium, residual soil	Lo and Chau (2003)
Faucon, French,2003 Debris flow	8.5×10^3	36.5×10^3	3~50	45×10^3	81	Tills, kame terraces and moraines	Remaître et al. (2009)
Fjærland, Norway, 2004 Debris flow	25×10^3	215×10^3	4~60	240×10^3	90	Quaternary till and older debris-flow material	Breien et al. (2008)
Dolomites, Italy, 1997 Debris flows	600	5400	7~30	6000	90	Postglacial sediments	Berti et al. (1999)

Studying entrainment, being an important part of debris flow analysis, will help the interpretations and understandings of significant changes in the mass during the flow process. Presently entrainment analysis often adopts a static approach in which shear stresses are calculated in the soil in the flow channel. The Mohr Coulomb criterion is used to determine the depth of failure in the soil in calculating the depth of erosion. Depth-averaged approach was used to describe erosion process (Bouchut et al. 2016 and Iverson and Ouyang 2015). However, in granular flow, material at the surface of the bed can be eroded by progressive scouring which is physically in particle scale. McCoy et al. (2012) and Reid et al. (2011) studied the scouring

process in the channel bed adopting field experiments. Mangeney et al. (2010) and Farin et al. (2014) carried out several laboratory experiments to study this process. The progressive scouring refers to the propagation of the entrainment front. This may result in more material being eroded than considering shear failure alone using a static approach. Presently, there is no model that can capture the progressive scouring mechanism and very little research has been done to understand this process. The purpose of this paper is to understand the progressive souring mechanism, to develop a numerical model that can calculate the amount of entrainment and to incorporate the model into debris flow analysis.

3.3. Review of previous work

3.3.1. Debris flow entrainment models

During the movement of a debris, material from the channel boundary are often eroded and mixed with the main body of the debris and becomes part of it (Iverson 2012). There are various models in calculating the amount and rate of entrainment in debris flow analysis (Iverson and Ouyang 2015). Some efforts have been made in the past to estimate the volume of erosion and incorporate basal entrainment. The models for estimating the amount of material incorporated from channel bed can be roughly summarized as analytical models and empirical models. In the analytical approach, there are basically two approaches in calculating entrainment: the static approach and the dynamic approach. Newton's Law of Motion or force equilibrium are used to calculate the entrainment rate or depth of erosion of the channel base. Shear stress and shear resistance are the most important factors in calculating entrainment. Diffusion process caused by difference of sediment concentration between erodible channel bed and the main body of the debris is also considered as one possible mechanism of entrainment (Iverson and Ouyang 2015). On the other hand, in the empirical approach the entrainment rate is empirically related to flow

velocity or shear stress exerting on the erodible bed. The coefficient of correlation between entrainment rate and flow velocity or shear stress is often determined by model calibration based on a large number of case histories.

In the static approach, static shear stresses are calculating beneath the channel bed under the debris and failure is considered when the static shear stress exceeds the shear strength of the material. The depth in which failure occurs is determined and the amount of material is calculated which will be added to the main body of the debris. In the dynamic approach, the rate of entrainment is calculated based on the rate of erosion of the material at the channel bed. The rate of erosion is determined based on shear failure at the surface and the material is removed from the surface depending on the velocity of flow of the main body of the debris (Medina et al. 2008, Iverson and Ouyang 2015 and Bouchut et al. 2016). It is assumed in this approach that the velocity of newly eroded material is the same as the average velocity of the debris flow (Fraccarollo and Capart 2002, Medina et al. 2008 and Ionescu et al. (2015). Bouchut et al. (2016) and Ionescu et al. (2015) proposed a model based on depth-averaged approach in which variation of static/flowing interface is considered as the erosion rate. Compared with other models, this model is deduced directly from the viscoplastic constitutive law. This model can show the continuity of shear stress and velocity across static/flowing interface.

Egashira et al. (2001) proposed a formula to calculate the erosion rate assuming that the slope of the channel bed is always adjusted to the angle corresponding to the limiting equilibrium conditions. The material in the channel left behind by an unsaturated debris will approach the limiting equilibrium slope angle. Geometrical relationship between the initial bed slope and equilibrium slope angle is incorporated into the mass conservation law of the eroded material to obtain the entrainment rate.

The entrainment model proposed by van Asch et al. in 2004 (Luna et al. 2012) is a one dimensional dynamic debris flow model that takes into account the entrainment concept based on the generation of excess pore water pressure under undrained loading on the in-situ material. Flow is treated as laminar, single phase and as an incompressible continuum process. Due to the moving mass flowing on top of the erodible bed, loading on the bed deposits is generated. The model calculates this applied load on the in-situ soil through changes in the vertical normal stress and shear strength caused by the debris flow. The increase in pore water pressure is calculated based on Skempton's (1954) equation. The depth of erosion is approximated using the relationship between the factor of safety at the bottom and top of soil in the channel.

Iverson (2012) considered the behavior of a slide block descending an erodible slope with the ability of incorporating soil from the bed. Newton's Second Law was first applied on the sliding material. Then, Coulomb friction rule was applied and basal friction resistance calculation was improved by taking the shear rate into account. The frictional resistance consists of a constant component of frictional resistance and a velocity-dependent component. After considering the rate-dependent friction, entrainment rate based on the change in weight of the sliding block was obtained. . Iverson and Ouyang (2015) considered the rapid change of stress, density and flow velocity between two layers: moving upper layer and static lower layer. A new entrainment model is proposed based on depth-integrated mass and momentum conservation equations.

De Blasio et al. (2011) suggested a semi-empirical model to calculate entrainment. In the semi-empirical model, the entrainment rate is dependent solely on the tangential component of weight at the base and on the average velocity of the debris flow. Critical shear stress was used as the thereshold to determine the occurance of entrainment. Data from the Fjæland debris flow was

used to determine the dynamic quantities and erosion effects in calibrating the model. This model seems promising since it relates debris flow velocity and basal shear stress to entrainment.

It is seen that the current approach in entrainment calculation considers shear failure of the soil in the channel base. Often static shear strength parameters are used.

3.3.2. Debris flow entrainment experiments

Flume experiments are normally conducted to test the entrainment of debris flow. Egashira et al. (2001) and Papa et al. (2004) built a small scale experimental flume, 10 cm wide by 20 cm high with 12º slope. The erodible bed, consisted of particles having uniform grain size, was placed at the lower part of the flow channel. The same material was used for the debris-flow body. During the test, the debris had different solid concentration which resulted in different erosional profile of the bed with different equilibrium slope angle. Particles and sediment flux concentration were varied in the test to understand the impact of solid concentration on entrainment rate.

Mangeney et al. (2010) constructed a similar flume for entrainment tests. A 20 cm long by 14 cm wide tank was placed at the crest of the channel which is evenly covered by granular material. In the experiments, subspherical, cohesionless and highly rigid glass beads, ranging from 600 μm to 800 μm, fill the tank and erodible bed. The thin layer of erodible bed was formed by cutting the supply of the steady uniform flow to allow the layer to deposit. The thickness of the erodible bed varied from 0 mm to 6.5 mm. Slope angle changed from 0º to 30° during the test. The effect of slope angle and thickness of erodible channel on runout distance was studied. The shape of the granular mass during movement was recorded and analyzed. It is concluded that runout distance increases almost linearly as a function of the thickness of the erodible bed suggesting that erosion is mainly “supply dependent”. The runout distance increases about 40% on the slope

close to the repose angle of the grains. As well, erosion is positively related with the slope angle that means erosion increases with the increase of slope angle. Farin et al [18] found that there is a critical value of slope angle, around 10º to 16º in the experiments, below which the erodible bed has no effect on runout distance or no difference can be detected after comparing the results from the channel bed with and without erodible material. However, if the flows over an erodible bed, larger than the critical slope angle, the runout distance increases by up to 50% comparted with the over a rigid bed.

A series of large-scale experiments were conducted between 1992 and 2013 using the USGS debris flow flume for gravel, sand and mud-size particles on erodible bed sediment with different moisture content (Iverson and Denlinger 2001; Iverson et al. 2004; Iverson et al. 2011; Iverson, R. M. 2012). The USGS facility is located about 45 miles east of Eugene, Oregon, in the United States of America (USA). The experimental flume is a 95 m long, 2 m wide and 1.2 m deep reinforced concrete channel. The properties of the erodible bed including moisture content and type of material, and solid concentration and grain composition in the tank were varied in the experiment. Different characteristics of granular flow were measured in each test. In this entrainment study, it is found that increase in water content usually leads to an increase in the rate of entrainment. On the basis of progressive shear entrainment, a preliminary theory on entrainment has been developed. Iverson's theory postulate that entrainment is accompanied by increased flow momentum and speed only if large positive pore pressures develop in wet bed sediments when the sediments are overridden by the debris. The increase in pore pressure facilitates progressive scouring of the bed, reducing the basal friction and resulting in an increase in the flow speed, mass and momentum (Iverson et al. 2011).

Sovilla et al. (2006) studied 18 snow avalanches that occurred between 1997 and 2003 in Switzerland and Italy. Information such as velocities, pressures and flow depths were collected. The average depths of erosion were estimated in “potential entrainment areas”. Based on the analysis on the mechanism of the entrainment process, a cohesionless dense snow avalanche model have been developed. In this model, the total entrainment rate is assumed to be a function of the location, velocity and time of the avalanche.

3.3.3. Introduction on runout calculation

In continuum modelling, there are two approaches in formulating the equations for debris flow runout analysis. The first approach is based on the Law of Conservation of Momentum. The debris is divided into slices in two dimensional analysis, or columns in three dimensional analysis, and the motion of individual slices can be calculated by applying Newton’s Law of Motion. An example of this force based formulation is the Dynamic Analysis Model (DAN) developed by Hungr (1995). There are also other depth-averaged models in debris flow runout calculation such the models proposed by Bouchut et al. (2016) and Iverson and Ouyang (2015).The second approach is based on the Law of Conservation of Energy. The energy formulation has been developed by Wang et al. (2010). The motion of the debris can be calculated by considering the energy dissipation on the boundary as well as internal dissipation of the mass of the debris in a Lagrangian framework (Wang 2008). The momentum formulation of the first approach cannot take into account the internal energy dissipation. Lateral pressure and basal resistance on individual slices are determined using the Rankine and Mohr-Coulomb theories. The momentum equations for the overall sliding mass are not required in the calculation.

In analyzing debris flow with significant amount of entrainment, an entrainment model should be incorporated into a runout model to simulate the erosion process, inclusion process and movement process. The energy-based runout model has been selected to incorporate entrainment model in this study.

3.4. Formulation of the progressive scouring model

It has been demonstrated that sediment entrainment will occur progressively from the sediment surface rather than by a mass failure along the bedrock-sediment interface (McCoy et al. 2012; Reid et al. 2011). In this study, an erosional mechanism that considers material lying on the channel bed being eroded progressively downward in a rolling motion is examined. This process is called progressive scouring. The current methods in entrainment calculations mainly consider shear failure under the channel bed. The equation to calculate the depth of entrainment based on basal shearing mode of erosion has been developed (Medina et al. 2008a, Iverson and Ouyang 2015 and Bouchut et al. 2016). However, the progressive scouring process in particle scale is not considered in the models. This could lead to an error in the estimation of the rate of erosion in granular flow. To address this deficiency, the proposal model takes into account surface erosional effects by considering progressive scouring and shear failure in the channel bed. In developing the model, it is assumed that friction between particles satisfy the requirement for a "pure" rolling motion. However in entrainment prediction, the friction between particles is needed to determine the types of motion which includes rolling and sliding motions.

3.4.1. Analysis of shear failure and rolling motion

3.4.1.1 Rolling motion

In order to develop a theoretical framework for the progressive scouring process, soil particle is assumed to be round. The formulation is based on 2D analysis. Although 2D analysis is a simplification of 3D analysis, it provides the response of the structure in the 2D plane. In some cases, the 3D world can be simplified into a 2D plane which can reasonably capture all the physical characteristics of the 3D reality. Therefore, in the 2D model, soils can be represented by round 2D particles.

In calculating the drag force for the initiation of the rolling action, it is assumed that a particle will rotate around a point *O* as shown in Figure 3-1 where T_R is the drag force required to initiate particle rolling, θ is the slope angle of the channel bed, *m* is the mass of the particle (for *2D*, $m=\pi R^2\rho_b$), ρ_b is the density of bed sediment particle, *g* is the gravity acceleration, R is the radius of the rolling particles, α_0 is the angle between the channel surface and the line connecting the centers of two adjacent particles. For soil with variable particle sizes, R is assumed to be equal to $d_{50}/2$. F is the required friction between two adjacent particles during rolling. N is the normal force existing on a particle. ā is the translation acceleration which has same direction as particle moving direction. a_x and a_y are x-component and y-component of ā.

Based on particle rolling analysis presented in Appendix A, it can be shown that the force required for impending motion is given by:

$$T_R = \frac{\pi\ R^2\ \rho_b\, g\ \cos\left(\theta+\alpha_0\right)}{\sin\alpha_0} \qquad [3\text{-}1]$$

Equation [3-1] is based on the moment balance about contact point *O* which can be used to calculate the drag force required to initiate the rolling action. The equations governing the motion of the particle after it starts to move are given in Appendix A.

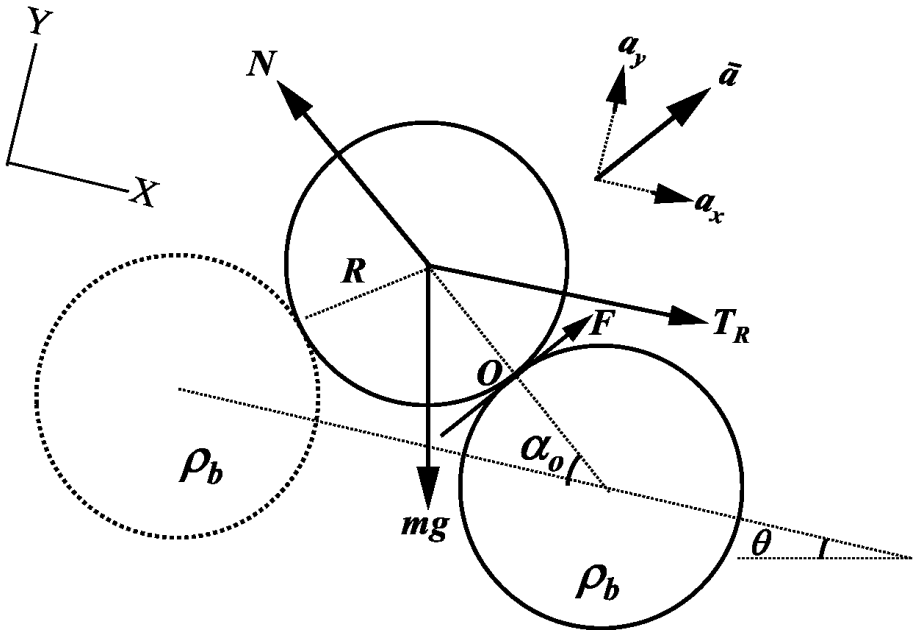

Figure 3-1: Free body diagram of particle when rolling occurs

3.4.1.2 Shear failure calculation

In addition to the rolling motion, material can be eroded in the channel bed due to shear failure. In this case, material will be sheared progressively with the thickness of the first layer is equal to the particle diameter or mean particle diameter in the case of non-uniform size particles. When a particle starts to move, the driving force is equal to the resisting force. Hence,

$$T_s = \left(\rho_f \, g \, h + \rho_b \, g \, 2R \right) \cos\theta \, \tan\phi \, 2R - \rho_b \, g \, 4R^2 \, \sin\theta \qquad [3\text{-}2]$$

where T_s is the shear force required for incipient motion of the particles, T_r is the shear resistance, ϕ is the internal friction angle, ρ_f and ρ_b are density of debris flow and bed sediment, respectively.

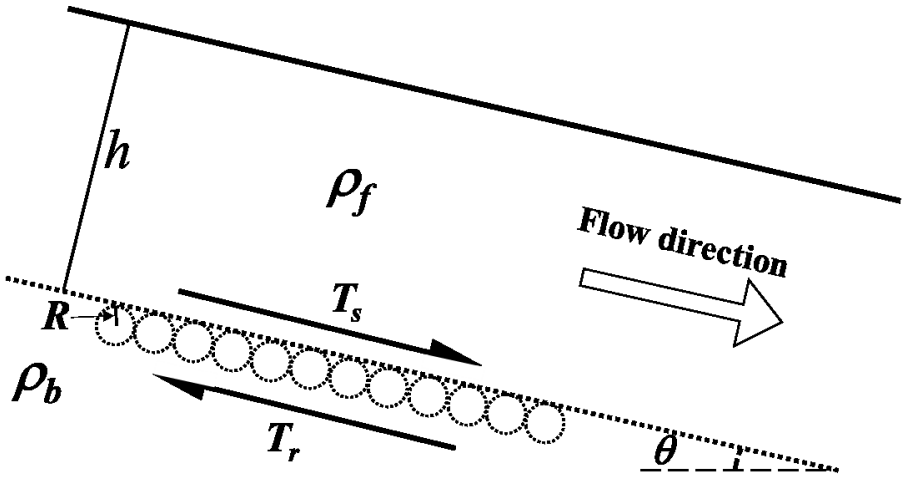

Figure 3-2: Definition sketch of shear erosion

3.4.1.3 Rolling mechanism versus sliding mechanism

Equation [3-1] calculates the drag force required for the initiation of the rolling motion and Equation [3-2] provides the drag force for the sliding mechanism. The actual mechanism that will occur in a particular situation depends on the smaller one of these two forces.

Consider the difference of the two drag forces as follows:

$$T_R - T_s = \frac{\pi R^2 \rho_b g \cos(\theta+\alpha_0)}{\sin\alpha_0} - 2R^2 g \rho_b \left(\frac{\rho_f}{\rho_b}\frac{h}{R}\cos\theta \tan\phi + 2\cos\theta\tan\phi - 2\sin\theta \right) \quad [3\text{-}3]$$

Rearranging Equation [3-3], it becomes:

$$T_R - T_s = 2R^2 \rho_b g \left[\frac{\pi \cos(\theta+\alpha_0)}{2\sin\alpha_0} - \left(\frac{\rho_f}{\rho_b}\frac{h}{R} + 2 \right) \cos\theta \tan\phi + 2\sin\theta \right] \quad [3\text{-}4]$$

When $T_R = T_s$

$$\frac{\pi \cos(\theta+\alpha_0)}{2 \sin\alpha_0} - \left(\frac{\rho_f}{\rho_b}\frac{h}{R}+2\right)\cos\theta \tan\phi + 2 \sin\theta = 0 \qquad [3\text{-}5]$$

$$\tan\phi = \frac{\frac{\pi \cos(\theta+\alpha_0)}{2 \sin\alpha_0} + 2 \sin\theta}{(\frac{\rho_f}{\rho_b}\frac{h}{R}+2)\cos\theta} \qquad [3\text{-}6]$$

If $\tan\phi > \frac{\frac{\pi \cos(\theta+\alpha_0)}{2 \sin\alpha_0} + 2 \sin\theta}{(\frac{\rho_f}{\rho_b}\frac{h}{R}+2)\cos\theta}$ for a material, then $T_R < T_s$, progressive scouring will occur before basal shearing for a coarse granular material with high internal friction angle. It means that particles will rotate first. If T_R is kept constant and it is less than T_s, particle will always be eroded by rolling motion. Figure 3-3 shows the general division between rolling and shearing motion. In reality, it is more likely that bed sediment can be eroded by both mechanisms at different times (Li and Komar 1986).

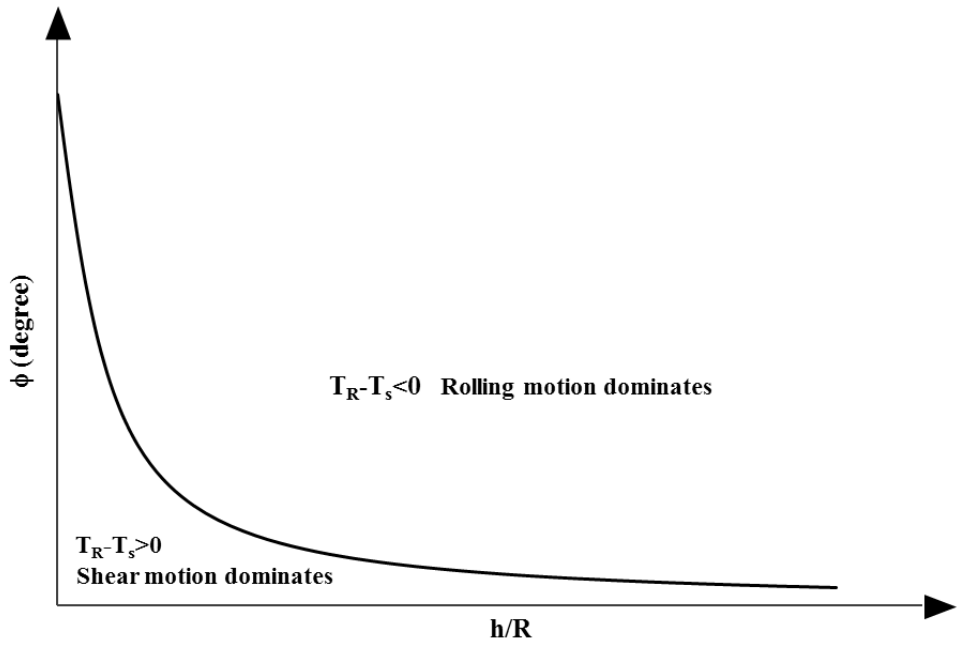

Figure 3-3: Threshold between rolling motion and shear failure

It is seen that omitting the progressive scouring mechanism may lead to underestimating the total volume of the debris.

3.4.2. Derivation of new entrainment model

3.4.2.1 Selection of motion of entrainment

There are two modes of erosion: progressive scouring and basal shearing. First it is necessary to calculate the shear forces required for rolling and shearing motions. If the actual shear force is less than these limiting values, no erosion is expected. If $T_R < T < T_s$, particles will be mainly eroded by rolling. If T is greater than both of them, particle will be moved by both rolling and sliding motions (Figure 3-4).

Figure 3-4: Changes in the entrainment modes

3.4.2.2 New entrainment model

To develop the equations for the progressive souring mode of erosion, it is necessary to consider simple geometry and particle configurations. In this formulation, uniform size spherical particles (circles rod with unit length in *2D* analysis), have been used. In this formation process, 2D analysis is performed. It is recognized that real soils are not spherical in shapes and they are not uniform in sizes. However the equations for the uniform size and spherical shape particles provide the form of the expression to calculate the rate of erosion for this mode of failure. Modifications of this theoretical equation may be necessary when applying it to analyze real debris flow.

Drag forces due to the moving debris above the bed are assumed to apply at the center of the particles. Particle is considered to be eroded when it rolls over the crest of another particle. Valyrakis et al. (2013) compared the minimum flow energy supplied for entrainment by saltation and rolling assuming the same order of magnitude of energy transport coefficients. It was revealed that a greater amount of mechanical work is required for saltating grains. Shodja and Nezami (2003) analyzed the distribution of all contact normal forces (combined rolling and sliding) and confirmed that rolling is the dominant mechanism. If there is no slipping between a particle and the underlying substrate, the particle will roll along the bed and it becomes part of

the debris. Newton's Law of Motion is applied to calculate the acceleration, velocity, and displacement of the particle.

Supposed that friction coefficient satisfies the requirement for rolling without slipping between particles. If there is slippage between particles and its underlying substrate, sliding motion will occur. Again, Newton's Law of Motion will be used to calculate the movement of the particle. Appendix A shows the derivation of the equations for both sliding and rolling mechanisms.

In order to determine if progressive scouring by rolling action occurs before basal shear failure, the drag force requires to initiate rolling should be less than the drag forces required for basal shear failure. The expressions to calculate initiation drag forces for both cases are presented in Appendix A.

3.4.2.3 The calculation of rolling time t

Entrainment rate is defined as the change of the depth of erosion in a unit time, therefore it is necessary to estimate the time (t) needed for a particle to move from the initial location to the crest of adjacent particle. The angle for a particle to rotate before it becomes part of the debris flow can be calculated once the initial resting angle α_0 is known. Based on the angular velocity of the moving particle, see Appendix A, the rolling time t can be estimated.

As α_0 varies for each location, time t should be calculated specifically for each α_0. The relationship between t and α_0 is shown in Figure 3-5. It can be seen from the figure that t decreases with the increase of α_0. Determination of α_0 will be discussed in the following section.

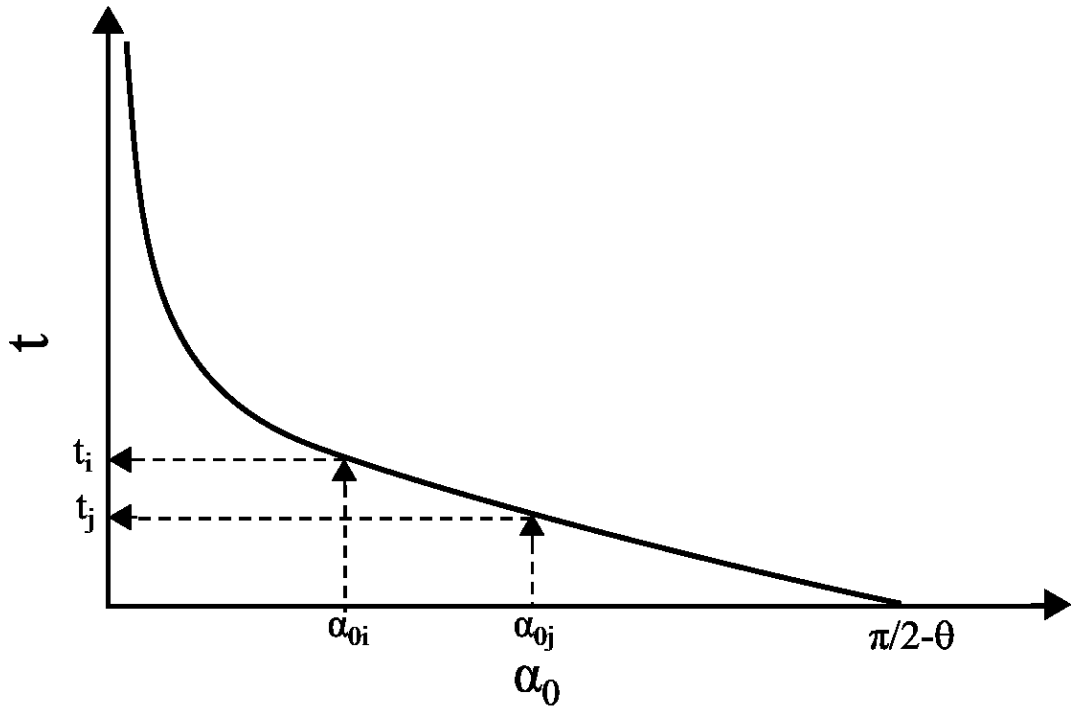

Figure 3-5: t_n against α_0 for constant drag force

3.4.3. Entrainment rate estimation

To incorporate the entrainment time into entrainment rate calculation in a continuum model, a probability density function (PDF) of the initial resting angle α_0 is introduced to relate the entrainment time to entrainment rate. The PDF provides the probability distribution of the relative location between two adjacent particles.

3.4.3.1 Relative location of adjacent particles

Firstly, different possible locations and configurations between two particles are considered and shown in Figure 3-6. The classification of these different cases is based on the position of particle 1 in one of the four quadrants of particle 2. The four quadrants are divided by two lines perpendicular to each other. One of them is the line parallel to the slope surface.

Particle 1 is the moving particle and particle 2 is the non-moving particle which particle 1 must override. It is interesting to note that if only the relative location between two adjacent particles is considered, Case I and Case III are the same. Similarly, Case II and Case IV are also the same. For Case II, if particle 1 is located in the second quadrant, for equilibrium, there must be another particle 3 keeping particle 2 stable. Therefore it means that the arrangement of particles 2 and 3 in Case II is the same as the arrangement of particles 1 and 2 in Case I. Hence, all the cases can be simplified into only one case, Case I. Therefore the formulation below is based on Case I.

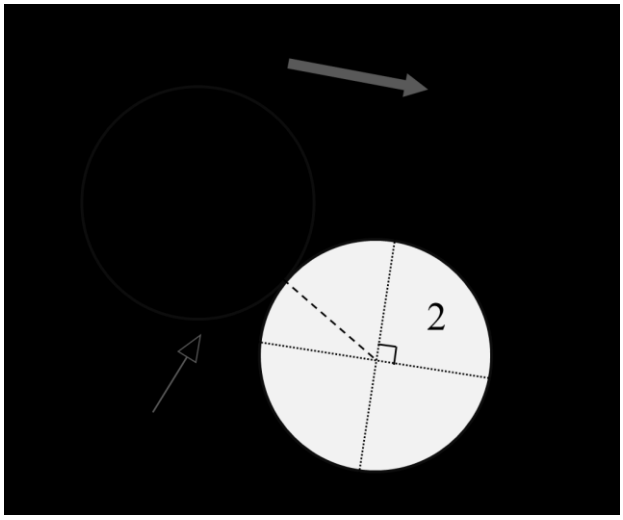

Case I

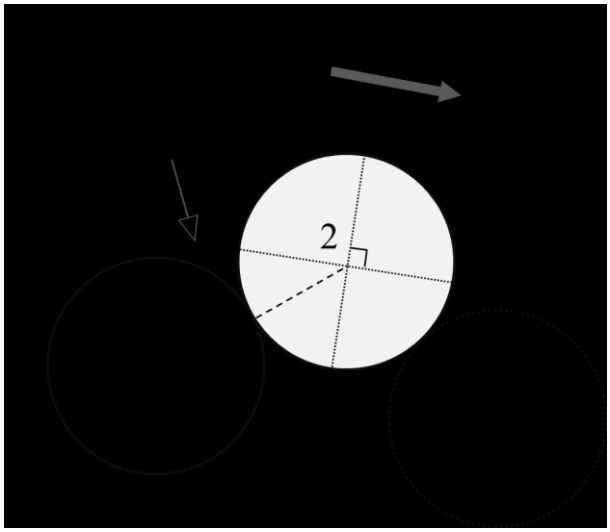

Case II

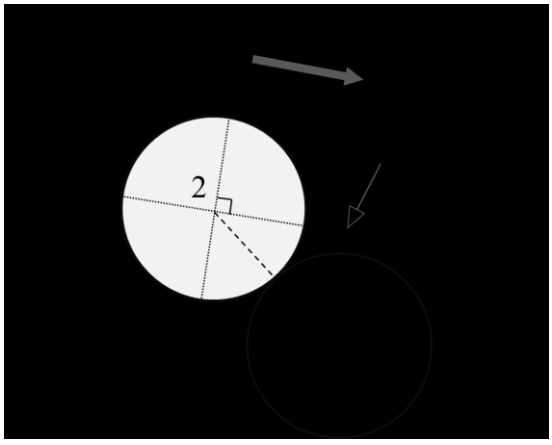

Case III

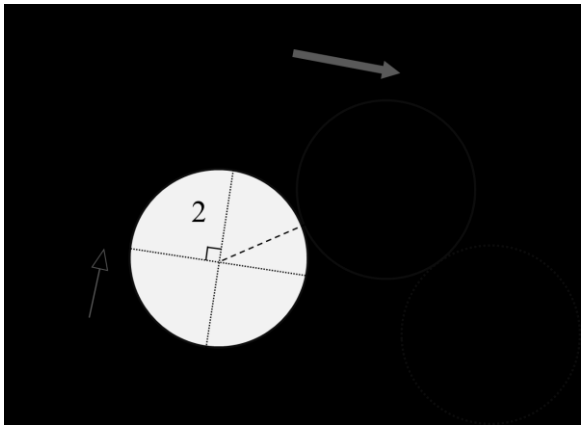

Case IV

Figure 3-6: Possible configurations of two particles in 2D cases

3.4.3.2 Characteristics of the entrainment of two adjacent particles

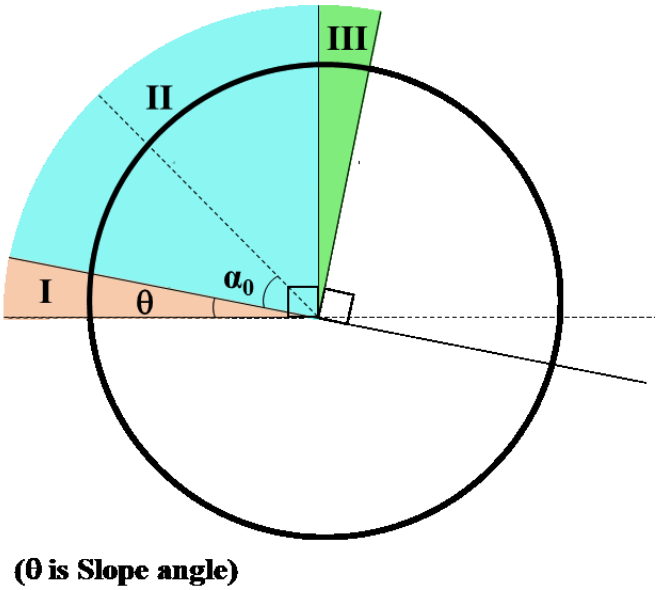

Figure 3-7: Range of angles of each region on the non-moving particle

According to the relative locations between the moving and non-moving particles, the region upstream of the non-moving particle can be divided into three regions (Figure 3-7): Region I - particle 1 cannot be eroded by rolling; Region II - particle 1 can be eroded; Region III - Unstable region for particle 1 and it has already eroded. Therefore, the erodible depth for Region III is zero.

In this framework, it is assumed that the probability of α_0 in the range $[(\pi/2)-\theta, \pi/2]$ is zero since these particles should have already been eroded. Since the range of the independent variable using the normal distribution function goes from negative infinity to positive infinity, the PDF of the normal distribution function should be normalized in the range $[0, (\pi/2)-\theta]$, see Figure 3-8. P_{nor} is modified to P_{mod} and average distribution is also shown in Figure 3-8.

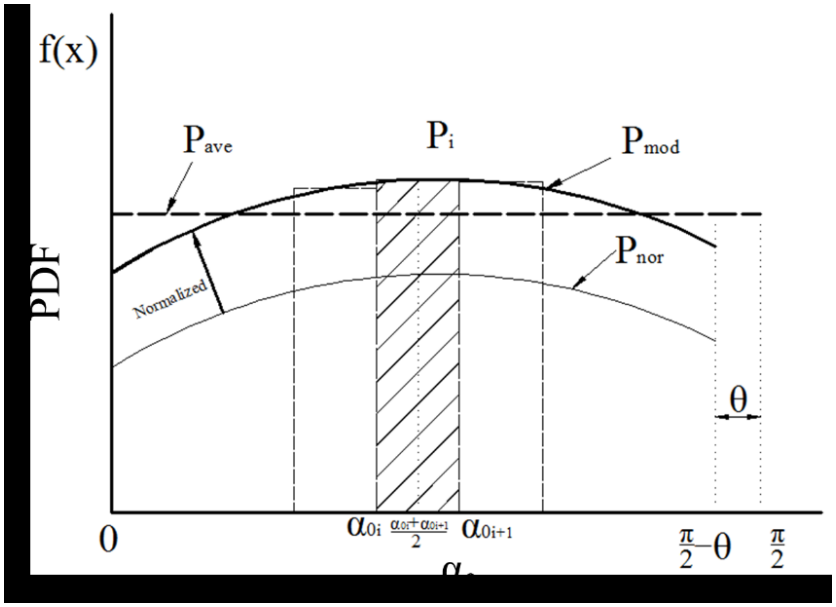

Figure 3-8: Probability density function of normal distribution and average distribution

3.4.3.3 Definition of depth of erosion

When one particle is removed by rolling action over time *t*, a layer of material is considered to be eroded. Therefore the depth of erosion is defined as the change of ground level between before and after one particle has been eroded (Figure 3-9) and the entrainment rate is defined as the change in depth over time *t*. The depth of erosion and the entrainment rate can be expressed in two different coordinate systems. If x-axis is the horizontal axis and y-axis is the vertical axis, the depth of erosion is $2R\ sin(\alpha+\theta)$. If x-axis is parallel to the slope and y-axis is perpendicular to the slope, the depth of erosion becomes $2R\ sin\alpha$. The latter coordinate system is adopted here.

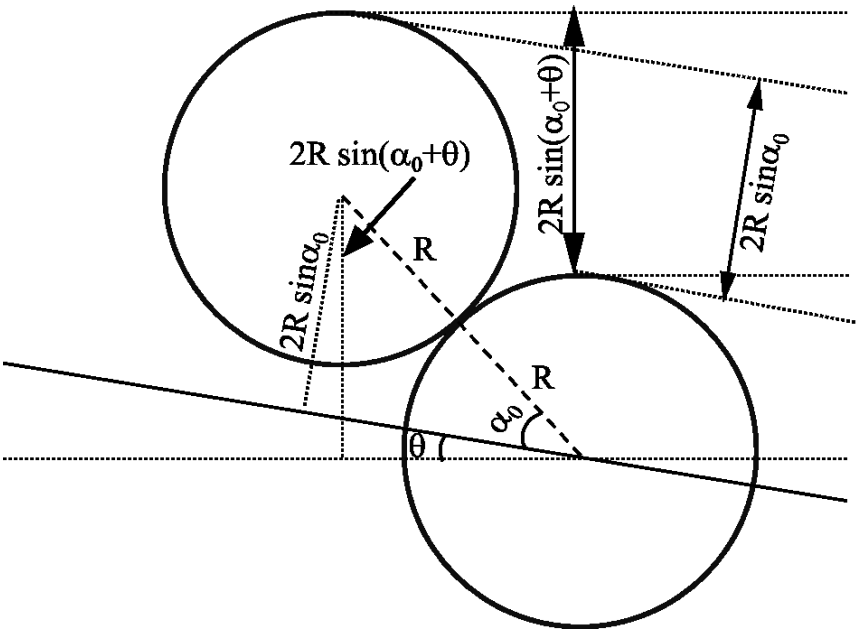

Figure 3-9: Eroded depth used for the calculation of entrainment rate

3.4.3.4 Estimation of entrainment rate

Based on the calculated the depth of erosion and the time required for one particle to move from its initial location to become part of the debris, the entrainment rate can be calculated. The entrainment rate is defined as the depth of erosion which is equal to $2R\sin\alpha_o$ as shown in Figure 3-9, divided by the time it takes for the particle to roll over.

To calculate the rate of erosion at a location along the debris, the entrainment rate of each particle is first calculated. The entrainment rate of a particle can be calculated from Equation [3-7]. The time it takes for a particle *i* to rotate from its initial contact position to the top of the adjacent particle is denoted as t_i. The depth of erosion is equal to the difference in height perpendicular to the slope surface between the two particles as shown in Figure 3-9. The rate of erosion for different values of α_0, $\dot{E}_i$, can be calculated from the depth of erosion over t_i as shown in Equation [3-7].

$$\dot{L}_t = \frac{\alpha_{0i}}{t_i} \qquad [3\text{-}7]$$

It is assumed in Equation [3-7] that once the particle moves over to the top of the non-moving particle, in front of it, it is considered as part of debris. When shear force exerted on the particles is greater than the friction on the particles, the entrainment mode changes from rolling motion to sliding motion. The frictional force F in Figure 3-1 will change to the opposite direction. The entrainment time t_i, in Equation [3-7], is the summation of the time required for the rolling motion and sliding motion. The time needed for particles with different α_{0i} to be eroded are plotted in Figure 3-5. It is shown that if α_0 approaches zero, the time needed for entrainment is infinite. Conversely, when α_0 is equal to $(\pi/2-\theta)$, t_i approaches zero.

Since α_0 varies from one location to another microscopically and it is not practical to determine α_0 for a channel bed, a PDF for α_0 is used to calculate the entrainment rate. It is assumed that α_0 varies from zero to $(90-\theta)$ degrees according to a probability density function of α_0. The entrainment rate is given by:

$$\dot{L} = \sum_{i=1}^{n} \dot{L}_t \qquad [3\text{-}8]$$

It means that once the entrainment rate corresponding to a certain α_0, calculated from Equations. [3-7] and [A-9], is known and mean value and standard deviation in PDF are given, the entrainment rate of loose packed particles can be estimated based on the shear stress applied. Selecting a proper parameters in the PDF is important in the entrainment calculation. Functional parameters such as the mean value of the normal distribution PDF can be measured for a specific site (Fenton et al. 1977), but it can only apply to that site. These parameters can also be estimated

based on the relationship between void ratio and internal friction angle, and the relationship between particle protrusion and void ratio (Okada et al. 2007; Shimobe et al. 1997).

The distribution of the entrainment rate for different α_0 is plotted in Figure 3-10. It is shown that the entrainment rate calculated from the normal distribution function is greatly affected by the type of probability density function. Besides, it is obvious that integration of the entrainment rate calculated using the average distribution function is much larger than that using the normal distribution function.

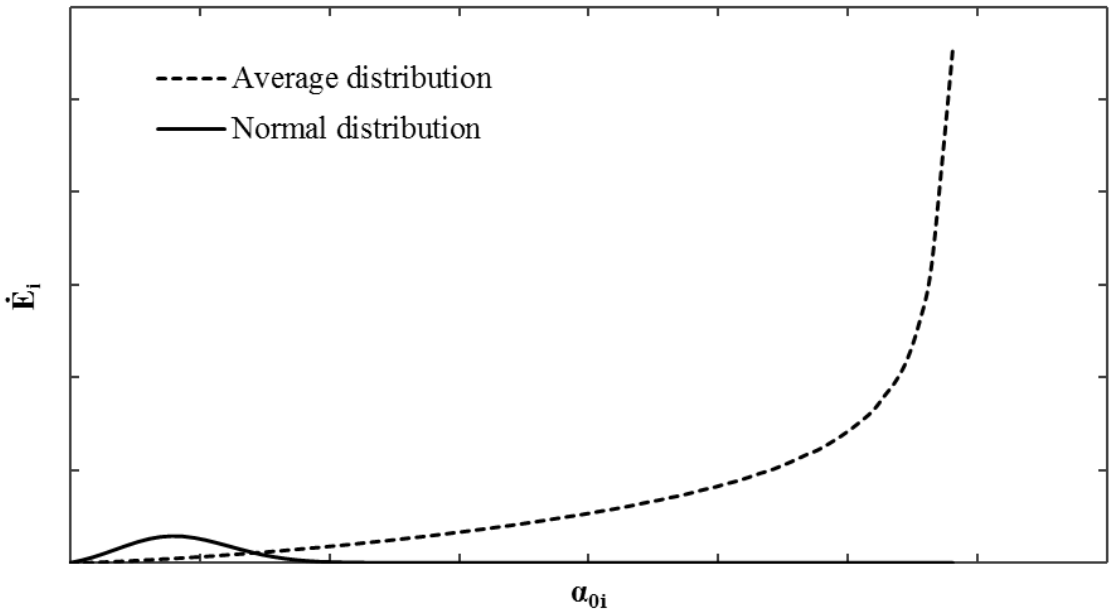

Figure 3-10: Comparison of the distribution of entrainment rate calculated based on normal distribution and average distribution PDF

3.4.4. Mean value of α_0

The value of α_0 cannot be easy measured in the field. However it is shown that α_0 can be related to a pivoting angle, θ_p, see Figure 3-11. From the geometrical relationship, it is found that α_0 is equal to $(\pi/2-\theta_p)$. Li and Komar (1986) measured the pivoting angle using a board which served

as the inclined slope, hinged at one end with a pulley system, so that movement was smooth and could then be held in position once the pebble rotation took place. From the geometry of the apparatus, the grain pivoting angle is equal to the slope of the inclined board at the instant of first movement (Figure 3-11b).

Figure 3-11: Schematic graph of pivoting angle. (a) shows the relationship between pivoting angle and α_0 when particles are lying on a plane; (b) indicates the configuration of particles before inception motion

Figure 3-12 shows the results of the pivoting angles for uniform-size spherical particles measured by Li and Komar (1986) using the system discussed above. The relationship between the pivoting angle and the diameter of particles in the bed is fitted using the empirical relationship suggested by Bridge and Bennett (1992). The experimental results indicate that the pivoting angle decreases with increase of the diameter of the spherical particles. This relationship may be used to select an appropriate pivoting angle when frictional properties of the particles in the channel bed are not available.

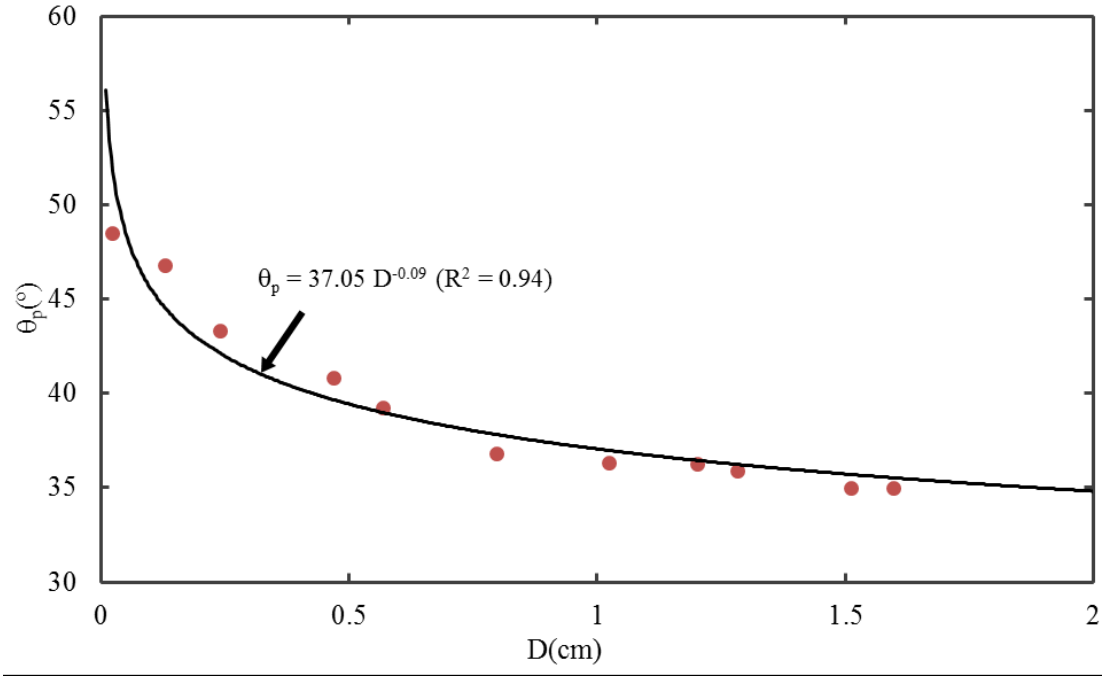

Figure 3-12: Pivoting angle for uniform spherical particles obtained from experiments (Li and Komar, 1986)

Since the pivoting angel is associated with the angle of repose which reflects the frictional properties of particles in the channel bed, theoretical values of θ_p can be estimated from the angle of repose of the material in the channel bed. Therefore, mean value of α_0 in the PDF can be obtained from the relationship in Figure 3-11a.

3.4.5. Determination of α_{0min} and t

Normally for debris flow in the field, the shear stress applied on the channel bed changes with time. Therefore the shear force should vary in the calculation. The shear stress can be calculated using a constitutive model, the selection of which is based on the flow type, solid concentration, particle size etc. For more details, please see Wang et al. (2010). Once the shear force is known at a certain time t, it is possible to determine the minimum angle of α_0, α_{0min}, at which the particles begin to be eroded (Figure 3-15).

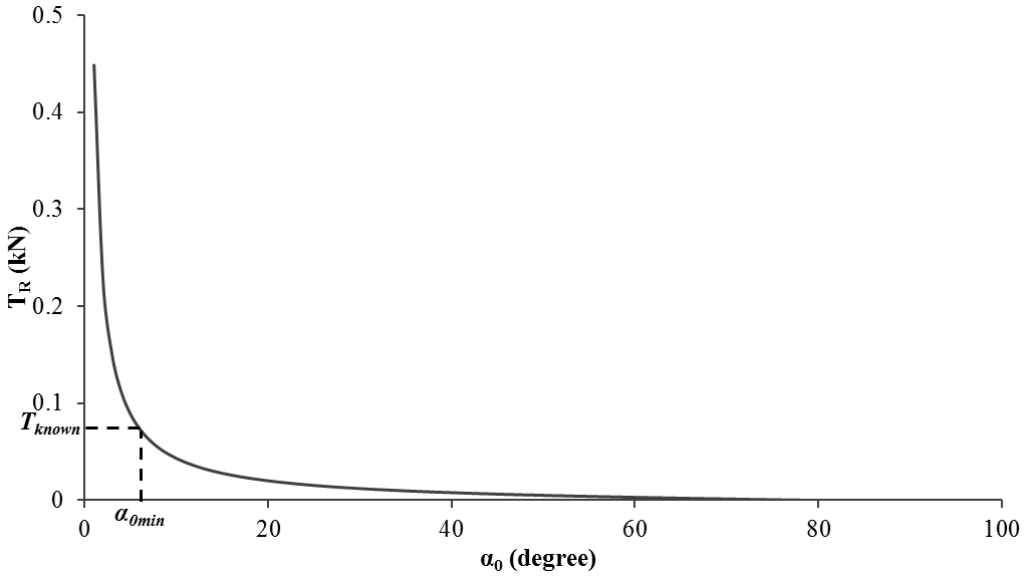

Figure 3-13: Plot of drag force T_R against α_0 from which α_{0min} can be found

For α_{0i} in Figure 3-16, if the drag force is equal to T_1 or T_2, t is equal to t_1 and t_2 respectively, but if T_i is lower than T_2 such as T_3 , the entrainment time will be infinite. This is because the force applied on the particles cannot satisfy the requirement of t for the movement.

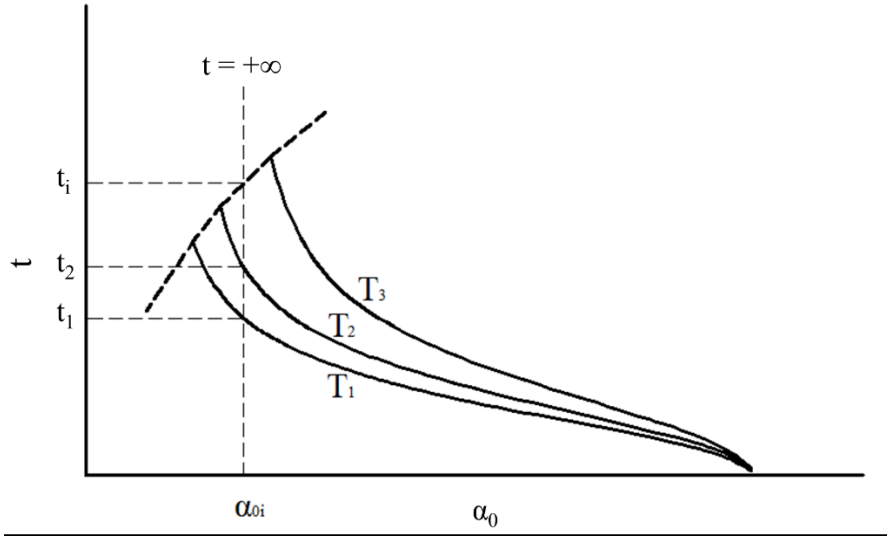

Figure 3-14: Schematic graph of the distribution of entrainment time against α_0

Once t for different T_R is determined, the entrainment rate for different α_0 can be obtained using the new entrainment model. The summation of the entrainment rate for different T_R is equal to the total entrainment rate. The relationship between the entrainment rate and the drag force can be used to estimate the entrainment rate of debris flow with varied basal drag forces.

3.5. Variation of drag force and rotational velocity

3.5.1. Variation of drag force

A sensitivity analysis of each term in the model is carried out by varying each parameter in the model. T_R is the force needed for a single particle to roll. The parameters used for testing the variation of T_R and R are listed in Table 3-2. Parameters are kept constant except the one used for the variation test.

Table 3-2: Initial parameters used to test the variation of drag force for different α_0, θ and R in the new entrainment model

Parameters	ρ(kg/m^3)	R(m)	θ(°)	α_0(°)
Value	2600	0.01	0	1

In order to clarify the variation of drag force with respect to α_0, θ and R in the model, using the parameters listed in Table 3-2, the required drag force to initiate entrainment for different slope angles, particle sizes and α are determined. Figure 3-15 and Figure 3-18 show that the normalized required drag force to mobilize the particle decreases rapidly with increase of normalized α_0 and normalized slope angle.

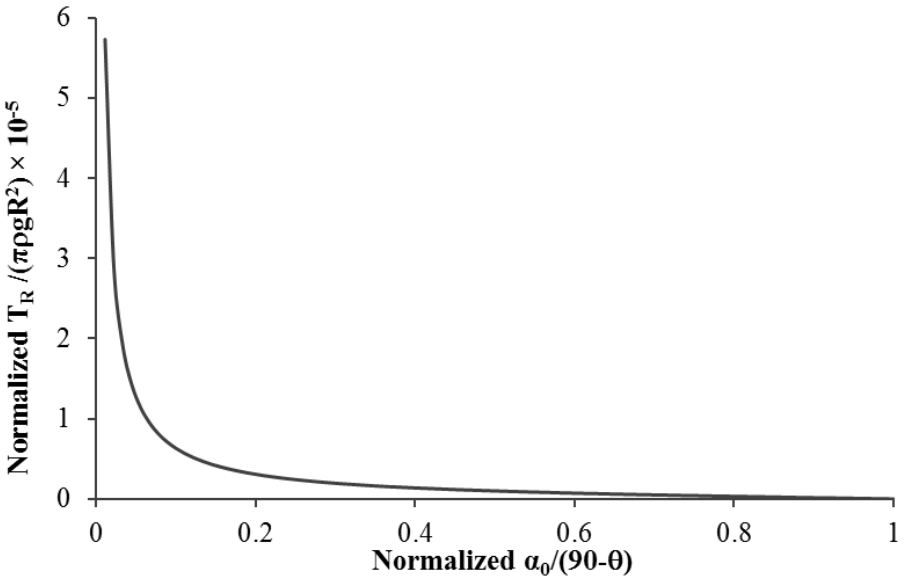

Figure 3-15: Variation of normalized T_R for different normalized α_0

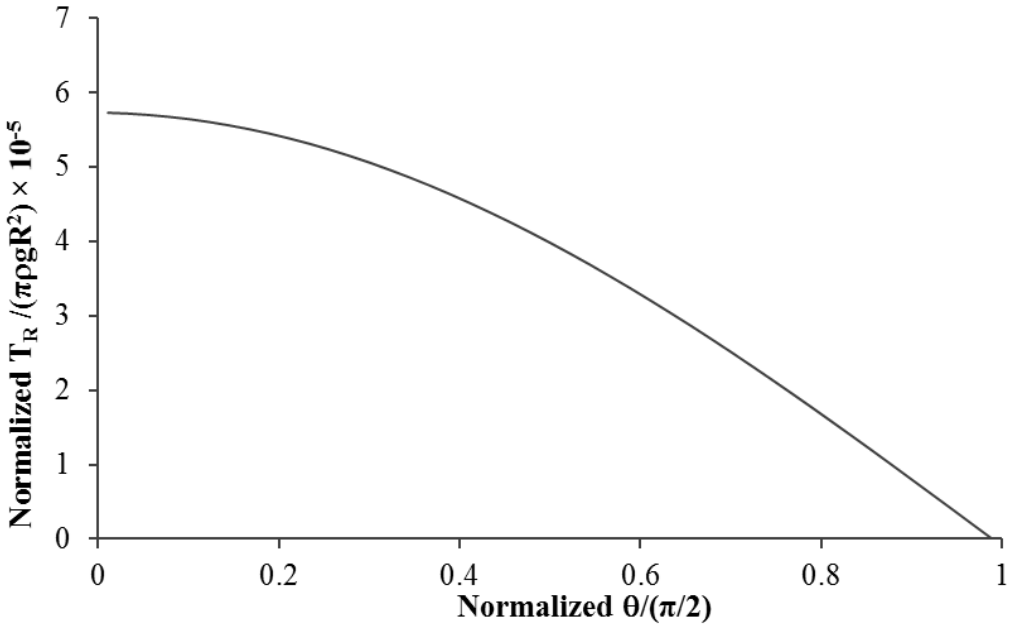

Figure 3-16: Variation of normalized T_R for different normalized slope angle (θ)

However with an increase in the particle size, the drag force needed for the incipient motion of the particle increases as shown in Figure 3-19. The curve is in concave shape. Since shear stress is calculated in most of the simulation using a constitutive model, the variation of shear stress

with respect to the normalized *R* is also plotted. Shear stress is calculated by dividing the drag force by the maximum projected area of the particle in X-Z plane. Figure 3-20 shows that shear stress is also found to be linearly increasing with the increase of the normalized particle size.

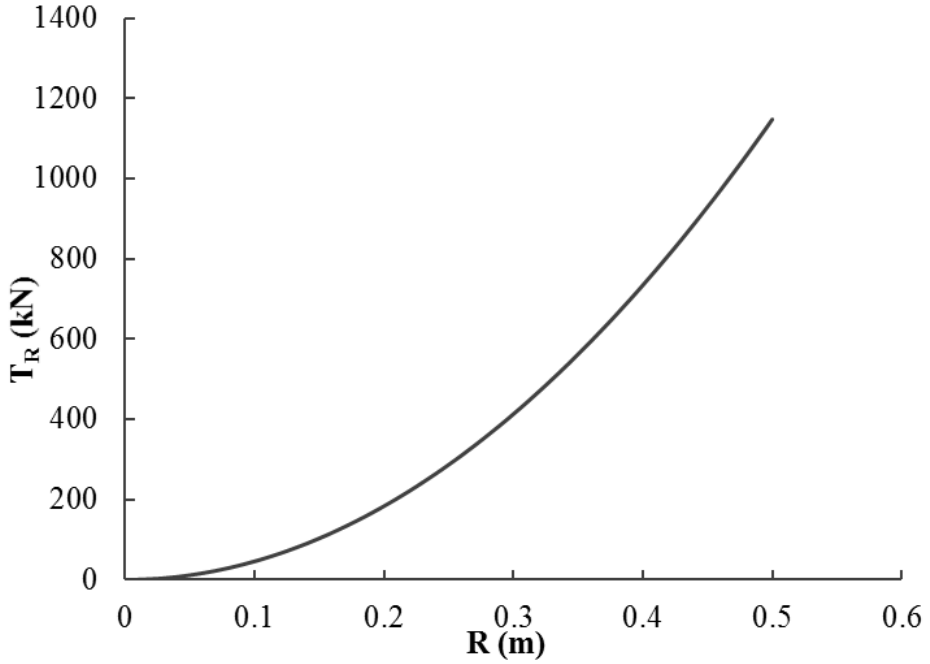

Figure 3-17: Variation of drag force T_R for different particle radius *R*

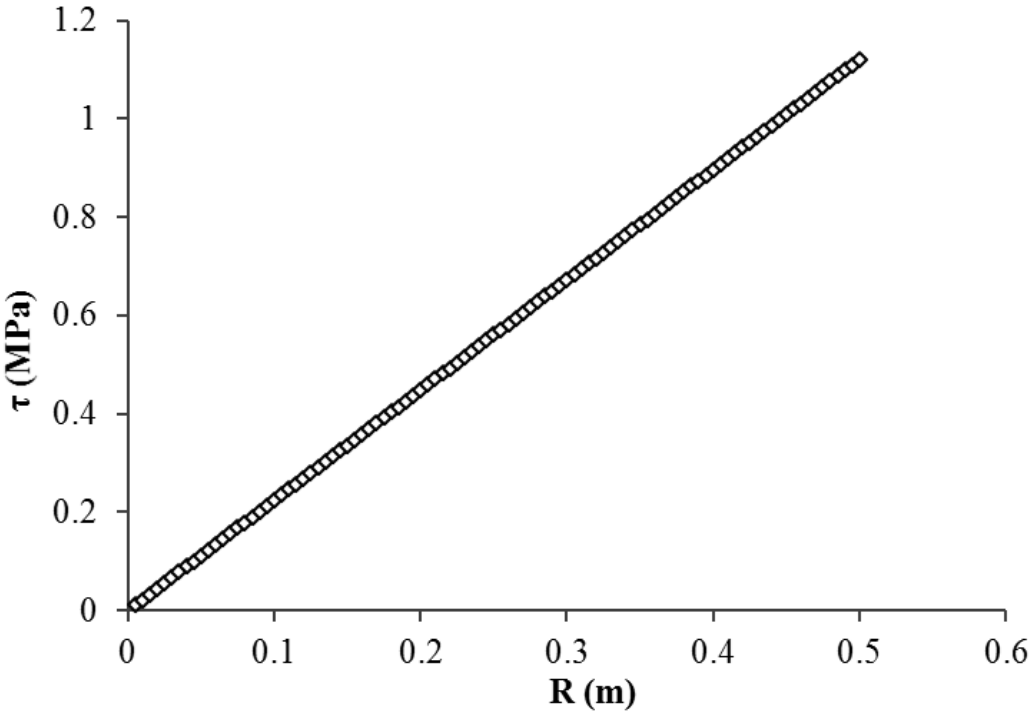

Figure 3-18: Variation of required shear stress for different particle radius R

3.5.2. Variation of change of α_t

To understand the change of α_t with respect to time in the entrainment model, α_t, $d\alpha_t/dt$, and $d^2\alpha_t/dt^2$ against time are plotted. The initial conditions are θ = 0º, T= 4600 N, α_0 = 1° respectively. T= 4600 N is the force required for mobilize the particle with α_0 = 0.1° which is the angle that will be used in testing the effect of α_0 on the rolling motion later. This force can be a smaller value but it must be larger than the minimum required force. Moreover the required force varies according to the radius of the particles, the slope angle and α_0. θ = 0º and α_0 = 1° are assumed as the initial conditions in changing α_t in the simulation.

Figure 3-22a shows the change in the normalized α_t with respect to the normalized time for different α_0. The values of α_0 vary from 0.1º to 89°. For a particle located at a position with α_{t0} = 0.1º, rotation is slow and it almost stays at the original position without rotation after 60% of the

total rotation time has passed. On the contrary, a particle at α_{t0} = 89º completes around 40% of total required rotation in the same normalized time. A particle with larger α_0 starts to accelerate more rapidly at an earlier stage.

Figure 3-22b indicates that particles lying on a steep slope are easier to be mobilized. Figure 3-22c shows the relationship between normalized angle and normalized time under different shear forces. It is apparent that larger drag force could mobilize the particle earlier and cause the particle to rotate more in the same normalized time.

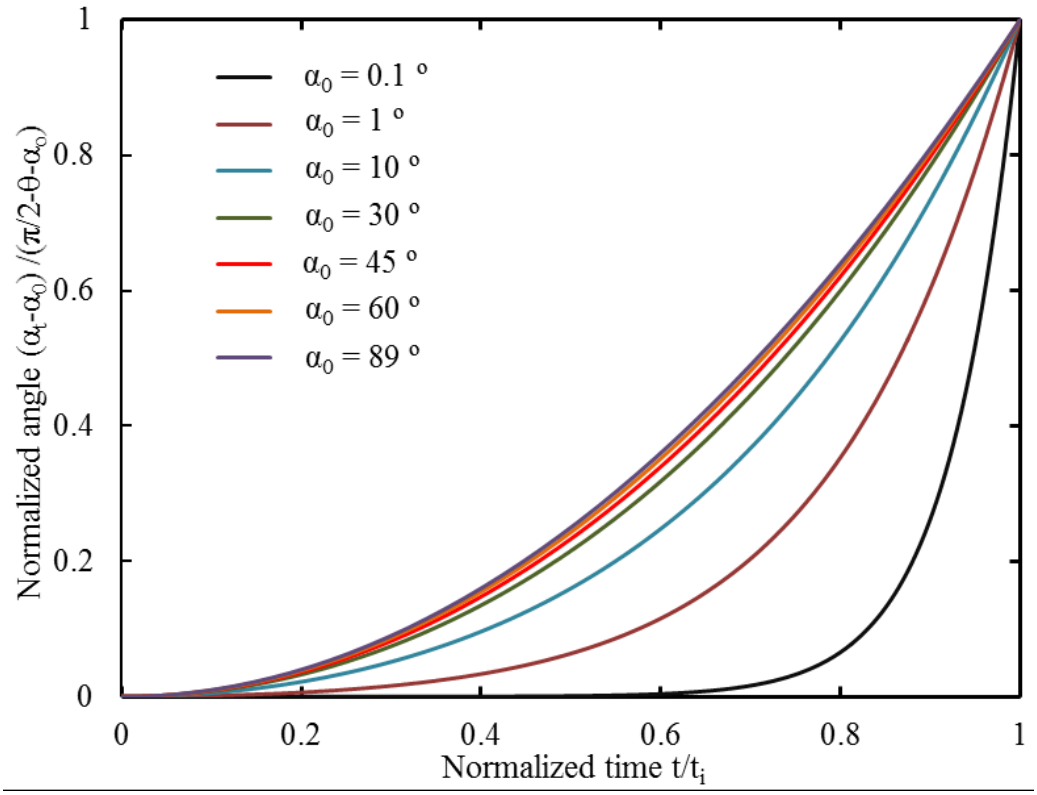

(a)

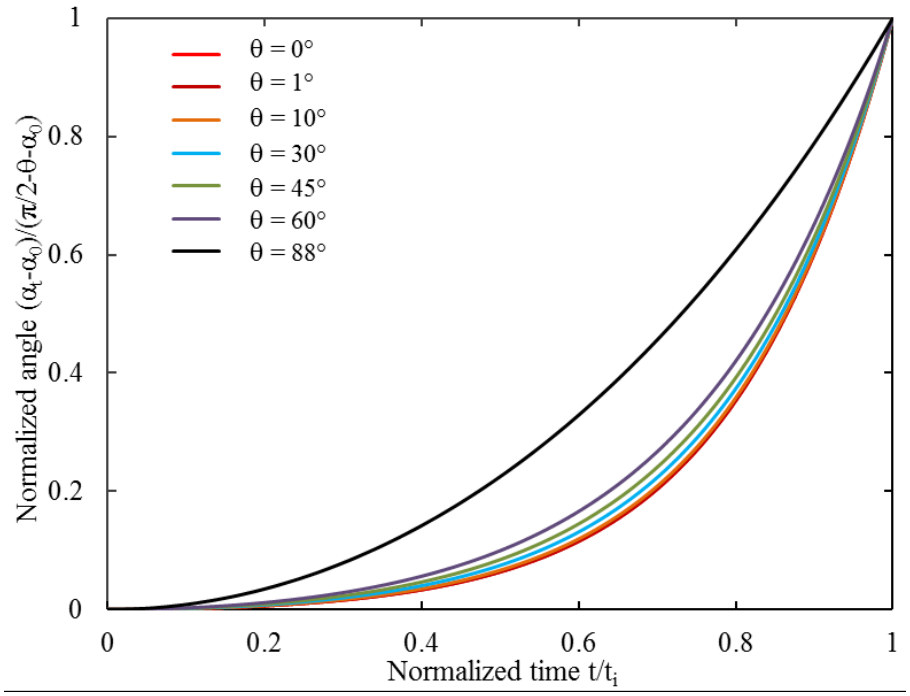

(b)

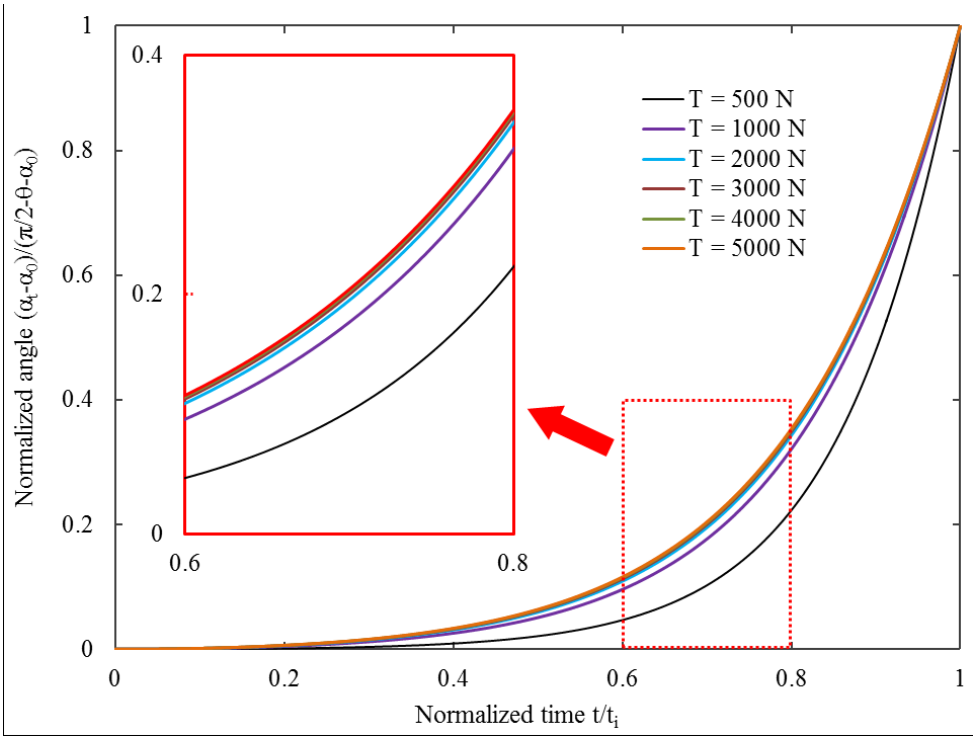

(c)

Figure 3-19: Variation of normalized α_t for different normalized time. (a) T =4600 N and θ = 0º. (b) T =4600 N and α_0 = 1º. (c) α_0 = 1º and θ = 0º.

Figure 3-20 shows the change of angular velocity and angular acceleration during the erosion process. Angular velocities and angular accelerations are normalized based on their maximum value when the particle moves to the top of the adjacent particle.

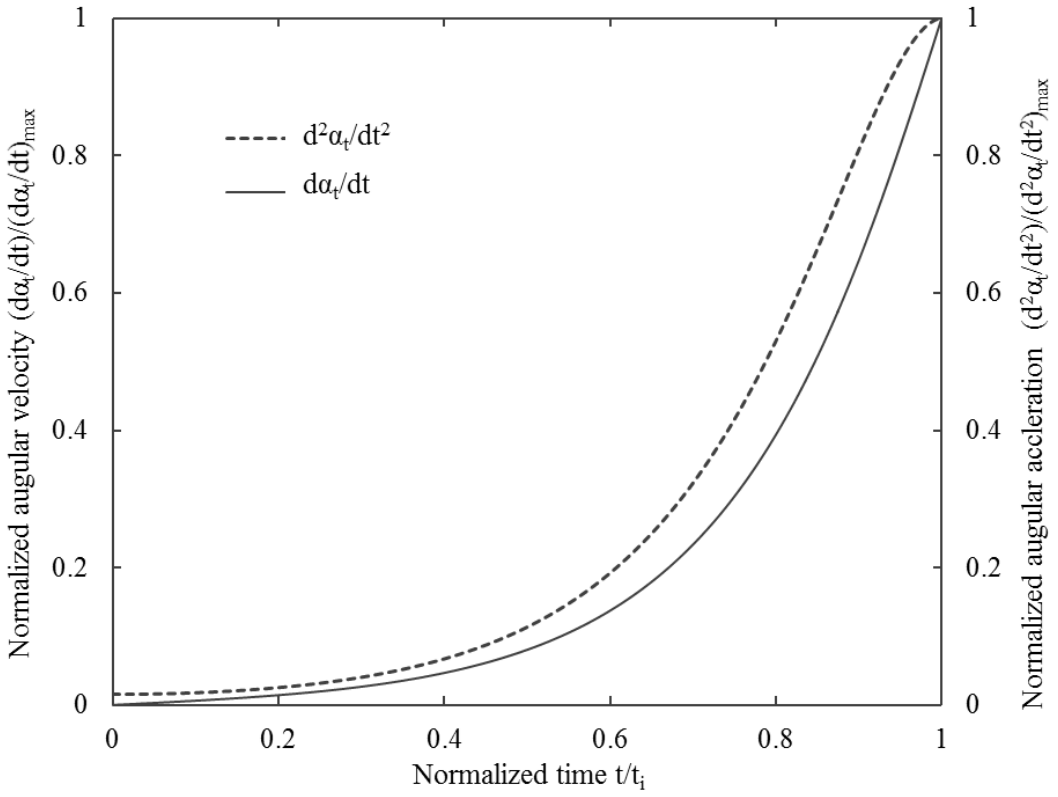

Figure 3-20: Variation of $d\alpha_t/dt$, and $d^2\alpha_t/dt^2$ in the calculation

Translational accelerations of the moving particle are shown in Figure 3-21. In plotting Figure 3-21, it is assumed that the particle is always moved by a rolling motion. Angular accelerations are normalized by the maximum total acceleration. The x-component of the acceleration increases when the total acceleration increases. However, the y-component of the acceleration starts to decrease after reaching its maximum value which is mainly due to the shape of the adjacent particle.

In the calculation, the difference between the friction provided by two adjacent particles and that required for pure "rolling" motion varies. If the difference becomes smaller and the friction between those two particles is less than what is required for a "pure" rolling motion at a given time, sliding will occur. Therefore, the calculations for $d\alpha_t/dt$, and $d^2\alpha_t/dt^2$ are only for "pure" rolling motion.

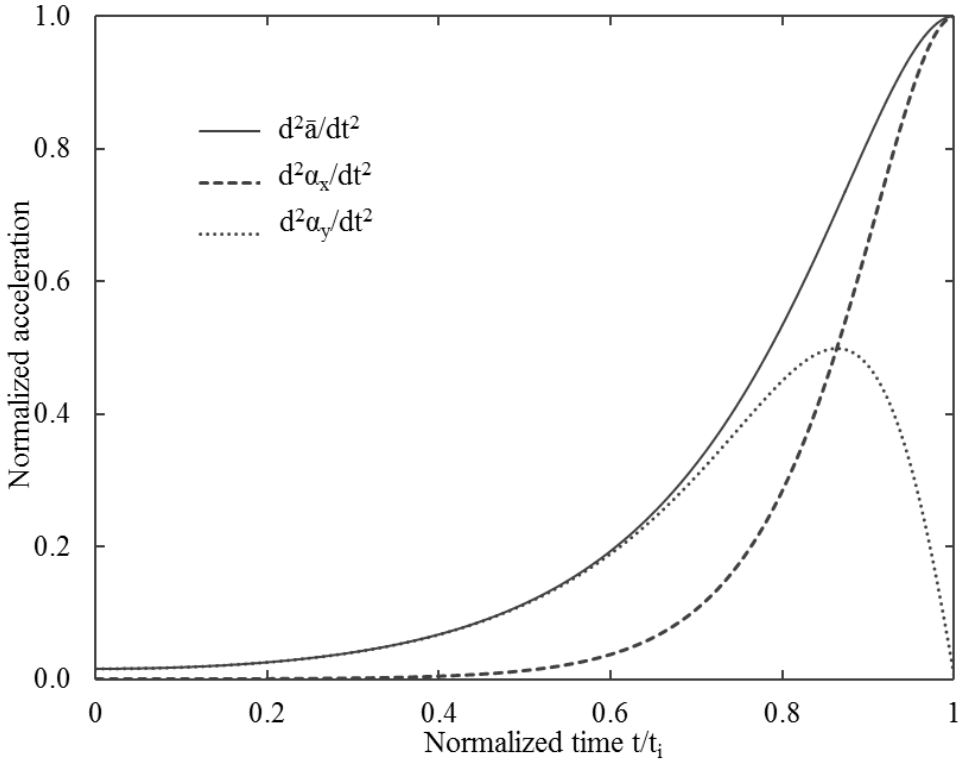

Figure 3-21: Normalized total X and Y translational acceleration and normalized time

3.5.3. Variation of PDF of α_0

Since the relative location between two adjacent particles is very difficult to determine, a PDF of α_0 is introduced to take into account the effect of particle configurations on the calculation of the rate of entrainment. In the normal distribution PDF, if α_0 is uniform, the parameter controlling the shape of the normal distribution PDF is the standard deviation σ. As σ and the mean value μ

of α_0 affect the shape of the normal distribution (Figure 3-22), selecting appropriate values for σ and μ is important.

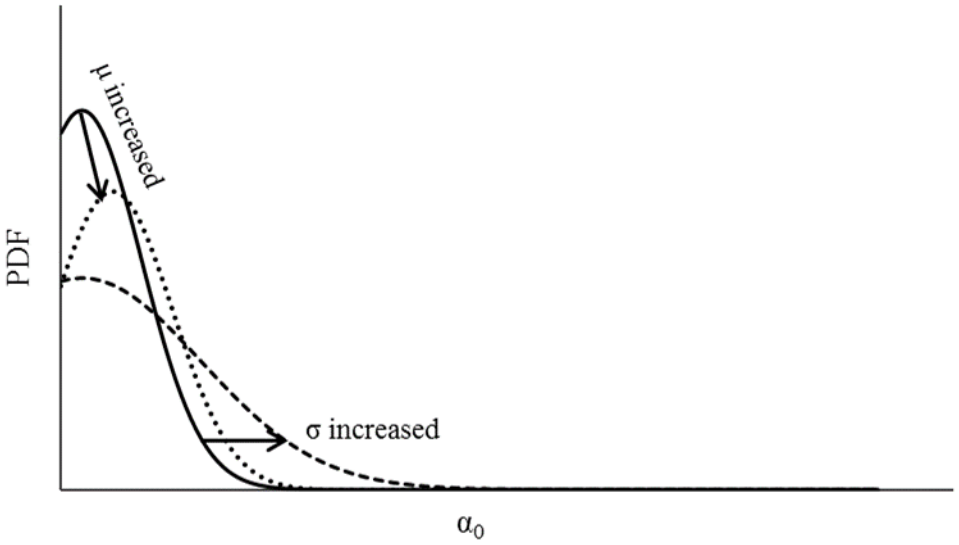

Figure 3-22: Effect of σ and μ on the normal distribution PDF

3.6. Model evaluation

In the entrainment model verification, an ideal situation is expected in which the channel width is constant and particle is known. Therefore, results from debris flume tests conducted by Iverson (2011) on June 2, 2009 are used. The flume was constructed on a slope 95 m long with a 2m wide concrete channel at an angle of 31° with respect to horizontal (Reid et al., 2011). A sand-gravel-mud (37% sand, 56% gravel, and 7% mud size (silt/clay) grains by dry weight) mixture was used in the test. Most of the gravel size grains in both mixtures were rounded and moderately bladed in form, whereas the sand was mostly sub-angular with different particle sizes and shapes. The static internal friction angle measured from tilt-table test with about 2 kPa confining stress was close to 39° for rough bed (Iverson et al. 2011).

Results from the experiment with relatively dry (volumetric water content = 0.18) bed sediments show that 16 scour sensors located within a drier bed sediment remained undisturbed as the debris flow overrode them. Only 1-2 cm of the uppermost bed sediment had been eroded according to the post-flow excavation (Reid et al. 2011). The time for the man-made debris flow to cross the erodible sediment bed was around *6s*. This means that the mean entrainment rate of this test is about 0.0016 m/s~0.0032 m/s.

Since particle sizes are not uniform in most soils, the median particle diameter d_{50} is often used to correlate with soil properties (Bittelli et al. 1999; Iverson et al. 2010). For simplification, it is assumed that particle sizes of bed sediments are uniform and d_{50} is used in the calculation.

According to the results of sieve analysis conducted by Iverson et al. (2010), the material has a d_{50} = 4mm. The effective size d_{50} is used in the characteristic size in the current calculation. The solid density of the particle is assumed to be 2700 kg/m^3. The parameters used in the simulation are summarized in Table 3-3.

Table 3-3: Parameters used for estimating the relationship between shear stress and entrainment rate

Parameters	Particle size d_{50} (mm)	Particle density (kg/m^3)	θ(°)	α_0(°)
Values	4	2700	31	1

Based on the parameters in Table 3-3, the required drag force for the inception of motion of a particle is 17 N which is the maximum required force to mobilize the particles with $\alpha_0 \geq 1°$. Therefore, $\alpha_0 = 1°$ and $T = 17N$, are used in this 2D entrainment calculation which will also give a complete response curve of entrainment rate for different values of α_0 starting from $1°$ in the parametric study.

The time needed for particles to be eroded is calculated using Equation [A-9] in Appendix A. Figure 3-23 shows that $\dot{E}_{max}$ from the normal distribution finally reaches a constant value, 0.0087m/s, equal to the entrainment rate calculated based on the average distribution PDF.

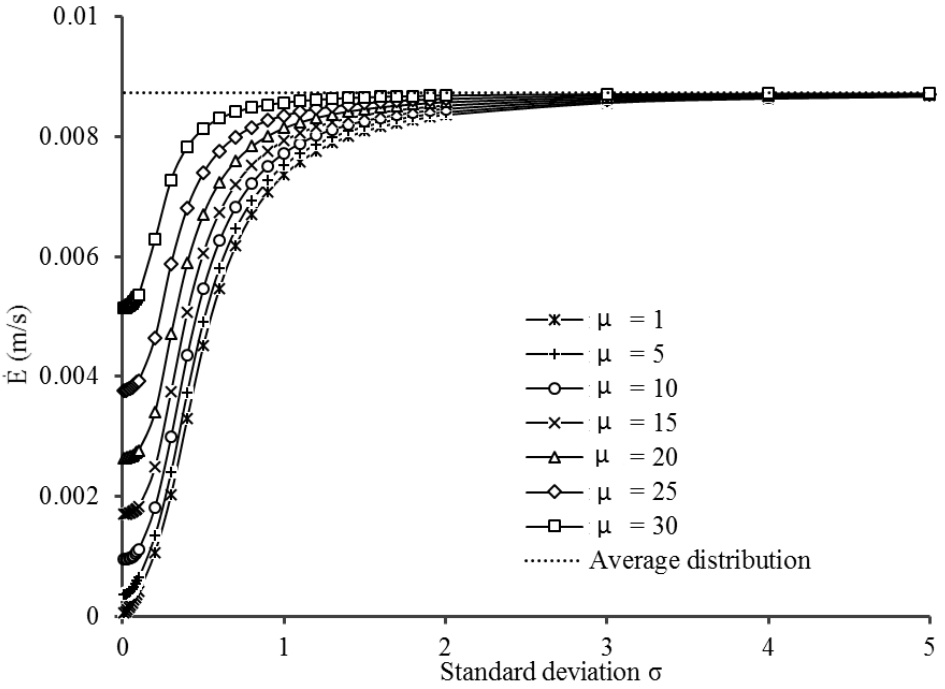

Figure 3-23: Back-analysis of flume experiments conducted by USGS

The time for a particle located at different positions to rotate to the top of the adjacent particle is different. Figure 3-24 indicates the change of t_i of for the particles with different α_0 under different shear forces. When larger force is applied on the particle, less time is consumed for a particle with larger α_0 to rotate from initial position to the point at which it becomes a part of debris. The distribution of t_i agrees with the analyzed results in Figure 3-14.

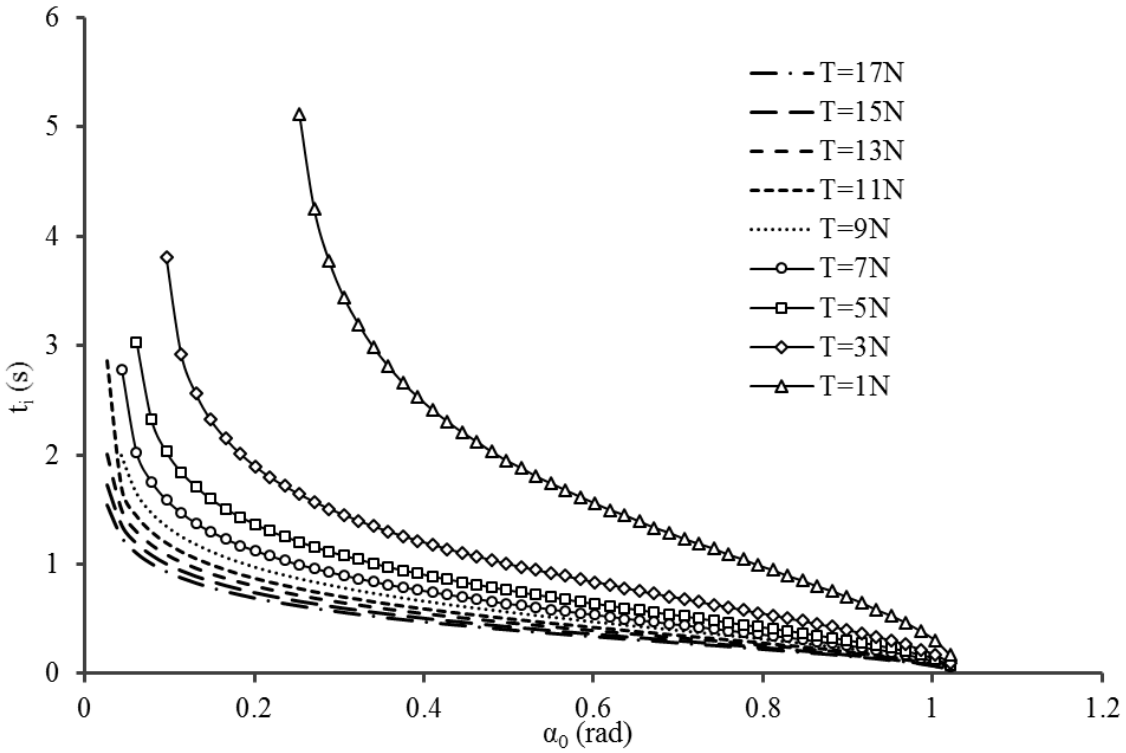

Figure 3-24: Calculation results of t_i for different drag forces

From these results, it is seen that particles with smaller α_0 need more time to be eroded which means the rate of erosion is lower. However, the entrainment rate is also dependent on the probability for particles located at different position.

Figure 3-25 shows the distribution of the modified entrainment rate, $\dot{E}_i P_i$, with the variation of α_0. Based on the relationship between the diameter of particle and the pivoting angle as shown in Figure 3-12, it is seen that α_0 should be around 48º. It is noted that material lying on the channel bed in the flume experiments would not be compacted to the same extent as in the experiments in measuring the pivoting angle. Therefore, α_o estimated from the pivoting angle experiment is an upper bound value. According to the calibration results, an average value of α_0 for the normal distribution PDF is found to be 25º. The standard deviation of α_0 is 0.1. Therefore, the drag force, T, is the only variable in calculating the distribution of $\dot{E}_i P_i$. Figure 3-25 shows that under higher

drag forces, higher entrainment rate is expected. However after the entrainment rate reaches the maximum value, it starts to decrease instead of continuing to increase since fewer particles are found in this range based on the normal distribution PDF.

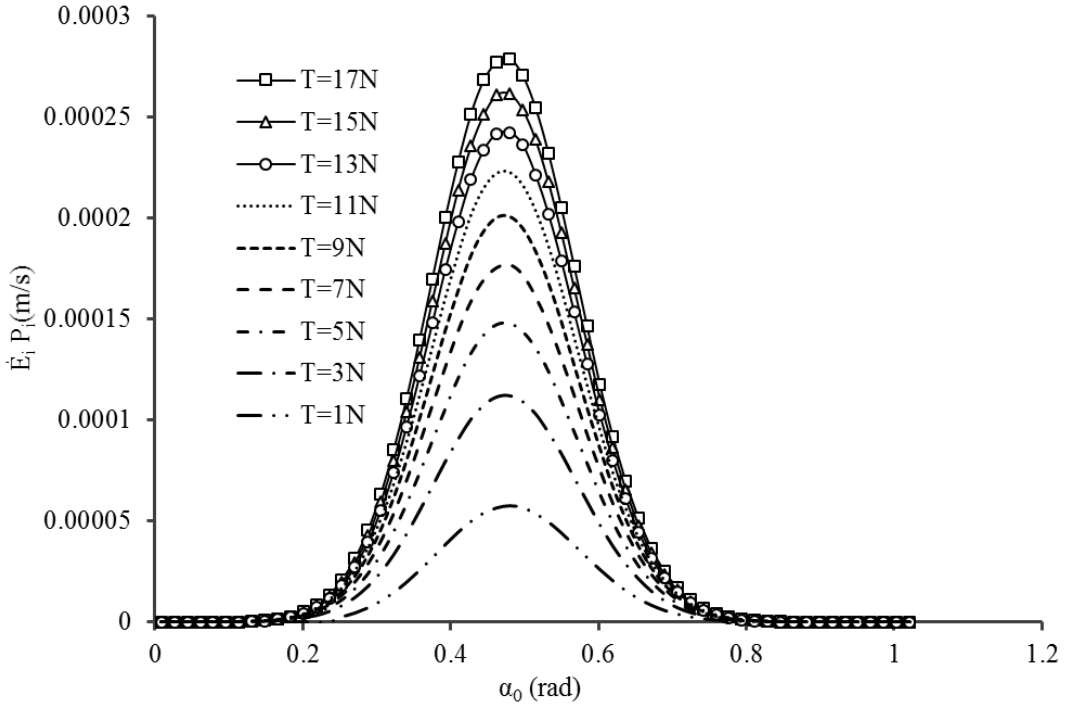

Figure 3-25: Normal distribution of E_i with varying drag force

By calculating the area under the curves in Figure 3-25 , the entrainment rates corresponding to each drag force are obtained. To relate the entrainment rate to the basal shear stress, drag force is converted to shear stress by dividing the force by the area of the particle projected to the channel slope. Figure 3-26 shows that increase in shear stress could cause more particle to be eroded. The estimated maximum entrainment rate corresponding with maximum shear stress is also plotted in Figure 3-26. The maximum shear stress is calculated using Coulomb friction model according to the internal friction angle, 39°, and observed normal stress at x= 32m, 5.04 kPa, from Iverson et al. (2010). Pore water pressure is neglected since bed sediment is relatively dry. The results show that the observed entrainment, 0.0032 m/s, is very close to the calculated value, 0.0038 m/s based

on the current model. The relationship in Figure 3-26 can be only be used to estimate the entrainment rate of the flume experiment with the same flume properties since the entrainment rate is dependent on the slope angle, particle size etc.

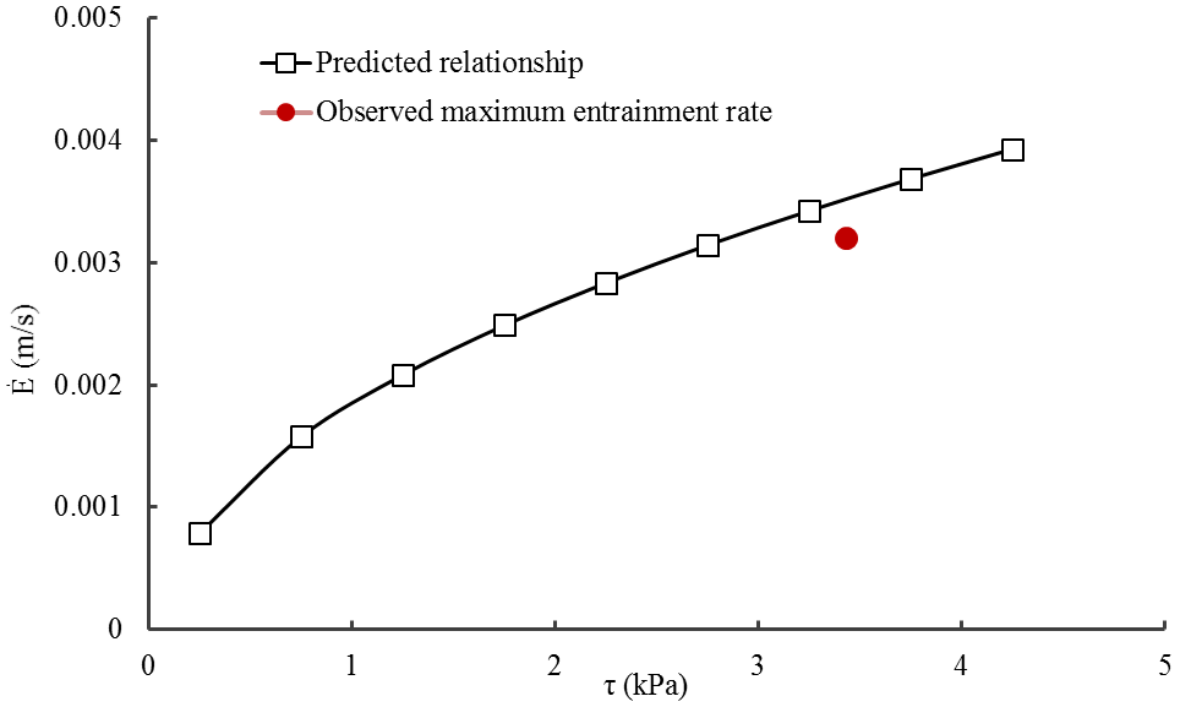

Figure 3-26: The relationship between the entrainment rate and shear stress obtained based on configurations of flume experiment (Iverson et al. 2010)

3.7. Conclusion

A new entrainment model has been proposed that takes into consideration both rolling and sliding motion rather than simply considering shear failure in existing analyses. In this new model, the rate of erosion which is equal to the available depth of erosion divided by the erosion time, is dependent on the particle size, soil density, slope angle, driving force and probable locations of two adjacent particles which is estimated from the pivoting angle. A PDF for the α_0 is used to take into account the variability and distribution of particles spatially. The variation of

drag force and rotational velocity as well as the change of the normalized angle for different slope angle and α_0 with respect to the normalized time are studied. The results show that the particle rotates slower during the first half of rotation than the second half.

The new model is calibrated using flume experiment. In the calibration, it is assumed that the friction between two adjacent particles satisfies the requirement for "pure" rolling motion. A relationship between shear stress and entrainment rate is obtained using the new model. The results are compared with the maximum entrainment rate observed. The results indicate that the new model can calculate a reasonable entrainment rate for flume experiment. If the friction cannot satisfy the requirements for "pure" rolling motion, both rolling motion and shear failure should be considered.

Study results of the variation of parameters indicate that the variation is reasonable according to the analysis of physical process. Back analysis of the results from the flume laboratory demonstrates that the new model has the ability to calculate the entrainment rate of granular flow.

Acknowledge: This study is sponsored by the Natural Science and Engineering of Canada Discovery grant.

Reference

Berti, M., Genevois, R., Simoni, A., and Tecca, P. R. (1999). Field observations of a debris flow event in the Dolomites, Geomorphology, 29(3-4), 265-74.

Bittelli, M., Campbell, G. S., and Flury, M. (1999). Characterization of particle-size distribution in soils with a fragmentation model. Soil Science Society of America Journal, 63(4), 782-788.

Bouchut, F., Ionescu, I. R., and Mangeney, A. (2016). An analytic approach for the evolution of the static-flowing interface in viscoplastic granular flows.

Breien, H., De Blasio, F. V., Elverhøi, A., and Høeg, K. (2008). Erosion and morphology of a debris flow caused by a glacial lake outburst flood, Western Norway, Landslides, 5(3), 271-80.

Bridge, J. S., and Bennett, S. J. (1992). A model for the entrainment and tranport of sediment grains of mixed sizes, shapes and densites, Water Resources Research, 28(2), 337-63.

Cundall, P. A., and Strack, O. D. L. (1979). A discrete numerical model for granular assemblies, Géotechnique, 29(1), 47-65.

De Blasio, F. V., Breien, H., and Elverhoi, A. (2011). Modelling a cohesive-frictional debris flow: an experimental, theoretical, and field-based study, Earth Surface Processes and Landforms, 36(6), 753-66.

Egashira, S., Honda, N., and Itoh, T. (2001). Experimental study on the entrainment of bed material into debris flow, Physics and Chemistry of the Earth, Part C: Solar, Terrestrial & Planetary Science, 26(9), 645-50.

Fannin, R.J., Busslinger, M., and Jordan, P. (2012). Debris flow travel distance: Field traverse data and regional guidelines for terrain stability assessment, Proceeding of the 11th International and 2nd North American Symposium on Landslides, Editors: Erik Eberhardt, Corey Froese, A. Keith Turner and Serge Leroueil, Banff Canada, June 3-8, 2012, Balkema, Taylor and Francis Group, London, 1: 751-756.

Farin, M., Mangeney, A., and Roche, O. (2014). Fundamental changes of granular flow dynamics, deposition, and erosion processes at high slope angles: Insights from laboratory experiments. Journal of Geophysical Research: Earth Surface, 119(3), 504-532.

Fenton, J. D., and Abbott, J. E. (1977). Initial Movement of Grains on a Stream Bed: The Effect of Relative Protrusion, Proceedings of the Royal Society of London Series a-Mathematical Physical and Engineering Sciences, 352(1671), 523-537.

Fraccarollo, L., and Capart, H. (2002). Riemann wave description of erosional dam-break flows, Journal of Fluid Mechanics, 461, 183-228.

Hungr, O. (1995). A model for the runout analysis of rapid flow slides, debris flows and avalanches, Canadian Geotechnical Journal, 32(4), 610-23.

Hungr, O., Evans, S. G., Bovis, M. J., and Hutchinson, J. N. (2001). A review of the classification of landslides of the flow type, Environmental & Engineering Geoscience, 7(3), 221-38.

Hungr, D., and Evans, S. G. (2004). Entrainment of debris in rock avalanches: An analysis of a long run-out mechanism, Geological Society of America Bulletin, 116, 1240-1252.

Ionescu, I. R., Mangeney, A., Bouchut, F., and Roche, O. (2015). Viscoplastic modeling of granular column collapse with pressure-dependent rheology. Journal of Non-Newtonian Fluid Mechanics, 219, 1-18.

Iverson, R. M., and Denlinger, R.P. (2001). Flow of variably fluidized granular masses across three-dimensional terrain 1. Coulomb mixture theory, Journal of Geophysical Research, 106, 537-552.

Iverson, R.M., Logan, M., and Denlinger, R. P. (2004). Granular avalanches across irregular three-dimensional terrain: 2. Experimental tests, Journal of Geophysical Research, 109, F01015, doi:10.1029/2003JF000084.

Iverson, R. M., Logan, M., LaHusen, R. G., and Berti, M. (2010). The perfect debris flow? Aggregated results from 28 large-scale experiments. Journal of Geophysical Research: Earth Surface (2003–2012), 115(F3).

Iverson, R. M., Reid, M. E., Logan,M., LaHusen, R. G., Godt, J. W., and Griswold, J. P. (2011). Positive feedback and momentum growth during debris-flow entrainment of wet bed sediment, Nature Geoscience, 4(2), 116-121.

Iverson, R.M. (2012). Elementary theory of bed-sediment entrainment by debris flows and avalanches, Journal of Geophysical Research, 117, F03006, doi:10.1029/2011JF002189.

Iverson, R. M., and Ouyang C.J. (2015). Entrainment of bed material by Earth-surface mass flows: Review and reformulation of depth-integrated theory. Reviews of Geophysics, 53, doi:10.1002/2013RG000447.

Li Z. L., and Komar, P. D. (1986). Laboratory measurements of pivoting angles for applications to selective entrainment of gravel in a current, Sedimentology, 33(3), 413-23.

Lo, K. H., and Chau, K. T. (2003). Debris-flow simulations for Tsingshan in Hong kong, Proceedings of the Third International Debris-Flow Hazards Mitigation: Mechanics, Prediction, and Assessment (DFHM) Conference, Editors: Rickenmann, D., and Chen, C.L., Savos, Switzerland, September 10-12, 2003, Millpress, Rotterdam, 577-588.

Luna, B. Q., Remaitre, A., van Asch, T. W. J., Malet, J. P., and van Westen, C. J. (2012). Analysis of debris flow behavior with a one dimensional run-out model incorporating entrainment, Engineering Geology, 128, 63-75.

Mangeney, A., Roche, O., Hungr, O., Mangold, N., Faccanoni, G., and Lucas, A. (2010). Erosion and mobility in granular collapse over sloping beds, Journal of Geophysical Research, 115, F03040, doi:10.1029/2009JF001462.

McCoy, S. W., Kean, J. W., Coe, J. A., Tucker, G. E., Staley, D. M., and Wasklewicz, T. A. (2012). Sediment entrainment by debris flows: In situ measurements from the headwaters of a steep catchment, Journal of Geophysical Research, 117, F03016, doi:10.1002/jgrf.20041.

McDougall, S., and Hungr, O. (2005). Dynamic modelling of entrainment in rapid landslides, Canadian Geotechnical Journal, 42(5), 1437-1448.

Medina, V., Bateman, A., and Hurlimann, M. (2008a). A 2D finite volume model for bebris flow and its application to events occurred in the Eastern Pyrenees, International Journal of Sediment Research, 23(4), 348-360.

Medina, V., Hürlimann, M., and Bateman, A. (2008b). Application of FLATModel, a 2D finite volume code, to debris flows in the northeastern part of the Iberian Peninsula, Landslides, 5(1), 127-142.

Moffat, R., Fannin, R.J., and Garner, S. J. (2011). Spatial and temporal progression of internal erosion in cohesionless soil, Canadian Geotechnical Journal, 48(3), 399-412.

Okada, Y., and Ochiai, H. (2007). Coupling pore-water pressure with distinct element method and steady state strengths in numerical triaxial compression tests under undrained conditions, Landslides, 4(4), 357-369.

Papa, M., Egashira, S., and Itoh, T. (2004). Critical conditions of bed sediment entrainment due to debris flow, Natural Hazards and Earth System Sciences, 4(3), 469-474.

Reid, M. E., Iverson, R. M., Logan, M, LaHusen, R. G., Godt, J. W., and Griswold, J. P. (2011). Entrainment of bed sediment by debris flows: Results from large-scale experiments, Debris-flow Hazards Mitigation, Mechanics, Prediction, and Assessment, 367-374.

Remaître, A., Malet, J. P., and Maquaire, O. (2009). Sediment budget and morphology of the 2003 Faucon debris flow (South French Alps): scouring and channel-shaping processes. Proceedings of the International Conference 'Landslide Processes': from geomorphological mapping to dynamic modelling, Editors: Malet, J.P., Remaître, A., and Bogaard, T., Strasbourg, France, February, 6-7, 2009, CERG Editions, Strasbourg, 75-80.

Schurch, P., Densmore, A. L., Rosser, N. J., and McArdell, B. W. (2011). Dynamic controls on erosion and deposition on debris-flow fans, Geology, 39 (9), 827-830.

Shimobe, S., and Moroto, N. (1997). A new engineering classification chart for densification of granular soils, Proceedings of the Third International Conference on Ground Improvement Geosystems, Editors: Schlosser, F., and Davies, M. C. R., London, UK, 3-5 June, 1997, Thomas Telford, London, 31-36.

Shodja, H. M., and Nezami, E.G. (2003). A micromechanical study of rolling and sliding contacts in assemblies of oval granules, International journal for numerical and analytical methods in geomechanics, 27(5), 403-424.

Skempton, A.W. (1954). The pore-pressure coefficients A and B, Géotechnique, 4 (4), 143-147.

Sovilla, B., Burlando, P., and Bartelt, P. (2006). Field experiments and numerical modeling of mass entrainment in snow avalanches. Journal of Geophysical Research, 111, F03007, doi:10.1029/2005JF000391.

Valyrakis, M., Diplas, P., and Dancey, C.L. (2013). Entrainment of coarse particles in turbulent flows: An energy approach, Journal of Geophysical Research: Earth Surface, 118(1), 42-53.

Wang, X. B. (2008). Geotechnical analysis of flow slides, debris flows, and related phenomena (Doctoral dissertation). University of Alberta, Edmonton, Canada.

Wang, X. B., Morgenstern, N. R., and Chan, D. H. (2010). A model for geotechnical analysis of flow slides and debris flows, Canadian Geotechnical Journal, 47 (12), 1401-1414.

4. NUMERICAL SIMULATION OF 2D GRANULAR FLOW ENTRAINMENT ON ERODIBLE SURFACE USING DEM

4.1. Abstract

To understand the entrainment process inside the granular flow, numerical experiments have been conducted by building a Discrete Element Method (DEM) model using the commercial program PFC2D. Flow channel, 8 m long and 15 degrees in slope, is setup with monitoring points located at the upper part of the erodible region. Particles, ranging from 3 mm to 4 mm, are placed in the erodible channel and in the tank, located at crest of the slope. In the test, velocities, including translational velocity, rotational velocity and average velocity, total volume, shear stresses are monitored using measurement circles. The sizes of measurement circles have been varied to see its impact on the results. It is found that an appropriate size of measure circles that can include 20 to 30 particles should be used. Results of the numerical experiment are compared with analytical results. Shear stresses at the interface between flowing and immobile particles, change of eroded depth and entrainment rate are used in the verification process. It is found that the monitored shear stresses in PFC model agree well with the shear stresses calculated using Mohr-Coulomb frictional relationship. The calculated depth of erosion using the analytical model is also compared with numerical experiment. Insight gained from the numerical experimental shows that the assumptions made in the new entrainment model are reasonable and it can be used to estimate the entrainment rate in debris flow analysis.

4.2. Introduction

4.2.1. Debris flow entrainment

Many debris flow events have significant amount of entrainment resulting in a substantially larger final volume than its initial volume (Remaître et al. 2009; Xu et al. 2012). This is mainly caused by the incorporation of loose granular material lying on the flow channels during the flow process (Iverson 2012). Entrainment can significantly change the mechanics and characteristics of debris flow thus making prediction and back analysis of debris flow much more difficult (McDougall and Hungr 2004).

4.2.2. Debris flow entrainment model

There are different models in calculating the amount and rate of entrainment in debris flow analysis. Basically, two approaches have been used: the static approach and the dynamic approach. In the static approach, static shear stresses are calculating beneath the channel bed under the debris and failure is considered when the static shear stress exceeds the shear strength of the material. The depth in which failure occurs is determined and the amount of material is calculated which will be added to the main body of the debris. In the dynamic approach, the rate of entrainment is calculated based on the rate of erosion of the material at the channel bed. The rate of erosion is determined based on shear failure at the surface and the material is removed from the surface based on the velocity of flow of the main body of the debris (Medina et al. 2008).

Egashira et al (2001) proposed a formula to calculate erosion rate assuming that the slope of the channel bed is always adjusted to the angle corresponding to limiting equilibrium conditions. The material in the channel left behind by an unsaturated debris will approach the limiting equilibrium slope angle. Geometrical relationship between the initial bed slope and equilibrium

slope angle is incorporated into mass conservation law of eroded material to obtain the entrainment rate.

The entrainment model proposed by van Asch et al. in 2004 (Luna et al. 2012) is a dynamic one dimensional debris flow model that takes into account the entrainment concept based on the generation of excess pore water pressure under undrained loading on in-situ material. Due to the moving mass flowing on top of the erodible bed, a loading on the bed deposits is generated. The model calculates this applied load on the in-situ soil through changes in the vertical normal stress and shear strength caused by the debris flow. The increase in pore water pressure is calculated based on the Skempton (1954) equation. The depth of erosion is approximated using the relationship between the factor of safety at the bottom and top of soil in the channel.

Iverson (2012) considered the behavior of a slide block descending an erodible slope with the ability of incorporating soil on the static bed. Newton's second law was applied on the sliding material. Then, Coulomb friction rule was applied and basal friction resistance calculation was improved by taking the shear rate into account. The friction resistance consists of a constant component of friction resistance and a velocity-dependent component. After considering the rate-dependent friction, entrainment rate based on the change in weight of the sliding block was obtained. Iverson and Ouyang (2015) updated the equation for estimating basal erosion rate. Jump conditions at the interfaces between each layer, which descripts the sudden change of shear stress and horizontal velocity in the debris, were considered in the derivation.

4.2.3. The new entrainment model

In the new entrainment model, it is considered that granular particles lying on channel bed are eroded progressively. Granular particles are abstracted as uniform size sphere (disk in the case of

$2D$ analysis). According to analysis carried out by Wu and Chou (2003), rolling is considered as the dominant motion in the entrainment process. However both rolling and shearing motions should be considered in the calculation of entrainment rate. Particles are mobilized due to shear stress exerting on the particles and will rotate around the point contact with the adjacent particle downstream. Newton's Law of Motion is applied to calculate acceleration, velocity, and displacement of the particle. It is also assumed in the new entrainment model that once the particle moves over another particle, in front of it, it will become part of flowing debris.

4.2.4. Use of PFC2D in debris flow runout simulation

Cundall (1971) introduced a discrete element method to study rock-mechanics problems and then applied to soils by Cundall and Strack (1979). PFC2D model is developed using DEM, which is capable of describing the mechanical behaviours of assembles of particles by calculating the contact forces and displacements of each individual particle in response to its interaction with adjacent particles. Newton's second Law and force-displacement Law are used to calculate the motion of the particles. The assembly of particles continue to move until forces are in equilibrium or the mechanical energy has been completely dissipated by friction and/or system damping.

Banton (2009) simulated channelized granular flows by considering the particle properties and basal surface properties. It was found that rebound coefficient between particles is important in the simulation when the flow is turbulent with a high velocity gradient. Three laboratory experiments, granular materials released from a rough inclined slope, carried out by Savage and Hutter (1991) and Hutter et al. (1995) were simulated. In the simulation, Banton (2009) adopted spherical particles which could enhance the particle rolling and runout distance. The simulation results agreed with that observed very well, therefore it was suggested that DEM technique is able to

simulate the physical process during channelized laboratory experiment of unigranular mass avalanches.

The dynamic response of colluvium accumulation slopes in Sichuan Province of China was studied by He et al. (2010), since epicentre of Wenchuan earthquake occurred in 2008 is located in this region. The accumulations was considered as discontinuity in the simulation. Horizontal shearing waveforms of Wenchuan earthquake were used for the study of dynamic response. It was concluded that material properties and interface in the accumulation affected the velocity a lot.

Li et al (2012) simulated rapid movement and sudden failure of slope triggered by rainfall. Fluidization of the flowslide was simulated. It is indicated that residual friction coefficient is relatively important on the travel distance, height and location of debris flow fan. Also, geometry of slip surface had a great influence on the deformation of sliding mass.

Effect of debris flow on retaining wall and earthfills was tested using PFC2D by Li et al (2010) and Salciarini et al. (2010). A slope with constant inclined angle was constructed and a retaining wall was placed away from the toe of the slope. By varying the size of the retaining wall and particle properties, influence of geometry and particles properties was examined by measuring the impact force exerted on retaining wall.

Though plenty of numerical flume experiments has been conducted, very few of them has taken entrainment into account in numerical flume experiment using PFC2D (Higashitani et al. 2009). This paper aims to creatively analyze the entrainment using PFC2D. A flume with erodible bed is designed. Entrained volume, displacement and front velocity are monitored to test the availability of the new entrainment model.

4.3. Model setup

4.3.1. Idealized model and geometry

To simulate the entrainment process, an idealized model with debris and erodible bed channel was constructed using PFC2D (Figure 4-1). The model is mainly composed of three parts: acceleration section, erosional section and deposition section. The reason of using acceleration part is to provide enough kinetic energy when the particle reaches the particles erosional section. The erosional section, 0.15m in depth, is the key part of this experiment. It is mainly consisted of frictional particles with diameter ranging from 3 mm to 4 mm which is the same as the particles in the tank. Finally, these particles are deposited as deposition zone. Since cohesionless particles are considered here, no bonds, including parallel bond and contact bond, exist between them. Model parameters and material properties are summarized in Table 4-1.

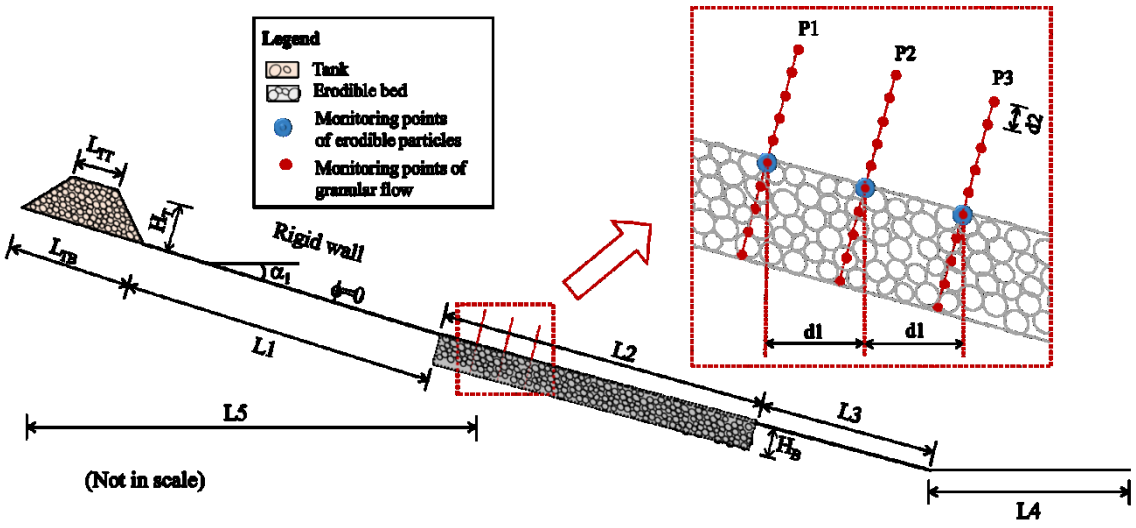

Figure 4-1: Geometrical sketch of the idealized PFC model in the numerical experiment

Table 4-1: Geometrical parameters of the slope and tank

Parameters	Value	Parameters	Value
α_0 (°)	15	d1 (m)	0.2
L1 (m)	3	d2 (m)	0.0375
L2 (m)	2	L_{TT} (m)	0.3
L3 (m)	3	L_{TB} (m)	0.6

Parameters	Value	Parameters	Value
L4 (m)	2	H_T (m)	0.3
L5 (m)	4	H_B (m)	0.15
Particle size (m)	0.003~0.004	Density of particles (kg/m^3)	2600

4.3.2. Introduction on setting up PFC2D model

Based on the idealized model, flume experiments are carried out using PFC2D. Tank filled with particles is put at the top of channel. The depth of erosion is estimated by trial and error, since if erodible bed is too deep, this will significantly increase the computing time at each step and finally increase runtime. And the particles at the bottom of erodible zone do not move and involve into the simulation after the main body of the debris has passed the erodible zone. The horizontal length of erodible channel also needs to be set to an approximate value based on previous estimation.

Before generating the particles, walls used to simulate the rigid bed are generated first. Stiffness including shear stiffness and normal stiffness are larger than that of the particles to prevent particles from crossing the walls. As it is prohibited that walls cannot overlap each other in PFC2D, overlapped wall used for generating erodible bed is deleted before putting the tank on the channel bed. Friction between the tank and the particles is assigned a smaller value. Otherwise, the particles at the bottom of the tank cannot slide into channel. In the simulation, frictionless wall is used for the bottom of the tank.

Particles are modelled as circular disks with unit thickness and filled the region enclosed by the walls. Gravity is applied. After preliminary equilibrium has been reach, walls covering the particles are removed. It is noted that the initial stress caused by compaction during the particle generation process should be released first, otherwise particles will move randomly with high acceleration. Therefore particles need to be stabilized again. There may be some stresses built up at the toe of the slope, they do not significantly affect the simulation process as long as the particles

remain unbounded (Remaître et al. 2008). The main body of the debris and the material in the erodible bed are represented by 5,092 and 6,392 particles, respectively with size ranging from 0.003m to 0.004m. Since it is practically difficult to generate particles as much as in the actual debris flow, this number of particle in this simulation is acceptable.

The model is evaluated by examining the average velocity, total volume, rotational velocity and entrainment rate. Circular particles will roll and consequently a small number of particles will roll ahead and separate from the main body of the debris. In the simulation, if the particles move out of the right of deposition zone. The particles will not be considered as part of debris. The average velocity is defined as the average velocity of all moving particles. Variation of the average velocity means that moving mass encounters the slope having different friction coefficient. To calculate the change in volume, particles with displacement greater than a threshold value that is considered as about twice of mean particle size are assumed to be part of the flowing debris. Then, the volume of debris can be reckoned according to the number of mobilized particles and average porosity of the debris. Rotational velocities of the erodible and flowing particles are monitored using measurement circles in PFC2D.

4.3.3. Parameters setting in the PFC2D model

Using the DEM to simulate granular flow requires the determination of appropriate geometric and rheological parameters between the particles as well as for the basal surface (Banton et al. 2009). The determination of parameters is based on the published papers (Teufelsbauer et al. 2009; Zhou and Ng 2010). Parameters used in the numerical experiment are shown in Table 4-2.

Table 4-2: Parameters setup in modelling (for channel bed and tank)

Items		Microscopic mechanical parameters of PFC model
Particle size	Maximum radius (m)	0.4
	Minimum radius (m)	0.3
	PDF	Uniform distribution
Particle density		2600
Porosity		0.2
Particle normal stiffness (N/m)		1e9
Particle shear stiffness (N/m)		1e9
Contact bond normal and shear strengths		0
Ball-ball friction		0.6
Ball normal stiffness (N/m)		1e10
Ball shear stiffness (N/m)		1e10
dt scale		1e-5
Local damping coefficient		0
Viscous damping coefficient (normal)		0.3
Viscous damping coefficient (shear)		0

In determining the model parameters, interparticle bonding strength are set to be zero since only rolling motion is considered in the model. By default, the friction coefficient at the ball-wall contacts equals the minimum friction coefficient of the ball and the wall. In the model, particles in the main body of the debris and in the erodible bed have the same material properties since they are essentially the same material. To prevent particle from flying away after removing the wall what was used for particle generation, the velocities of the particles are set to zero after each calculation loop in the initial stage.

Local and viscous damping are used to dissipate kinetic energy in order to arrive a steady state solution in a reasonable number of cycles. Local damping is used to apply damping force to each ball or clump (collection of particles) with magnitude proportional to the unbalanced force. Instead, viscous damping is applied at the contact by imposing normal and shear forces at each

contact directly proportional to the relative velocities at the contact. The default values for local and viscous damping ratio are 0.7 and 0, respectively (Itasca, 2002).

In calculating local damping, Newton's Second Law is modified by including the damping force as:

$$F_{(i)} + F^{d}_{(i)} = m_{(i)}\, a_{(i)};\ \text{i} = 1, 2, 3 \qquad [4\text{-}1]$$

where $F_{(i)}$, $m_{(i)}$ and $a_{(i)}$ are the generalized force, mass and acceleration components, respectively; $F_{(i)}$ includes contribution from gravity force; and $F^{d}_{(i)}$ is the damping force which is given by:

$$F^{d}_{(i)} = -\alpha \left| F_{(i)} \right| sign\left(v_{(i)} \right) \qquad [4\text{-}2]$$

where α is local damping coefficient and $v_{(i)}$ is the generalized velocity.

$$v_{(i)} = \begin{cases} \dot{} & = 1, 2 \\ \dot{} & = 3 \end{cases} \qquad [4\text{-}3]$$

$$\text{sign}\left(\text{y}\right) = \begin{cases} +1, & if\ y > 0 \\ -1, & if\ y < 0 \\ 0, & if\ y = 0 \end{cases} \qquad [4\text{-}4]$$

In calculating viscous damping, normal and shear components of a damping force are given by

$$D_i = c_i \left| V_i \right| \qquad [4\text{-}5]$$

where c_i is the damping constants, V_i is the relative velocity at the contact, and the subscript i refers to one of the two components of the contact force (i =1 means normal force, and i=2 shear force). Instead of specifying the damping constants, the critical damping constant is specified. The relationship between damping constant, c_i, and critical damping constant is

$$c_i = \beta_i c_i^{crit} \quad [4\text{-}6]$$

where β is critical damping ratio. When β < 1, the system is said to be underdamped or lightly damped; when β >, the system is said to be overdamped or heavily damped. c^{crit} is the critical damping constant, which is given by

$$c_i^{crit} = 2m\omega_i = 2\sqrt{mk_i} \quad [4\text{-}7]$$

where ω_i is the natural frequency of the undamped system, k_i is the contact tangent stiffness and m is the effective system mass.

4.4. Numerical experiment results

To test the effects of entrainment on debris flow runout, particles located as specified coordinate are monitored (Figure 4-1). Runout distance and velocity of debris flow are obtained by monitoring moving and stationary particles in the flow channel. A total of 30 locations, distributed evenly in three cross sections, are being monitoring. Since it is possible that there are particles inside the measurement circles, particles closest to those points are being monitored. To monitor entrainment rate dynamically, stresses and variations of the height at the interface between moving and stationary particles are calculated. The locations of flowing particles at different time is shown in Figure 4-2. Since entrainment starts when the moving particles reaches the erodible bed, the location of moving particles at different time during erosion is analyzed. When particles are being eroded to become part of the moving mass, the color of the particles will be changed to the same color as the moving particles.

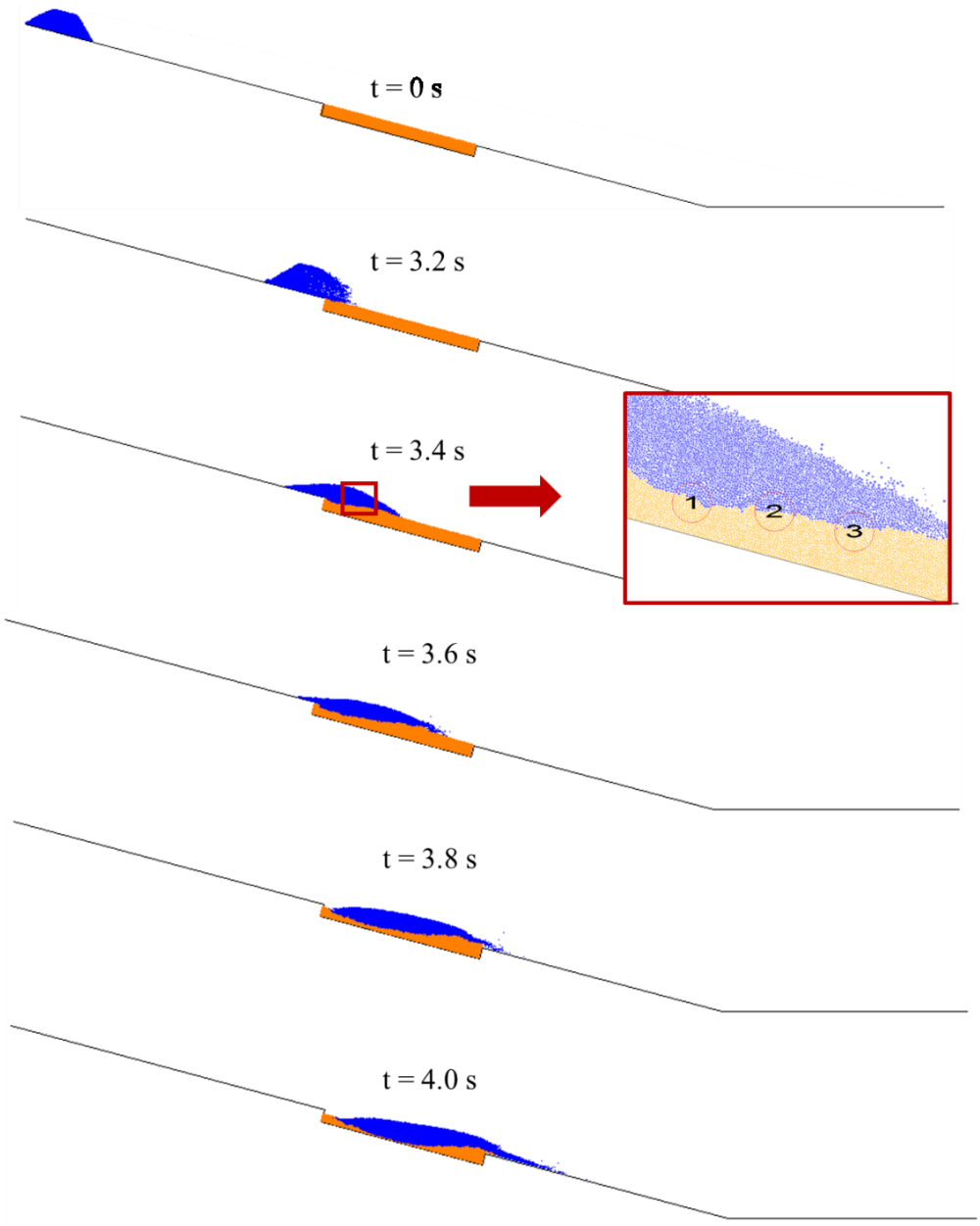

Figure 4-2: Dynamic location of moving granular flow and close up of measurement circles

4.4.1. Simulation results of granular flow

During the simulation process, average velocity and total volume are being monitored. Average velocity is calculated based on all moving particles. Total volume is defined as the volume of all particles mobilized, blue particles in Figure 4-2. The calculated velocity and total volume are

shown in Figure 4-3. The average velocity increases linearly until the moving particles reach the erodible bed. The maximum velocity, around 2.10 m/s, occurs at the beginning of entrainment process. After that, the average velocity decreases continuously until t= 4.5s. The average fluctuates around 0.9 m/s. Variation of the total volume of the moving particles starts at t=3.2s. Therefore, analysis of simulation results will focus on the velocities and total volume in the shaded region, between t=3.2s and t= 4s, as shown in in Figure 4-3.

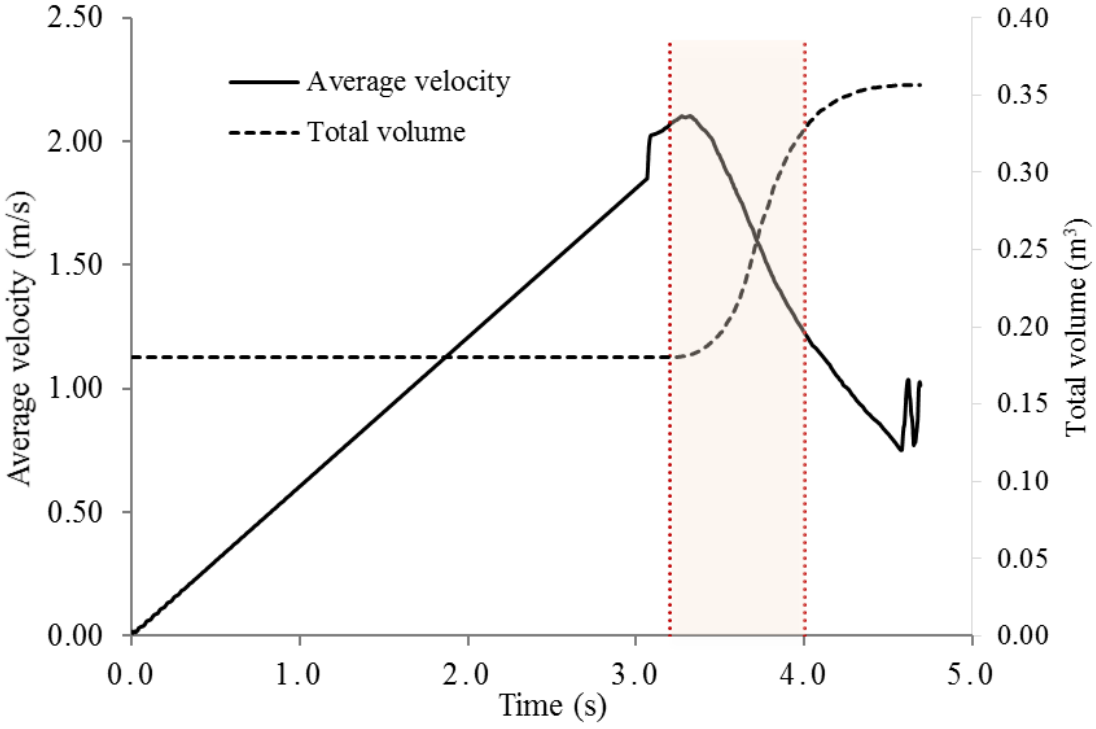

Figure 4-3: Average velocity of moving particles

4.4.2. Calculated results at the monitored points

The calculated rotational velocity of the particles closest to monitoring points at the erodible channel surface are also shown Figure 4-4. These particle are selected at the initial stage of this numerical experiment and their rotational velocities are tracked throughout the flow process. Physically, particles closest to the surface of the erodible channel at P1 are moved first and then

particles at P2 and P3 are moved consecutively. Positive value indicates counterclockwise rotation according to the default setting in PFC2D. The time when particles start to rotate is when erosion starts. It means that the rotational velocities correspond with physical analysis though negative rotational velocities observed that are probably caused by particles climbing over the monitored particles.

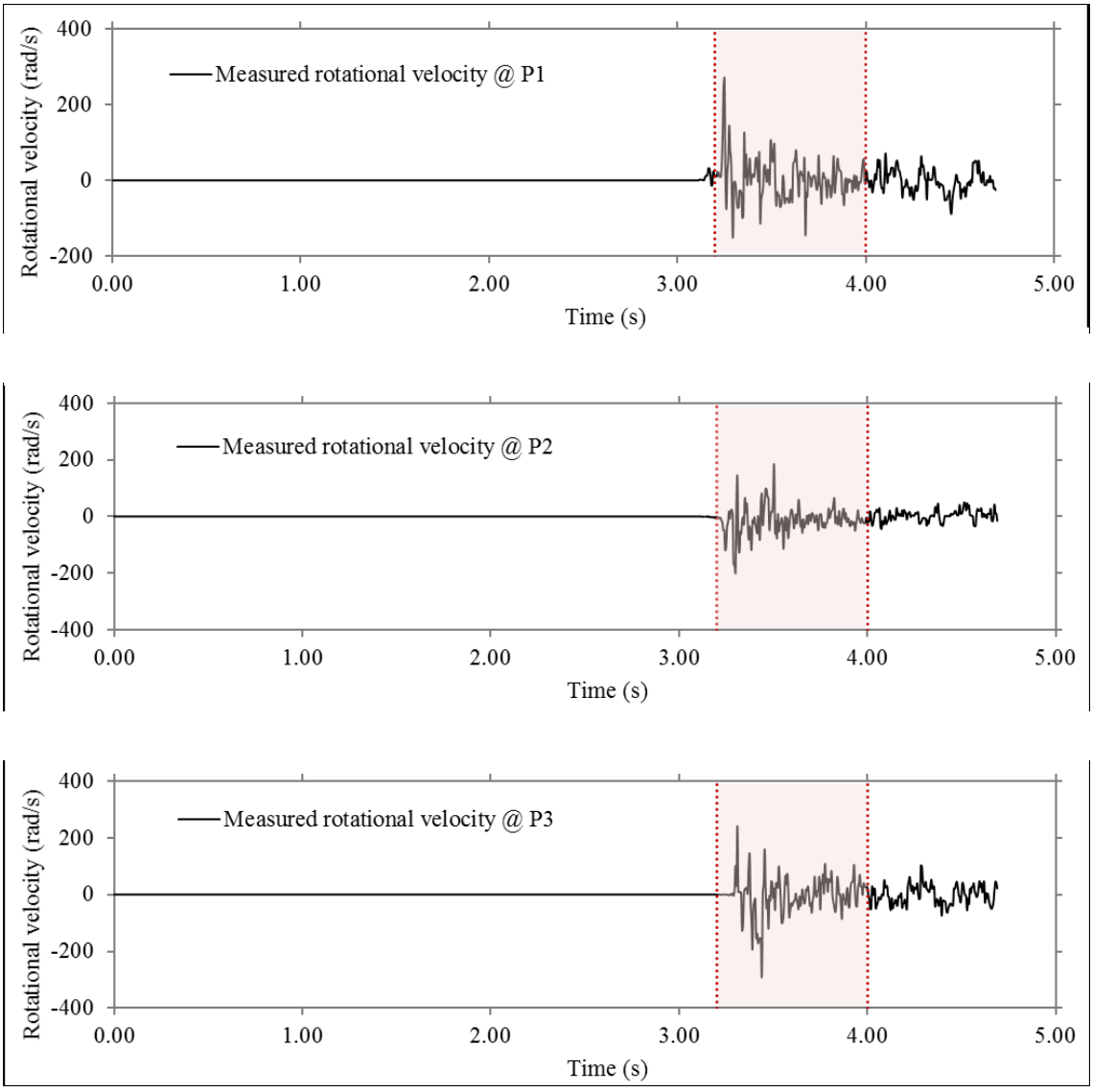

Figure 4-4: Variation rotational velocities of particles at monitoring points

In PFC2D, contact forces and particle displacements are calculated at the micro level. Since they cannot be compared directly to a continuum model, averaging procedures are used to calculate macro stresses. The average stress tensor, $\bar{\sigma}_{ij}$, in a volume V of material, is defined as:

$$\bar{\sigma}_{ij} = \frac{1}{V}\int_{V} \sigma_{ij} dV \qquad [4\text{-}8]$$

where $\bar{\sigma}_{ij}$ are the components of stresses in volume V.

According to contact forces, contact orientations and region porosity, the average stress tensor, $\bar{\sigma}_{ij}$, is estimated using stress-measurement procedure developed by Potyondy and Cundall (2004). In the estimation, it is assumed that there is no body force, particles satisfy full-force equilibrium and parallel-moment equilibrium is not satisfied. Outward normal stress is considered as positive value. Force per unit length of particle boundary are converted to a stress quantity by dividing the force by the thickness of the element. Since shear stress along the flow channel is needed, stress transformation is necessary after calculating the normal and shear stresses (Figure 4-5).

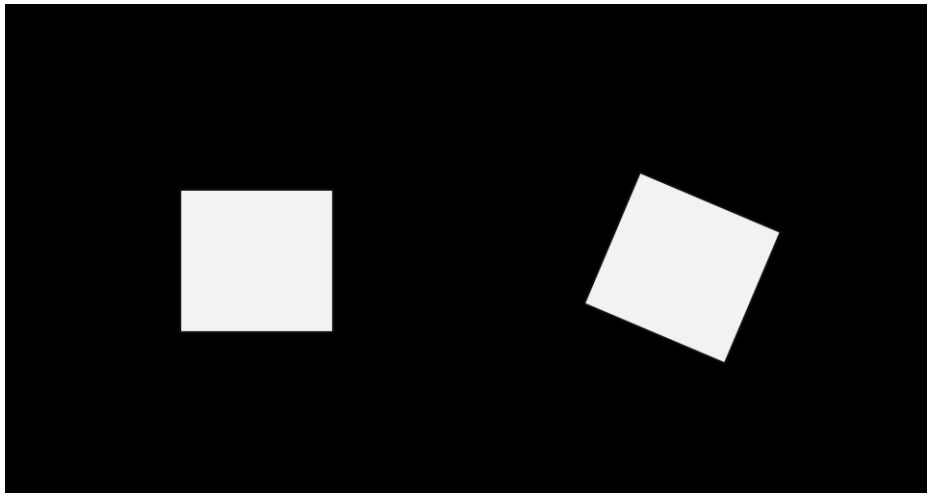

Figure 4-5: Stress transformation during to slope of the erodible bed

The size of measurement circle can affect the calculated values. To see the effect of the size of measurement, various sizes are used in the calculation of the shear stresses. The results are plotted in Figure 4-6. It is obvious that the shear stress converges to a single value if the size of the measurement circle increases.

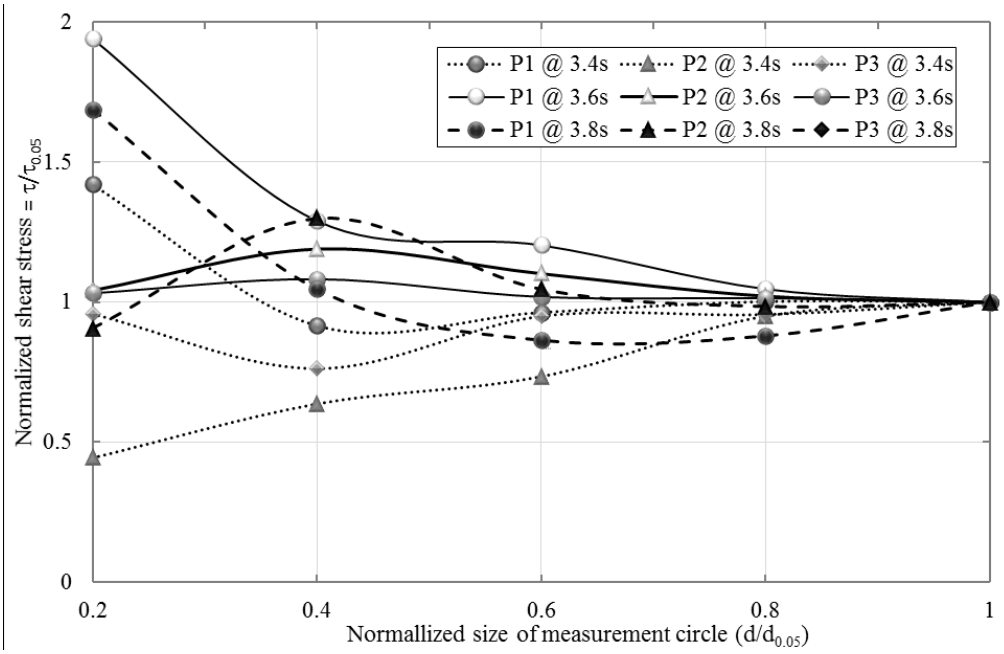

Figure 4-6: Sensitivity analysis of the size of the measurement circle on shear stress

To clarify the distribution of x-velocity, rotational velocity and shear stress in the granular flow, they are calculated during the flowing process along the cross sections as shown in Figure 4-1. The results are plotted in Figure 4-7. Since friction dominates the properties of granular flow, which is different from viscous flow in which viscosity dominates the flow properties, the largest x-velocity appears at the top of the flow channel, notably at B1 and C1. At A1, due to boundary effect, x-velocity of particles near the initial erodible surface is smaller than that below the initial erodible surface, however in B1 and C1, the calculated x-velocity is almost linearly distributed similar as simple Couette flow.

Rotational velocity at the monitored sections varies considerably between positive and negative values with depth. Since particles override each other, underlying particles requires larger force to be moved than the particles above. When the upper particle roll forward, counter clockwise rotation, the lower particles then roll backward, clockwise rotation, due to friction at the contact. This results in rapid changes in the direction of rotation between positive and negative values with depth.

Shear stresses also vary along the cross sections. However shear stresses are increasing from top to bottom in the moving particles. Since stresses are calculated using average values in a volume depending on porosity, it is expected that shear stresses will vary a little bit along the cross sections.

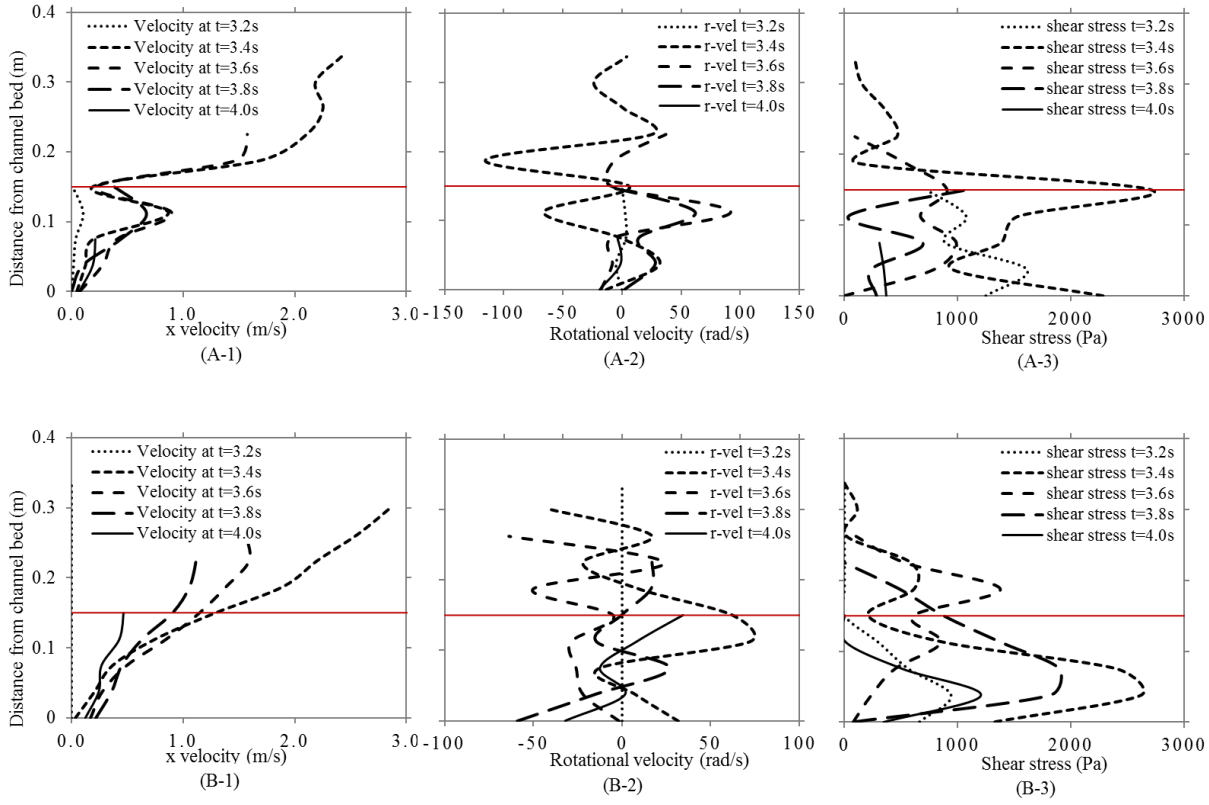

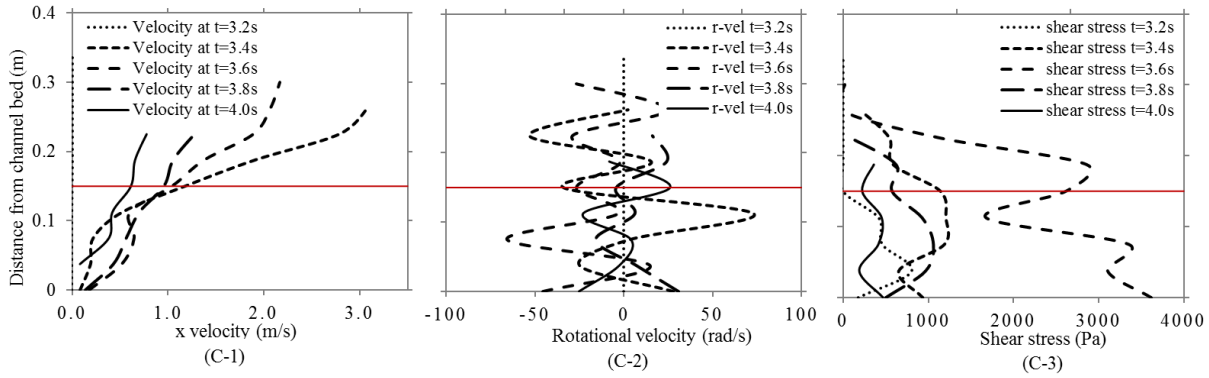

Figure 4-7: Flow properties along monitored cross sections

(A-1, B-1 and C-1 are monitored x-velocity along cross sections P1, P2 and P3. A-2, B-2 and C-2 are monitored rotational velocity along cross sections P1, P2 and P3. A-3, B-3 and C-3 are monitored shear stress along cross sections P1, P2 and P3, which have been transformed to the direction parallel to flow channel)

4.5. Setup of analytical entrainment model

4.5.1. Description of analytical entrainment model

Traditional analytical entrainment models consider shear failure in the erodible bed. It is assumed that shear stress at the base of the moving particles is sufficiently high to erode material lying on the channel bed. There are basically two approaches in calculating entrainment: static approach and dynamic approach. In the static approach, failure occurs when the static shear stress exceeds the shear strength of the material. (Medina et al. 2008). Entrainment depth is calculated based on force equilibrium of erodible layer. In the dynamic approach, the rate of erosion is calculated based on the unbalanced shear stress parallel to the flow channel according to Newton's Second Law of Motion. The amount of entrained material thereby depends on excess momentum (Medina et al. 2008).

It is considered that granular particles lying on the channel bed are eroded progressively in the new entrainment model. Granular particles are modelled as uniform size sphere. Particles are being moved due to shear stress applied on the particles. According to Cheng et al. (2003) and Shodja et al. (2003), drag force to initiate rolling action is normally less than that required for basal shear failure. Therefore it is considered that rolling motion is the dominant motion in initial stage of entrainment for granular material. However both rolling motion and shear failure should be considered in the analysis.

In calculating the drag force for the initiation of the rolling action, it is assumed that a particle will rotate around point *O* as shown in Figure 4-8. Drag forces arising from the moving debris above the bed are assumed to apply at the center of the particle. It is assumed that the particle will rotate around the contact point with the adjacent particle located downstream. Newton's Law of Motion is applied to calculate the acceleration, velocity, and displacement of the particle. The equation governing the motion can be written as:

$$\frac{TR}{\left(I+mR^2\right)}sin\alpha_t - \frac{mgR}{\left(I+mR^2\right)}\cos\left(\alpha_t+\theta\right) = \frac{\partial^2\alpha_t}{\partial t^2} \qquad [4\text{-}9]$$

where T is the drag force required to initiate rolling, R is the radius of the particles (For a granular assembly with different particle sizes, d_{50} is used.), I is moment inertial which is equal to m $(3R^2 + L^2)/12$, L = 1m for 2D, m is the mass of the particle (for 2D, $m=\pi R^2\rho_b$), ρ_b is the density of bed sediment particle, α_t is the angle between channel bed and connection line of centers of those two particles, θ is the slope angle, g is the gravity acceleration, $\partial^2\alpha_t/\partial t^2$— angular acceleration and t is time.

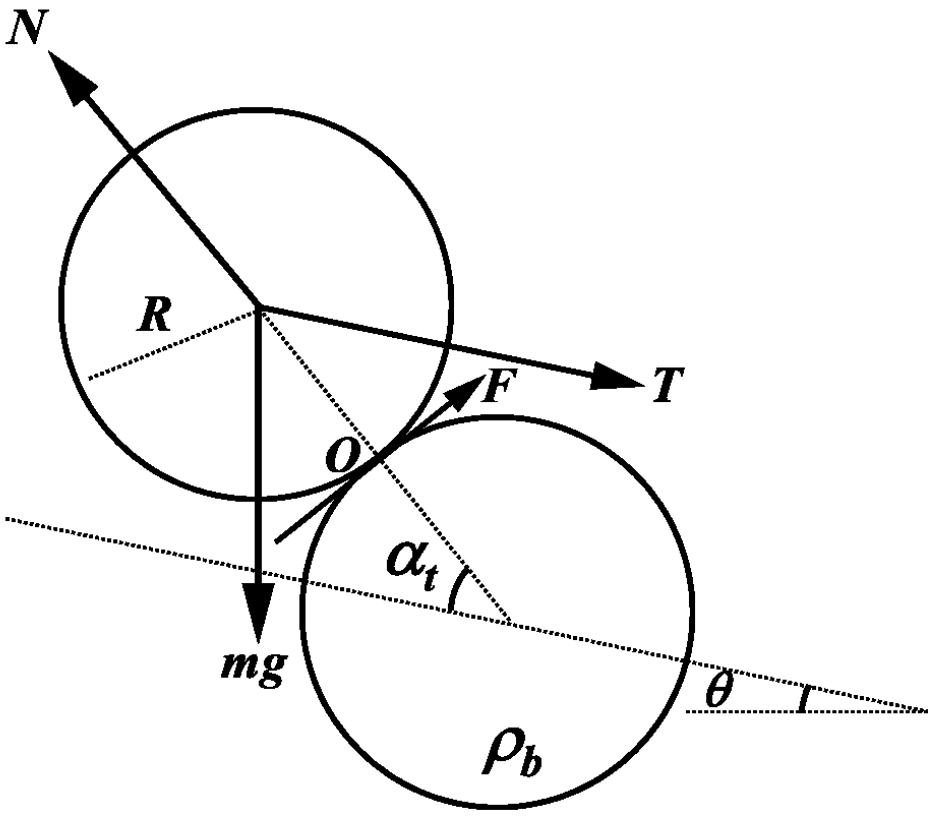

Figure 4-8: Free body diagram of a particle when rolling occurs

It is also assumed in the derivation that once the particle moves over the adjacent particle downstream, it will be considered to become part of flowing debris. Based on Equation [4-7], the entrainment time, the time required for one particle to move from initial location into debris, can be calculated. The entrainment rate is defined as the height of particle exposed to the flow divided by the time needed for it to be eroded. Therefore for different α_0, the initial condition of α_t, entrainment rate, $\dot{E}_i$, is defined as:

$$\dot{E}_i = \frac{2R\sin\alpha_{0i}}{t_i} \qquad [4\text{-}10]$$

t_i is the time required for one particle to roll from its initial position, α_0, to vertical line at which α_t equals $(\pi/2-\theta)$, because it was assumed that once the particle moves over another particle, it

will be considered as part of debris flow. Therefore, for a given shear force applied on the particle, t_i, can be determined from equation [4-7]. When the shear force applied on the particle is larger than the friction at the particle contact, the entrainment mode changes from rolling motion to sliding motion.

Since α_0 varies considerably in the granular assembly and it is not easy to determine individual angles at each particle contact, a statistical approach is used to provide an estimate on the values and variations of α_0. It is assumed that the variation of α_0 can be approximated using a probability density function (PDF). The model parameters for a PDF have significant effects on the calculations of entrainment. Strictly speaking, parameters like mean value of normal distribution function would be possible to measure on site (Fenton and Abbott 1977), but it only can apply to the site where the test was made. It can also be estimated using relationship between void ratio and internal friction angle, and relationship between particle protrusion and void ratio (Okada et al. 2007). The overall entrainment rate $\dot{E}$ can be determined from individual particle entrainment rate $\dot{E}_i$ and the probability density function P_i as:

$$\dot{E} = \sum_{i=1}^{n} \dot{E}_i P_i \qquad [4\text{-}11]$$

where n is the number divisions of the probability density function in the approximation over the range of the values of α_0. For instance, if the increment of α_0 is 1 degree from 0 to 90 degree, n will be equal to 91.

4.5.2. Model parameters for the analytical calculation

The value of α_0 cannot be easy measured in the field. However it is shown that α_0 can be related to a pivoting angle. In the simulation, pivoting angle of angular particle, ϕ_p, is estimated using

the empirical relationship from Li and Komar (1986). The average slope angle is used here. The mean value of the normal distribution PDF is calculated to be 33º based on the relationship that $\alpha_0 = (\pi/2-\phi_p-\theta)$. A standard deviation value equal to 0.1 is used. The average particle size, 3.5 mm, used in the PFC simulation is also used in the analytical model. The particle density used in the calculation is the same as that used in the PDF simulation.

The contact friction angle, ϕ_μ, is not the same as the aggregate angle of friction ϕ_{cv} at critical state. Caquot (1934) related ϕ_μ and ϕ_{cv} using:

$$\tan\phi_{cv} = \frac{1}{2}\pi\tan\phi_\mu \qquad [4\text{-}12]$$

Bishop (1954) also developed an approximate solution verified using double measured values ϕ_μ and ϕ_{cv}.

$$\sin\phi_{cv} = \frac{15\tan\phi_\mu}{10+3\tan\phi_\mu} \qquad [4\text{-}13]$$

In the calculating entrainment, equation [4-10] is used to relate the friction angle in PFC simulation to the friction angle in the probabilistic entrainment model. According to the friction angle in PFC simulation, an internal frictional angle is calculated based on the equation above which will be equal to the mean value of PDF in probabilistic entrainment model. Standard deviation equal to 0.01 is used in the calculation.

4.6. Validation and comparison of simulation results

4.6.1. Verification of calculated shear stress

To evaluate the new entrainment model, shear stress, variation of erodible depth and entrainment rate are compared with the results from PFC numerical experiment along sections P1, P2 and P3.

Shear stress is defined as the stress always along the slope. Shear stresses at the interfaces between the granular flow and the immobile particles are compared to that calculated using the Coulomb friction model and the Voellmy fluid model in the runout model (Figure 4-9). The height of the flowing particles used in calculating the shear stresses in the Coulomb friction model and the Voellmy fluid model is measured at a 0.05s interval in the entrainment process in PFC2D. In shear stress calculation, the turbulence coefficient in the Voellmy fluid model is equal to 100 m/s^2 which is selected based on the suggestion of Luna et al. (2012).

The components representing normal stresses in Coulomb friction model and Voellmy fluid model are obtained from the measurement circles by stress transformation. The friction coefficient and turbulent coefficient are selected as mentioned above. The shear stress are then calculated using the Coulomb friction model and Voellmy fluid model. The component representing shear stress along slope in PFC experiment can also be obtained by stress transformation according to the stresses calculated using measurement circles represented by soli dot in Figure 4-9. It can be seen from the figure that there are discrepancies between calculations from PFC model and the constitutive models. The shear stress from PFC model matches that estimated using the Voellmy fluid model initially. However, at a later stage, the PFC calculated shear stress is closer to the stresses calculated using the Coulomb friction model. The

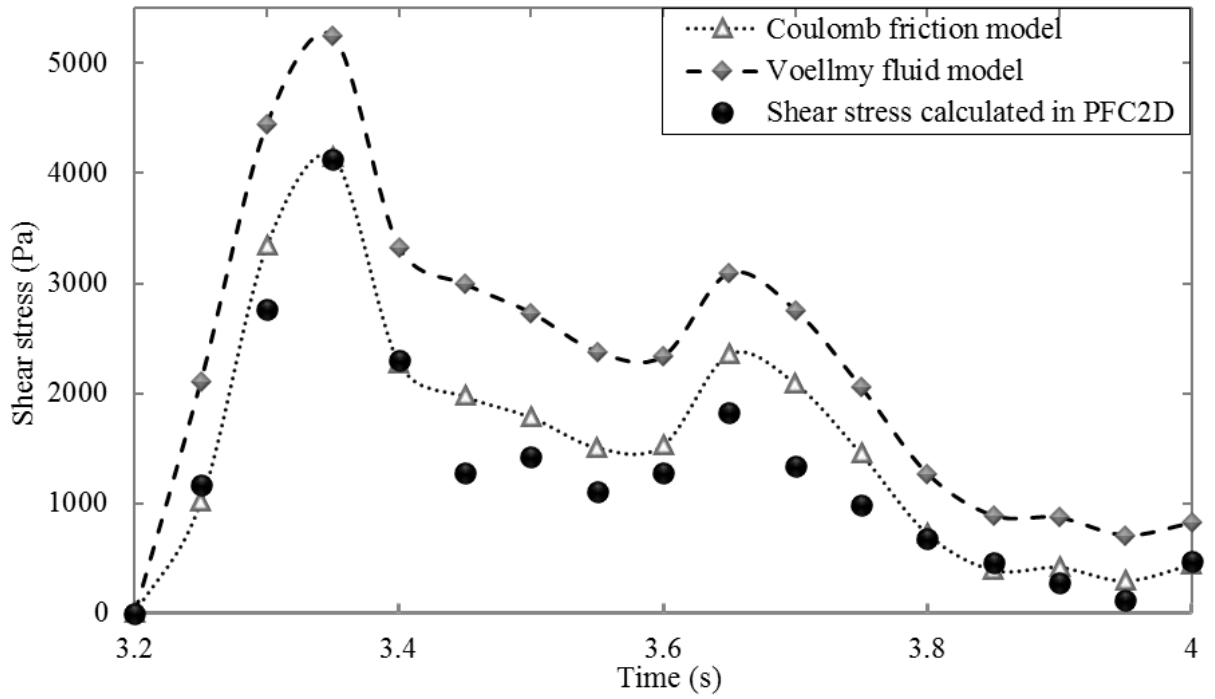
Coulomb friction model
Voellmy fluid model
Shear stress calculated in PFC2D
Shear stress (Pa)
Time (s)
0
1000
2000
3000
4000
5000
3.2
3.4
3.6
3.8
4

(a)

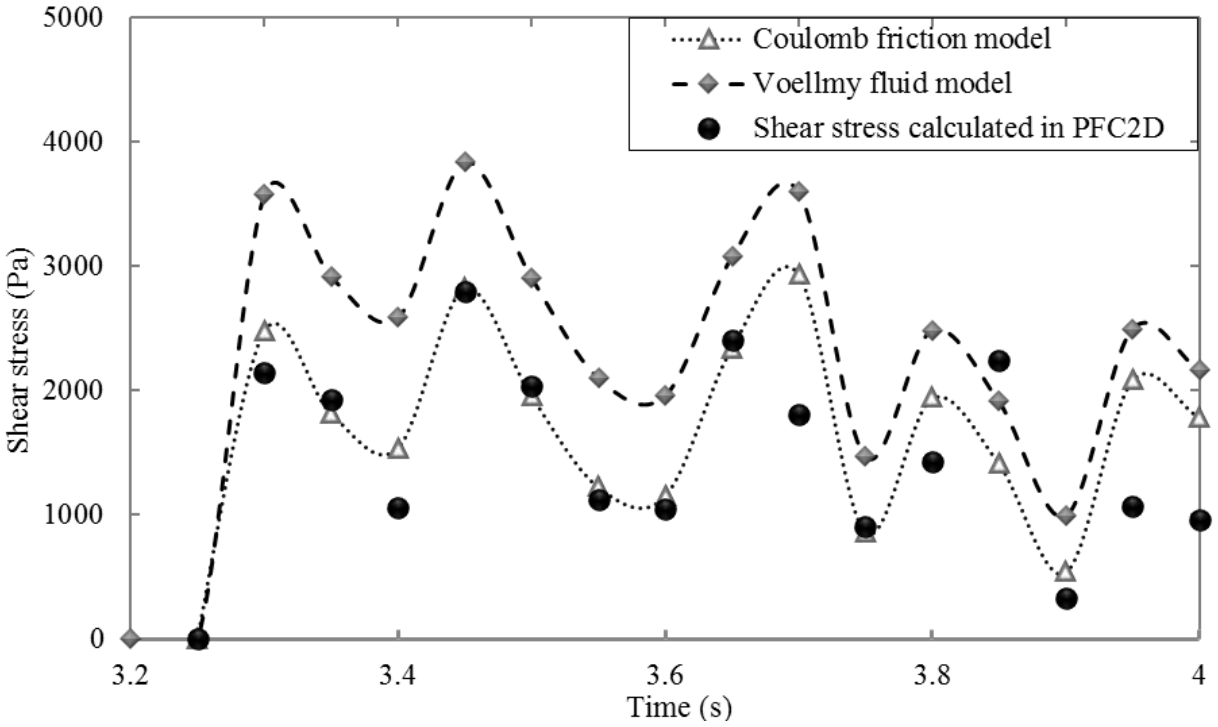
Coulomb friction model
Voellmy fluid model
Shear stress calculated in PFC2D
Shear stress (Pa)
Time (s)
0
1000
2000
3000
4000
5000
3.2
3.4
3.6
3.8
4

(b)

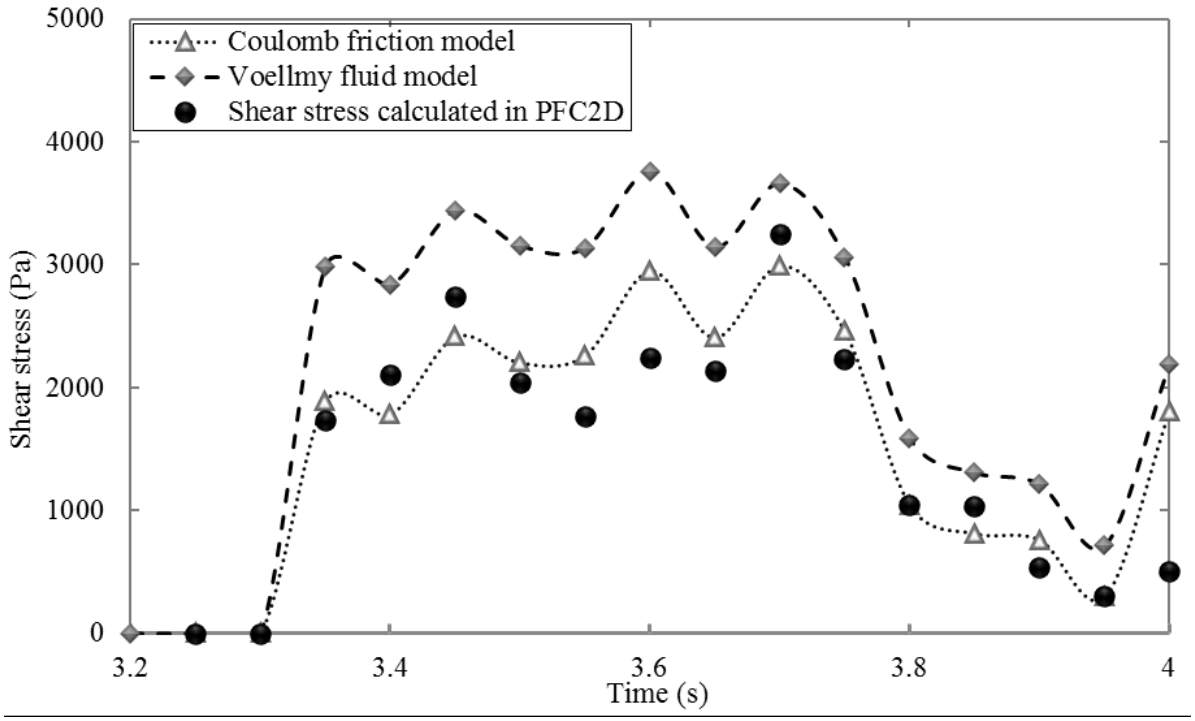

(c)

Figure 4-9: Verification of shear stress monitored and calculated at interface between moving particle and immobile particles. (a), (b) and (c) are comparison results from P1 to P3, respectively.

4.6.2. Verification of eroded depth

The entrainment depth in PFC experiment is defined as the variation of the interface between moving particles and stable bed. Figure 4-10 shows that entrainment starts until the moving particles reach erodible zone and entrainments almost stop if the moving particles reach the rigid boundary (channel bed), considered as not erodible.

To evaluate entrainment, the calculated depths of erosion using PFC and the entrainment model are compared in Figure 4-10. The depths of erosion estimated using the entrainment model agree well with that determined at P1, P2 and P3 until time equals to t = 3.8 s at which time the moving

particles reach the rigid wall. When moving particles reach this boundary, the interface will not change any more no matter what is the magnitude of shear stress applied on channel bed. The discrepancies after t = 3.8 s are mainly caused by the reason mentioned above. It means after t = 3.8s, although the shear stress calculated in PFC is not equal to zero, the entrainment rate should be equal to zero. However, this discrepancy is not large as the moving particles fully stop less than 0.2 s later. Overall, the starting and ending times of entrainment from P1 to P3 also agree well based on the two type of analyses. The accuracy of the estimated starting time of entrainment is based on the time step adopted for the calculation of shear stresses. This can be overcome by monitoring the variation of shear stress at specified location.

The equation proposed by Medina et al. (2008) is also used to calculate the entrainment rate. In this calculation, bulk density is calculated according to the density of the particles and void ratio when particles are generated. Mean velocity of flow is the average velocity of all moving particles. Net shear stress are calculated by subtracting the resistant stress estimated using Coulomb Friction Model from the driving stress calculated from the PFC model.

Figure 4-10 shows the depth of erosion calculated using the dynamic model and the progressive scouring entrainment model named as analytical model in previous section. To estimate the variation of entrainment depths between calculated values using the dynamic model and the progressive scouring model and that calculated in PFC experiment, Euclidean distance of calculated depth of erosion using different entrainment models and the depth of erosion from the numerical experiment are shown in Table 4-3. It is obvious that the depth of erosion calculated using the new entrainment model are closer to the calculated depth of from the PFC model.

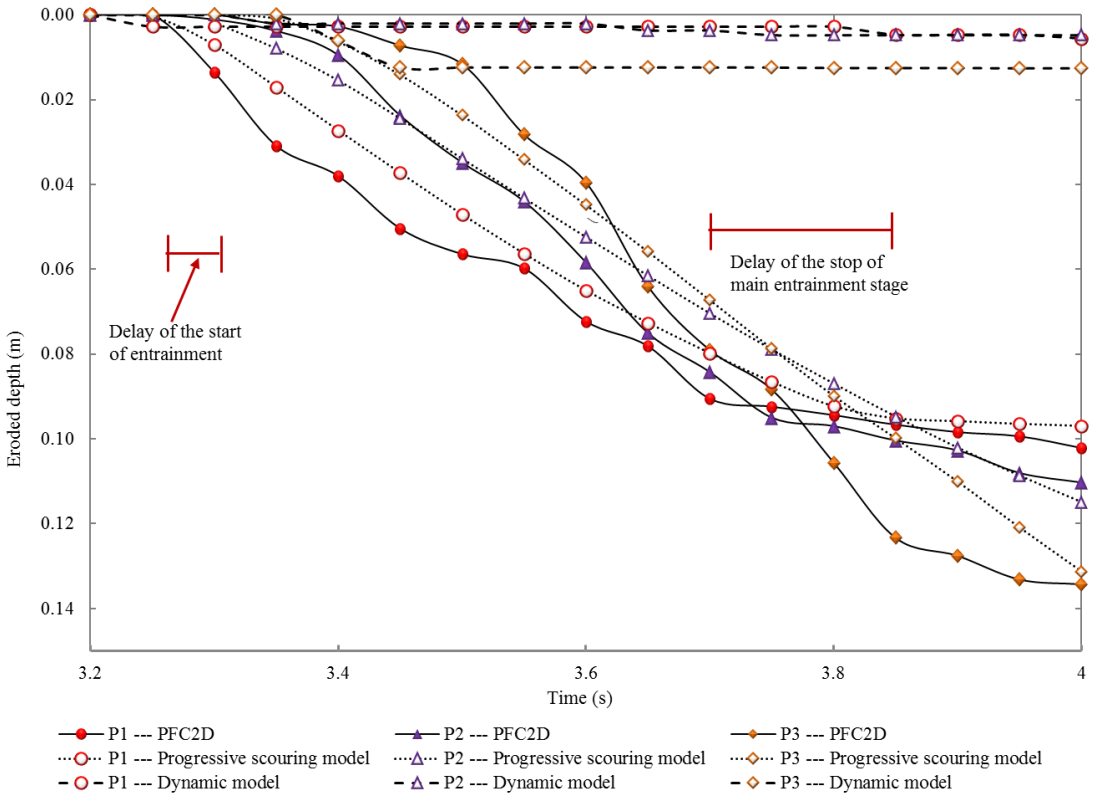

Figure 4-10: Comparison of analytical and PFC2D simulated eroded depth at the interface

Table 4-3: Euclidean distance of calculated entrainment depth between dynamic entrainment model and PFC experiment, and between progressive scouring entrainment model and PFC experiment at different locations

Entrainment models	P1	P2	P3
Progressive scouring model	0.02988	0.02957	0.04277
Dynamic entrainment model	0.28402	0.27437	0.27830

4.6.3. Verification of the rate of erosion

The rate of erosion is calculated by dividing the depth of erosion by the time during the erosion process. The new entrainment model is verified by comparing the entrainment rate between progressive scouring model and the PFC results. The various methods of calculating the entrainment rates are presented in Figure 4-11. The redThe entrainment rates of each cross section are differentiated by different symbols. The deviation of entrainment rate calculated can

be explained by the errors in identifying the erosion depth in discrete model which is different from continuous model.

The calculated entrainment rate from the progressive scouring entrainment model at P1 varies between 0.13m/s and 0.21m/s, while the entrainment rates of the other two lines change almost evenly along the diagonal line. By monitoring the entrainment process at P1, it is found that the boundary effect affects the entrainment calculation since the height of moving mass is probably overestimated which is used to calculate the shear stress in the progressive scouring entrainment model. It is because some of the particles at the top part of the flow are not fully in contacted with underlying particles in PFC model. These particles do not contribute to the development of shear stress on the flow channel.

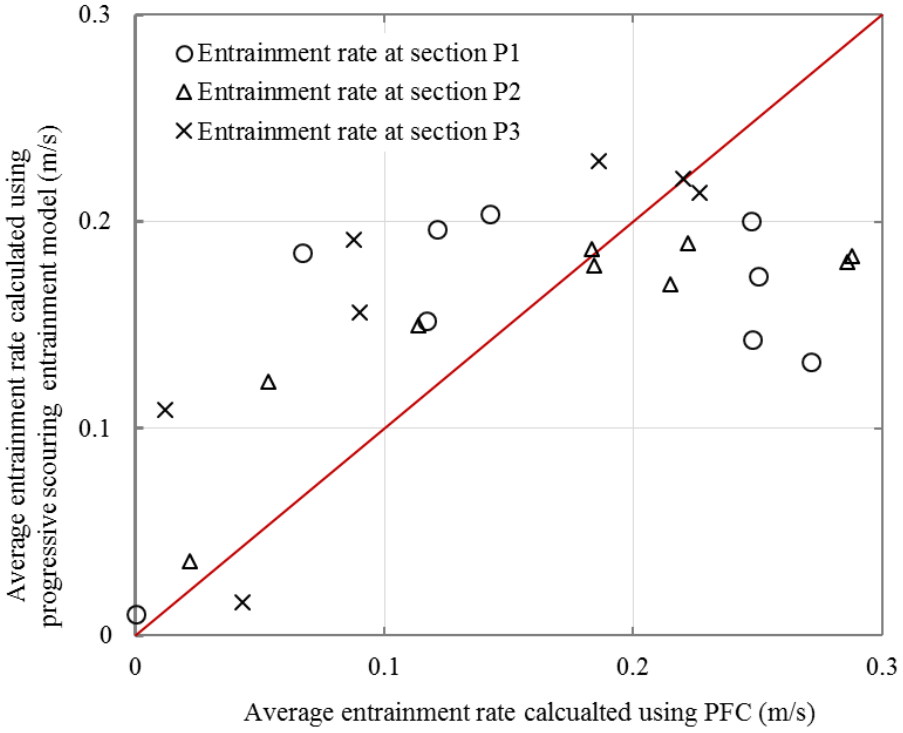

Figure 4-11: Comparison of entrainment rate between entrainment runout model and PFC2D simulation

4.7. Discussion and conclusion

To study the entrainment process using PFC, a flume with source zone, erodible zone and deposition zone is constructed. The determination of the slope angle, size of tank and depth of erodible channel bed should be based on calculation time expected and calculation capacity of the compute. The height of the erodible channel is critical in the experiments. The erodible part can be neither too shallow, since it will be eroded to a rigid wall quickly, and nor too deep, as it will then need more calculation time at each step. Therefore, calculation time and visible entrainment process should be balanced. Moreover, to prevent the flying the particles, stiffness of particles in the tank and erodible channel should be set as a small value before overlapping of particles is observed at the bottom part of the erodible channel.

Since it is assumed that rolling motion is the main process in the progressive scouring entrainment model, rotational velocities of the particles located at three different cross sections are monitored. Observed results indicate that rotational velocities at the monitoring spots suddenly increase when entrainment starts. The increase can indicate that the rolling motion is an essential part in entrainment process and should be incorporated into the entrainment process with sliding motion. A change of rotational velocity between positive and negative values is induced by the interaction between adjacent rigid particles and/or particle and wall.

The shear stresses applied on channel bed are calculated in PFC using measurement circles based on stress transformation. The stresses perpendicular to the slope which are also calculated using measurement circles in PFC are used to calculate shear stress adopting Mohr-Coulomb friction model and Voellmy fluid model. The results indicate that the shear stresses calculated using Mohr-Coulomb friction model are closer to that calculated using PFC.

The entrainment rate in PFC simulation is determined by the change of interface between moving particles and immobilized particles. The entrainment rate is also calculated using progressive scouring model and dynamic entrainment model based on the shear stresses calculated using Mohr-Coulomb friction model. The parameters in the progressive scouring model is selected based on the parameters in the PFC including density, internal friction angle, and mean value of particle size. The comparison result of the variation of eroded depth demonstrates that the erosion process mainly occurs between 3.3s and 3.7s. The erosion depths calculated using PFC, the dynamic entrainment model and the progressive scouring entrainment model in this time range enable us to evaluate these models. The scatter plot substantiates that it is feasible to use the progressive scouring entrainment model to estimate the entrainment rate, in which rolling motion starts first. The calculated depths of erosion using the progressive scouring entrainment model and the dynamic entrainment model indicate that the previous one performs very well in the calculation of the entrainment rate.

Reference

Banton, J., Villard, P., Jongmans, D., and Scavia, C. (2009). Two-dimensional discrete element models of debris avalanches: Parameterization and the reproducibility of experimental results. Journal of Geophysical Research, 114, F04013, doi:10.1029/2008JF001161.

Bishop, A. W. (1954). Correspondence, Géotechnique, 4(1), 43-45.

Caquot, A. (1934). Equilibre des Massifs a' Frottement Interne. Stabilite des Terres Pulv6rents et Coherentes. Gauthier Villars, Paris.

Cheng, N. S., Law, A. W. K., and Lim, S. Y. (2003). Probability distribution of bed particle instability, Advances in Water Resources, 26(4), 427-433.

Cundall, P.A. (1971). A computer model for simulating progressive, large scale movements in blocky rock systems. Proceedings of the International Symposium on Rock Mechanics, Editors: anonymous, Nancy, France, October 4-6, 1971, Rubrecht, Germany, 2:129-136.

Cundall, P. A., and Strack, O. D. (1979). A discrete numerical model for granular assemblies. Géotechnique, 29(1), 47-65.

Egashira, S., Honda, N., and Itoh, T. (2001). Experimental study on the entrainment of bed material into debris flow, Physics and Chemistry of the Earth, Part C: Solar, Terrestrial & Planetary Science, 26(9), 645-650.

Fenton, J. D., and Abbott, J. E. (1977). Initial Movement of Grains on a Stream Bed: The Effect of Relative Protrusion, Proceedings of the Royal Society of London Series a-Mathematical Physical and Engineering Sciences, 352(1671), 523-537.

He, J. M., Li, X., Li , S. D., Yin, Y. P., and Qian, H. T. (2010). Study of seismic response of colluvium accumulation slope by particle flow code, Granular Matter, 12(5), 483-490.

Hutter, K., Koch, T., Plüss, C., and Savage, S. B. (1995). The dynamics of avalanches of granular-materials from initiation to runout. 2. Experiments, Acta Mechanica, 109(1-4), 127-165.

Iimura, K., Watanabe, S., Suzuki, M., Hirota, M., and Higashitani, K. (2009). Simulation of entrainment of agglomerates from plate surfaces by shear flows. Chemical Engineering Science, 64(7), 1455-1461.

Itasca, Consulting Group Inc., (2002). PFC2D Particle Flow Code in 2 Dimensions. User's Guide.

Iverson, R. M. (2012). Elementary theory of bed-sediment entrainment by debris flows and avalanches, Journal of Geophysical Research, 117, F03006, doi:10.1029/2011JF002189.

Iverson, R. M., and Ouyang C. J. (2015). Entrainment of bed material by Earth-surface mass flows: Review and reformulation of depth-integrated theory. Reviews of Geophysics, 53, doi:10.1002/2013RG000447.

Li, W. C., Li, H. J., Dai, F. C., and Lee, L. M. (2012). Discrete element modeling of a rainfall-induced flowslide, Engineering Geology, Engineering geology, 149, 22-34.

Li, X. P., He, S. M., Luo, Y., and Wu, Y. (2010). Discrete element modeling of debris avalanche impact on retaining walls, Journal of Mountain Science, 7(3), 276-281.

Li Z. L., and Komar, P. D. (1986). Laboratory measurements of pivoting angles for applications to selective entrainment of gravel in a current, Sedimentology, 33(3), 413-423.

Luna, B. Q., Remaitre, A., van Asch, T. W. J., Malet, J. P., and van Westen, C. J. (2012). Analysis of debris flow behavior with a one dimensional run-out model incorporating entrainment, Engineering Geology, 128, 63-75.

McDougall, S., and Hungr, O. (2004). A model for the analysis of rapid landslide motion across three-dimensional terrain, Canadian Geotechnical Journal, 41(6), 1084-1097.

Medina, V. H, Bateman, A., and Hurlimann, M. (2008). A 2D finite volume model for bebris flow and its application to events occurred in the Eastern Pyrenees, International Journal of Sediment Research, 23(4), 348-360.

Okada, Y., and Ochiai, H. (2007). Coupling pore-water pressure with distinct element method and steady state strengths in numerical triaxial compression tests under undrained conditions, Landslides, 4(4), 357-369.

Potyondy, D. O., and Cundall, P. A. (2004). A bonded-particle model for rock, International journal of rock mechanics and mining sciences, 41(8), 1329-1364.

Remaître, A, van Asch, Th. W. J., Malet, J. P., and Maquaire, O. (2008). Influence of check dams on debris-flow run-out intensity, Natural Hazards and Earth System Science, 8(6), 1403-1416.

Remaître, A., Malet, J. P, and Maquaire, O. (2009). Sediment budget and morphology of the 2003 Faucon debris flow (South French Alps): scouring and channel-shaping processes, Proceedings of the International Conference on Landslide Processes: from géomorphologie mapping to dynamic modelling, Editors: Malet, J.P. Remaitre, A. and Bogaard, T, Strasbourg, France, February 6-7, 2009, CERG, Strasbourg, 75-80.

Salciarini, D., Tamagnini, C., and Conversini, P. (2010). Discrete element modeling of debris-avalanche impact on earthfill barriers. Physics and Chemistry of the Earth, 35(3), 172-181.

Savage, S. B., and Hutter, K. (1991). The dynamics of avalanches of antigranulocytes materials from initiation to runout. 1. Analysis, Acta Mechanica, 86, 201-223.

Shodja, H. M., and Nezami, E. G. (2003). A micromechanical study of rolling and sliding contacts in assemblies of oval granules, International Journal for Numerical and Analytical Methods in Geomechanics, 27(5), 403-424.

Skempton, A.W. (1954). The pore-pressure coefficients A and B, Géotechnique, 4(4), 143-147.

Teufelsbauer, H., Wang, Y., Chiou, M. C., and Wu, W. (2009). Flow–obstacle interaction in rapid granular avalanches: DEM simulation and comparison with experiment. Granular Matter, 11(4), 209-220.

Wu, F. C., and Chou, Y. J. (2003). Rolling and Lifting Probabilities for Sediment Entrainment, Journal of hydraulic engineering, 129(2), 110-119.

Xu, Q., Shang, Y. J., van Asch, Th.W. J., Wang, S. T., Zhang, Z. Y., and Dong X. J. (2012). Observations from the large, rapid Yigong rock slide-debris avalanche, southeast Tibet, Canadian Geotechnical Journal, 49(5), 589-606.

Zhou, G. G., and Ng, C. W. (2010). Numerical investigation of reverse segregation in debris flows by DEM. Granular matter, 12(5), 507-516.

5. IMPLEMENTATION OF ENTRAINMENT ANALYSIS IN DRY GRANULAR FLOW RUNOUT MODEL

5.1. Abstract

A new entrainment calculation method has been incorporated into an energy-based debris flow runout model. Entrainment calculation is governed by a second order partial differential equation that is solved using the finite difference method. During entrainment, it is considered that the total mass is changing due to the inclusion of material from the channel bed. Simultaneously, the profile of the channel bed is adjusted accordingly due to surface erosion. Sensitivity analyses are carried out by varying model parameters such as internal friction angle, basal friction angle, turbulent coefficient, mean value of probabilistic density function (PDF) for resting angle etc. The sensitivity analysis results are evaluated by calculating the percentage change of the maximum entrainment rate, maximum frontal velocity of the debris, final total volume, longitudinal length of deposition, maximum debris flow height, and runout distance. It is shown that the mean value of PDF for the resting angle significantly affects the debris flow height, maximum entrainment rate and final total volume. Basal friction angle mainly has an effect on runout distance and longitudinal length of depositional fan. Measurements from Tsing Shan debris flow (1990) are used to study the model. Velocities at different channel sections estimated using superelevation method, runout distance and total volume are used to evaluate the simulation results. It is found that the simulated runout distance of debris flow and the maximum velocity at specified channel section are in good agreement with field observations.

5.2. Introduction on the entrainment model

In many debris flow events, flow channels are typically covered by surficial deposits, sometimes several meters thick of loose granular material. During the moving process of debris flow, material from the channel boundary are often eroded and mixed with the main body of the debris and becomes part of the flowing debris (Iverson 2012). The process of increasing the mass by eroding the material from the channel is called entrainment. There are various models in calculating the amount and rate of entrainment in debris flow analysis which includes static approach and the dynamic approach. In the static approach, static shear stresses beneath the debris are calculated and failure is considered when the static shear stress exceeds the shear strength of the material. The depth in which failure occurs is determined and the amount of material is calculated which will be added to the main body of the debris.

In the dynamic approach, the rate of erosion is determined based on shear failure at the channel surface and the material is removed from the surface based on the velocity of flow of the main body of the debris (Medina et al. 2008a). It is assumed in this approach that the velocity of newly eroded material is the same as the average velocity of the debris flow. However field observations indicate that the velocity of the newly eroded material is not same as the debris (Fraccarollo and Capart 2002; Medina et al. 2008b). The main difference between static and dynamic approaches are that, the rate of erosion is estimated based on the stress (force) equilibrium of erodible layer for static approach, instead of on the net driving shear stress which is the difference between shear stress and shear resistance.

Egashira et al (2001) proposed a formula to calculate erosion rate assuming that the slope of the channel bed is always adjusted to the angle corresponding to limiting equilibrium conditions. The material in the channel left behind by an unsaturated debris will approach the limiting equilibrium slope angle. Geometrical relationship between the initial bed slope and equilibrium

slope angle is incorporated into mass conservation law of eroded material to obtain the entrainment rate.

The entrainment model proposed by van Asch et al. in 2004 (Luna et al. 2012) is a dynamic one dimensional debris flow model that takes into account the entrainment concept based on the generation of excess pore water pressure under undrained loading on in-situ material. Flow is treated as laminar, single phase and as an incompressible continuum process. Due to the moving mass flowing on top of the erodible bed, a loading on the bed deposits is generated. The model calculates this applied load on the in-situ soil through changes in the vertical normal stress and shear strength caused by the debris flow. The increase in pore water pressure is calculated based on the Skempton (1954) equation. The depth of erosion is approximated using the relationship between the factor of safety at the bottom and top of soil in the channel. The model proposed by van Asch is similar to depth-integrated model except that it calculates the factor of safety for the erodible layers.

Iverson (2012) considered the behavior of a slide block descending an erodible slope with the ability of incorporating soil on the static bed. Newton's second law is first applied on the sliding material. Then, Coulomb friction rule is applied and basal friction resistance calculation is improved by taking the shear rate into account. The frictional resistance consists of a constant component of frictional resistance and a velocity-dependent component. After considering the rate-dependent friction, the rate of erosion based on the change in weight of the sliding block can be obtained. Iverson and Ouyang (2015) updated their theory with jump conditions between layers are considered.

De Blasio et al. (2011) suggested a semi-empirical model to calculate entrainment. In the semi-empirical model, entrainment rate depends solely on the tangential component of weight at the

base of the flow and on the average velocity of the debris flow. Critical shear stress is used as the thereshold to determine the occurance of entrainment. Data from Fjæland debris flow used for dynamic quantities and for erosion effects is utilized to calibrate the model. This model seems promising since it relates debris flow velocity and basal shear stress to entrainment.

5.3. Numerical model of entrainment

5.3.1. Mathematical model

Entrainment is a common phenomenon in debris flow. Conventional analytical entrainment models consider shear failure of erodible bed. It is assumed that shear stress in the channel bed due to debris flow is sufficiently high to incorporate erodible material lying on channel bed. In the static approach, static equilibrium between the flow frictional forces, τ_b, and the basal resistance forces, τ_{res}, should be satisfied at each computational time step (Medina et al. 2008a). If no equilibrium exists, the model estimates the magnitude of entrainment using equation [5-1].

$$\tau_b + h_{ent}\rho g \sin\theta = c + \left|h + h_{ent}\right| \rho g \cos\theta \tan\phi_{bed} \qquad [5\text{-}1]$$

where h_{ent} is the depth of erosion , θ is slope angle, c is the cohesion, h is flow height, g is gravitational acceleration and ϕ_{bed} is the bulk friction angle of the bed material.

In the dynamic approach, failure mode is considered as the same as that in the static approach except that Newton's Second Law of Motion is applied on the erodible material. Therefore the amount of entrained material depends on the availability of momentum (Medina et al. 2008b), given by:

$$\frac{\partial z}{\partial t} = \frac{(\tau_b - \tau_{res})}{\rho V} \qquad [5\text{-}2]$$

where $\partial z/\partial t$ is the rate of entrainment and V is the mean velocity of flow.

In the new entrainment model, granular particles lying on channel bed are eroded progressively. Granular particles are assumed to be uniform size spheres (disks in the case of 2D analysis). Particles are mobilized due to shear stress applied on the particles. According to the analysis by Cheng et al. (2003) and Shodja et al. (2003), the drag force to initiate rolling action is normally less than that required for basal shear failure. Therefore it may be considered that rolling motion is the dominant motion in the initial stage of entrainment. However both rolling motion and shear action should be considered in the calculation of entrainment. Drag forces due to the moving debris above the bed are assumed to apply at the center of each erodible particle. It is assumed that the particle will rotate around the point at which it contacts with the adjacent particle located downstream (Figure 5-1). Newton's Law of Motion is applied to calculate acceleration, velocity, and displacement of the particle. Taking moment about the point of contact between two particles, the rotational momentum equation is given by:

$$\frac{TR}{\left(I+mR^2\right)}sin\alpha_t - \frac{mgR}{\left(I+mR^2\right)}\cos\left(\alpha_t+\theta\right) = \frac{\partial^2\alpha_t}{\partial t^2} \qquad [5\text{-}3]$$

where T is the drag force required to initiate particle rolling, R is the radius of the rolling particle, I is moment inertial which is equal to $m\ (3R^2 + L^2)/12$, $L = 1m$ for $2D$, m is the mass of the particle (for $2D$, $m=\pi R^2\rho_b$), ρ_b is the density of bed sediment particle, α_t is the angle between channel bed and connection line of centers of those two particles, θ is the slope angle, g is the gravity acceleration, $\partial^2\alpha_t/\partial t^2$— angular acceleration and t is time. At this stage, the entrainment rate is calculated in $2D$ that means unit width ($1m$) is assumed in the calculation.

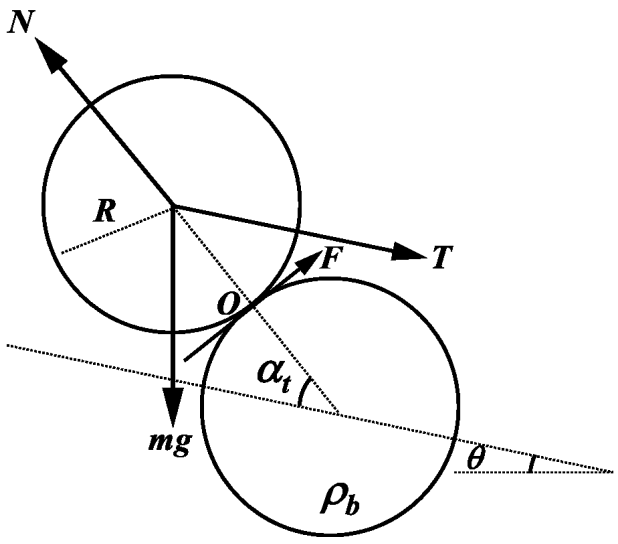

Figure 5-1: Free body diagram of particle when rolling occurs

It is also assumed in the derivation of this equation that once the particle moves over the adjacent particle located downstream, it will be considered as part of debris flow. Based on mathematical model of rolling motion (Equation [5-3]), entrainment time, the time required for one particle to move from its initial location into debris flow body, can be estimated. Hence the entrainment rate is defined as the height of particle exposed to the flow divided by time needed for it to be eroded. Therefore for different initial resting angles, α_0, the initial value of α_t, the entrainment rate, $\dot{E}_i$, is given by:

$$\dot{E}_i = \frac{2R\sin\alpha_{0i}}{t_i} \qquad [5\text{-}4]$$

where t_i is the time required for one particle to roll from the initial position, α_0, to vertical line at which α_t equals $(\pi/2-\theta)$, because it is assumed that once the a particle moves over the particle in front of it, it will be considered as part of moving debris. Therefore, if shear force exerted on the particle is known and the properties of the particle are determined, t_i, can be obtained from

equation [5-3]. When shear force exerted on the particles is larger than the friction between the particles, the moving process changes from the rolling motion to the sliding motion.

Since α_0 varies from point to point and it is not easy to determine its values for all points in the domain, a probabilistic approach is used to calculate the statistical distribution of α_0 for a given case. It is assumed that the value α_0 can be approximated by a probability density function (PDF). Selecting the proper parameters for the PDF is important in entrainment calculation. Some parameters like the mean value of the normal distribution function could be estimated from pivoting angle which could possibly be measured for a given site (Fenton et al. 1977). However the values are site specific. Alternatively it can also be estimated according to the relationship between void ratio and internal friction angle, and relationship between particle protrusion and void ratio (Okada et al. 2007). After a PDF has been determined and the entrainment rate for each specified value of α_0 is calculated, the overall entrainment rate can be calculated from:

$$\dot{E} = \sum_{i=1}^{n} \dot{E}_{\alpha_0} \qquad [5\text{-}5]$$

in which n is the number of division between *0* and *90* degrees based on the increment of α_0.

5.3.2. Numerical solution for entrainment calculation

The finite difference method is used to solve equation [5-3] numerically. Based on the forward difference scheme, the first and second derivative of α_t with respect to time are:

$$\frac{\partial \alpha_t}{\partial t} = \frac{\alpha_t^{i+1} - \alpha_t^{i}}{\Delta t} \qquad [5\text{-}6]$$

$$\frac{\partial^2 \alpha_t}{\partial t^2} = \frac{\alpha_t^{i+2} - 2\alpha_t^{i+1} + \alpha_t^{i}}{(\Delta t)^2} \qquad [5\text{-}7]$$

Therefore the finite different form of the entrainment equation is given by:

$$\frac{T\,R}{\left(I+m\,R^2\right)}\sin\alpha_t^i-\frac{m\,g\,R}{\left(I+m\;R^2\right)}\cos\left(\alpha_t^i+\theta\right)=\frac{\alpha_t^{i+2}-2\alpha_t^{i+1}+\alpha_t^i}{\left(\Delta t\right)^2} \qquad [5\text{-}8]$$

Two initial conditions are required. They are $\alpha_t\big|_{t=0}=\alpha_0$ and:

$$\left.\frac{\partial\alpha_t}{\partial t}\right|_{t=0}=0 \qquad [5\text{-}9]$$

Once these conditions are known, the time needed for α_t changing from α_0 to $(\pi/2-\theta)$ can be obtained from equation [5-8]. Therefore, t for each α_i, t_i, can be determined. Based on t_i, the depth of erosion for each α_0 can be determined. Utilizing the PDF, the entrainment rate for each slice for different values of α_0 can be obtained. Since the shear force underneath each slice is not same, T in equation [5-8] is different for each slice. Consequently, the individual particle entrainment rate and the overall entrainment rate can be calculated from equations [5-10] and [5-11] respectively:

$$\dot{L}_{k} \qquad \frac{\sin\alpha_{0i}}{t_i} \qquad [5\text{-}10]$$

$$\dot{L}_{k} \qquad \sum_{i=1}^{n} \qquad [5\text{-}11]$$

where subscript k is the slice number varying from $k=1$ to $k=n$.

5.4. Implementation of entrainment calculation in runout analysis

5.4.1. Runout model

As described in previous section, two approaches have been adopted to simulate debris flow runout process. Since the energy based runout model considers internal energy dissipation during

the movement of the debris which is important for the landslides with large deformation such as flow slides and debris flow (Wang et al. 2010), it is used to incorporate the new entrainment model.

As a slice-based model, the energy model determines the motion of each slice using the equations of energy conservation in the Lagrangian framework (Wang et al. 2010). The change of kinetic energy of a sliding mass is equal to the change of potential energy, work done by resistance force along the base of the sliding mass and deformation work. Lateral pressure and basal resistance on individual slices are determined from the Rankine and Mohr-Coulomb equations. The governing equation of the runout model is:

$$\frac{d}{dt}\left(\frac{1}{2}m\bar{u}^2\right) = mg\bar{u}\sin\theta + \frac{1}{2}mghe_{zz} + P_L\bar{u}_L\cos\theta_L - P_R\bar{u}_R\cos\theta_R - T\bar{u} - \int_V \tau_{ij}e_{ij}dV \quad [5\text{-}12]$$

where m is the mass of the slice, $\bar{u}$ is the mean velocity of the slice along the base of the slice, g is gravity acceleration, θ is the inclination of the base of the slice with respect to the horizontal, P_L and P_R are interslice forces exerted on left and right sides of the slice, T is the shear force acting along the base of the slice, τ_{ij} are components of the stress tensor and e_{ij} are components of the strain rate tensor. Figure 5-2 shows the components of force in equation above.

5.4.2. Incorporation of entrainment in runout analysis

Figure 5-2 shows the incorporation process of the progressive scouring model into the energy based runout model. Figure 5-2a indicates the initial state of the slices without entrainment process. The forces exerting on the slice are also labeled. Figure 5-2b indicates the incorporation process. The deformation of the slice, variation of the slice and change of the channel bed are also shown.

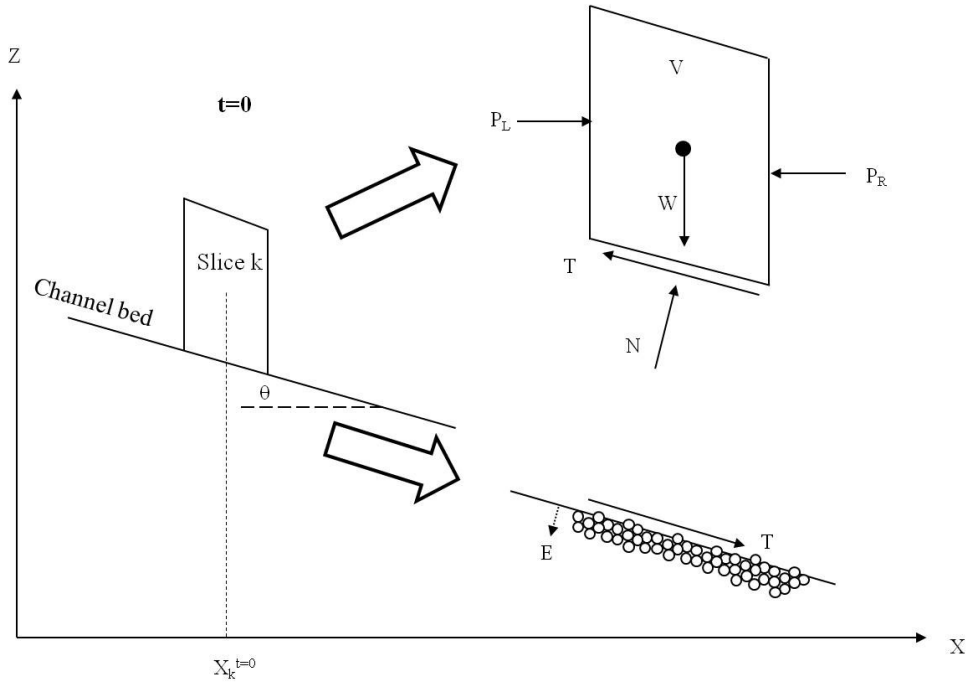

(a)

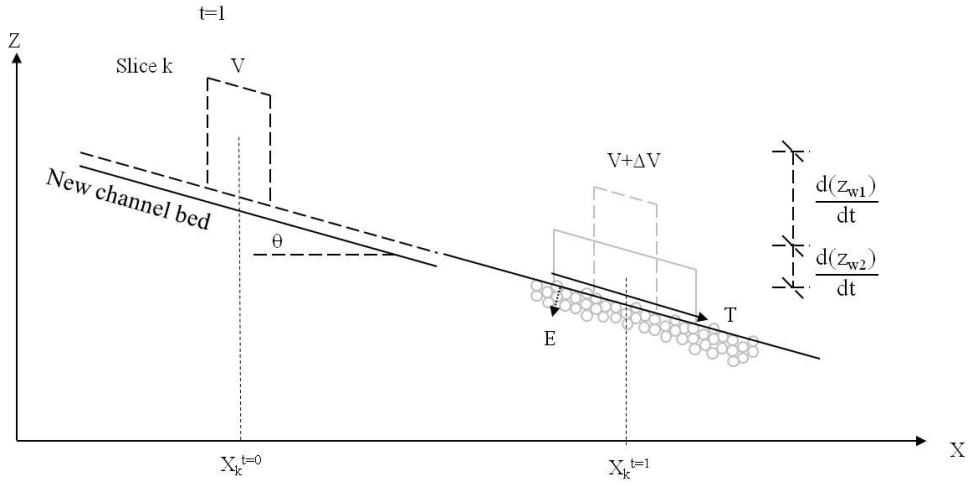

(b)

Figure 5-2: Schematic of entrainment process. ((a) shows forces acting on a single slice in the runout model before entrainment is incorporated; (b) indicates change of the slice after entrainment.)

During the entrainment process, the volume of moving debris is increased by eroding loose material lying on the channel bed. The elevation of channel bed is also changed due to erosion. Therefore it is essential to increase the volume of each slice due to entrainment since volume change could impact the shear stress acting on the channel bed. The change of slope angle is also important in the calculation of the rate of erosion. The change in volume in each time step and its effect on flow height are given by:

$$V_k^{t+\Delta t} = V_k^t + \Delta V \qquad [5\text{-}13]$$

$$\left(h_c\right)_k^{t+\Delta t} = \frac{V_k^{t+\Delta t}}{\left(x_b\right)_{k+1}^{t+\Delta t} - \left(x_b\right)_k^{t+\Delta t}} \qquad [5\text{-}14]$$

The depth of erosion under each slice is equal to the entrainment rate multiplies by the entrainment time. The entrainment volume of each slice in each time step is shown in Figure 5-3. If the displacement in each time step is less than width of the slice, $\Delta V = b\,\dot{E}\,\Delta t$ indicated in (i) (2D). Otherwise, entrainment volume should be estimated using $\Delta V = s\,\dot{E}\,\Delta t$ shown in (ii). During each time step, the entrainment rate is assumed constant underneath each slice. Souring due to slide deformation is neglected here. As the slice moves across the erodible zone, the sides of the entrainment area in Figure 5-3 are inclined which slope is equal to $\dot{E}\,\Delta t / b$. Generally if time step is small enough, $b\,\dot{E}\,\Delta t$ is adopted, which is closer to the real erosion process that is a progressive process. The depth of erosion of adjacent slides is accumulated. For slides having the same entrainment rate and displacement, the accumulated depth of erosion is illustrated in Figure 5-4. If the displacement and entrainment rate are not same, the principle of accumulation is identical, but the accumulated depth of erosion is undulate.

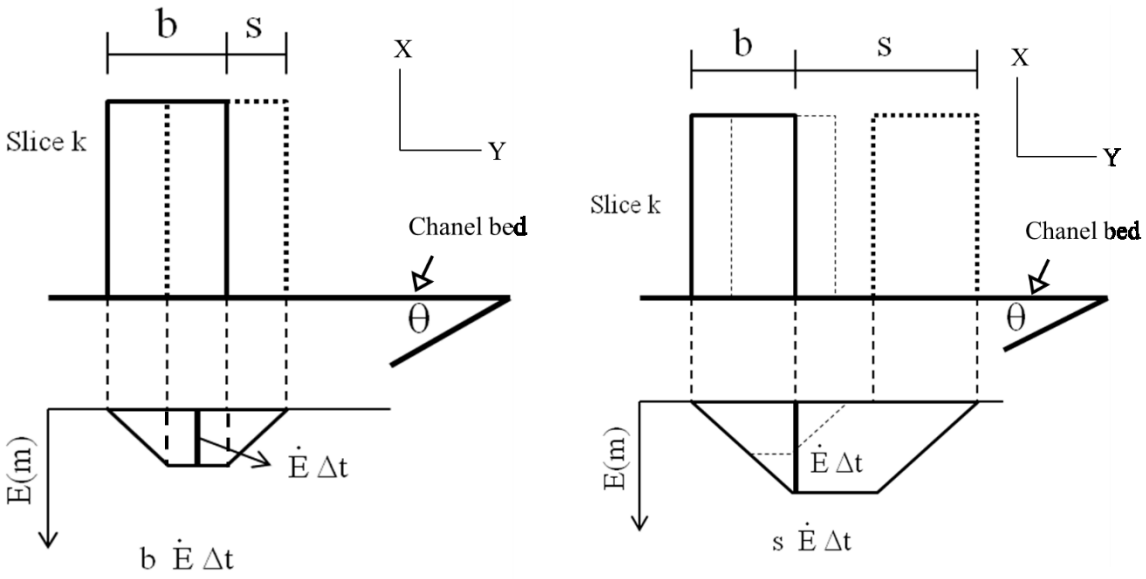

(i) **(ii)**

***b*--- width of slice; *s* --- displacement of slice;**

Figure 5-3: Schematic of entrainment caused by a moving slice

Figure 5-4: Accumulation of entrainment for three slices

The profile of the channel bed also changes due to entrainment which can be adjusted according to equation [5-15]. If no slice crosses bed points in each time step, elevation of bed points is modified by subtracting the depth of erosion of the slice just on the top of bed point if any. More points in defining the channel bed can be used for higher accuracy of entrainment variation along the channel bed. In addition, time step together with the velocity of each slice can impact the calculation of entrainment depth.

$$Z_{bi}^{t} = Z_{bi}^{t-1} - \sum_{m}^{n} \left(\quad \right) \qquad [5\text{-}15]$$

$\dot{L}_{bi}$ is determined by estimating the depth of erosion due to slices which crosses the bed point at each time step. *m* is the number of slices at the left of bed nodes at the end of each time step; *n* is the number of slices at the left of bed nodes before each time step; t_{ei} is time needed for the slice to cross the bed point

In the model, slices of unit width are simulated. It is suggested that the cross section of each slice can be abstracted into trapezoid shape with different slope ratio at two sides (Figure 5-5). In so doing, lateral friction force exerted on moving slides can be taken into account.

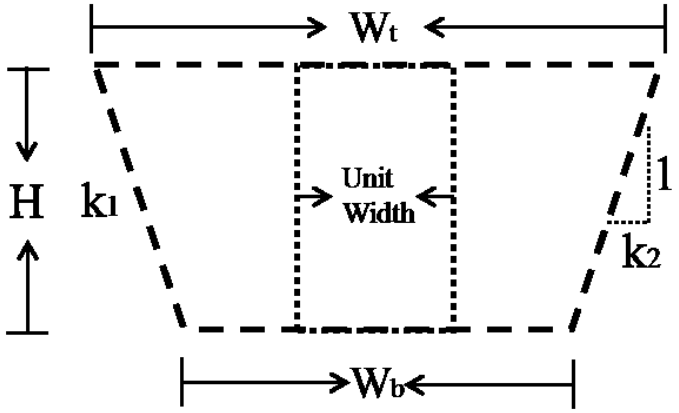

H--- height of debris; k_1--- slope ratio of left size; k_2--- slope ratio of right side; W_b--- width of channel base; W_t--- width of channel top;

Figure 5-5: Cross section of debris flow in the simulation

5.5. Sensitivity analysis of the entrainment runout model

After the new entrainment model is incorporated into the energy-based runout model, a sensitivity analysis of the model parameters has been carried out which includes mean value of PDF, internal friction angle, turbulent coefficient and basal friction angle. Sensitivity analysis results are presented by calculating the percentage change from the base case.

The critical parameters in rheological, entrainment and runout models are being studied. The parameters used for sensitivity test are varied one at a time. To make the sensitivity results comparable and consistence, each parameter is increased or decreased by the same values: 10% and 20%.

Since the entrainment model will be applied to study real case, profile from a real case, Tsingshan debris flow, is used, which will be also used a case for the application of the new runout out model with entrainment included. The selection of base case in sensitivity test is from the parameters measured in field (Lo and Chau 2003).

To evaluate the effect of changing model parameters on the results of the debris flow analysis, the maximum velocity at the front of the debris, runout distance, total volume and maximum entrainment rate are being evaluated and compared with the base case. The channel profile used in the analysis is shown in Figure 5-6. The profile is divided into three parts: trigger zone, erosion zone and deposition zone according to Lo and Chau (2003).

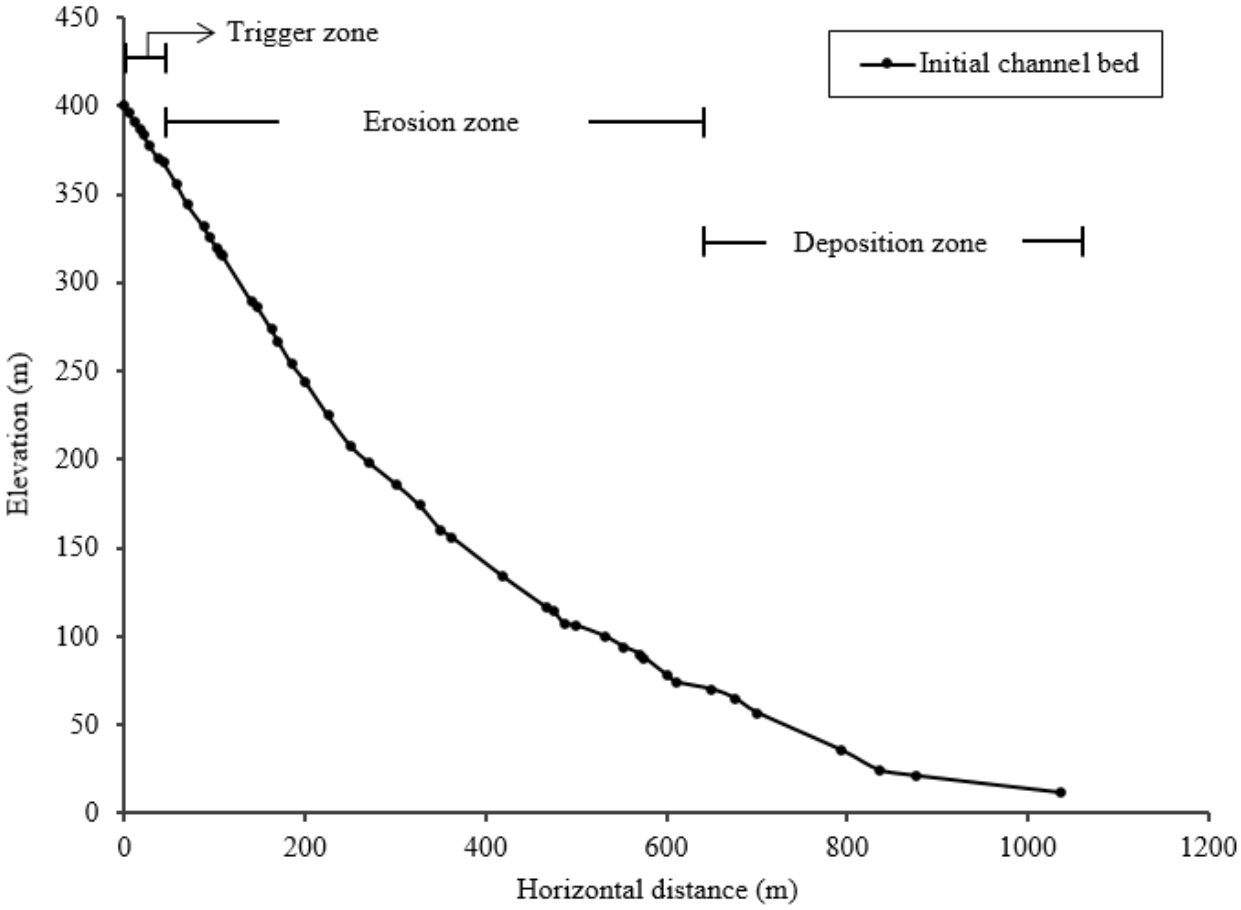

Figure 5-6: Longitudinal profile used in the sensitivity analysis

Table 5-1: Parameter for the base case in sensitivity analysis

Entrainment model parameters	Values	Runout model parameters	Values
Particle size d_{50} (mm)	50	Unit weight (kN/m^3)	20
Standard deviation	0.1	Internal friction angle (°)	25
Mean value of PDF (°)	18	Basal friction angle (°)	14
Expansion ratio	1.2	Turbulent coefficient (m/s^2)	300
Particle density (kg/m^3)	2600		

The results of sensitive analysis are shown in percentage change from the base case as shown in Figure 5-7. It is found that most sensitive soil properties in the model is basal friction angle. It has significantly impact on the runout distance, maximum debris flow height and longitudinal length of deposition zone. It also changes the maximum frontal velocity and final total volume

with lesser effects. Increasing the basal friction angle could greatly decrease the runout distance and longitudinal length of deposition.

The internal friction angle of the debris controls the lateral force between the slices. The interslice force can be in an active, passive or static state depending on the interslice relative velocities in the longitudinal direction. Based on the results from the sensitivity analysis, larger frontal velocity and longer runout distance are due to smaller internal friction angle.

The most important single parameter affecting entrainment is the mean value of the initial resting angle α_o in the probability density function. A 10% increase in the mean value of α_o results in 40% increase in entrainment. It also has an effect on the maximum front velocity. If the mean of value of α_o is increased by 20%, the total volume is increased around 91%, the entrainment rate is increase by 70% and the frontal velocity is increased by 16%. It also increases the runout distance and maximum height of the debris, but the changes are comparatively smaller.

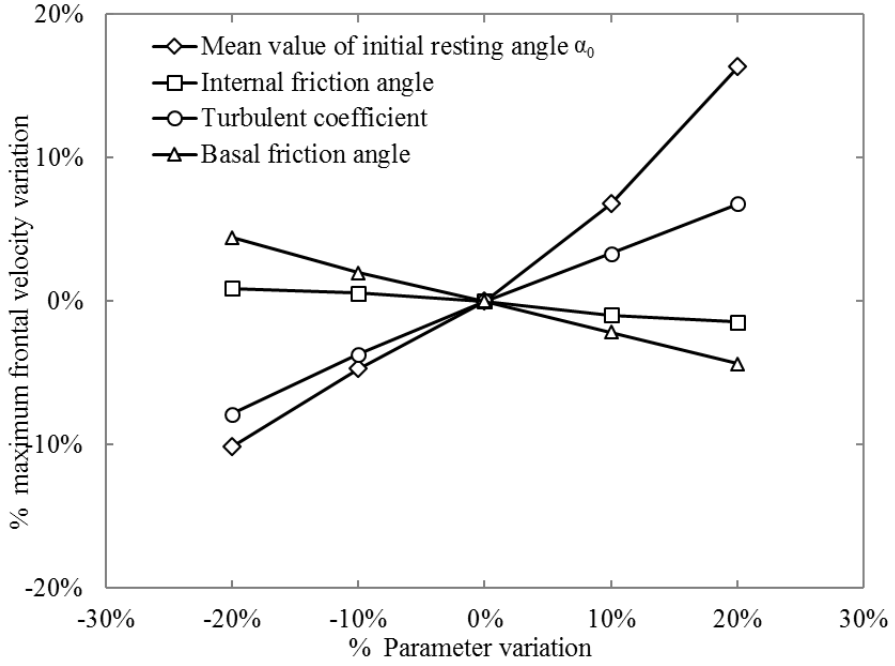

(a)

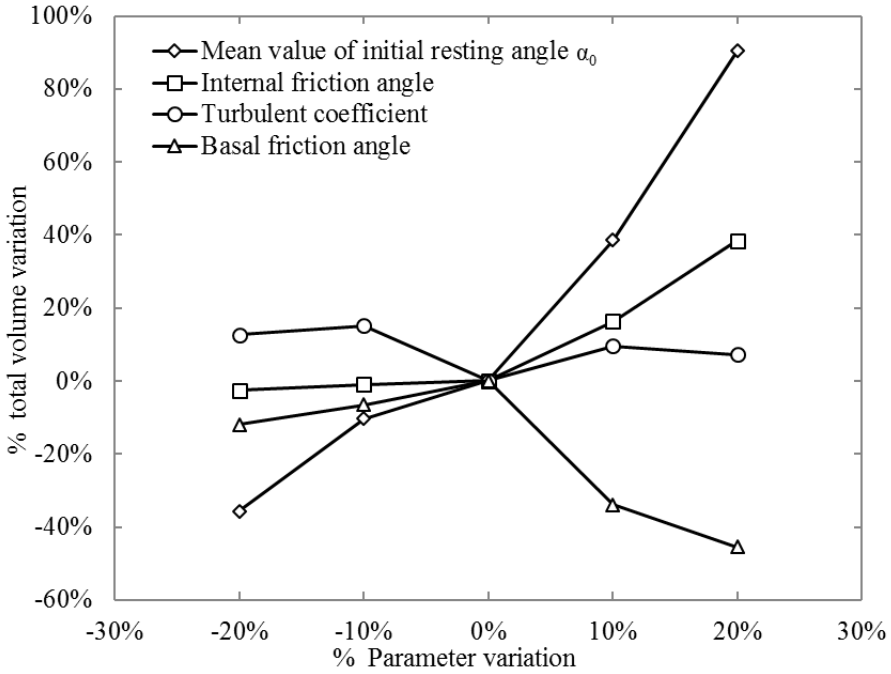
Mean value of initial resting angle α_0
Internal friction angle
Turbulent coefficient
Basal friction angle
% total volume variation
% Parameter variation
100%
80%
60%
40%
20%
0%
-20%
-40%
-60%
-30%
-20%
-10%
0%
10%
20%
30%

(b)

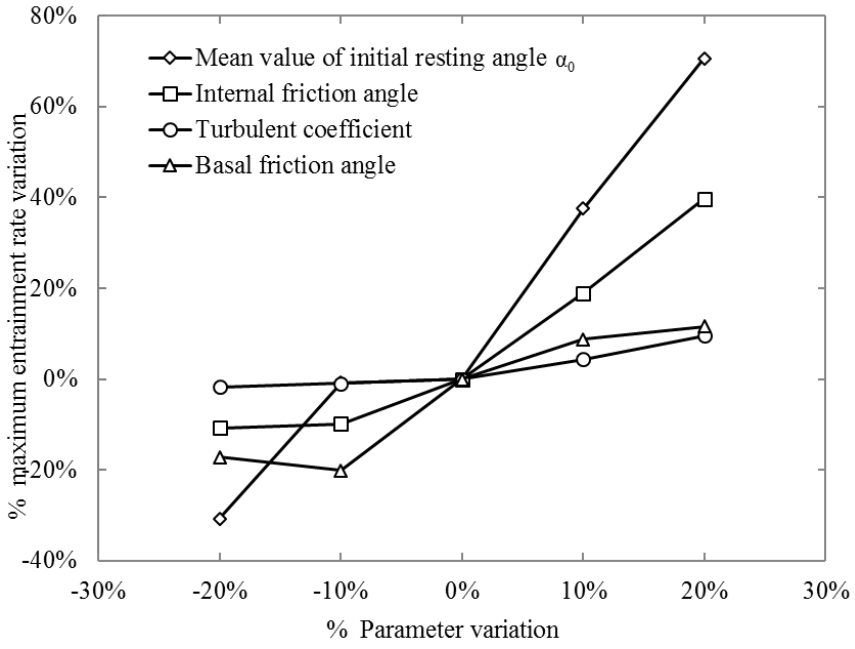
Mean value of initial resting angle α_0
Internal friction angle
Turbulent coefficient
Basal friction angle
% maximum entrainment rate variation
% Parameter variation
80%
60%
40%
20%
0%
-20%
-40%
-30%
-20%
-10%
0%
10%
20%
30%

(c)

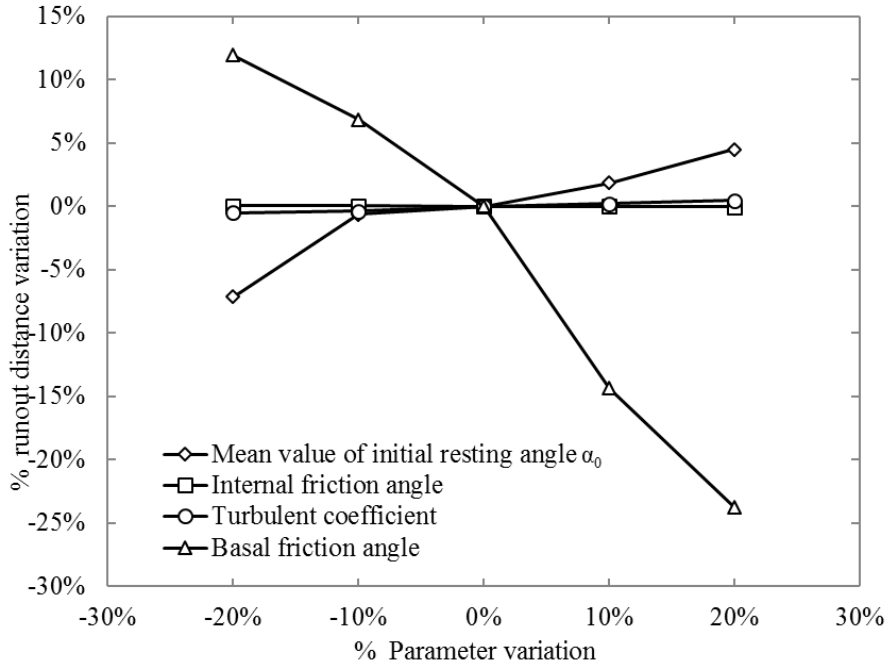
15%
10%
5%
0%
-5%
-10%
-15%
-20%
-25%
-30%
% runout distance variation
Mean value of initial resting angle α_0
Internal friction angle
Turbulent coefficient
Basal friction angle
-30%
-20%
-10%
0%
10%
20%
30%
% Parameter variation

(d)

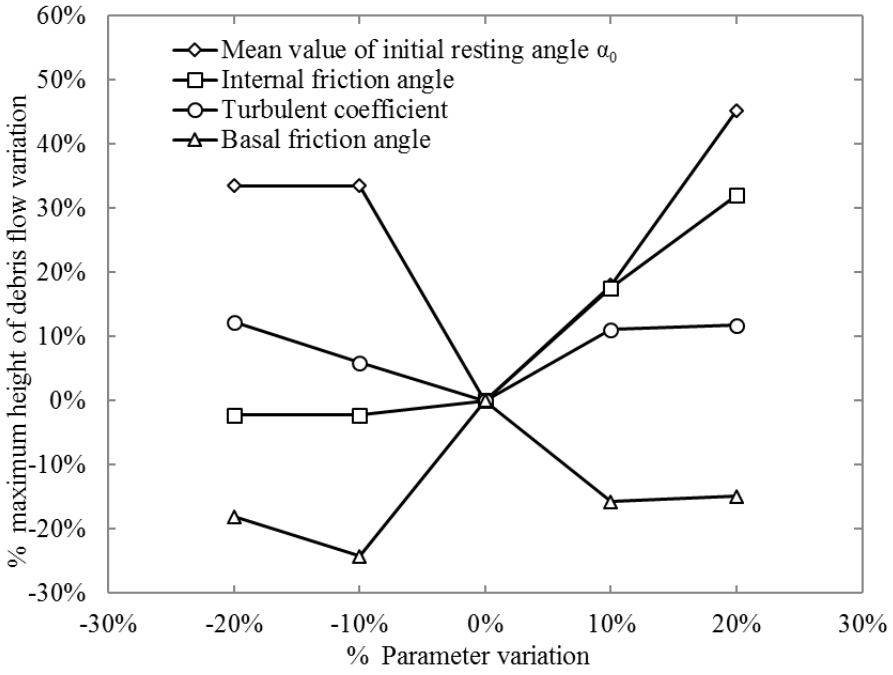
60%
50%
40%
30%
20%
10%
0%
-10%
-20%
-30%
% maximum height of debris flow variation
Mean value of initial resting angle α_0
Internal friction angle
Turbulent coefficient
Basal friction angle
-30%
-20%
-10%
0%
10%
20%
30%
% Parameter variation

(e)

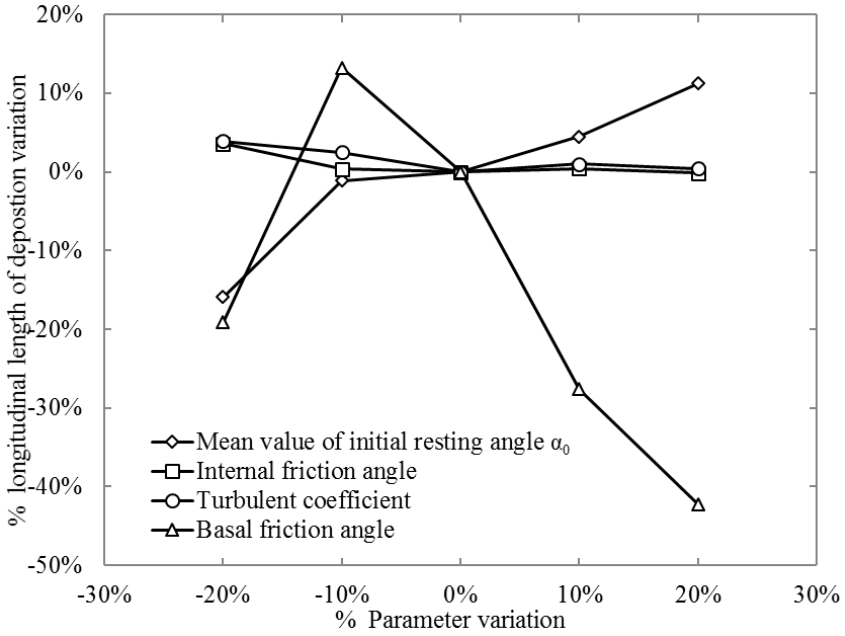

(f)

Figure 5-7: Variation percentage of debris flow properties by varying parameters in runout and entrainment models. (a) shows the variation of maximum frontal velocity, (b) shows the change of total volume, (c) indicates the variation of maximum entrainment rate, (d) shows the variation of runout distance, (e) show the variation in maximum height of debris flow and (f) is the variation longitudinal length of debris flow

The sensitivity test results demonstrate that mean value of PDF is mostly very sensitive in the calculation of maximum frontal velocity, total volume, maximum entrainment rate and maximum flow height. Turbulent coefficient is critical in the calculation of maximum frontal velocity. Basal friction angle is important in the calculation of runout distance and longitudinal distance of debris flow deposition fan. Therefore, in the modelling, the selection of the mean value of PDF should be very careful which can refer to the protrusion angle of granular particles.

5.6. Case study of Tsing Shan debris flow (1990)

5.6.1. Introduction

To apply the runout model with the entrainment model into a case study, a real case with significant entrainment, Tsingshan debris flow (1990) is chosen. The Tsing Shan summit and ridge tops are generally rounded with occasional isolated outcrop and gullied areas. The eastern side upper slopes has an overall gradient of about $45°$. The lower slopes flatten from $37°$ near the granite contact to $20°$ at the toe. The geology profile can be found at Lo and Chau (2003). The footslopes of Tsing Shan have an overall slope angle of about $10°$ south-east towards the pre-development coastline. The dash line in Figure 5-8 is used to obtain longitudinal profile that will be used in runout analysis.

The 1990 Tsing Shan debris flow occurred on the eastern flank of Tsing Shan (also called Castle Peak) Hong Kong (Figure 5-8), in the early morning of September 11, 1990. The event was triggered by a rockslide of volume 355 m^3 near the peak after a heavy rainstorm (Figure 5-9) (King 1996). As the debris travelled downslope along a drainage line, significant entrainment of the loose bouldery colluvium occurred. This process escalated the debris flow volume during movement. The final volume of the debris was estimated to be 19,000 m^3 with a travel length of around 1km. The widest lateral spread was 120 m and the deposit thickness was up to 2m (Lo and Chau 2003).

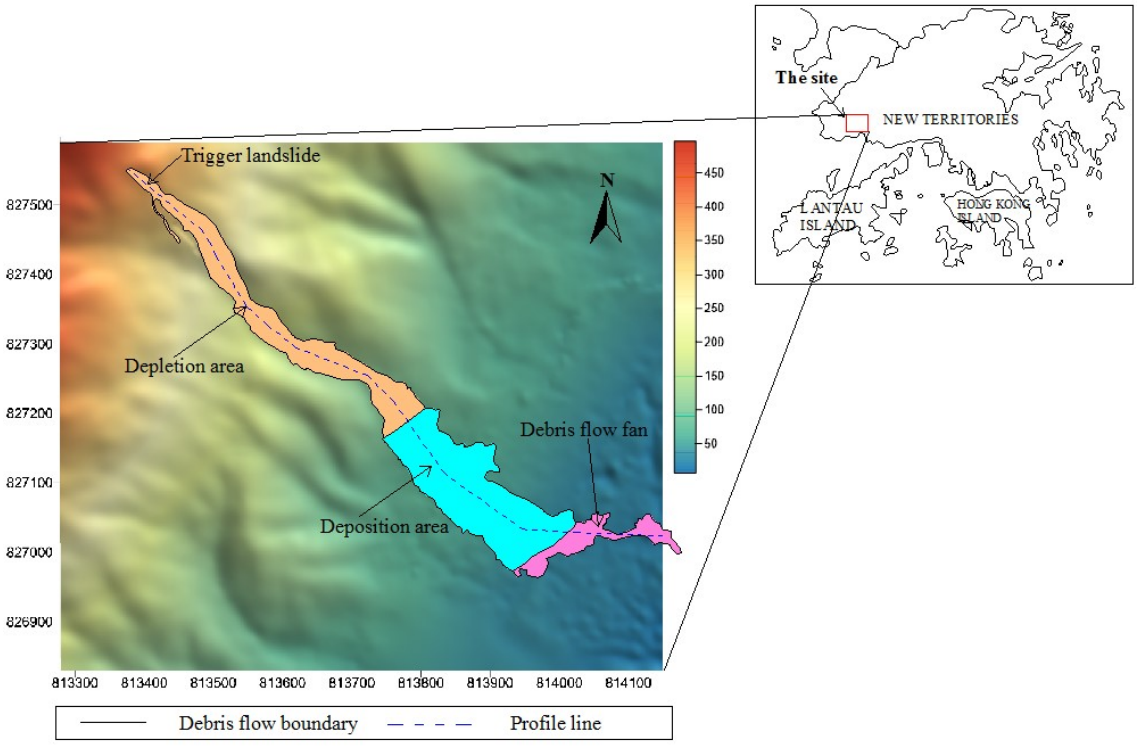

Figure 5-8: Location map & Digital Elevation Model of 1990 Tsing Shan debris flow

The summit and upper slopes of Tsing Shan are made of fine grained granite. Downslope from the granite on the lower slopes and footslopes of the eastern side of Tsing Shan, sedimentary and volcanic rocks of the Upper Jurassic being part of the Repulse Bay Volcanic Group. On the lower slopes these are the sedimentary rocks of the Tsing Shan Formation which comprises of sandstone, siltstone and mudstone with conglomerate and tuff. The debris flow scar is generally incised into deposits of colluvium. It starts on the granite upper slope, passes the sedimentary rocks and ends on the volcanic rocks and the footslope.

The closest rain gauge to the site of the Tsing Shan debris flow is located less than 1.5 km from the catchment. It is concluded that this rain gauge is likely to provide the best temporal distribution of rainfall in the catchment but the totals recorded values might be higher than that actually occurring in the catchment due to delayed orographic effect. Rain gauge data in 15

minute interval for the preceding 24 hours of the event are shown in Figure 5-9. It clearly shows that there was intense rainfall before the debris flow event.

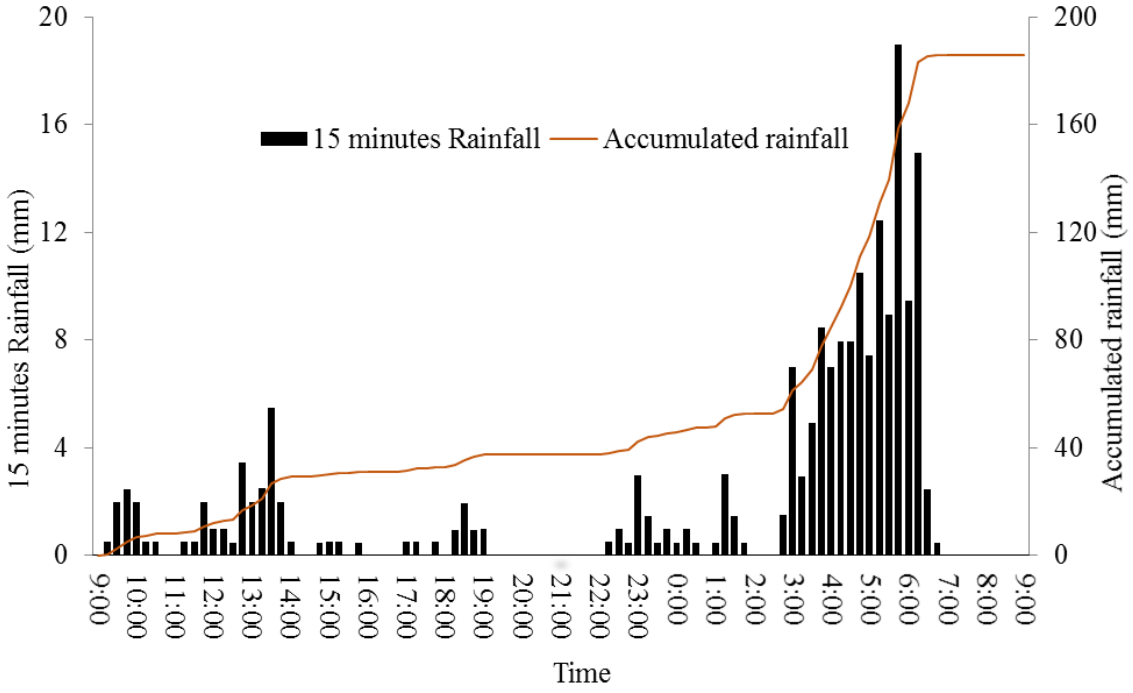

Figure 5-9: Rainfall Data from 10/09/90 to 11/09/90 (Rain gauge No. N07) (King. 1996)

The debris flow involved erosion and transportation of soil and rock from the flanks of Tsing Shan, and the deposition of the materials along the scar and at the toe of the slope. Entrainment and deposition volume at different sections was investigated. By measuring the area of each section from Figure 5-8, average entrainment and deposition depth are shown in Figure 5-10. The "maximum" entrainment and deposition depth are around 1.6 m and 2 m, respectively. If erosion depth is assumed to be evenly distributed along the path of the debris flow, the maximum depth of entrainment would be higher than the average value at some sections.

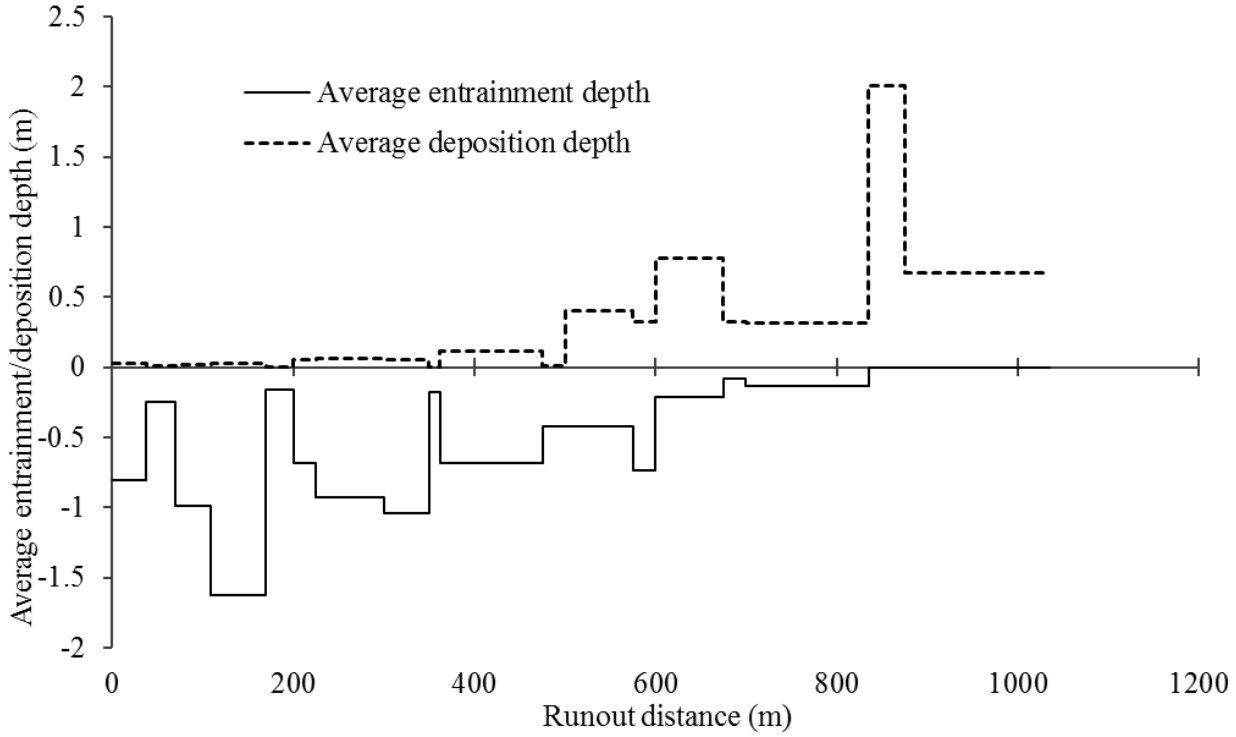

Figure 5-10: Average entrainment and deposition depth along the debris flow moving path (adopted from Lo and Chau 2003)

5.6.2. Parameters selection

In the runout analysis, parameters for the model are determined based on laboratory test and field investigation (King, 1996; Sun, Lam, and Tsui, 2003) and previous numerical simulation results (Hungr, 2008). To determine the particle size distribution in the erodible channel, two soil samples, D19 and D20, collected from the deposition area were tested (King, 1996). The grain size distribution of these two samples are shown in Figure 5-11. Since the samples only include particle size of less than 100 mm, the percentage of large size boulder is being estimated. The mean particle size in this case is approximately estimated as d_{50} = 50mm, which will be used in the entrainment analysis.

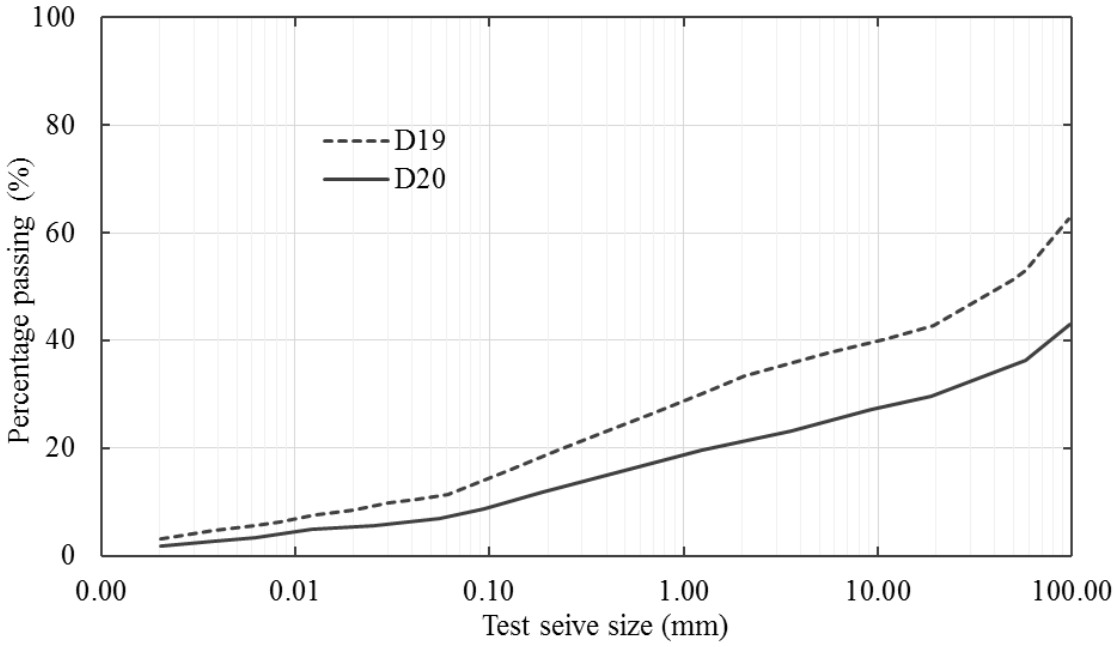

Figure 5-11: Estimated particle size distribution curve of debris (King, 1996)

Strictly speaking, α_0 is not a constant value. Instead, it varies along the channel and is different between locations. To simply the estimation, a constant value is used in the simulation. Generally, slope angle of a heap of loose granular particles is the angle of repose of those particles, so the maximum angle of a slope consisted of loose granular particles could indicate angle of repose of such particles. Therefore, it is supposed that maximum slope angle equals to angle of repose of such material. By relating the angle of repose to α_0 in the new entrainment model, mean value of normal distribution and standard deviation in the new model could be indirectly estimated. In this simulation, mean value of PDF equaling to 18º is adopted.

As in the entrainment calculation single particle is considered, the density of particle is used here. The density of particle mainly depends on the lithology of rock on site. When the particles settled on channel bed are mobilized into debris flow, their porosity normally increases, therefore expansion ratio is necessary to simulate this phenomenon. The expansion ratio is defined as the

ratio of change of density. Turbulent coefficient in the Voellmy fluid model is set as 300 m/s^2, according to previous analysis on this case (Hungr, 2008; Blanc, 2008).

Time step is also very important in runout simulation especially for complex topography. Δt_e is time step used to estimate the time needed for one particle to be removed from a fixed position. If large shear force is applied on the channel bed, smaller Δt_e should be used to minimize the error. To ensure the accuracy of simulation and use as little time as possible in the simulation, Δt and Δt_e, equalling to 0.001s, are originally used. In the simulation, Δt will adjust automatically according to the displacement of each slice. If the displacement of each slice in each time step is larger than the threshold value, Δt is adjusted to an appropriate value.

Internal and basal friction angle are selected based on the previous simulation. Summation of all the parameters used in the simulation are shown in Table 5-2. Entrainment model parameters are determined using them from laboratory testing results in the geotechnical report.

Table 5-2: Parameter used in modelling Tsing Shan debris flow (1990)

Parameters	Values
Unit weight (kN/m^3)	20
Internal friction angle (°)	35
Basal friction angle (°)	30
Particle size d_{50} (mm)	50
Mean value of α_0 (°)	23
Standard deviation	0.1
Expansion ratio	1.2

5.6.3. Simulation results

Debris flow velocities including front velocity, maximum and minimum velocity are shown in Figure 5-12. Maximum velocity appears when t = 17s. At initial few seconds, velocity of the front slide is the minimum one among all slides. After around 6 seconds later, the front one

moves with maximum velocity until debris flow stops. The gap between minimum and maximum velocity is undulant, but it is obvious that the average gap at first half part is smaller than that at second half part.

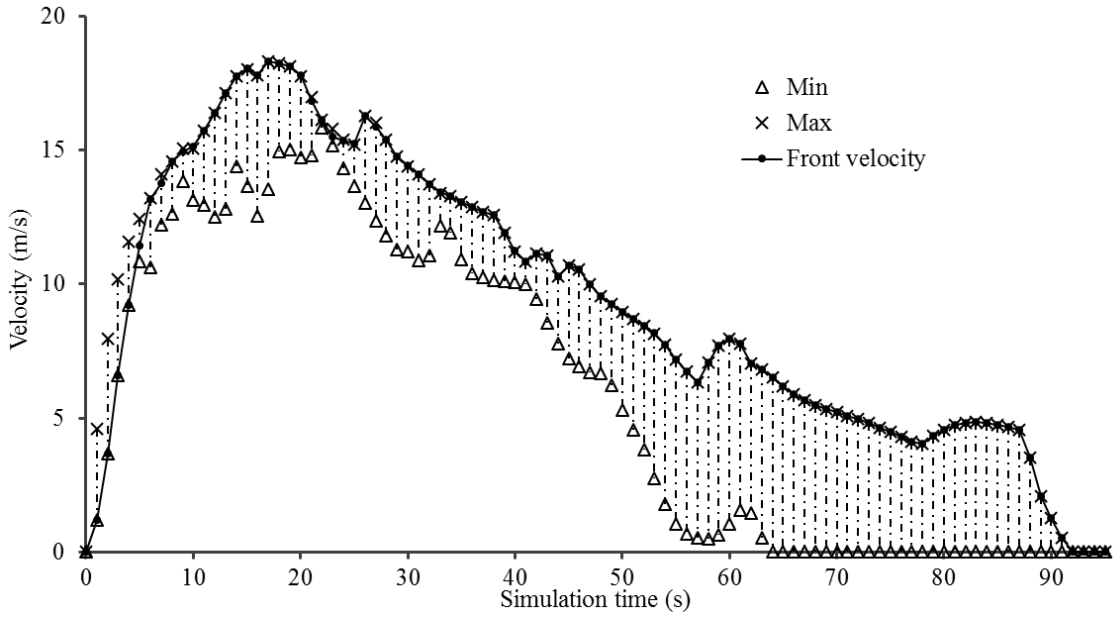

Figure 5-12: Variation of velocity along the channel bed

In Figure 5-13, location of first and last slice in the simulated are plotted. Meanwhile, maximum debris flow height is shown in the graph also. After around 50s, tail of debris flow almost stops at x = 500m when the front slice keeps moving. After few seconds later, position of maximum height stops moving. This will cause high shear stress applied on specified position for long time as Voellmy model is used in the simulation. Its effects on the rate of erosion and the depth of erosion are shown in Figure 5-14 and Figure 5-15.

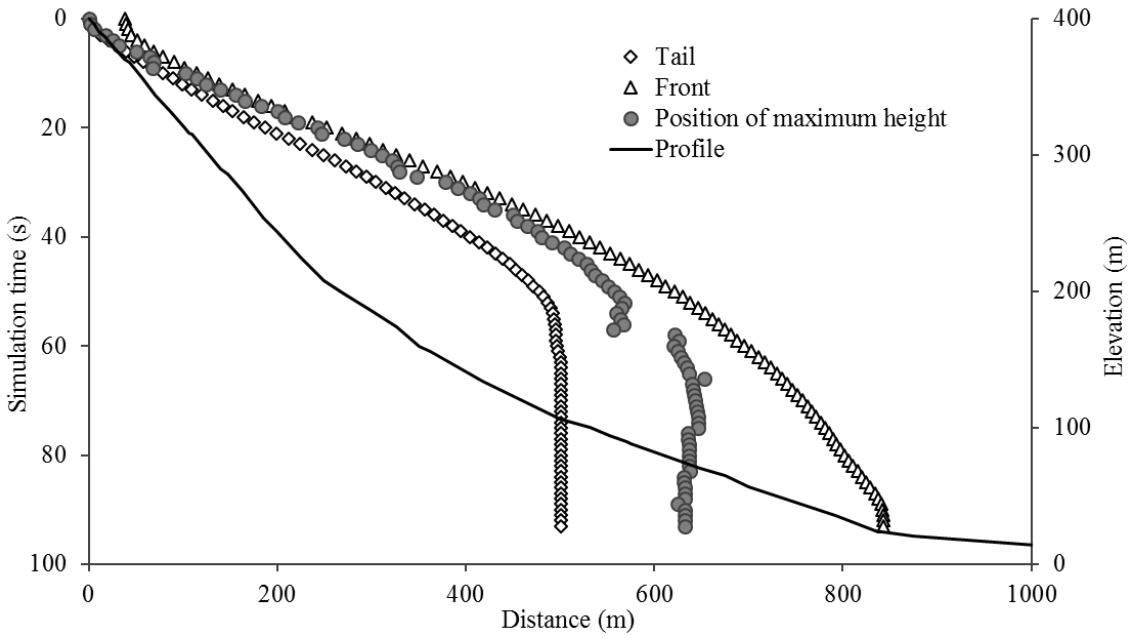

Figure 5-13: Location of tail and front of debris flow in the simulation

In Figure 5-13, after around 55 seconds, maximum height of debris stays at almost same location, this causes the height of debris increase almost linearly. The 2D simulation concerns a channelled flow modification resulting from the effect of lateral boundary discontinuity followed by free spreading. If the lateral spread is considered, the height will change a lot when the flow channel suddenly expands. The mean value of entrainment rate is around 0.17m/s. The depth of erosion is obtained by subtracting the height of flow channel after simulation from initial channel elevation. Maximum depth of erosion is 6.07m located at x≈550m. The peak in Figure 5-15 is in good agreement with maximum height of debris shown in Figure 5-13, and so is entrainment volume in Figure 5-16. Therefore, if maximum height of debris changes, the maximum depth of erosion and entrainment volume will also change.

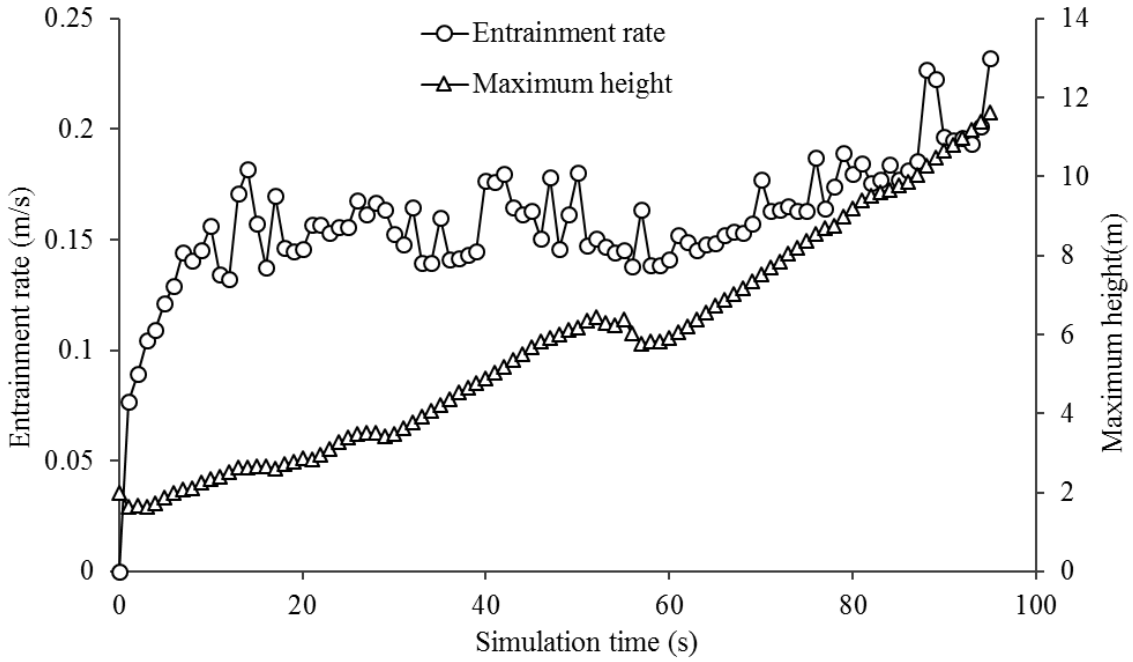

Figure 5-14: Maximum entrainment rate and flow height along the channel

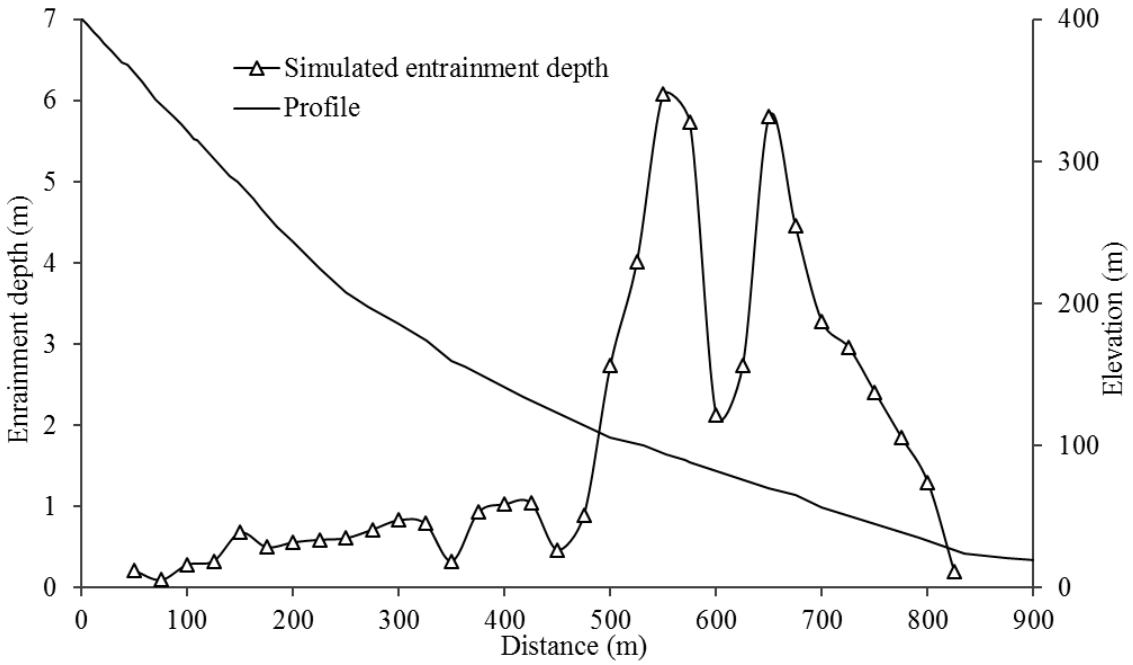

Figure 5-15: The depth of erosion along the channel

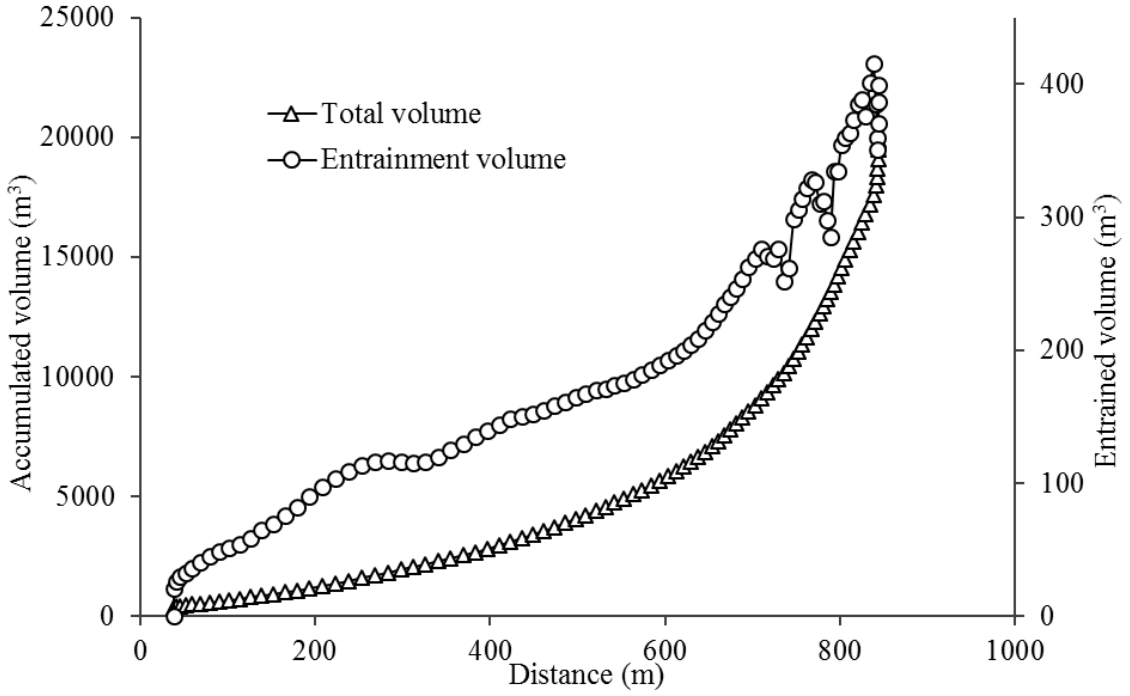

Figure 5-16: Variation of total volume along the channel bed

5.6.4. Evaluation of simulation results

Criteria used to evaluate results include front velocity, final profile and volume. The volume of final deposition investigated is about 20,000 m^3. The simulation yields a final volume of almost same number (Figure 5-16). The variation of channel width in the movement is shown in Figure 5-17. The debris flow path in the simulation, having constant width, is also indicated in the graph. Observed height and simulated height after debris flow are compared in Figure 5-18. It is clearly shown that width of flow channel is suddenly increased at 500m~750m section. This will cause the spreading of flow and lowering of flow height. Although the height of debris in the simulation, defined as deposition height minus initial channel height, is adjusted according to the local channel width, this still induces points at this section in Figure 5-18 are a bit away from line.

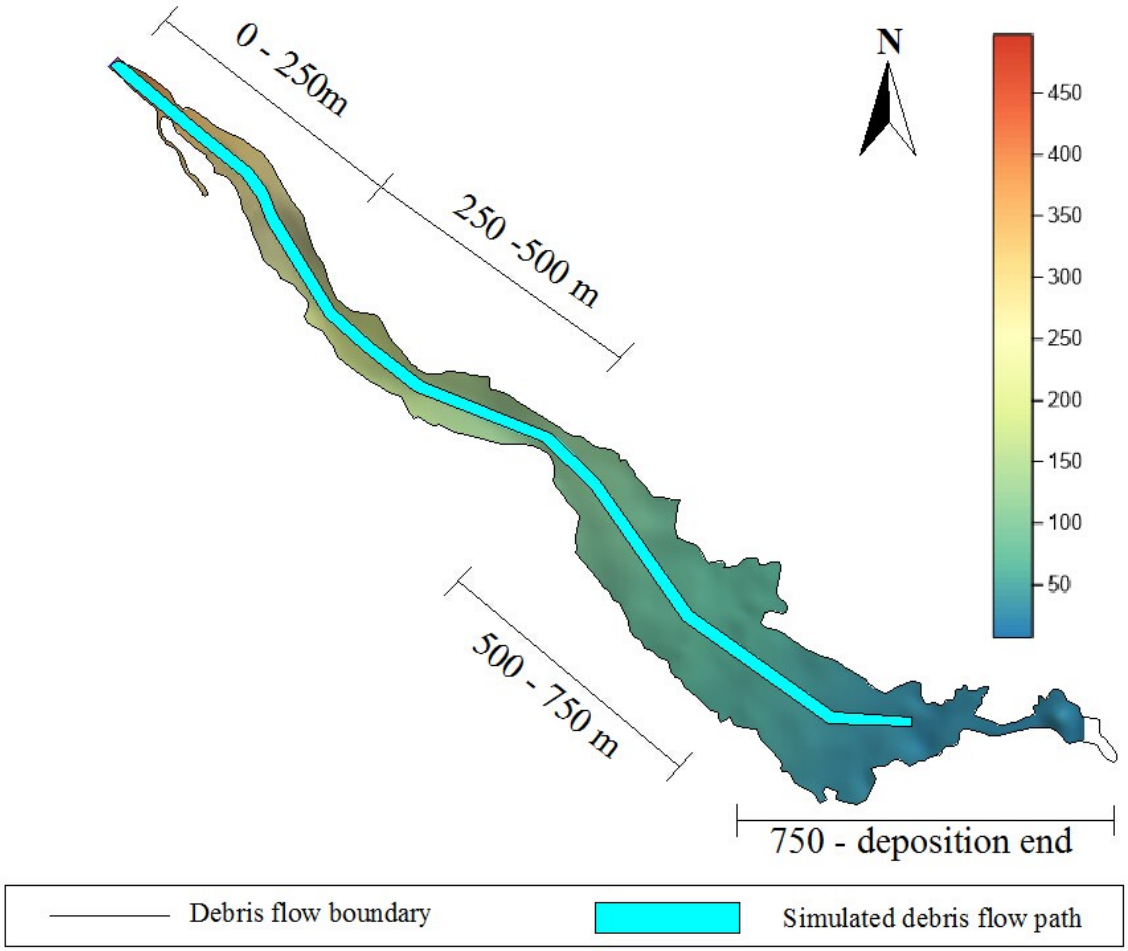

Figure 5-17: Variation of channel width in the debris flow

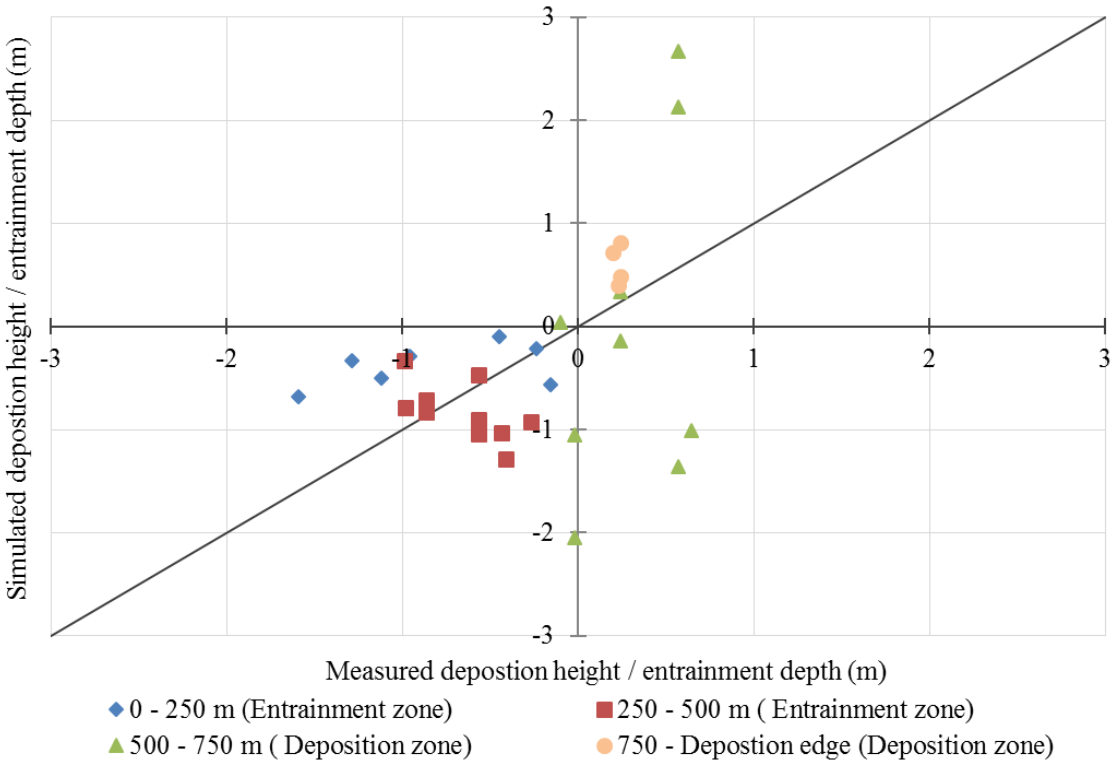

Figure 5-18: Scatter plot of observed and simulated height of debris flow

The maximum velocity is estimated from superelevation angle of the flow surface. The superelevation angles of the Tsing Shan debris flow are measured for four adjacent sections at Ch 350 and Ch 475 where the trail follows bends in the valley. It is calculated that the average velocities are 16.5 m /s and 12.5 m/s at Ch 350 and Ch 475, shown in Figure 5-19. Simulated velocities at both sections agree with measured velocity very well.

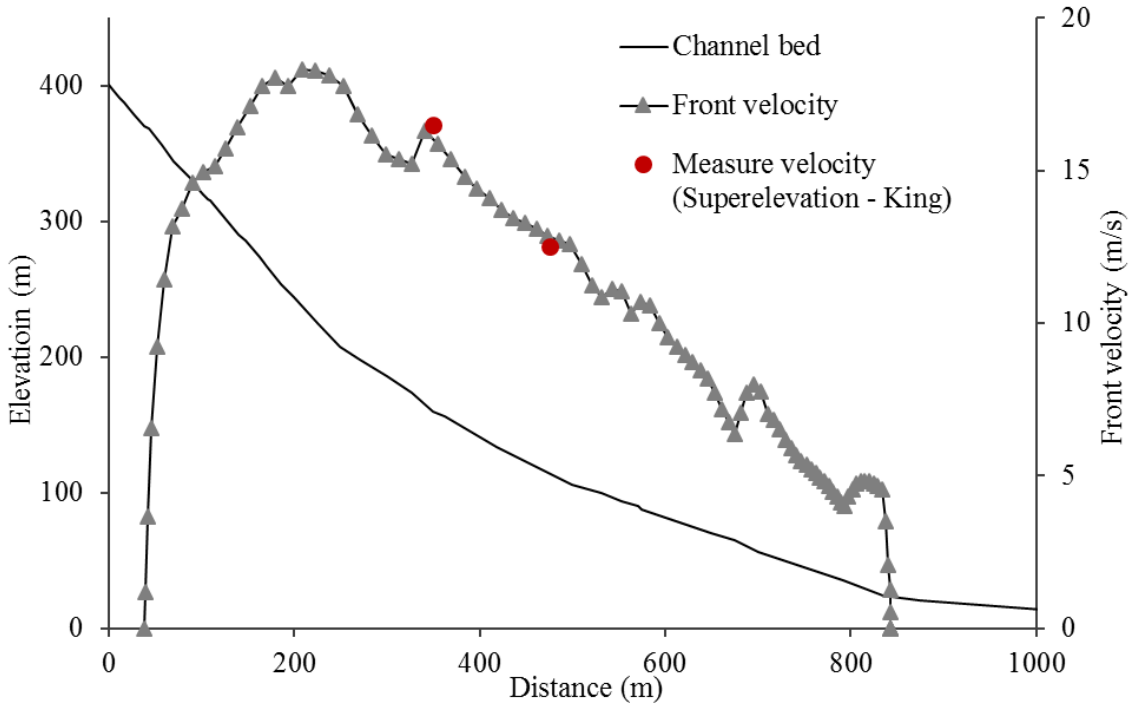

Figure 5-19: Simulated and measured velocity along flow channel

To test the influence of entrainment on debris flow velocity and runout distance, the simulated results are compared with that with no entrainment by using same parameter in the simulation (Figure 5-20). It is obvious that runout distance from the simulation with entrainment, 843m, is larger than that without entrainment, 573m. Velocity of flow having entrainment is almost always larger than that without entrainment, including maximum front velocity from simulation with entrainment, 18.3m/s, larger than that without entrainment, 13.3m/s. It means that omission of entrainment could underestimate front velocity and runout distance. This could be fatal in check-dam design as impulsive force would be underestimated.

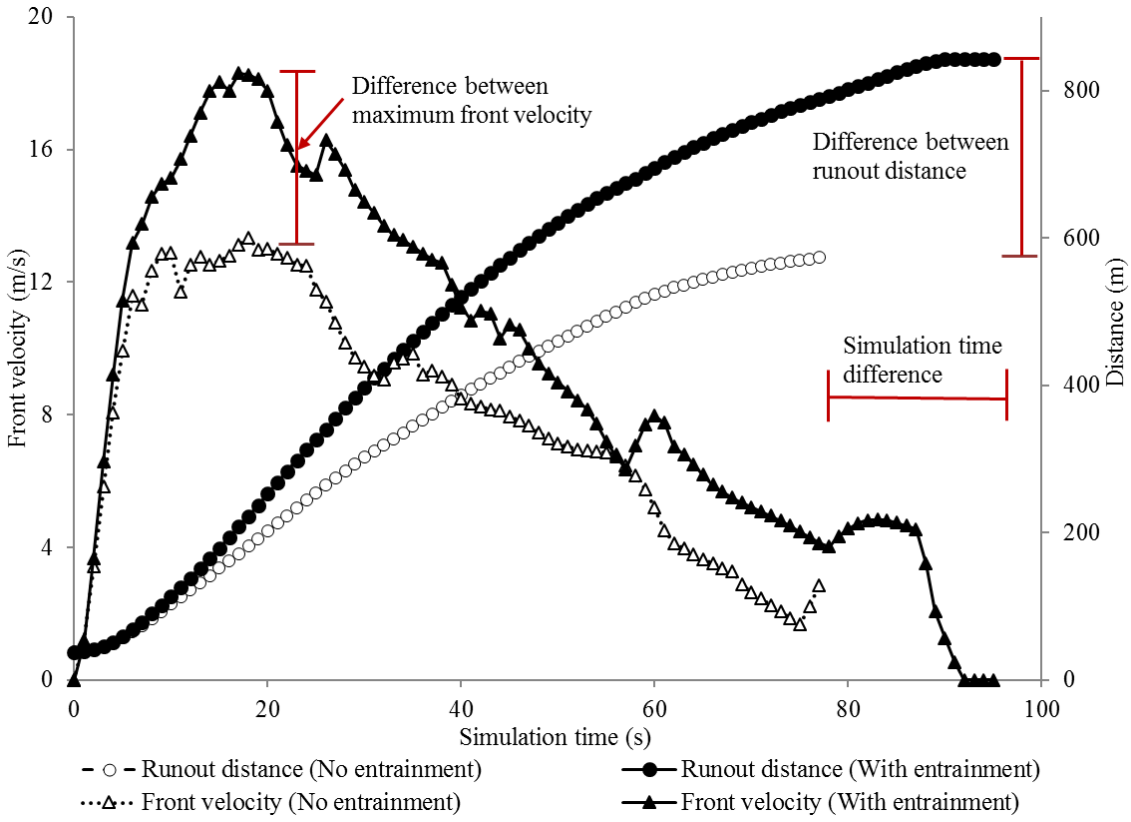

Figure 5-20: Comparison of maximum velocity and front velocity with and without entrainment in moving

5.7. Discussion and conclusion

Finite difference method is used to numerically solve the new entrainment model. It can save the time on simulation but it is only an approximate method. To increase the accuracy, other methods can also be employed in solving the second order differential equation, like Runge-Kutta method, but this could extend simulation time for same case. In the simulation, both sliding and rolling motion are considered. In so doing, progressively scouring of the particles lying the channel bed is successfully simulated.

In the sensitivity analysis of the entrainment runout model, soil properties and parameters influences the simulation results such runout distance, maximum front velocity and total volume.

Entrainment process is dominated by mean of PDF (μ). It affects not only entrainment rate, but also the front velocity as well as total volume. Runout distance is mainly influenced by channel basal friction angle. It also impacts entrainment rate, but it is not as important as μ in the simulation.

Time steps in estimating runout distance and entrainment rate also affect the entrainment rate. Smaller time step could show real physical process of entrainment and movement of debris flow, but it, at the same time, increases simulation time. In the new model, appropriate time step is dynamically adjusted according to criterion used to limit the deformation of the slices.

Back analysis of Tsing Shan debris flow (1990) is carried out. Entrainment is incorporated into a runout model to simulate the debris flow process. It is supposed that the flow moves as granular flow and erodible material is consisted of uniform loose packed granular particles, therefore excess pore water pressure and particle shape are neglected. It is clearly shown in the simulation results that adjustment of the total volume and channel profile are considered in the entrainment runout model. In our simulation, constant value of μ in normal distribution PDF is used. Strictly, μ is not same at each section and selection of its value can rely on the properties of channel bed such as the angle of repose of the erodible material. Besides, as only progressive souring is considered in the model, entire failure of the channel bank is not taken into account. This could induce errors in the estimation of debris flow volume.

The simulation results are compared with that observed. The total volume and maximum velocity are in good agreement with the event, but slight difference still exists between the results simulated and observed arising from suddenly change of width of flow channel. By simulating the debris flow on same channel using the entrainment runout model without considering entrainment and comparing the simulated results with that with entrainment, it is demonstrated

that ignoring entrainment underestimates the maximum velocity and runout distance. Therefore, impulsive force of debris at each section would also be underestimated. This is fatal in designing the construction in debris flow mitigation.

From the discussion above, it is indicated that the progressive scouring model considers both rolling and sliding motion of particle movement. Sensitivity analysis results show that μ of normal distribution PDF plays a vital role in entrainment estimation. To determine the value of μ, it is suggested that soil properties, such as the angle of repose, of erodible material lying on channel bed can be considered in selecting the appropriate value of μ. The results of the entrainment runout model reveals that taking progressive scouring into account in entrainment estimation can improve the simulation of debris flow runout. This will improve the accuracy of the quantification of natural hazards.

Reference

Blanc, T. (2008). Numerical simulation of debris flows with the 2D SPH depth-integrated model (Master's thesis). Institute for Mountain Risk Engineering, University of Natural Resources and Applied Life Sciences, Vienna, Austria

Cheng, N. S., Law, A. W. K., and Lim, S. Y. (2003). Probability distribution of bed particle instability, Advances in Water Resources, 26(4), 427-433.

De Blasio, F. V., Breien, H., and Elverhoi, A. (2011). Modelling a cohesive-frictional debris flow: an experimental, theoretical, and field-based study, Earth Surface Processes and Landforms, 36(6), 753-766.

Egashira, S., Honda, N., and Itoh, T. (2001). Experimental study on the entrainment of bed material into debris flow, Physics and Chemistry of the Earth, Part C: Solar, Terrestrial & Planetary Science, 26(9), 645-650.

Fenton, J. D., and Abbott, J. E. (1977). Initial movement of grains on a stream bed: The Effect of Relative Protrusion, Proceedings of the Royal Society of London Series a-Mathematical Physical and Engineering Sciences, 352(1671), 523-537.

Fraccarollo, L., and Capart, H. (2002). Riemann wave description of erosional dam-break flows, Journal of Fluid Mechanics, 461, 183-228.

Hungr, O. (2008). Numerical modelling of the dynamics of debris flows and rock avalanches. Geomechanics and Tunnelling, 1(2), 112-119.

Iverson, R. M., and Denlinger, R. P. (2001). Flow of variably fluidized granular masses across three-dimensional terrain 1. Coulomb mixture theory. Journal of Geophysical Research-Solid Earth, 106, 537-552.

Iverson, R. M., Logan, M., and Denlinger, R. P. (2004). Granular avalanches across irregular three-dimensional terrain: 2. Experimental tests, Journal of Geophysical Research, 109, F01015, doi:10.1029/2003JF000084.

Iverson, R. M. (2012). Elementary theory of bed-sediment entrainment by debris flows and avalanches, Journal of Geophysical Research, 117, F03006, doi:10.1029/2011JF002189.

Iverson, R. M., and Ouyang C. J. (2015). Entrainment of bed material by Earth-surface mass flows: Review and reformulation of depth-integrated theory. Reviews of Geophysics, 53, doi:10.1002/2013RG000447.

King, J. (1996). Tsing Shan Debris Flow. Special Project Report SPR 6/96. Geotechnical Engineering Office, Hong Kong.

Lo, K. H., and Chau, K. T. (2003). Debris-flow simulations for Tsing Shan in Hong kong, Proceedings of the Third International Debris-Flow Hazards Mitigation: Mechanics, Prediction, and Assessment (DFHM) Conference, Editors: Rickenmann, D., and Chen, C.L., Savos, Switzerland, September 10-12, 2003, Millpress, Rotterdam, 577-588.

Luna, B. Q., Remaitre, A., van Asch, T. W. J., Malet, J. P., and van Westen, C. J. (2012). Analysis of debris flow behavior with a one dimensional run-out model incorporating entrainment, Engineering Geology, 128, 63-75.

Medina, V., Bateman, A., and Hurlimann, M. (2008a). A 2D finite volume model for bebris flow and its application to events occurred in the Eastern Pyrenees, International Journal of Sediment Research, 23(4), 348-360.

Medina, V., Hürlimann, M., and Bateman, A. (2008b). Application of FLATModel, a 2D finite volume code, to debris flows in the northeastern part of the Iberian Peninsula, Landslides, 5(1), 127-142.

Okada, Y., and Ochiai, H. (2007). Coupling pore-water pressure with distinct element method and steady state strengths in numerical triaxial compression tests under undrained conditions, Landslides, 4(4), 357-369.

Shodja, H. M., and Nezami, E. G. (2003). A micromechanical study of rolling and sliding contacts in assemblies of oval granules, International Journal for Numerical and Analytical Methods in Geomechanics, 27(5), 403-424.

Skempton, A.W. (1954). The pore-pressure coefficients A and B, Géotechnique, 4(4), 143-147.

Sun, H., Lam, T., and Tsui, H. (2003). Design basis for standardised modules of landslide debris-resisting barriers. Technical Note No. TN 4/2003. Geotechnical Engineering Office, Hong Kong.

Wang, X. B., Morgenstern, N. R., and Chan, D. H. (2010). A model for geotechnical analysis of flow slides and debris flows, Canadian Geotechnical Journal, 47(12), 1401-1414.

6. RUNOUT AND ENTRAINMENT ANALYSIS OF AN EXTREMELY LARGE DEBRIS FLOW – A CASE STUDY OF YIGONG TIBET, CHINA[2]

6.1. Abstract

An extremely large rock avalanche occurred on April 9, 2000 at Yigong Tibet, China. It started with an initial volume of material of 90×106 m3 comprising mainly of loose material lying on the channel bed. The rock avalanche travelled around 10 km in horizontal distance and formed a 2.5 km long by 2.5 km wide depositional fan with a final volume of approximately 300×106 m3. An energy-based debris flow runout model is used to simulate the movement process with a new entrainment model. The entrainment model considers both rolling and sliding motions in calculating the volume of eroded material. Entrainment calculation is governed by a second order partial differential equation which is solved using the finite difference method. During entrainment, it is considered that the total mass is changed due to basal erosion. Also the profile of the channel bed is adjusted accordingly due to erosion at the end of each calculation time step. For Yigong the profile used in the simulation was extracted from a DEM (Digital Elevation Model) with a resolution of 30 m × 30 m. Measurements obtained from site investigation, including deposition depth and flow height at specific location, are used to verify the model. Ground elevations based DEM before and after the event are also used to verify the simulation results where access were difficult. It is found that the calculated runout distance and the modified deposition height agree with field observations. Moreover, the back-calculated flow

[2] This chapter has been published in *Landslides* Journal and is available online now (Kang, C., Chan, D., Su, F. et al. Landslides (2016). doi:10.1007/s10346-016-0677-7).

characteristics based on field observations, such as flow velocity, are also used for model verifications. The results indicate that the new entrainment model is able to capture the entrainment volume and depth, runout distance and deposition height for this case.

6.2. Introduction

6.2.1. Debris flow event and analysis

Debris flows are rapid mass movement in steep hilly terrains where earthly materials flow down in a valley or channel usually triggered by heavy rainfall. It is usually fast-moving with variable solid concentration and large runout distance. Due to its fast moving characteristics, debris flow is one of the most hazardous and unpredictable surface process that results in many losses of lives and property damages (Schurch et al. 2011). For example, between 2004 and 2010 there were 2,327 people killed by debris flow in China out of 6,910 who were killed by natural hazards. One recent example showing the destructive power of debris flow is the Zhouqu debris flow which occurred on August 7, 2010. It caught the residents of Zhouqu by surprise since the event occurred just before midnight killing 1,765 people and destroying more than 5,500 houses.

In order to assess the extent of damages caused by a debris flow event, numerical modelling and debris flow analysis are often carried out. There are several approaches in debris flow modelling. This includes the empirical approach, the discrete approach and the continuum approach. In the empirical approach, calculations of the volume, speed, runout distance and the extent of a debris flow is based on historical observations of a large number of events, see Fannin et al. (2012) and Moffat et al. (2011). In the second approach using the discrete method debris flow is modelled using many small elements that interact with each other, Cundall and Strack (1979). The third approach is based on continuum models in which the body of the debris is considered to be a

continuum. The formulation of the model is based on physical laws such as Newton's Law of Motion, the Law of the Conservation of Mass and the Law of the Conservation of Energy. The equations governing the motion of the debris are derived to calculate the flow characteristics, such as velocity, depth, runout distance etc., see Wang et al. (2010). Numerical techniques, such as the finite element method, finite different method or the block continuum method, are often used to provide the numerical solution for the debris flow analysis. Due to the complexity of rheology of debris material and the size of a typical debris flow, it is still not possible to adopt a discrete approach which requires large computation resources. The continuum model is more practical approach to obtain solutions for realistic debris flow problems.

6.2.2. Debris flow run-out simulation

In continuum modelling, there are two approaches in formulating the equations for debris flow runout analysis. The governing equations can be derived by applying the Law of Conservation of Momentum in numerical analysis or it can be derived based on the Law of Conservation of Energy. The first approach has been commonly used such as the Dynamic Analysis Model (DAN) developed by Hungr (1995). DAN has been widely used in debris flow runout simulation. DAN is based on an explicit solution of the Saint Venant equations incorporating a variety of constitutive relationships in describing debris flow characteristics.

The energy model adopts the Law of Conservation of Energy which also consider internal energy dissipation during the movement of the debris flow. As a slice-based model, the energy model determines the motion of each slice considering energy conservation in the Lagrangian framework (Wang 2008). Lateral pressure and basal resistance on individual slices are determined using the Rankine and Mohr-Coulomb theories. The momentum equations for the overall sliding mass are not examined during the calculation.

6.2.3. Debris entrainment and basal erosion

During the moving process of debris flow, material from the channel boundary are often eroded and mixed with the main body of the debris and becomes part of the flowing debris (Iverson 2012). This process of increasing the mass by eroding the material from the channel is called entrainment. There are various models in calculating the amount and rate of entrainment in debris flow analysis. There are basically two approaches in calculating entrainment: the static approach and the dynamic approach. In the static approach, static shear stresses are calculated beneath the channel bed under the debris and failure is considered when the static shear stress exceeds the shear strength of the material (Medina et al. 2008a). The depth in which failure occurs is determined and the amount of material is calculated which will be added to the main body of the debris. In the dynamic approach, the rate of entrainment is calculated based on the rate of erosion of the material at the channel bed. The rate of erosion is determined based on shear failure at the surface and the material is removed from the surface based on the velocity of flow of the main body of the debris (Medina et al. 2008a). It is assumed in this approach that the velocity of newly eroded material is the same as the average velocity of the debris. However field observations indicate that the velocity of the newly eroded material is not same as the debris (Fraccarollo and Capart 2002; Medina et al. 2008b).

Egashira et al (2001) proposed a formula to calculate erosion rate assuming that the slope of the channel bed is always adjusted to the angle corresponding to limiting equilibrium conditions. The material in the channel left behind by an unsaturated debris will approach the limiting equilibrium slope angle. Geometrical relationship between the initial bed slope and equilibrium slope angle is incorporated into mass conservation law of eroded material to obtain the entrainment rate.

The entrainment model proposed by van Asch et al. in 2004 (Luna et al. 2012) is a dynamic one dimensional debris flow model that takes into account the entrainment concept based on the generation of excess pore water pressure under undrained loading on the in-situ material. Flow is treated as laminar, single phase and as an incompressible continuum process. Due to the moving mass flowing on top of the erodible bed, a loading on the bed deposits is generated. The model calculates this applied load on the in-situ soil through changes in the vertical normal stress and shear strength caused by the debris flow. The increase in pore water pressure is calculated based on the Skempton's (1954) equation. The depth of erosion is approximated using the relationship between the factor of safety at the bottom and top of soil in the channel. The model proposed by van Asch is similar to the depth-integrated model except that it considers the factor of safety for the erodible layers. Although the interaction between the debris and the channel soil is considered here, entrainment rate is not taken into account. Besides, the effect of grain size is not considered in the entrainment process, which is important and it was illustrated by the experiments carried out by Egshira (2001)

Iverson (2012) considered the behavior of a slide block descending an erodible slope with the ability of incorporating soil on the static bed. Newton's second law was first applied on the sliding material. Then, Coulomb friction rule was applied and basal friction resistance calculation was improved by taking the shear rate into account. The frictional resistance consists of a constant component of friction resistance and a velocity-dependent component. After considering the rate-dependent friction, entrainment rate based on the change in weight of the sliding block was obtained.

De Blasio et al. (2011) suggested a semi-empirical model to calculate entrainment. In the semi-empirical model, entrainment rate depends solely on the tangential component of weight at the

base of the flow and on the average velocity of the debris flow. Critical shear stress is used as the thereshold to determine the occurance of entrainment. Data from Fjæland debris flow used for dynamic quantities and for erosion effects is utilized to calibrate the model. This model seems promising since it relates debris flow velocity and basal shear stress to entrainment.

After comparing the pros and cons and limitations of those models, a new progressively scouring model was developed. In applying the model to solve practical problems, the model was used to calculate the debris flow characteristics and entrainment at Yigong. The calculated flow characteristics such as debris flow height, the depth of erosion and thickness of debris deposition are compared with field observations.

6.3. Run-out model and the new entrainment model

6.3.1. Run-out model

As described earlier, two approaches has been applied to simulate debris flow runout process. Since the energy model considers the internal energy dissipation during mobilization, motion and deposition, it is employed to incorporate the new entrainment model.

In the slice-based model, the energy model determines the motion of each slice based on the energy conservation equations using the Lagrangian difference scheme (Wang et al. 2008). The change in kinetic energy of a sliding mass consists of changes in potential energy, work done by resistance forces along the base of the sliding mass and work due to internal deformation of the debris. Lateral pressure and basal resistance on individual slices can be calculated using the Rankine and Mohr-Coulomb equations. Longitudinal spreading is mainly due to velocity gradient ($\partial u/\partial x$) that results from a combination of forces acting on the debris which include

lateral earth pressure, gravitational force, and shearing resistance. The governing equation of the runout model is:

$$\frac{d}{dt}\left(\frac{1}{2}m\bar{u}^2\right) = mg\bar{u}\sin\theta + \frac{1}{2}mghe_{zz} + P_L\bar{u}_L\cos\theta_L - P_R\bar{u}_R\cos\theta_R - T\bar{u} - \int_V \tau_{ij}e_{ij}dV \quad [6\text{-}1]$$

where m is the mass of the slice, ū is the mean velocity of the slice along the base of the slice, g is gravity acceleration, θ is the inclination of the base of the slice with respect to the horizontal, P_L and P_R are interslice forces exerted on the left and right sides of the slice, T is the shear force acting along the base of the slice, τ_{ij} are components of the stress tensor and e_{ij} are components of the strain rate tensor. Detail formulation and discussion of the model can be found in Wang et al (2010) and Wang (2008).

6.3.2. The new entrainment model

In static approach of entrainment calculation, static equilibrium is considered between the flow frictional forces, τ_b, and the basal resistance forces, τ_{res}, in each computational time step (Medina et al. 2008a). If equilibrium does not exist, the model estimates the magnitude of entrainment from:

$$\tau_b + h_{ent}\rho g\sin\theta = c + \left|h + h_{ent}\right|\rho g\cos\theta\tan\phi_{bed} \quad [6\text{-}2]$$

where h_{ent} is the depth of erosion , θ is slope angle, c is the cohesion, h is flow height, g is gravity acceleration and ϕ_{bed} is the bulk friction angle of the bed material.

In dynamic approach, same failure mode is considered as that in static approach except that Newton's second law is applied on the erodible material. So, amount of entrained material depends on the availability of momentum (Medina et al. 2008b), given by

$$\frac{\partial z}{\partial t} = \frac{(\tau_b - \tau_{res})}{\rho V} \qquad [6\text{-}3]$$

where $\partial z/\partial t$ is the rate the rate of entrainment and V is the mean velocity of the flow.

In the new entrainment model, it is considered that granular particles lying on the channel bed is eroded progressively. Granular particles are modelled using uniform size sphere (disk in the case of 2D analysis). Particles are mobilized due to shear stress exerting on the particles. According to the analysis (Cheng et al. 2003; Shodja et al. 2003), normally initiation drag force for the rolling action is less than that required for basal shear failure. Therefore, it is reasonable to assume that rolling motion is the dominant motion in initial stage of entrainment. However both rolling motion and sliding motion are considered in the formulation of the entrainment model.

Based on the experiments from Fraccarollo and Capart (2002), it is obvious that the vectors representing the velocity of flow "particles" are almost parallel to the channel bed. Therefore, in the derivation of the equation, it is assumed that the forces acting on the particle are based on particle movement parallel to the sliding surface. Hence, the forces are assumed to be tangent to the slopes.

In calculating the drag force for the initiation of the rolling action, it is assumed that a particle will rotate around point O as shown in Figure 6-1. Drag forces due to the moving debris above the bed are assumed to apply at the center of the particles. It is assumed that the particle will rotate around the contact point with the adjacent particle located downstream. Newton's Law of Motion is applied to calculate the acceleration, velocity, and displacement of the particle. The moment equation is given by

$$\frac{TR}{\left(I + mR^2\right)} sin\alpha_t - \frac{mgR}{\left(I + mR^2\right)} \cos\left(\alpha_t + \theta\right) = \frac{\partial^2 \alpha_t}{\partial t^2} \qquad [6\text{-}4]$$

where T is the drag force required to initiate particle rolling, R is the radius of the rolling particles (d_{50} is adopted here), I is moment inertial which is equal to $m(3R^2+L^2)/12$, L=1m for 2D, m is the mass of the particle (for 2D, $m = \pi R^2 \rho_b$), ρ_b is the density of bed sediment particle, a_t is the angle between channel bed and connection line of centers of those two particles, θ is the slope angle, g is the gravity acceleration, $\partial^2\alpha_t/\partial t^2$ is angular acceleration and t is time.

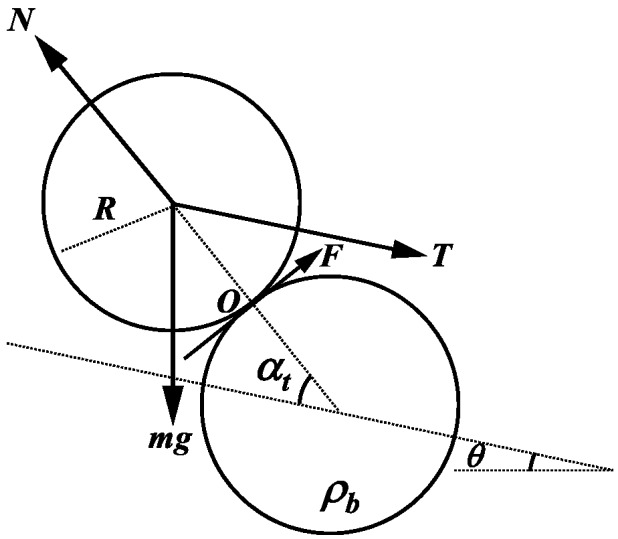

Figure 6-1 Free body diagram of particle when rolling occurs

It is also assumed in the derivation that once the particle moves over adjacent particle located downstream, it is considered to have been eroded and will be added to the total mass of the debris. Based on equation of rolling motion (Equation [6-4]), the entrainment time, which is the time required for one particle to move from initial position to become part of the debris, can be estimated. The entrainment rate is defined as the height of the particle exposed to the flow divided by the time needed for it to be eroded. So, for different α0, initial condition of αt, entrainment rate, $\dot{E}i$, is defined in Equation [6-5].

$$\dot{L}_i = \frac{2R_i \sin\alpha_{0i}}{t_i} \qquad [6\text{-}5]$$

t_i, in equation [6-5], is the time required for one particle to roll from the initial position, α_0, to the vertical position when α_t is equal to $(\pi/2-\theta)$. It is assumed in the derivation that once the particle moves to the top of the overriding particle downstream, it is considered to be part of debris. Therefore, if shear force exerted on the particle is known and particle properties are determined, t_i can be obtained by solving equation [6-4]. When shear force exerted on the particle is larger than the friction on the particle, the entrainment mode changes from rolling motion into sliding motion.

Since α_0 varies from one location to another and it is not easy to be determined, a probabilistic approach is adopted and α_0 is assumed to follow a probability density function (PDF) using a normal distribution. Selecting the parameters for the PDF is important in the entrainment calculation. The mean value of the normal distribution function can be estimated for a particular case (Fenton et al. 1977), but its value is site specific. The value of α_o can also be estimated from the relationship between void ratio and internal friction angle, and the relationship between particle protrusion and void ratio (Okada et al. 2007). After the PDF has been determined and the entrainment rate for each specified α_0 are known, the entrainment rate can be obtained from Equation [6-6].

$$\dot{L} = \sum_{i=1}^{n} \dot{L}_i(\alpha_{0i}) \qquad [6\text{-}6]$$

in which n is the number of division between 0 and 90 degrees based on the increment of α_0.

6.4. Description of Yigong rock avalanche

6.4.1. Geomorphology

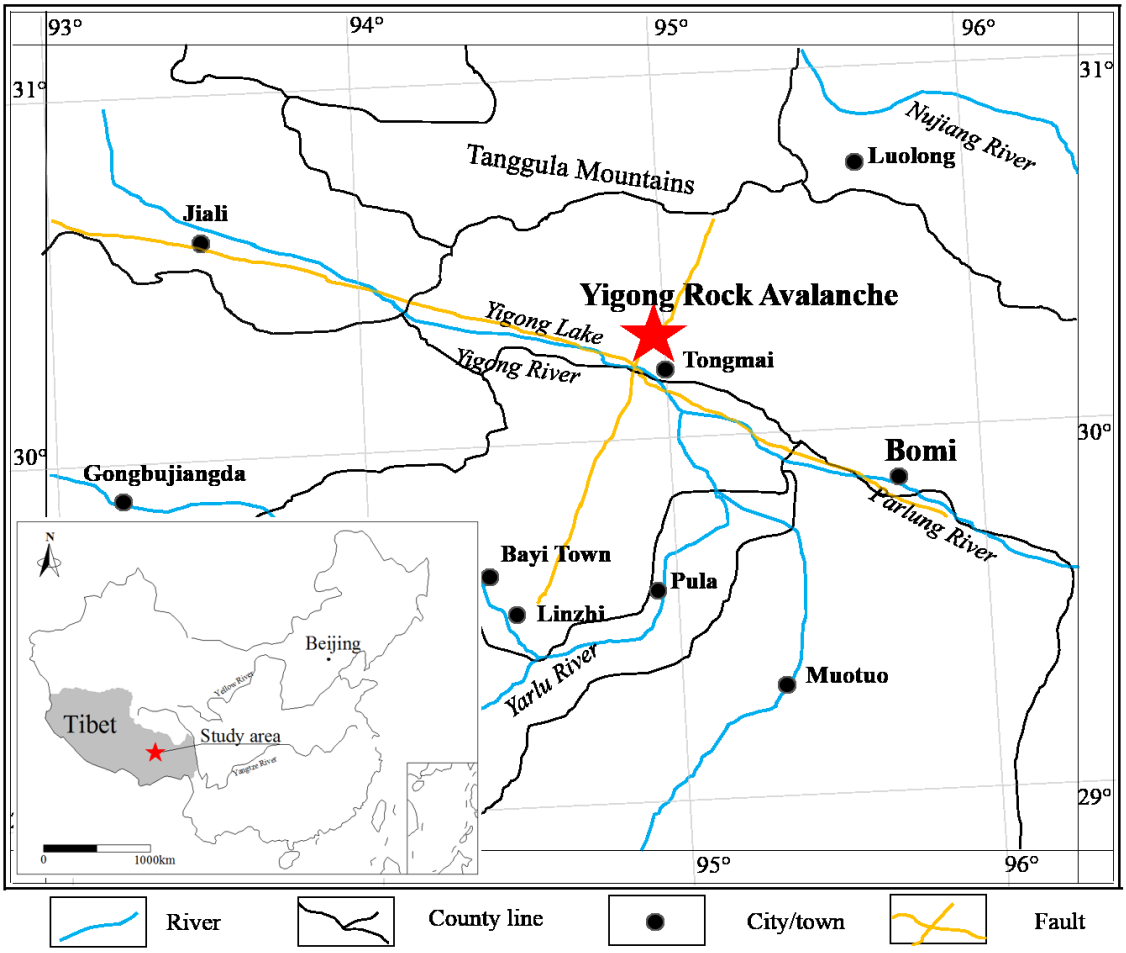

Figure 6-2: Geographical location of Yigong rock avalanche

On April 9th 2000, a rock avalanche occurred at Yigong, Tibet, China (Figure 6-2). This event is considered as one of largest non-seismic mass movement in recent years (Zhang et al. 2013). The Yigong rock avalanche (YRA) is located at N30º12'03", E94º58'03", Zamu Creek, a tributary of the Yigong River (Lv et al. 2002). Zamu Creek is a typical channeling valley. The slopes of its lateral mountains are between 30° and 35°. The bottom width of the creek is between 50m and 150m (Zhang et al. 2013). The elevation at the source zone of the rock avalanche is about 5,350 m, and the elevation of the Yigong River bed is about 2,188m (Figure 6-3) (Wang 2006). The

runout path is plotted in Figure 6-3 denoted by line P-P', which is also the profile line used in the current simulation.

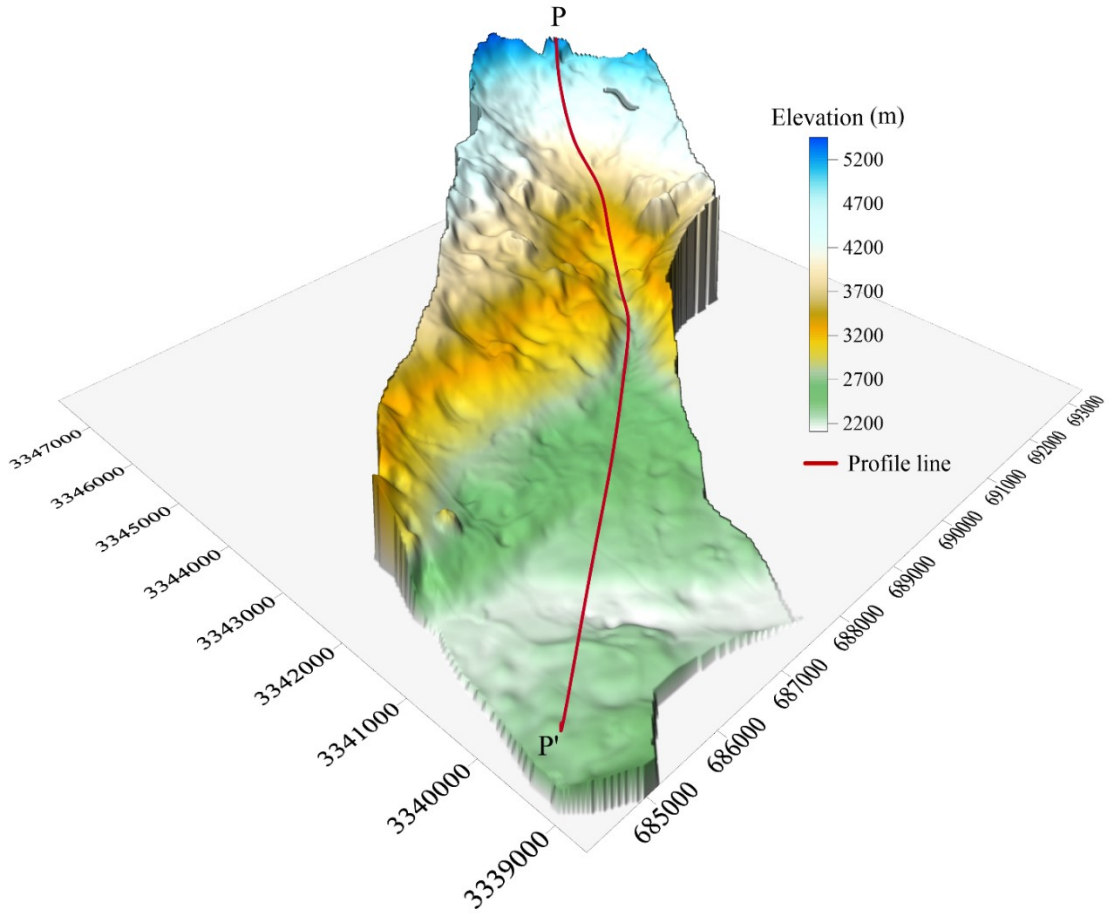

Figure 6-3: Digital elevation model of Yigong Rock Avalanche

6.4.2. Features of source area

The source area of YRA is situated at the top of the catchment area of Zamu Creek with a drainage area of 20.2km^2 and length of 7.9km. The total bare source zone of YRA is about 12.9km^2. The elevation of the source ranges from 4,000m to 5,525m. The geometric centre of the rock slide has an elevation of about 4,600m (Xu et al. 2012). The bare rock is mainly consisted of granite, but due to two intersecting faults in this region, geological activities and physical

weathering process, a wedge-shaped sliding body was formed in source area. From the digital elevation model (DEM) before and after the occurrence of the rock avalanche, it is estimated that source volume was around $90\times10^6 m^3$ with 318m in maximum depth (Figure 6-4) (Wang 2006). In Figure 6-4, the negative number means the decrease in elevation after the rock avalanche.

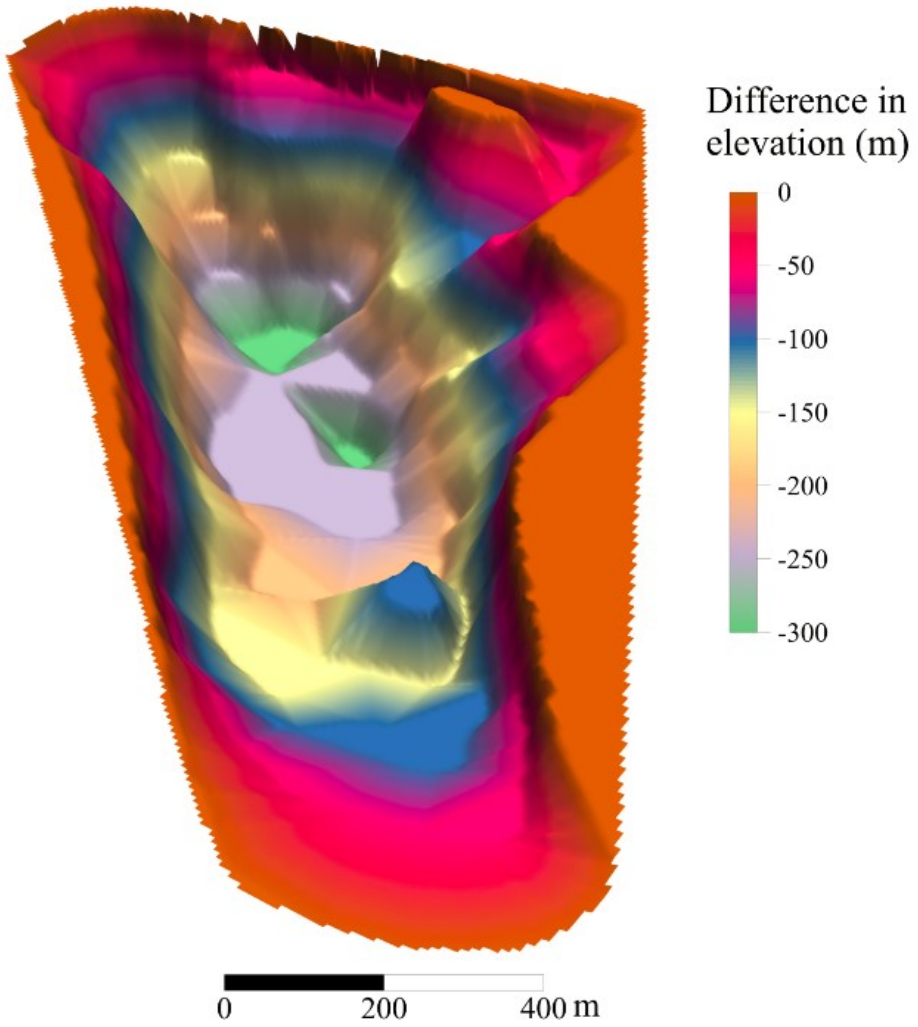

Figure 6-4: Variation of elevation at source area of YRA (Revised from Wang (2006))

6.4.3. Time and duration of the event

According to seismogram of the nearest seismic station, the Linzhi seismic station which is located 110 km southeast of the site, the first vibration of the ground occurred at 19:59:42. The

energy released from the tremor is equivalent to a 2.9 magnitude earthquake. After that two consecutive 3.5 magnitude earthquakes were detected (Ren et al, 2001). This coincides with the description from a local residence whose home is 10 km away from the source area of rock slide and 300 m away from the western margin of final debris deposition. The eyewitness recalled that the ground was shaking violently at around 20:00 (Xu et al. 2012). Therefore, it can be concluded that the event occurred at around 20:00 on April 9, 2000.

Since YRA occurred suddenly, there was no data collected for the elapsed time. The time deduced from recorded seismic wave indicated that this event lasted for at least minutes (Ren et al. 2001). A farmer, who was working at Yigong Tea Farm at the time, cited that from the time he saw a cloud of thick smoke to the time he saw the debris flowed out of the Zamu Creek is around minutes. Others have quoted that the duration of this event is around 10 minutes (Yin 2000). Although the elapsed time varies from 3 to 10 minutes, it is nonetheless that this event lasted a short time.

6.4.4. Description of velocity, run-out distance and height during its movement

For such a rapid large rock avalanche, it is very difficult to monitor the velocity during the event since not only it occurs randomly, but also it is difficult to install monitoring devices so that it will not be damaged. Normally velocity is deduced from seismic surveillance data and the estimated average velocity is around 48 m/s. Local citizens who was working near the outlet of Zamulong Creek described that nine gales were felt at the outlet. Destroyed tress and charred trees along the channel also affirmed that the rock avalanche moved with a very high speed (Figure 6-5).

Field investigation showed that YRA climb over the mountain near the outlet of Zamu Creek (Figure 6-5). The picture taken at point A at the top right corner shows that the debris had reached that location. The photo at point B shows the cross section of deposition fan. It is obvious that the deposited material lies on top of the old debris deposition fan and the new deposition height is around 60 to 70 m. The elevation difference between the deposition and peak of mountain is about 200m. Adding the thickness of the deposition, it is suggested that maximum flow height of YRA at that site is nearly 200m if super elevation is not considered. YRA stopped after it reached the south bank of Yigong River. Therefore the horizontal travel distance is around 10km (Yin 2000). This distance is estimated along the flow channel.

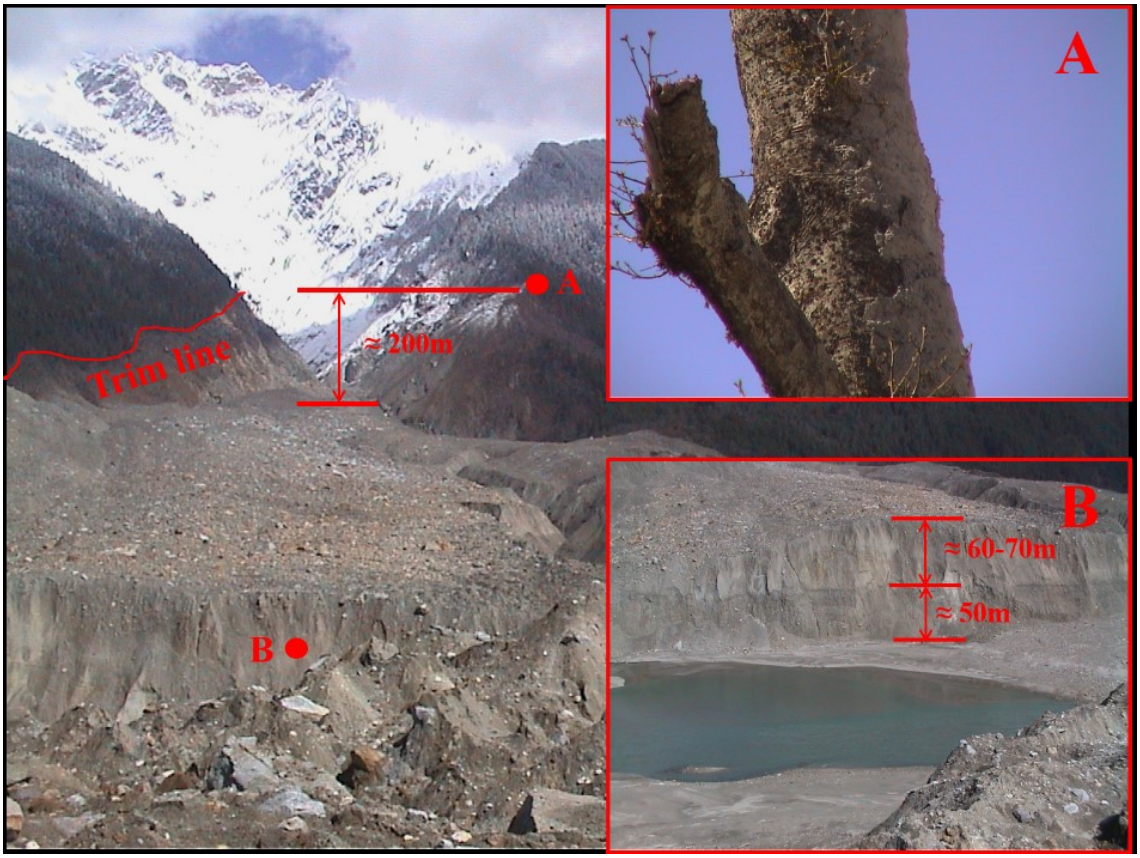

Figure 6-5: Evidence of flow height near the outlet of Zamu Creek (Photography by Chen 2015)

6.4.5. Description of entrainment and final deposition

During the sliding process, drag force exerted by the sliding debris could erode materials lying on the channel bed. This process could increase the volume of the final deposition and increase the velocity of moving debris. The entrainment zone in Zamu Creek is mainly composed of loose colluvial materials, distributed not only on the creek banks, but also on the channel bed. Erodible material in Zamu Creek is mainly located at an elevation between 3,000m and 4,000m.

Deposition zone consists of boulders moved from source area and loose debris materials in the entrainment zone. In this region, particle size changes from the central area to deposition boundary. The accumulated debris at the central area in the deposition zone composes mostly of bounders having a diameter over 3m, and the total volume of the boulders is around $30\times10^3 m^3$.

Elevation variation of Zamu Creek before and after YRA is shown in Figure 6-6. It seems that the maximum elevation variation is around 500m which is larger than that reported by Wang (2006). The DEM used to plot the elevation variation map is based on survey a few month after the event. Snow melt and other topographic evolution process may introduce errors in the elevations.

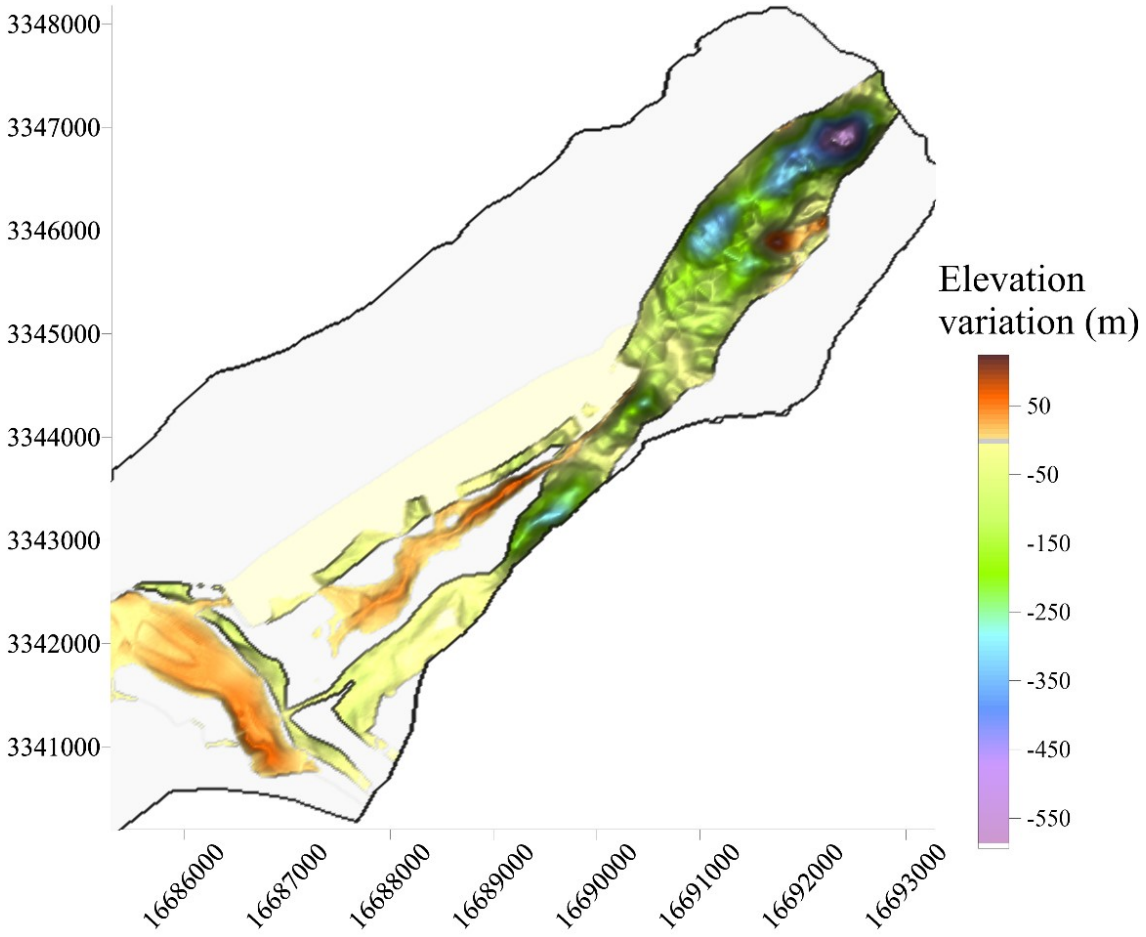

Figure 6-6: Elevation variation obtained by subtracting DEM after event from that before event

As grain size in rock avalanche fan varies from very fine particle to boulders, it is very difficult to sample particles of all sizes for sieve analysis, so coarse particles which size is greater than 400mm were excluded in sampling process. The observed largest particle is around 22m (Figure 6-7). Grain size distribution of sampled fine particles is shown in Figure 6-8.

Figure 6-7: Observed largest particle embedded into deposition fan (Photography by Chen 2015)

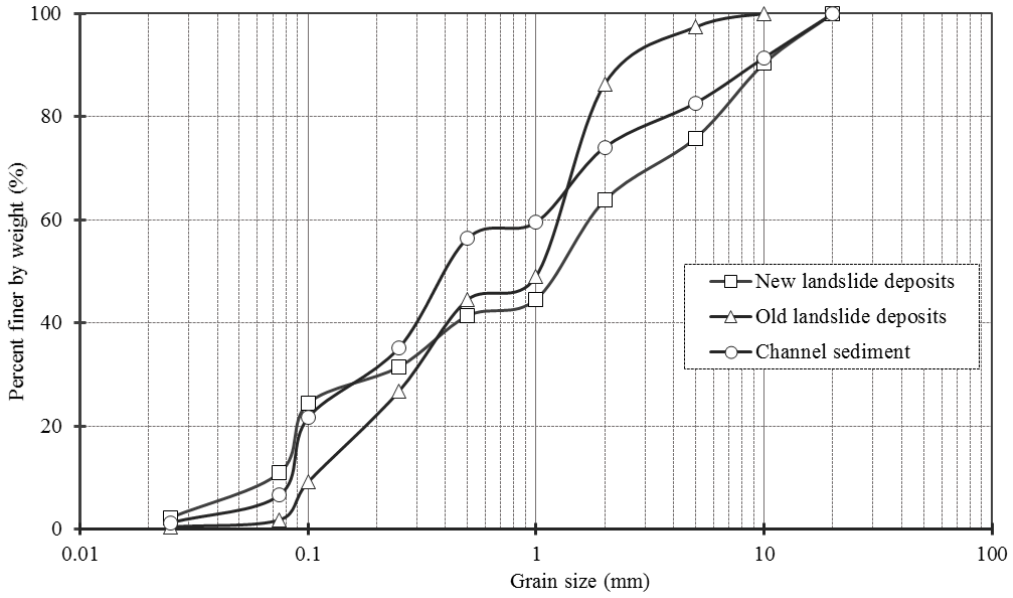

Figure 6-8: Grain size distributions of fine particles (d < 400mm) sampled from runout path of YRA (Test carried out by Zhou)

Interpretation of remote sensing images shows that the total volume of YRA is about 300 million m^3 (Wang and Lv. 2001). From the aerial photo after the event, it is measured that YRA formed a 2,500m long and 2,500m wide deposition fan. Zoning map of deposition fan is shown in Figure 6-9 and the longitudinal profile is shown in Figure 6-10. Average depth of the deposit is 60m-70m (Yin. 2000).

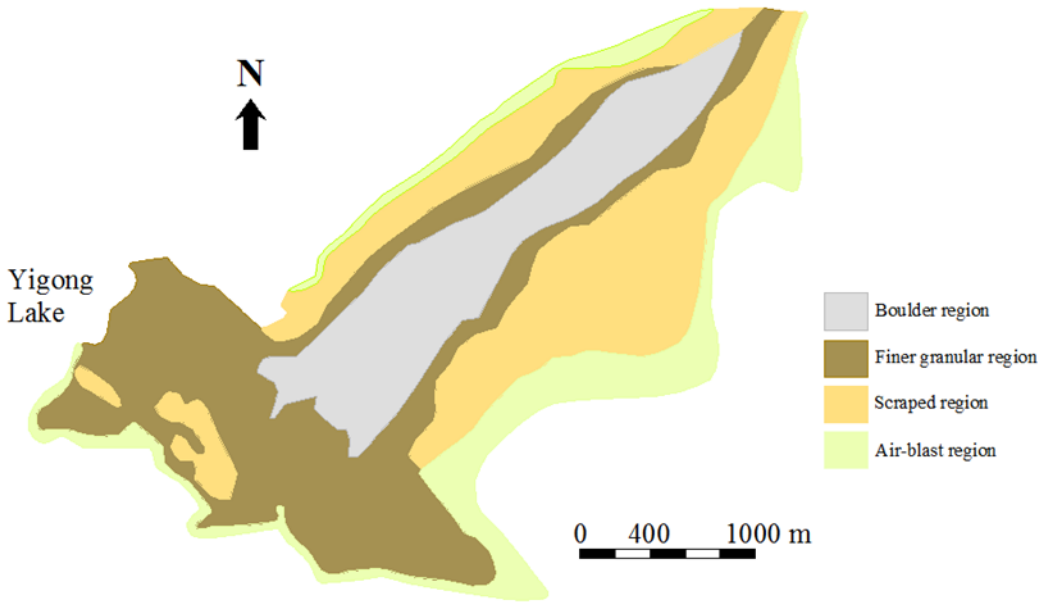

Figure 6-9: Zoning map of deposition fan of YRA (Zhang and Yin 2013)

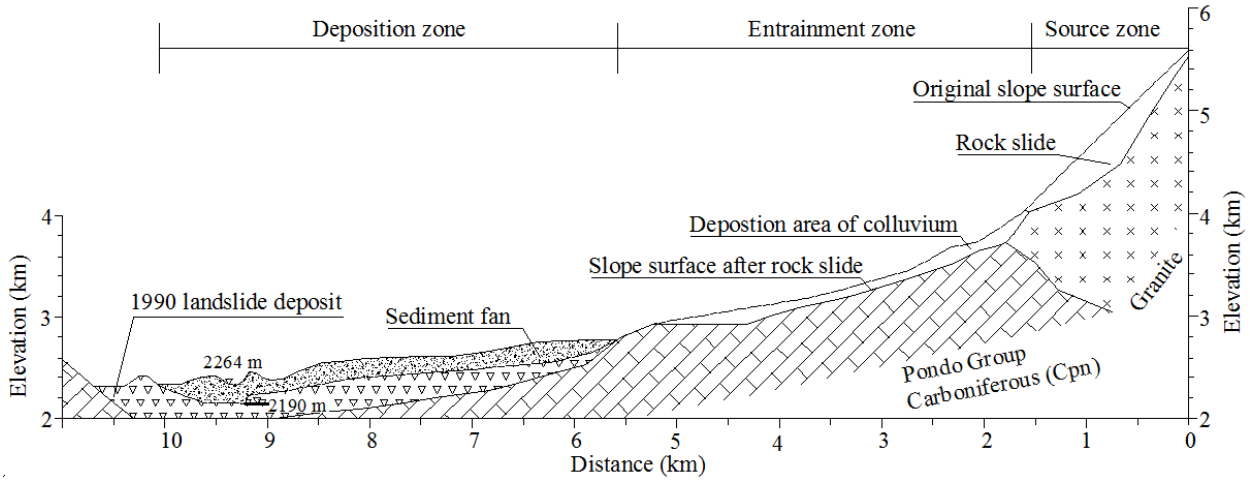

Figure 6-10: Longitudinal profile along YRA path

Since small size rock avalanche frequently occurred. A discharge channel was excavated in the deposition fan in 2000. The shape of deposition fan has been changed considerably, but the main features of YRA were still visible when field investigation was conducted in 2002. The elevation of the channel bed is about 2,190m (Yin 2000). Surveyed topographic map measured using total station shows that the deposition fan has been cut down by about 100m (Figure 6-11).

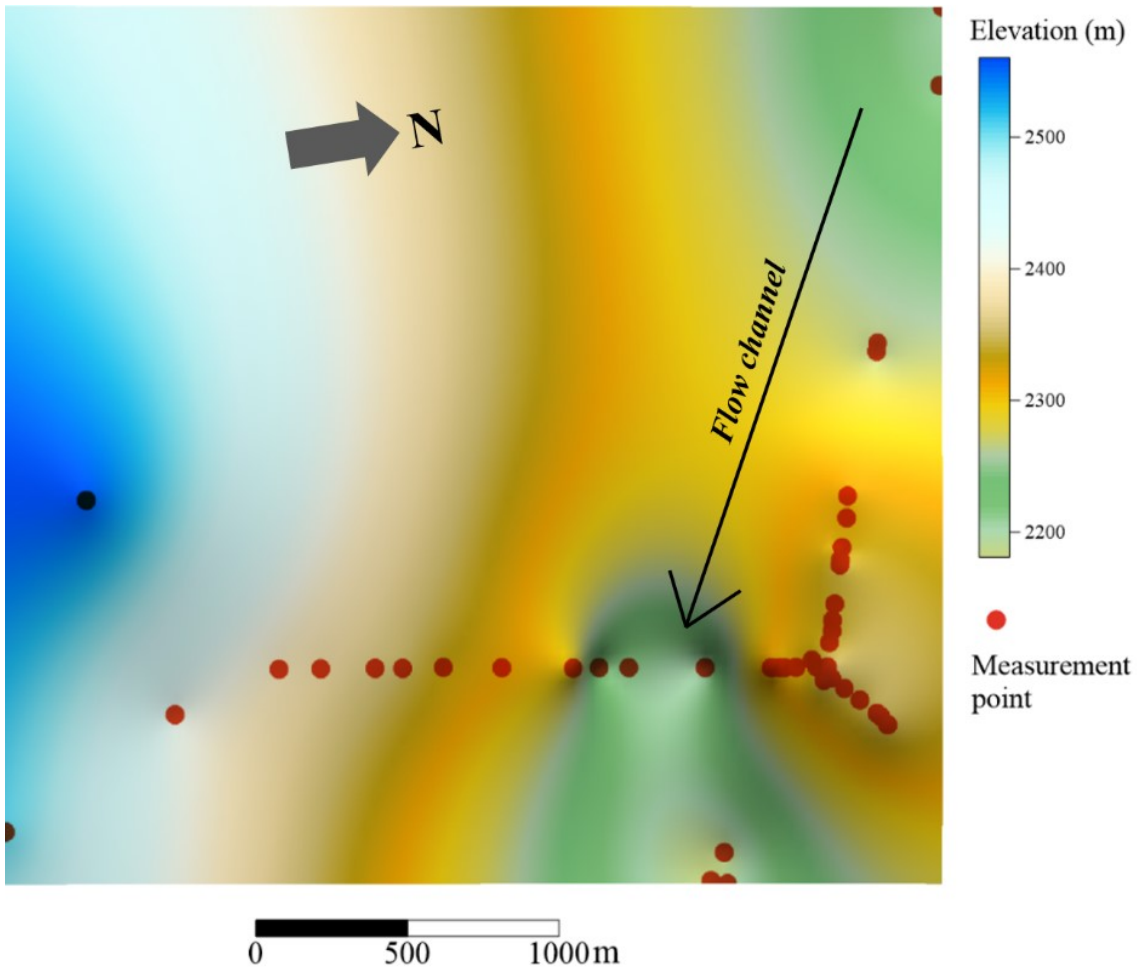

Figure 6-11: Terrain of deposition fan surveyed 2 years later

6.4.6. Consequence of the Yigong Rock Avalanche

Although the YRA is an extremely large rock avalanche in recent year, fortunately there was no casualties reported. However a barrier dam was formed and it blocked the Yigong River (Figure 6-12). The water surface elevation before this event was constant at about 2,210m, and the total amount of water in Yigong Lake was $70\times10^6 m^3$. After the river was blocked, water surface level rose rapidly (Lv et al. 2002). A 30 m deep discharge channel was completed on June 3, 2000 and the lake level started to drop on June 10, 2000, see Figure 6-13, (Liu et al. 2013). It took almost one week for the water level in the lake to return to the river level before the event. Unfortunately 4,000 people were stranded in this process putting their lives at risk. Besides, many villages and farmland were flooded (Yin 2000).

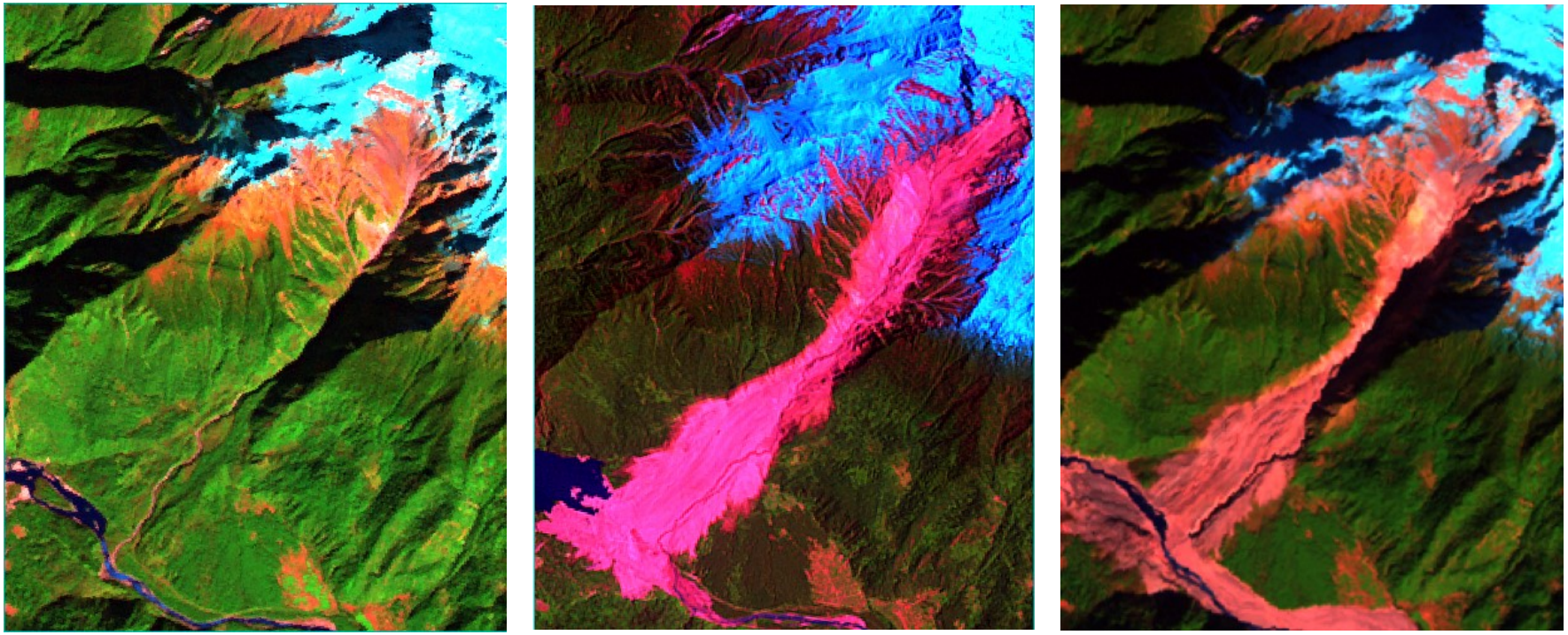

(a) Pre-event (LandsatTM-5, 1998-12-15) **(b) Post-event (LandsatTM-7, 2000-05-20)** **(c) Post-event (LandsatTM-7, 2000-12-30)**

Figure 6-12: Aerial photos at different time indicated that (a) there is an old debris fan (1900), (b) the river was blocked by YRA (2000) and (c) flow channel after overtopping of the dam (Wang, 2006, Lv et al., 2002)

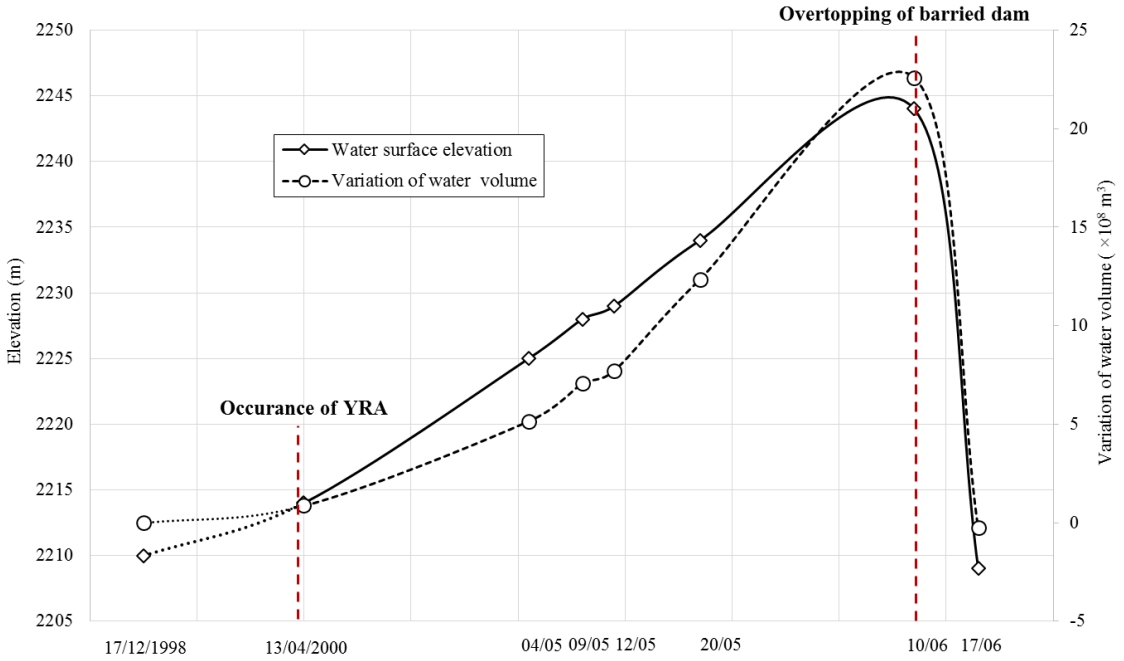

Figure 6-13: Variation of Yigong lake elevation

6.4.7. Possible triggers and evidence of the triggering mechanism

Since two faults, an east-west Jiali right-handed strike slip fault and south-north Yigong-Lulang strike slip fault, cross Zamu creek (Xu et al. 2012), with large temperature difference between day and night, joints and fissures are well developed at this region (Zhou et al. 2000).

Since there was no record of seismic activity before the rock avalanche, variation of temperature and rainfall become the most likely triggers of YRA. As the temperature record of one weather station cannot accurately describe the weather change of a small area few kilometers away from this station, according recorded land surface temperature at three weather stations around Yigong area, see Figure 6-14a, the Ground Surface Temperature (GST) and precipitation were interpolated using Inverse Distance Weighting Method. The interpolated results are shown in Figure 6-14b and c. It is clearly shown that large differences in GST between day and night time were detected. Due to the variation of temperature, snow melts when temperature rises above

zero, and water freezes if temperature drops below $0^{o}C$. This freeze-thaw process can induce to active physical weathering. In this freezing process, the force of expansion caused by freezing of water could result in the development of fissures and crack. In the thawing process, melted water can fill the pores caused by crack development. Also, the new filled water could cause the increase in pore water pressure in the cracks and the decrease in effective stress. When the shear stress exceeds the shear strength of the material, a wedge can form and it may slip suddenly from the mountain top.

Figure 6-14b indicates that the mean GST in this region rose from -0.6°C to 10.7°C 10 days before the occurrence of YRA while the highest GST increased from 9.7°C to 46.7°. Although the mean temperature dropped to 5.9°C 3 days before the event, it rose to around 11.4°C one day before the event. On the day of the event, the highest GST was 36.0°C. It was also recorded that the highest daily temperature of this area mostly appeared at around 16:00 to 18:00 (Zhou et al. 2000). Adding the time needed for heat conduction in rock blocks and air in open spaces between rock blocks, this may explain why this event occurred few hours late after 18:00.

The interpolated daily precipitation shows that there were only 2mm-4mm precipitation one day before YRA see Figure 6-14b. This amount of water is not enough to reduce the strength or increase the driving force for the material at source area. If surface evaporation is taken into account, the water is lesser. Therefore, it is most likely that melted snow provides the source of water for loosely packed material lying on channel bed since the mean GST was higher than the freezing point. Therefore, it means that variation in temperature resulted in changes in snow and ice melting causing pore water pressure to increase is the main trigger for the occurrence of YRA.

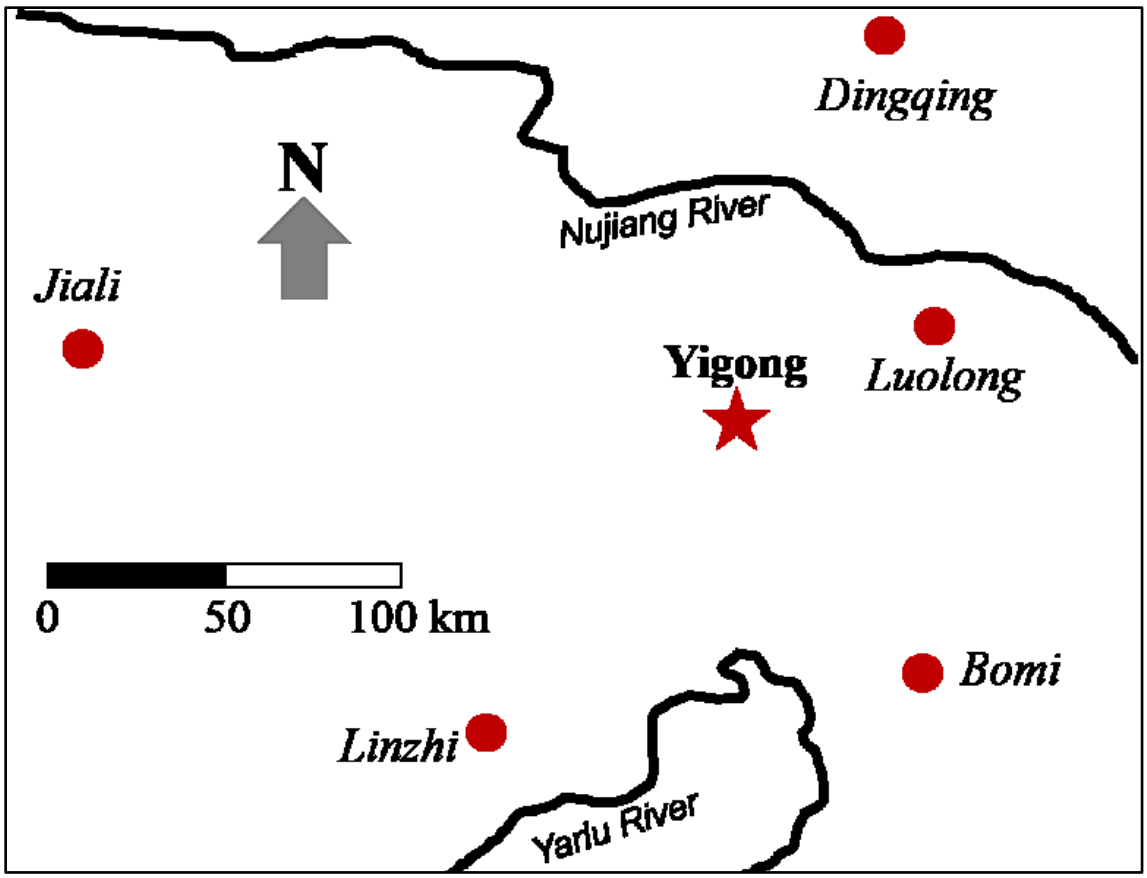
Dingqing
N
Nujiang River
Jiali
Yigong
Luolong
0
50
100 km
Bomi
Linzhi
Yarlu River

(a)

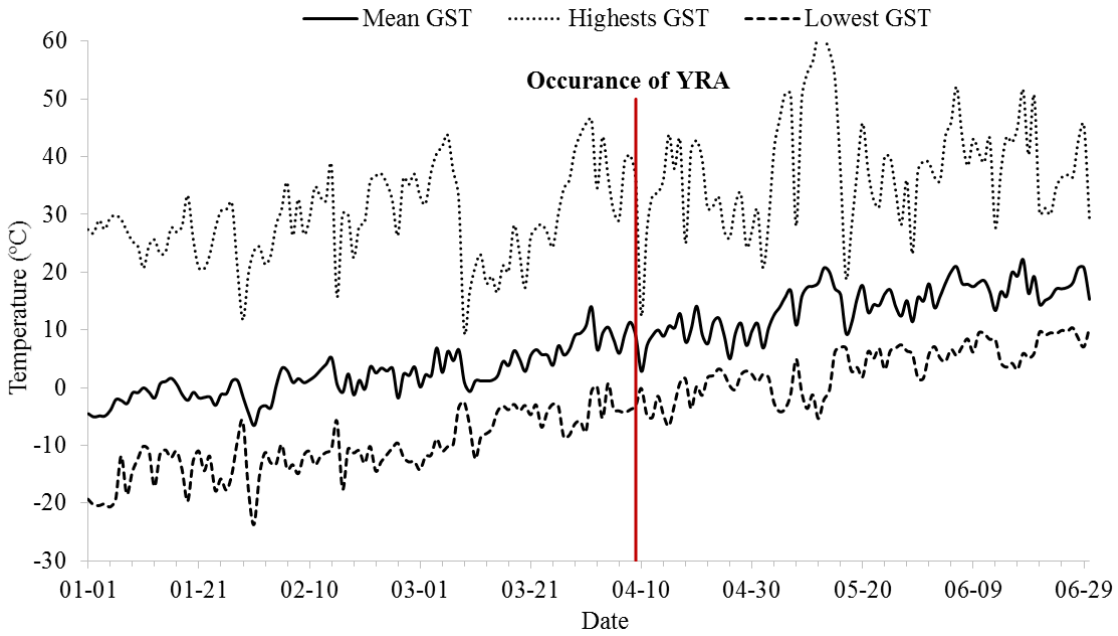
Mean GST
Highests GST
Lowest GST
Occurance of YRA
Temperature (°C)
60
50
40
30
20
10
0
-10
-20
-30
01-01
01-21
02-10
03-01
03-21
04-10
04-30
05-20
06-09
06-29
Date

(b)

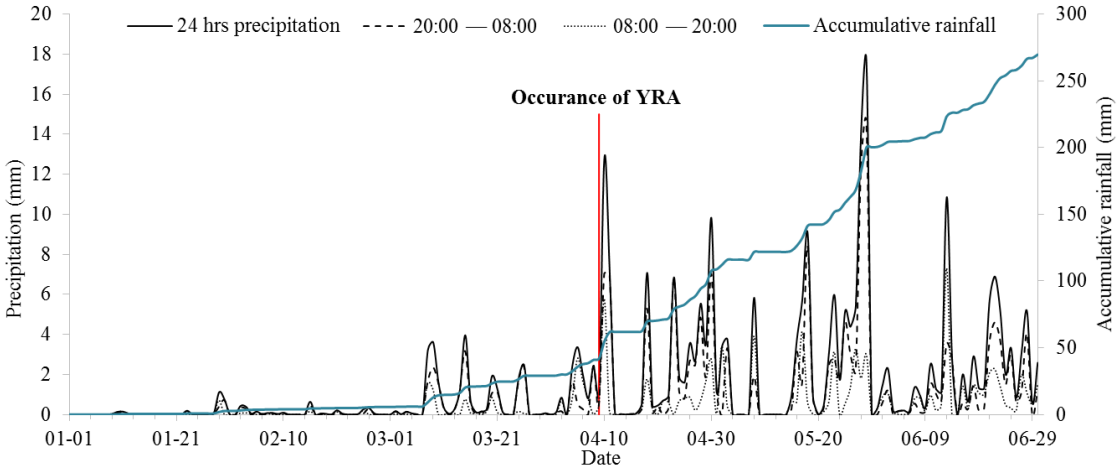

(c)

Figure 6-14: Ground surface temperature and precipitation before and after the event interpolated from surrounding weather stations. (a) weather stations located around Yigong area; (b) and (c) are ground surface temperature and precipitation interpolated from the stations shown in (a).

6.5. Runout and entrainment analysis

According to the data collected in the field, granular particles deposited at the rock avalanche fan mainly came from the source area and transported from the entrainment zones. If the entrainment zone is close to the deposition fan and rock fragmentation has not taken place, particles located in the entrainment region should be about the same size as those in the deposition zone. Although samples can be collected in the deposition fan, it is very difficult to conduct sieve analysis since the particle ranges from very fine (clay) to very large (boulder). Therefore, a practical way to estimate the medium size of the material is to analyze the composition of the material. According to the description of the loose material at the deposition area (Xu et al.,

2012) and particle size distribution curve obtained from the laboratory test, it is estimated that the medium size, d_{50}, of the material is around 300 mm.

Since it is nearly impossible to measure α_0 for all particles in place, an indirect method to estimate the mean of normal distribution is used here. The value of α_0 may be obtained from the pivoting angle and the slope angle. In the simulation, the pivoting angle of the angular particle, ϕ_p, is estimated using the empirical relationship from Li and Komar (1986). The average slope angle can be obtained from the digital elevation model. A mean value of the normal distribution PDF of 12º is calculated based on the relationship $\alpha_0 = (\pi/2-\phi_p-\theta)$. Based on the results of sensitivity analyses, the standard deviation is found to be equal to 0.1 for this case. When the particles are eroded, close-packed particles mobilized and becomes loose. Porosity of the eroded material increase. This will cause the expansion of the material. Based on the Law of Conservation of Mass, a bulking factor is defined as ratio between the density of the material in the channel bed and the density of the debris. In the calculation, the volume of the eroded material in the debris is equal to the volume before it is eroded times the bulking factor.

The Voellmy model is used to calculate the shear stress exerting on channel bed. Xu et al. (2012) used the friction angles ranging from 0.52º to 20º on different longitudinal sections of YRA. Since the model is developed based on dry granular flow, a lower friction angle and basal friction angle are suggested to offset the effect of water on the soil friction. An internal friction angle of 13º and basal friction angle of 12º were used in the simulation which is smaller than that used by Xu et al. (2012). A turbulent coefficient of 500 m/s^2 indicating the roughness of flow surface is adopted in the simulation which is a little bit larger than the medium value suggested for rock avalanche (Luna et al. 2012), but it is still within the reasonable range of values. Parameters used in the simulation are summarized in Table 6-1.

Table 6-1: Parameters in the simulation

Run-out model parameters	Values
Unit weight (kN/m^3)	20
Internal friction angle (°)	13
Basal friction angle (°)	12
Turbulent coefficient (m/s^2)	500
Entrainment model parameters	
Particle size d_{50} (mm)	300
Standard deviation of α_0 (°)	0.1
Mean value of α_0 (°)	12
Particle density (kg/m^3)	2,600
Bulking factor	1.3

The longitudinal profile shown in Figure 6-10 is divided into three zones from top to bottom: source zone, entrainment zone and deposition zone. In the simulation, original slope surface changes due to the entrainment at medium part of the profile. Based on the observed source volume and area of source material in 2D, a uniform width, 173m, is calculated which keeps constant in the simulation. The number of slices could impact the calculation results. To investigate the sensitivity of the number of slice on the model results, the source material is divided into 50 slices in another run. The difference in runout distance, velocity and total volume are 0.6%, 0.1% and 1%, respectively. After evaluating the required time for the calculation and resolution of calculated results, the model with 30 slices is adopted.

6.6. Simulation Results

6.6.1. Results of runout and entrainment analyses

In the simulation, the front velocity of the rock avalanche was calculated. The calculated front velocity of YRA increases in the first 30 seconds and then gradually drops when the material reaches a relatively flat area as shown in Figure 6-10. A plot of the velocity versus path distance is shown in Figure 6-15. The maximum velocity occurred at a path distance around 3500m. At about 140s, the front of the debris almost stopped moving but the remaining part kept moving at

a very small velocity. The change of profile of YRA at different time stage is shown in Figure 6-16.

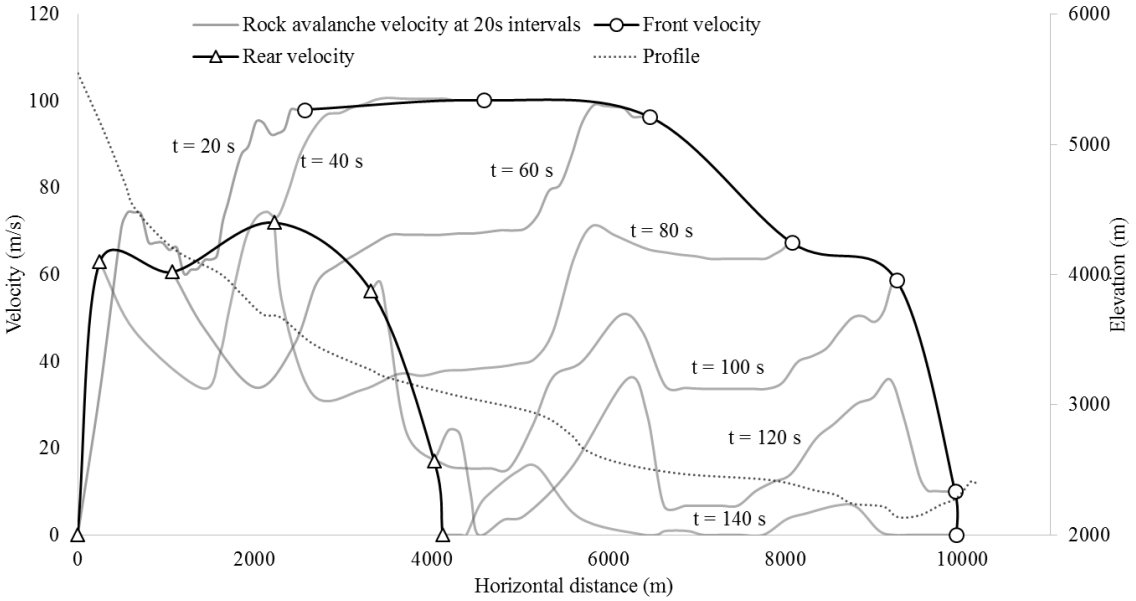

Figure 6-15: Velocity and its variation in the simulation

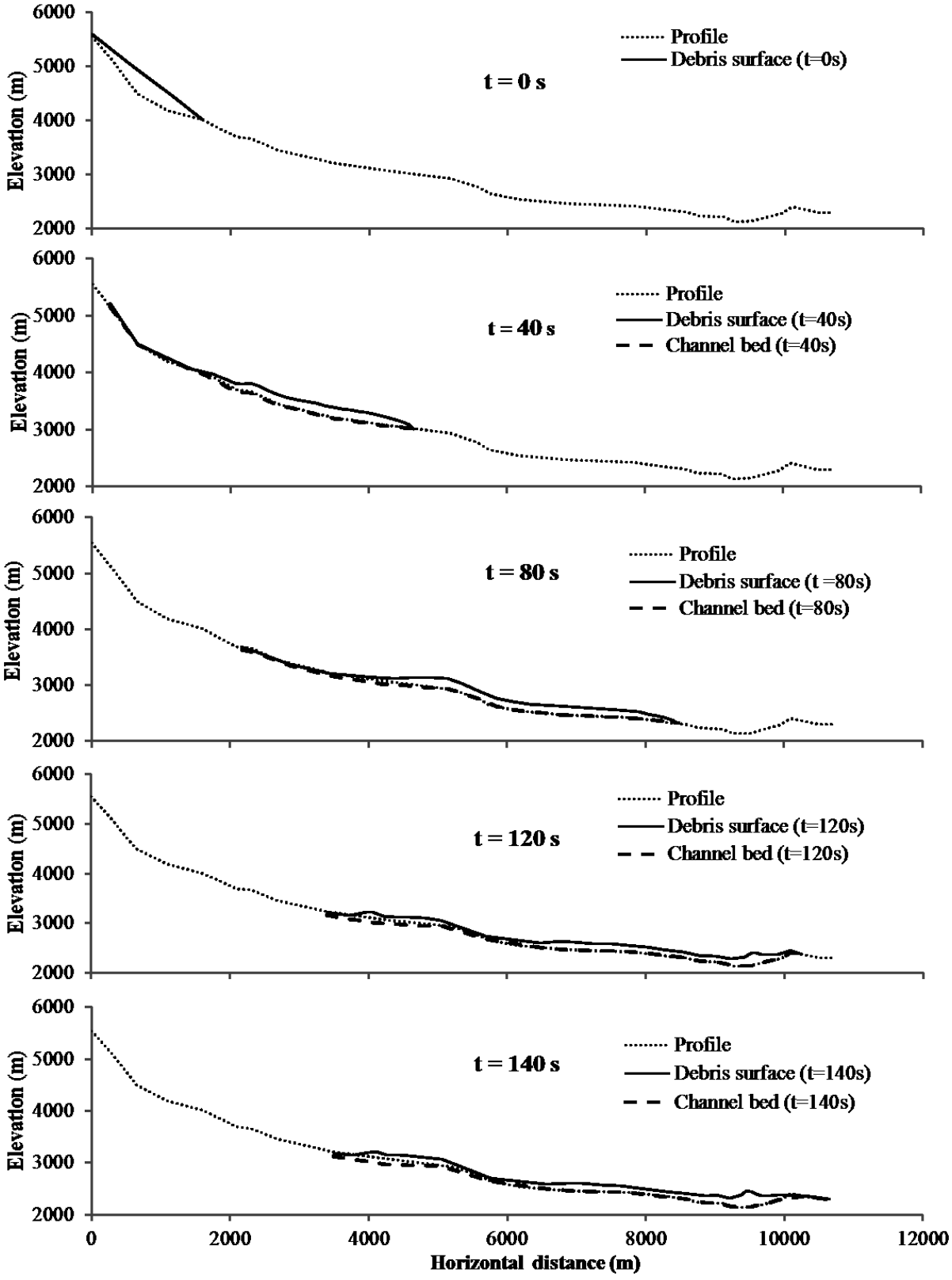

Figure 6-16: Change of profile in each simulation steps

Since YRA has a large initial volume travelling at high velocity, the entrainment rate is expected to be very large. The depth of erosion is assumed to be 280m in runout analysis using DAN (Zhang 2013). The entrainment rate of each slice at different time stage in this simulation is shown in Figure 6-17. The maximum entrainment rate is 1.79m/s at the initial stage (Figure 6-18). The entrainment rate increases after 100s since the accumulated flow height has increased. This is an important drawback in 2D analysis. At first half of the analysis, the entrainment rate increases to 1.7m/s rapidly varying between 1-2m/s before the debris stops moving. The maximum height of the rock avalanche decreased with time until the front suddenly reaches the flat area. The calculated maximum height of debris in the deposition area is about 320m. The calculated maximum depth of erosion is 108m located at x=4,218m (Figure 6-19).

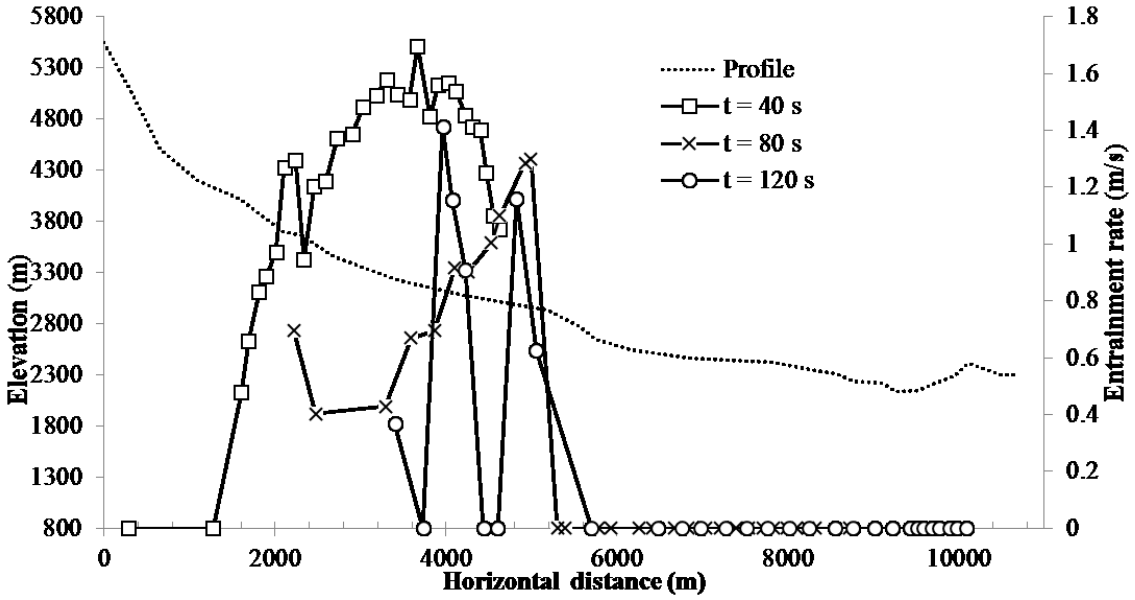

Figure 6-17: Entrainment rate along the channel at different time stage

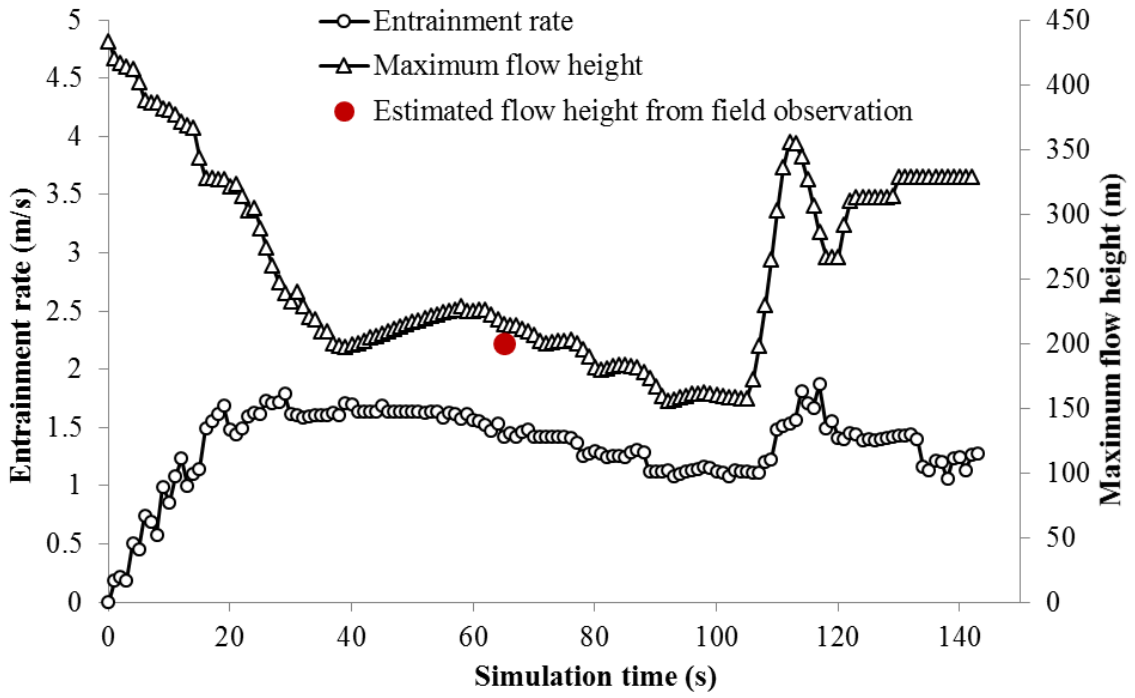

Figure 6-18: Maximum entrainment rate and flow height in the simulation of 2000 Yigong Rock Avalanche

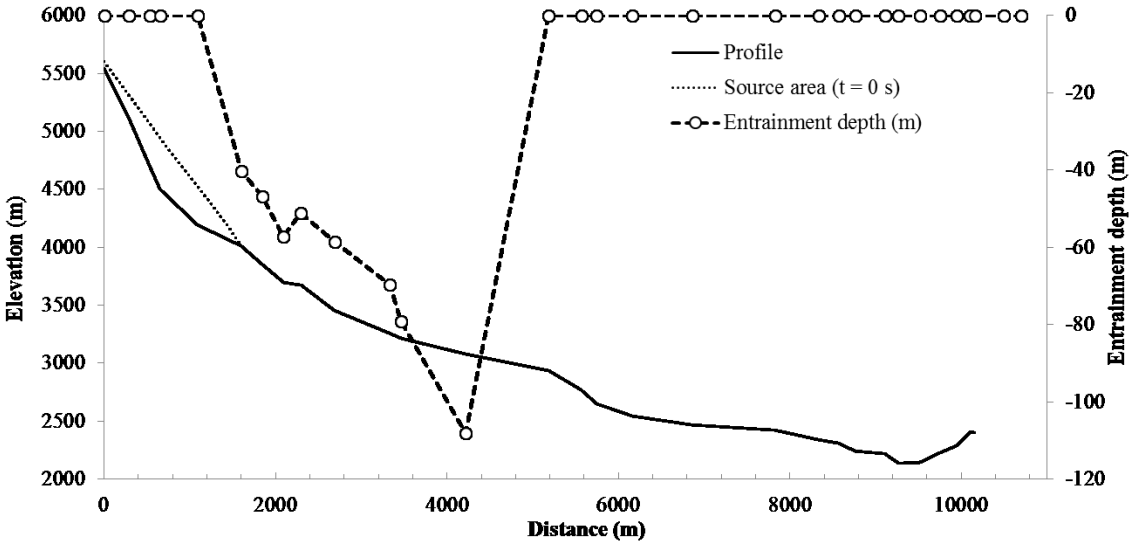

Figure 6-19: Simulated depth of erosion along the channel

The initial volume of the debris starts at $90\times10^6 m^3$ and increases gradually until the front has moved about 10km (Figure 6-20). When the front has almost stopped, the total volume is still

increasing due to the entrainment in the tail region. The maximum increase in volume of $1.03\times10^6 m^3$ occurred at a run-out distance of about 5161m. The front velocity at that location is higher than 100m/s. The calculated accumulated volume is not as large as that observed in the field due to neglecting bank entrainment and broadening of flow channel in the entrainment zone.

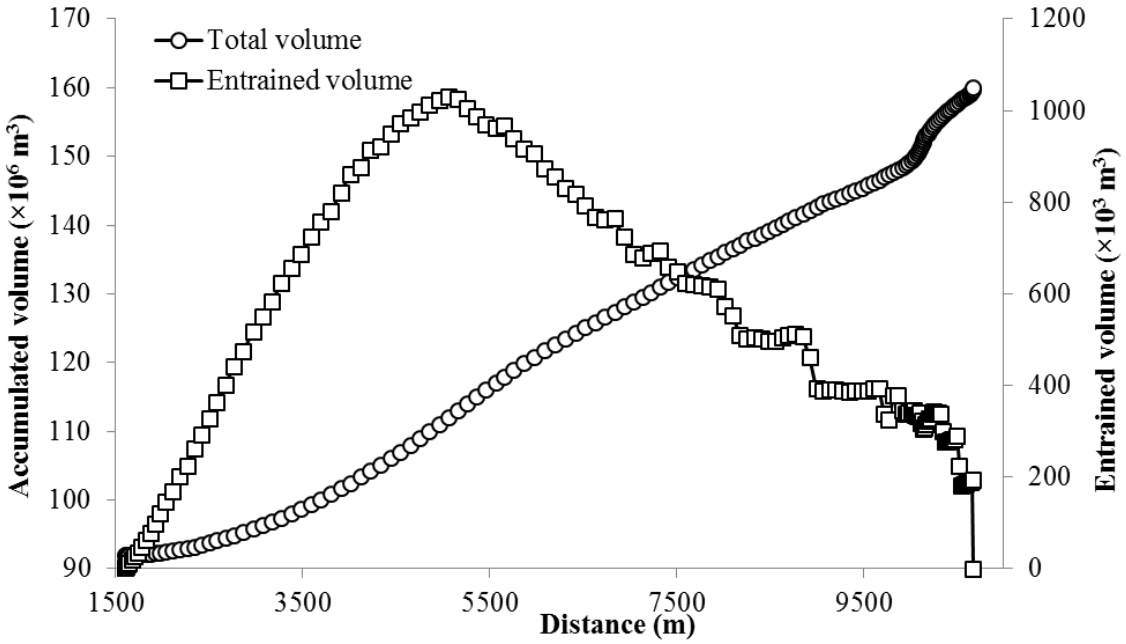

Figure 6-20: Entrainment volume and total volume in the simulation

6.6.2. Validation of modelling results

Validation of the runout and entrainment model is based on field observations such as the estimated runout distance and deposition height. Also, results from published literature are used in evaluating the model. In the model the calculated runout distance is about 10km which matches the field observation. Since the width of flow channel doesn't change a lot in entrainment zone, based on the volume of the debris, the depth of entrainment can be calculated. The calculated depth of erosion is the change of the elevation of bed points in the calculation

which is adjusted to the direction perpendicular to the slope surface. The observed depth of entrainment versus the calculated values at entrainment zone with a 100m interval are shown in Figure 6-21.

To compare the calculated final height of the depositional fan in 2D with field observation which is in 3D, the calculated depositional height has to be adjusted to represent the field situation. A correction coefficient, C_{LS}, for lateral spreading is defined as

$$C_{LS} = W_{\mathrm{mod}el} / W_{fan} \qquad [6\text{-}7]$$

where W_{model} and W_{fan} are, respectively, the channel width in the model and width of deposition fan. W_{model} is the width of channel calculated by dividing the total volume of source material by total area of source material in 2D profile. W_{fan} is the average width of the deposition fan. A volume and height (h_{fan}) relationship and volume and width (W_{fan}) relationship can be found for this area based on the digital elevation model of deposition fan. Based on this relationship, an equivalent width (W_{fan}) can be determined for a rectangular model cross section with the same debris height (h_{fan}) and the same volume. Since the debris flow channel on site is always triangle, the cross section of debris flow channel is changed to rectangle before calculating W_{fan}. The final deposition height is modified by multiplying the correction coefficient, see Figure 6-22. The average flow height measured using a total station is also shown in the figure. It is seen that the modified deposition height is very close to the average value although there are some variations at some points.

YRA is described as a very rapid rock avalanche, but there are very few evidences that can directly provide a measurement of its actual velocity. From the trees destroyed by air pressure wave on two sides of valley and the slurry attached on the trees on the top of a mountain located

at left side of the outlet, it can be assumed that YRA occurred with a very high velocity. The calculated maximum velocity is around 110m/s which agrees reasonably well with the value calculated by Zhang (2013) using DAN 3D. This is a controversial value since this is a very high velocity compared with velocity observed in other cases although description from witness and charred tress along the channel indicated YRA has a very high velocity, but such high peak velocity, 81-100 m/s, has been reported by Evans et al (1989) for case of Pandemonium Creek rock avalanche.

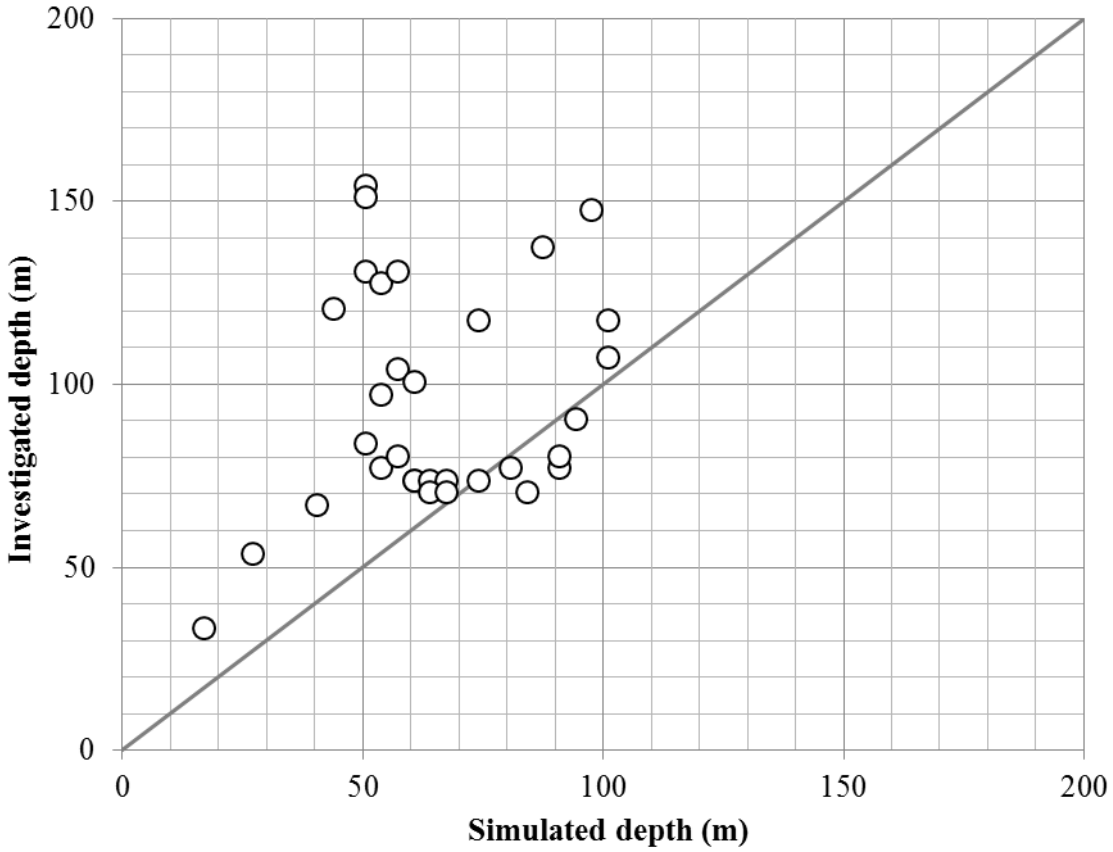

Figure 6-21: Scatter plot between observed depth of erosion in field after event and the calculated depth of erosion

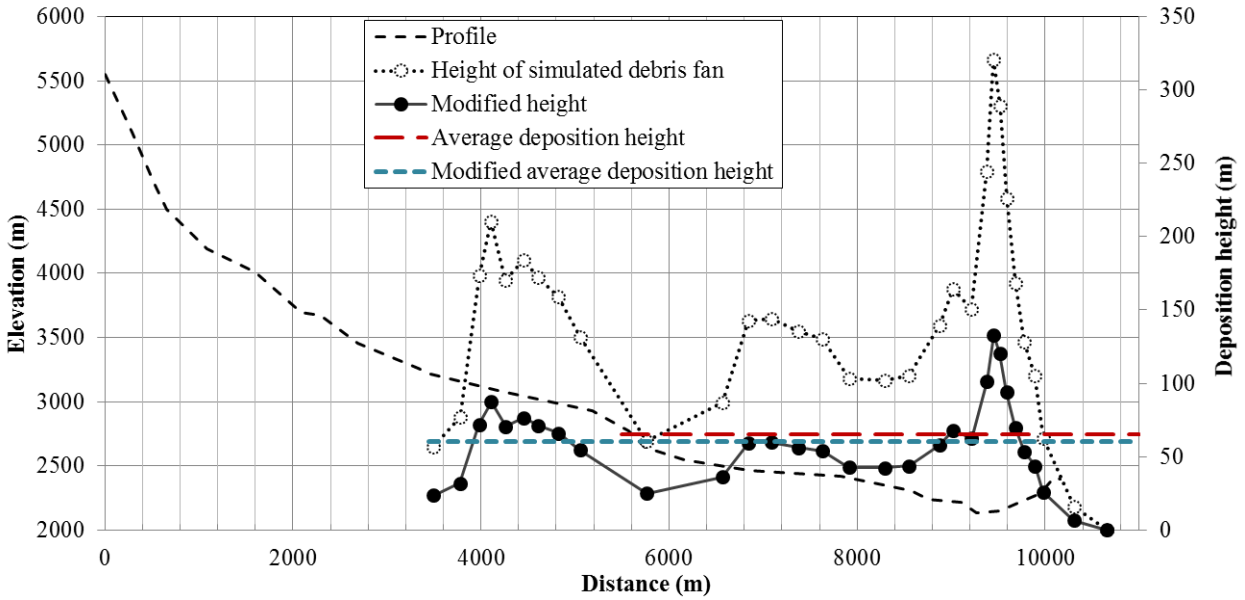

Figure 6-22: Modified deposition fan by taking lateral spreading into consideration

To test the effect of entrainment on YRA, the simulation results are compared with and without entrainment, see Figure 6-23. It is obvious that the runout distance from the simulation with entrainment is around 1,000m further than that without entrainment. The front velocity with entrainment is also higher than that without entrainment. This is mainly caused by the increase in potential energy with the introduction of more material in the debris. Moreover, the entrained material will generate more basal friction. The combination of these effects lead to the difference in the runout distance and maximum velocity. Although the differences are not large, since the velocity and runout distance are relatively large due to the scale of the problem, a small increase in velocity and runout distance mean a large increase in kinetic energy. Consequently, the increase in kinetic energy will cause more damages and destructions. The incorporation of entrainment in the debris flow calculation provides a more rational approach than simply assuming a constant volume from start to finish or an empirical assignment of additional mass to the model at specific locations.

At the same time, simulation time for no entrainment is shorter than that with entrainment. It means that omission of entrainment could underestimate the front velocity and runout distance. This could have negative effects in mitigation measures of natural hazards by underestimating the extent and speed of the debris.

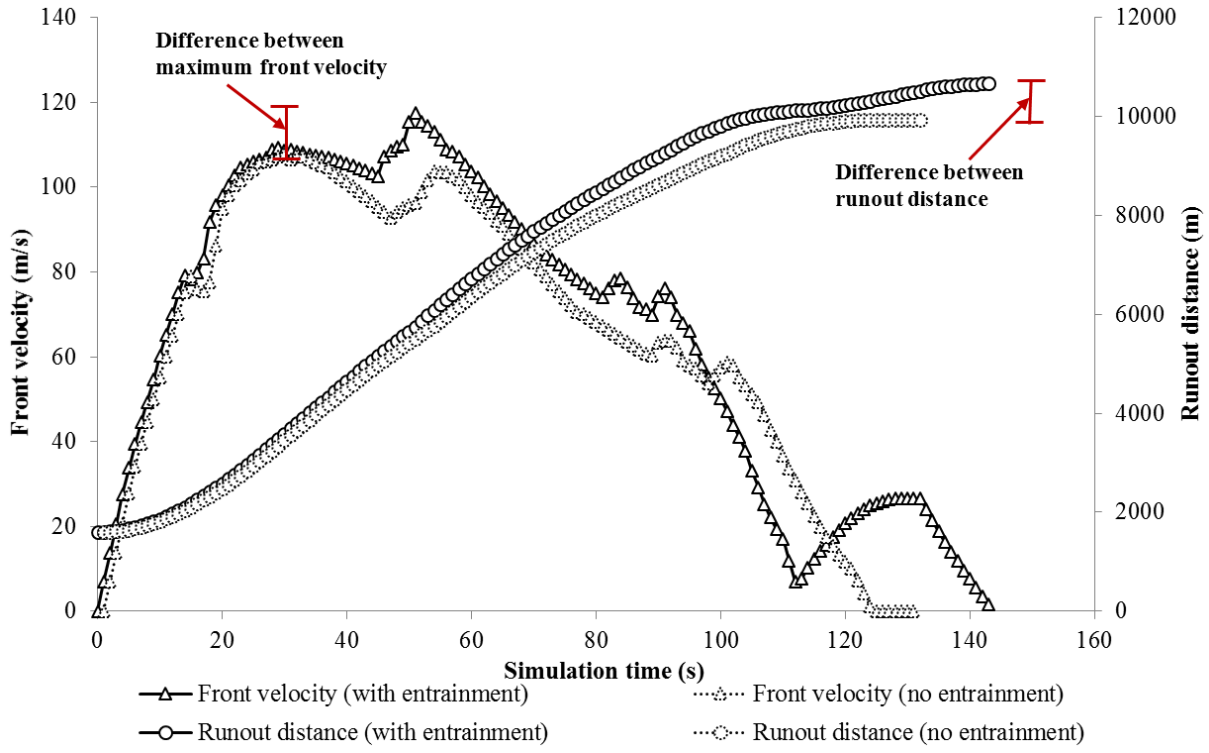

Figure 6-23: Comparison of maximum velocity and front velocity of YRA with and without entrainment

6.7. Discussion and conclusion

YRA is an extremely large mass movement in recent years. According to the metrological record of weather stations near the Yigong area, rainfall should not be the main trigger of the rock avalanche. Instead, it was found that the most likely triggering mechanism is temperature variation, which resulted in snow/ice melting in cracks and fissures causing the increase in pore water pressure and the decrease in effective stress. Eventually, the slide detached from slope

when the shear stress overcomes the shear strength of the rock mass. The YRA occurred at late afternoon when highest GST just pasted few hour ago, this is another evidence that indicates occurrence of YRA is related to the variation of temperature.

It is clearly shown in the simulation results of YRA that the calculated run-out distance and flow height at specific locations match reasonably well with the observed value. Also the variation in elevation in the entrainment zone is another indication that the model is reasonable in capturing entrainment. The deposition height of the debris cannot be compared directly with field observation using a two dimensional model. The height of the debris can cause changes in shear stresses on the channel bed which will change the entrainment rate and depth of erosion. In this model, a lateral spreading correction coefficient is introduced to relate the 2D model with 3D reality. Also the assumption of uniform particle size on the channel bed can increase the discrepancy between calculated results and observed values.

Although the maximum calculated entrainment rate shows some variation with time, the variation is not large except in places where the channel bed is slopping steeply. Entrainment rate of each slice has no regularity along the flow path at different time stage. Entrainment rate in the new model is dependent on slope of flow channel and properties of erodible material. Therefore, estimation of entrainment should be taken those factors into account.

The proposed entrainment model calculates entrainment volume with time. This is more reasonable in considering progressive scouring since material are eroded gradually. Therefore the model can be used to simulate entrainment of channel eroded by flow at different elapsed time. Moreover channel bed elevation is adjusted after each time step to reflect changes due to entrainment which provides a more realistic simulation. This is more important in short channel with a lot of entrainment than a long channel with little entrainment.

Shearing of layers of material refers to the shear failure of material calculated based on static shearing resistance. Instead, the sliding motion refers to the sliding movement of the particle relative to the base material when the low friction is not sufficient to resist motion at the particle contact with the base, otherwise, the rolling motion occurs. This model not only incorporates the rolling motion of entrainment, it also consider the sliding motion of particle and shearing layers of materials which is often the only mechanism considered in many entrainment model. Incorporating the rolling motion in entrainment calculation provides a new concept in advancing the understanding the mechanism of entrainment in debris flow analysis.

One of the uncertainty in the proposed entrainment model is the method in determining the mean value and standard deviation in the PDF (probability density function). Since the particles in the field are not all spherical in shape and particle size varies a lot, particle protrusion relative to each other is difficult to measure. Therefore particle properties cannot be easy captured using only one PDF. In the case of YRA, the parameters were determined by trial and error based on field observations and empirical relationship.

Acknowledge: This study is sponsored by the Key Project of National Natural Science Foundation of China (Grant No. 41030742), the Major Projects of National Natural Science Foundation of China (Grant No. 41190084) and the Natural Science and Engineering of Canada Discovery grant. The data used in this study is provided by the Institute of Mountain Hazards and Environment, CAS. The aerial photo and DEM are obtained from the Ministry of Land and Resources of the P.R.C.

Reference

Chen, X. Q. (2015). Evidence of flow height near the outlet of Zamu Creek [Fig. 5] (Personal communication, 11 11 2014).

Chen, X. Q. (2015). Observed largest particle embedded into deposition fan [Fig. 7] (Personal communication, 11 11 2014).

Cheng, N. S., Law, A. W. K., and Lim, S. Y. (2003). Probability distribution of bed particle instability, Advances in Water Resources, 26(4), 427-433.

Cundall P. A., and Strack O. D. L. (1979). A discrete numerical model for granular assemblies, Geotechnique, 29, 47-65.

De Blasio, F. V., Breien, H., and Elverhoi, A. (2011). Modelling a cohesive-frictional debris flow: an experimental, theoretical, and field-based study, Earth Surface Processes and Landforms, 36(6), 753-766.

Egashira, S., Honda, N., and Itoh, T. (2001). Experimental study on the entrainment of bed material into debris flow, Physics and Chemistry of the Earth, Part C: Solar, Terrestrial & Planetary Science, 26(9), 645-650.

Evans S. G., Clague J. J, Woodsworth G. J., and Hungr O. (1989). The Pandemonium Creek rock avalanche, British Columbia. Canadian Geotechnical Journal, 26(3), 427-446.

Fannin, R.J., Busslinger, M., and Jordan, P. (2012). Debris flow travel distance: Field traverse data and regional guidelines for terrain stability assessment, Proceeding of the 11th International and 2nd North American Symposium on Landslides, Editors: Erik Eberhardt, Corey Froese, A. Keith Turner and Serge Leroueil, Banff Canada, June 3-8, 2012, Balkema, Taylor and Francis Group, London, 1: 751-756.

Fenton, J. D., and Abbott, J. E. (1977). Initial Movement of Grains on a Stream Bed: The Effect of Relative Protrusion, Proceedings of the Royal Society of London Series a-Mathematical Physical and Engineering Sciences, 352(1671), 523-537.

Fraccarollo, L., and Capart, H. (2002). Riemann wave description of erosional dam-break flows, Journal of Fluid Mechanics, 461, 183-228.

Hungr, O. (1995). A model for the runout analysis of rapid flow slides, debris flows, and avalanches, Canadian Geotechnical Journal, 32(4), 610-623.

Iverson, R. M. (2012). Elementary theory of bed-sediment entrainment by debris flows and avalanches, Journal of Geophysical Research, 117, F03006, doi:10.1029/2011JF002189.

Li Z. L., and Komar P. D. (1986). Laboratory measurements of pivoting angles for applications to selective entrainment of gravel in a current, Sedimentology, 33 (3), 413-423.

Liu N., Chen Z. L., Cui P., and Chen N. S. (2013). Dammed lake and risk management. Beijing: Science press. (In Chinese)

Luna, B. Q., Remaitre, A., van Asch, T. W. J., Malet, J. P., and van Westen, C. J. (2012). Analysis of debris flow behavior with a one dimensional run-out model incorporating entrainment, Engineering Geology, 128, 63-75.

Lv, J. T., Wang, Z. H., and Zhou, C. H. (2002). A tentative discussion on the monitoring of the Yigong landslide-blocked lake with satellite remote sensing technique. Acta Geoscience Sinica, 23(4), 363-368. (In Chinese).

Medina, V. H, Bateman, A., and Hurlimann, M. (2008a). A 2D finite volume model for bebris flow and its application to events occurred in the Eastern Pyrenees, International Journal of Sediment Research, 23(4), 348-360.

Medina, V. H., Hurlimann, M., and Bateman, A. (2008b). Application of FLATModel, a 2D finite volume code, to debris flows in the northeastern part of the Iberian Peninsula, Landslides, 5(1), 127-142.

Moffat, R, Fannin, R. J., and Garner, S. J. (2011). Spatial and temporal progression of internal erosion in cohesionless soil, Canadian Geotechnical Journal, 48(3), 399-412.

Okada, Y., and Ochiai, H. (2007). Coupling pore-water pressure with distinct element method and steady state strengths in numerical triaxial compression tests under undrained conditions, Landslides, 4(4), 357-369.

Ren, J. W., Shan, X. J., Shen, J., Ge, S., Zha, S., Deng, G. Y., Zhang, J., and Suo, R. (2001). Geological characteristics and kinematics of the rock fall-landslide in Yigong，Southeastern Tibet, Geological Review, 47(6), 642-647. (In Chinese).

Schurch, P., Densmore, A. L, Rosser, N. J., and McArdell, B.W. (2011). Dynamic controls on erosion and deposition on debris-flow fans, Geology, 39 (9), 827-830.

Shodja, H. M., and Nezami, E. G. (2003). A micromechanical study of rolling and sliding contacts in assemblies of oval granules, International Journal for Numerical and Analytical Methods in Geomechanics, 27(5), 403-424.

Skempton, A.W. (1954). The pore-pressure coefficients A and B, Geotechnique, 4(4), 143-147.

Wang, X. B. (2008). Geotechnical analysis of flow slides, debris flows, and related phenomena (Doctoral dissertation). University of Alberta, Edmonton, Canada.

Wang, X. B, Morgenstern, N., and Chan, D. (2010). A model for geotechnical analysis of flow slides and debris flows, Canadian Geotechnical Journal, 47(12), 1401-1414.

Wang, Z. H. (2006). Large scale individual and slide remote sensing'. Earth Science Frontiers, 13(5), 516-523. (In Chinese).

Wang, Z. H., and Lv J. T. (2001). Understand Yigong landslide in Tibet based on the satellite image'. Journal of Remote Sensing, 5(4), 312-316. (In Chinese).

Xu, Q., Shang, Y. J., Van Asch, T. W. J., Wang, S. T., Zhang, Z. Y., and Dong, X. J. (2012). Observations from the large, rapid Yigong rock slide– debris avalanche, southeast Tibet. Canadian Geotechnical Journal, 49(5), 589-606.

Yin, Y. P. (2000). Charateristics and mitigation study on the gigantic Yigong avalanche of Bomi, Tibet, China. Hydrogeology&Engineering Geology, 4, 8-11. (In Chinese).

Yin, Y. P. (2000). Introduction on the gigantic Yigong avalanche of Bomi, Tibet, China. The Chinese Journal of Geological Hazard and Control. 11(2), 100. (In Chinese).

Zhou, G. Y., and Yi, Y. Z. (2000). ADCP monitoring in emergency treatment of Yigong massive landslide in Tibet. Yangtze River, 31(9), 30-32. (In Chinese).

Zhang, M., and Yin, Y. P. (2013). Dynamics, mobility-controlling factors and transport mechanisms of rapid long-runout rock avalanches in China, Engineering Geology, 167, 37-58.

Zhang, Y. J. (2013). Study on dynamic characteristics of typical rock avalanches on canyon area (Master's thesis). Shanghai Jiaotong University, Shanghai, China. (In Chinese).

Zhou, G. D., (2015). Grain size distributions of fine particles (d < 400mm) sampled from runout path of YRA [Fig. 8], (Personal communication, 04 11 2014).

Zhou, G. D., (2015). Small size rock avalanche occurred on one side of valley in Zamu creek [Fig. 10], (Personal communication, 04 11 2014).

7. ENTRAINMENT ANALYSIS OF FOUR CASES HISTORIES

7.1. Abstract

During the moving process of debris, material from the channel boundary is often eroded and mixed with the main body of the debris flow and becomes part of the debris. This process can increase the mass of debris flow by eroding the material from the channel. A new entrainment model that considers progressive scouring is incorporated with an energy runout model to simulate entrainment process of debris flow. Four case histories have been studied: Niumian Rock Avalanche (NRA), Fjærland debris flow, Faucon debris flow and Zymoetz River rock avalanche (ZRRA). Volumes, including entrainment volume and total volume, average velocity, runout distance, entrainment rate and flow height have been calculated using the runout model. Field observations, including flow velocity, flow height, the depth of erosion at specific section, run-out distance and total volume at deposition fan, are being used to evaluate the calculated results for each case. It is found that the calculated run-out distance, frontal velocity and total volume agree well with field observations except the calculated depth of erosion and total volume due to neglect of lateral spreading effect in 2D analysis. For comparison, the Niumian rock avalanche is also analyzed using the dynamic entrainment model.

7.2. Introduction

7.2.1. Debris flow event

Debris flow is one of the most hazardous and unpredictable surface process that results in many losses of lives and property damages. Many of them have significant amount of entrainment resulting in a substantially larger final volume than its initial volume (Breien, 2005; Remaître et al., 2009; Tang et al., 2012). Entrainment can change the mechanics and characteristics of flow

thus making prediction and back analysis of debris flow much more difficult (Iverson, 1997; Iverson et al., 2001; Iverson et al., 2004). The rate of this process is mainly affected by the shear stress applied on the bed sediment, the internal friction between the particles, the velocity of the flowing debris, the slope angle of the channel, the cohesion of the bedding material and the pore water pressure generated due to shearing of fine grained materials in the bed (Iverson et al., 2011; Takahashi, 1991).

7.2.2. Debris flow entrainment analysis

Debris flow entrainment has been studied in laboratory and field experiments (Mangeney et al., 2010; McCoy et al., 2012). Several models, including empirical model and analytical model, are developed (De Blasio et al., 2011; Egashira et al., 2001; Iverson, 2012; Medina et al., 2008a).

There are basically two approaches in calculating entrainment: the static approach and the dynamic approach. In the static approach, static shear stresses beneath the debris are calculated and failure is considered when the static shear stress exceeds the shear strength of the material. The depth in which failure occurs is determined and the amount of material is calculated which will be added to the main body of the debris. In the dynamic approach, the rate of entrainment is calculated based on the rate of erosion of the material at the channel bed. The rate of erosion is determined based on shear failure at the surface and the material is removed from the surface based on the velocity of flow of the main body of the debris (Medina et al. 2008a). It is assumed in this approach that the velocity of newly eroded material is the same as the average velocity of the debris flow. However field observations indicate that the velocity of the newly eroded material is not same as the debris (Fraccarollo and Capart 2002; Medina et al. 2008b).

Egashira et al (2001) proposed a formula to calculate erosion rate assuming that the slope of the channel bed is always adjusted to the angle corresponding to limiting equilibrium conditions. The material in the channel left behind by an unsaturated debris will approach the limiting equilibrium slope angle. The geometrical relationship between the initial bed slope and equilibrium slope angle is incorporated into mass conservation law of eroded material to obtain the entrainment rate.

The entrainment model proposed by van Asch et al. is a dynamic one dimensional debris flow model that takes into account the entrainment concept based on the generation of excess pore water pressure under undrained loading on in-situ material (van Asch et al. (2004)). Flow is treated as laminar, single phase and as an incompressible continuum process. Due to the moving mass flowing on the erodible bed, a loading is applied on the bed deposits. The model calculates the loading through changes in the vertical normal stress and shear strength caused by the debris flow (Luna et al. 2012). The increase in pore water pressure is calculated based on the Skempton (1954) equation. The depth of erosion is approximated using the relationship between the factor of safety at the bottom and top of soil in the channel. This model is similar to the dynamic model except that it involves the FOS for erodible layer.

Iverson (2012) considered the behavior of a slide block descending an erodible slope with the ability of incorporating soil on the static bed. Newton's second law is applied on the sliding material. Then, Coulomb friction rule is used and basal friction resistance calculation is improved by taking the shear rate into account. The friction resistance consists of a constant component of friction resistance and a velocity-dependent component. After considering the rate-dependent friction, entrainment rate based on the change in weight of the sliding block is obtained.

De Blasio et al. (2011) suggested a semi-empirical model to calculate entrainment. In the semi-empirical model, entrainment rate depends solely on the tangential component of weight at the base of the flow and on the average velocity of the debris flow. Critical shear stress is used as the thereshold to determine the occurance of entrainment. The measurements from Fjæland debris flow is used in the model calibration. This model seems promising since it relates debris flow velocity and basal shear stress to the calculation of the rate of erosion.

In this paper, a new analytical model is used to perform the entrainment simulation. In the new entrainment model, it is considered that granular particles lying on channel bed are eroded progressively. Both rolling motion and shear failure are considered in the simulation. Newton's Law of Motion is applied to calculate the acceleration, velocity, and displacement of the particle. Then, the rate of erosion is calculated according to the particle acceleration and eroded depth. The entrainment model is then incorporated with an energy based runout model.

7.2.3. Study cases

Four case studies, NRA (China), Fjærland debris flow (Norway), Faucon debris flow (France) and ZRRA (Canada), will be presented in this chapter. The locations of the cases are shown in Figure 7-1. These cases are chosen since there are detailed information about the debris flow publically. Also there is significant entrainment in these cases. Here is a brief description of the cases.

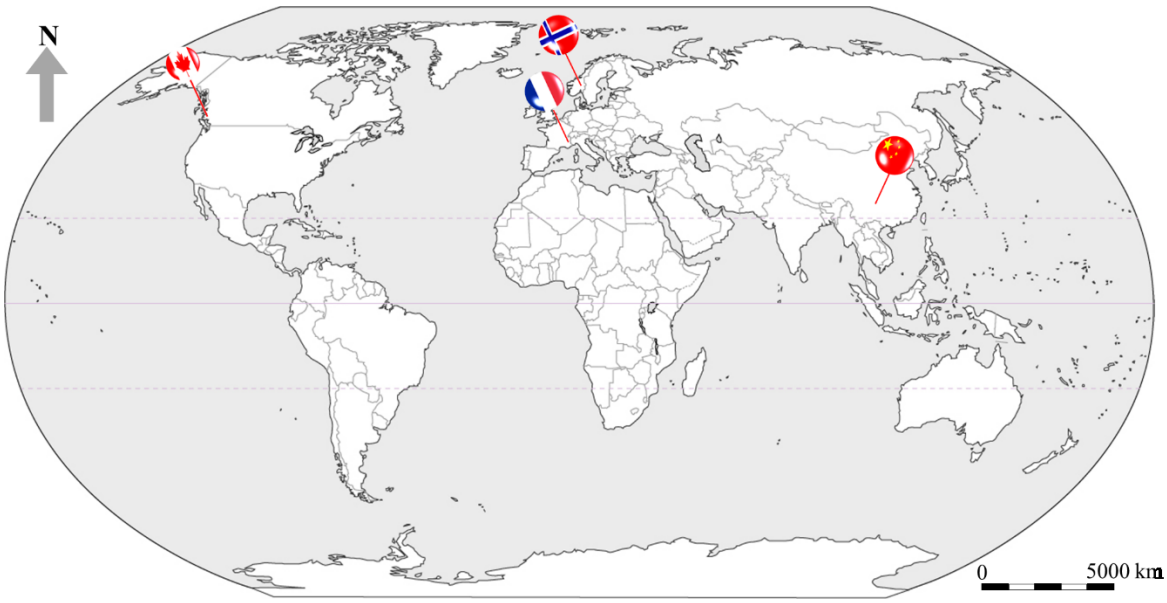

Figure 7-1: Location of case studies on the world map

The Niumian Rock Avalanche (NRA) is located in western China and it was triggered by earthquake. The case has been investigated by Xing et al. (2014). The geological condition and properties of NRA has been described by Xing et al. (2014) and Zhang (2013). Velocities at 5 different cross sections were estimated using superelevation and runup methods. Xing et al. (2014) studied this case using DAN3D model. The final volume and run-out distance have been estimated according to the field investigation. The Voellmy model was used to describe the rheological properties of NRA.

The second case is chosen from Norway Fjærland debris flow (2000). Breien et al. (2008) investigated this case focusing on the hydrological and geomorphological issues. Erosion and bulking process, volume at source area and deposition fan have been estimated quantitatively. The modified BING model was used to describe the rheological property. The entrainment volume was estimated using a semi-empirical model in which entrainment rate is dependent on the average velocity of the debris and critical shear stress for erosion.

Remaître et al. (2008) studied the geomorphological condition and flow behavior of the Faucon debris flow (2003). The entrainment process was simulated using 1D debris flow model in which entrainment calculation is based on limit equilibrium condition (Luna et al., 2012). A Bingham fluid rheology is introduced to estimate resistance term.

ZRRA is a recent rock slide-debris flow that mobilized a great amount of material from the channel. It has been back-analyzed by McDougall (2006) using DAN3D model. Coulomb-friction model and Voellmy model are used to simulate the rheological properties of the flow in the model. Entrainment rate is estimated based on the difference between initial and final volume. It is suggested that entrainment is an essential part for the successful simulation of this type of landslides.

Although there are good agreements in the back analysis of those cases, progressive scouring mechanism has not taken into account in the calculation of the rate of erosion. A new entrainment model incorporated with an energy based runout model is used here to back analyze these cases. In the simulation, the entrainment rate is dynamically determined. Criteria used to evaluate the simulation include the estimated velocity, observed height, the measured depth of erosion, run-out distance and total volume at deposition fan. Uncertainty in the model is analyzed and correlations between the mean value of the probability density function of the friction angles and the slope angles are studied.

7.3. Runout model and entrainment model

7.3.1. Run-out model

As described in previous section, two approaches have been applied to simulate debris flow runout process. The new entrainment model is incorporated into the energy based runout model.

In the slice-based model, the energy based runout model determines the motion of each slice using equations of energy conservation with the Lagrangian difference scheme (Wang et al. 2008). The change of kinetic energy of a sliding mass consists of potential energy change, work done by resistance force along the base of the sliding mass and deformation work. Lateral pressure and basal resistance on individual slices are defined by the Rankine and Mohr-Coulomb equations. The governing equation of the runout model is shown in equation [7-1].

$$\frac{d}{dt}\left(\frac{1}{2}m\bar{u}^2\right) = mg\bar{u}\sin\theta + \frac{1}{2}mghe_{zz} + P_L\bar{u}_L\cos\theta_L - P_R\bar{u}_R\cos\theta_R - T\bar{u} - \int_V \tau_{ij}e_{ij}dV \quad [7\text{-}1]$$

where m is the mass of the slice, $\bar{u}$ is the mean velocity of the slice along the base of the slice, g is gravity acceleration, θ is the inclination of the base of the slice with respect to the horizontal, P_L and P_R are interslice forces exerted on the left and right sides of the slice, T is the shear force acting along the base of the slice, τ_{ij} are components of the stress tensor and e_{ij} are components of the strain rate tensor. Detail formulation and discussion of the model can be found in Wang et al (2010) and Wang (2008).

7.3.2. The new Entrainment model

Conventional analytical entrainment models consider shear failure of erodible bed. It is assumed that bed shear stress of flow is sufficiently high to incorporate erodible material lying on channel bed. In static approach, it is considered that static equilibrium is satisfied between the flow frictional forces, τ_b, and the basal resistance forces, τ_{res}, (Medina et al. 2008a). If equilibrium is not satisfied, the model estimates the magnitude of entrainment from:

$$\tau_b + h_{ent}\rho g\sin\theta = c + \left|h + h_{ent}\right|\rho g\cos\theta\tan\phi_{bed} \quad [7\text{-}2]$$

where h_{ent} is the depth of erosion, θ is slope angle, c is the cohesion, h is flow height, g is gravity acceleration and ϕ_{bed} is the bulk friction angle of the bed material.

In dynamic approach, the same failure mode is considered as that in static approach except that Newton's second law is applied on the erodible material. Therefore, amount of entrained material depends on the availability of momentum (Medina et al. 2008b), given by:

$$\frac{\partial z}{\partial t} = \frac{(\tau_b - \tau_{res})}{\rho V} \quad [7\text{-}3]$$

where $\partial z/\partial t$ is the rate the rate of entrainment and V is the mean velocity of the flow.

In the new entrainment model, it is considered that granular particles lying on channel bed are eroded progressively. Granular particles are abstracted as uniform size particle. Particles are mobilized due to shear stress exerting on the particles. According to the analysis (Cheng et al. 2003; Shodja et al. 2003), normally initiation drag force for the rolling action is less than that required for basal shear failure. Therefore, it is considered that rolling motion is the dominant motion in the initial stage of the entrainment process. Both rolling motion and shear failure are considered in the development of the entrainment model. Drag forces due to the moving debris above the channel bed are assumed to apply at the center of the particles. It is assumed that the particle will rotate around the contact point with the adjacent particle downstream. Newton's Law of Motion is applied to calculate the acceleration, velocity, and displacement of the particle. Moment equation is given by:

$$\frac{TR}{\left(I + mR^2\right)} sin\alpha_t - \frac{mgR}{\left(I + mR^2\right)} \cos\left(\alpha_t + \theta\right) = \frac{\partial^2 \alpha_t}{\partial t^2} \quad [7\text{-}4]$$

where T is the drag force required to initiate particle rolling, R is the radius of the rolling particles (d_{50} is adopted here), I is moment inertial which is equal to $m(3R^2+L^2)/12$, $L=1m$ for

2D, m is the mass of the particle (for 2D, $m = \pi R^2 \rho_b$), ρ_b is the density of bed sediment particle, α_t is the angle between channel bed and connection line of centers of those two particles, θ is the slope angle, g is the gravity acceleration, $\partial^2\alpha_t/\partial t^2$ is angular acceleration and t is time.

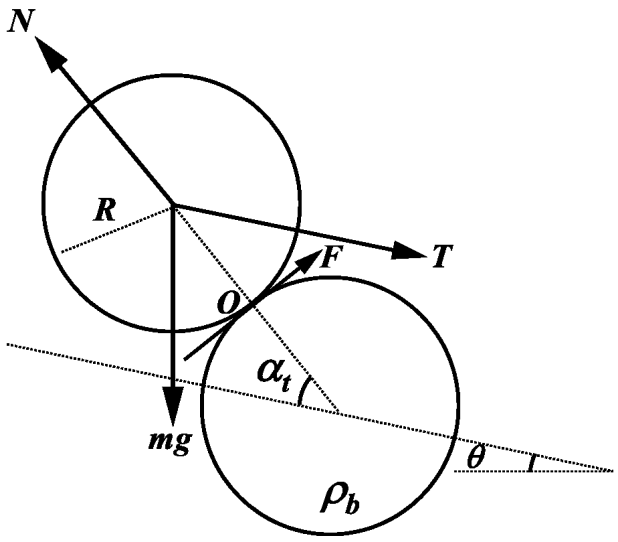

Figure 7-2: Free body diagram of particle when rolling occurs

It is also assumed in the derivation that once the particle moves over adjacent particle located downstream, it will be considered as part of debris flow. Based on mathematical model of rolling motion (Equation [7-4]), entrainment time, the time required for one particle to move from initial location into debris flow body, can be estimated. Entrainment rate is defined as the height of particle exposed to the flow divided by time needed for it to be eroded. Therefore, for different α_0, initial condition of α_t, entrainment rate, $\dot{E}_i$, is defined in Equation [7-5].

$$\dot{E}_i = \frac{2R_i(1-\cos\alpha_{0i})}{t_i} \qquad [7\text{-}5]$$

t_i, in equation [7-5], is the time required for one particle to roll from the initial position, α_0, to vertical position when α_t is equal to $(\pi/2-\theta)$. It is assumed in the derivation that once the particle

moves to the top of the overriding particle downstream, it is considered to be part of debris. Therefore, if shear force exerted on the particle is known and particle properties are determined, t_i can be obtained by solving equation [7-4]. When shear force exerted on the particles is larger than the friction on the particles, the entrainment mode changes from rolling motion into sliding motion.

Since α_0 varies from one location to another and it is not easy to be determined, a probabilistic approach is adopted and α_0 is assumed to follow a probability density function (PDF) using a normal distribution. Selecting the parameters for the PDF is important in the entrainment calculation. The mean value of the normal distribution function can be estimated for a particular case (Fenton et al. 1977), but its value is site specific. The value of α_0 can also be estimated from the relationship between void ratio and internal friction angle, and the relationship between particle protrusion and void ratio (Okada et al. 2007). After the PDF has been determined and the entrainment rate for each specified α_0 are known, the entrainment rate can be obtained from Equation [7-6].

$$\dot{E} = \sum_{i=1}^{n} \dot{E}_{(\alpha_i - \alpha_{i-1})} \qquad [7\text{-}6]$$

in which n is the number of division between 0 and 90 degrees based on the increment of α_0.

7.4. Niumian rock avalanche

7.4.1. Description of Niumian rock avalanche (NRA)

NRA is located in the Niumian Valley, south of Wenchuan, Sichuan China. The debris flow was triggered by Wenchuan earthquake which happened on May 12, 2008 (Figure 7-3, (a)). The source area, adjacent to the fracture zone of the fault, had a length of 514 m, with an area of 1.9

$\times 10^5$ m^2 (Figure 7-3, (b)). It was situated at an elevation between 1,300 m and 1,800 m. After detaching from the source area, the debris ran down rapidly and scoured material on its path. Finally, it stopped before the Min River. Scouring and deposition area were located at elevations between 900 m and 1300 m.

The rocks exposed in the landslide area are mainly consisted of Neoproterozoic plagiogranite, Triassic sandstone and Quaternary deposits (Xing et al. 2014). The source area is located in the Neoproterozoic plagiogranite. The slope in the rock outcrop area is covered by the Quatermary and diluvial deposits. The fault in the study area is the Yinxiu-Beichuan Fault, the fault responsible for the Wenchuan earthquake. Besides, joints and crack are well developed which causes the rock in source area break into blocks.

The study region is located in humid subtropical monsoon climate. The average annual precipitation is 1285.1 mm (Zhang, 2013). There are many small streams, including study valley, that belong to Min River stream.

The velocities of the rock avalanche at different cross sections were estimated from run-up and superelevation techniques (Figure 7-3, (b)). The run-up phenomenon appeared at points 1, 3 and 5. The superelevation method was used to calculate velocities at points 2 and 4. The estimated velocities from point 1 to 5 were 19.8 m/s, 20 m/s, 36 m/s, 22 m/s and 19 m/s respectively (Xing et al. 2014).

By subtracting the elevations of the post-event digital elevation model from pre-event digital elevation model, the volume at source area was estimated to be approximately 3,725,000 m^3. The final deposited volume estimated on site was 7,500,000 m^3. The deposition material at the midpoint of the channel consisted of 60% to 65% gravel to boulder sized debris, ranging in size from 2 to 50 cm. Deposition at downstream of channel was composed of gravel to bounder sized

debris. The average thicknesses at this two parts were 10 m and 28 m, respectively (Xing et al., 2014).

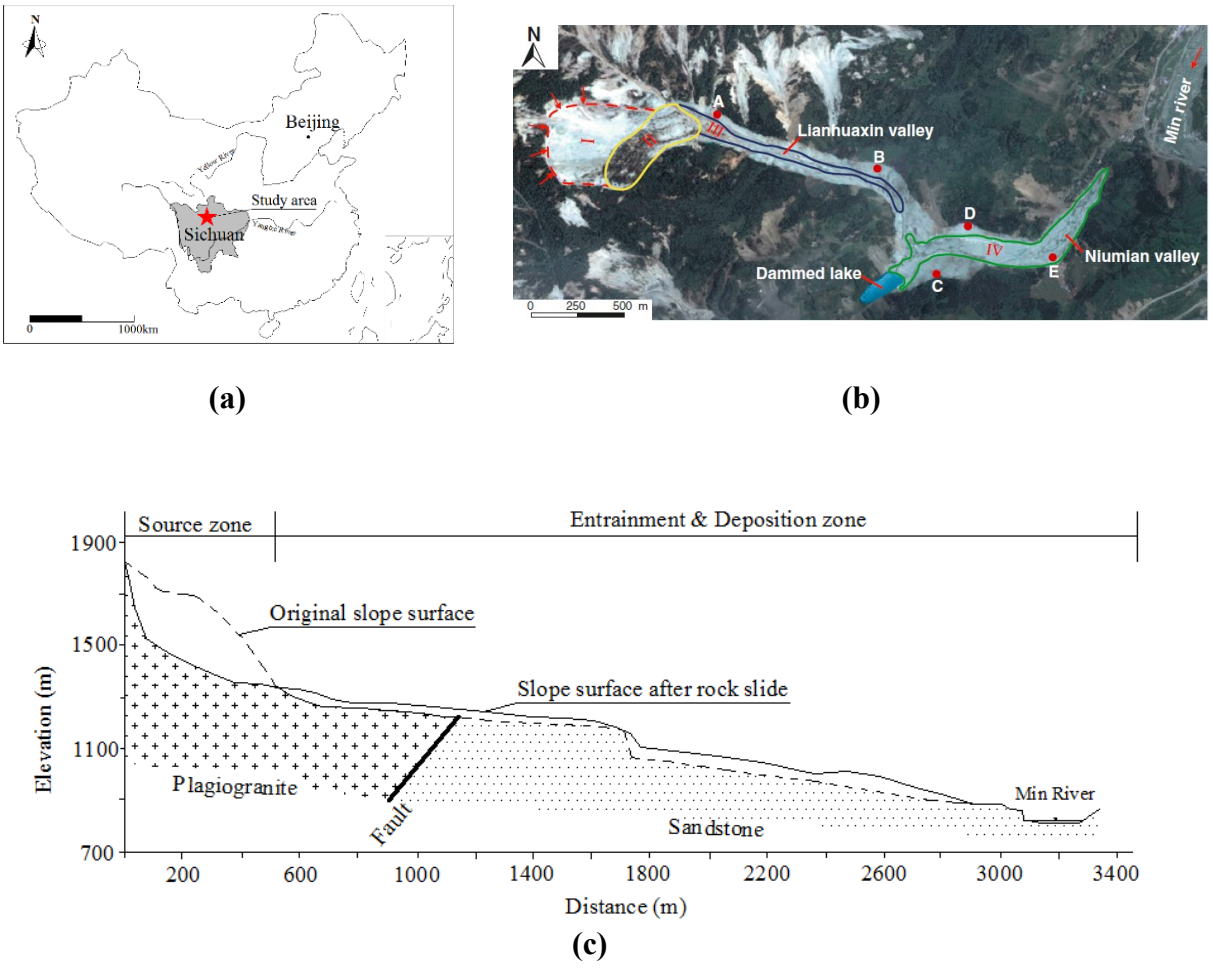

Figure 7-3: (a)Location of Niumian Valley rock avalanche, Sichuan, China; (b) Aerial photo Niumian Valley rock avalanche (Xing et al. 2014); (c) Longitudinal profile of the channel of Niurmian Valley rock avalanche.

7.4.2. Parameter selection

In the simulation, the selection of parameters for NRA is mainly based on information collected from site investigation (Zhang, et al., 2013 and Xing et al., 2014). The mean particle size lying

on the channel bed and the unit weight of debris are deducted from particles size at the deposition zone. Vollemy model is suggested in the simulation of this case. Since study area is located near Yingxiu–Beichuan Fault, Quaternary deposits are distributed along the flow channel (Xing et al. 2014). Therefore, a friction angle, 11º which is lower than that of sandstone, around 25º, is adopted which is the same value as that used in the back analysis of Xing et al. (2014). The turbulent coefficient is chosen to be 2,000 m/s^2, although it is larger than the suggested value by Luna et al. (2012). Internal friction angle is set as 14º smaller than that adopted by Xing et al. (2014) in runout simulation. The mean value of α_0 is suggested to determine based on pivoting angle of the particles lying on the channel bed and average slope angle. After considering the shape factor of these particles not sphere, 7º is adopted as the mean value. Standard deviation is set as 0.1. The maximum friction coefficient between clean rocks is around 0.7 which is adopted as particle contact friction coefficient. This principles are also used in the selection of mean value of α_0, standard deviation of α_0 and particle contact friction coefficient for following cases.

To determine the parameters that should be used in the calculation, frontal velocity generally should be matched with the change of basal frictional coefficient that is considered as the factor mainly controlling runout distance. Varying mean value of α_0 can result in a change of entrainment rate. In this process, basal friction angle is also adjusted accordingly since increase of total volume could lead to change of runout distance as the increase of potential energy resulting from the erosion of channel bed. Moreover, if high shear stress is expected that is driving force for the erosion, turbulent coefficient should be adjusted, however, it is not sensitive as mean value of α_0 in the calculation of entrainment rate. Internal friction angle is an important factor in the calculation of flow height. The first try of parameter selection refers to the back analysis results using other models if available. The principle of parameter calibration is the

same for following cases. All the parameters used in the simulation of NRA are summarized in Table 7-1.

Table 7-1: Parameters in the Niumian rock avalanche study

Parameters	Values
Unit weight (kN/m^3)	20*
Internal friction angle (º)	14
Basal friction angle (º)	11*
Turbulent coefficient (m/s^2)	2,000*
Particle size d_{50} (mm)	100
Mean value of α_o (º)	7
Standard deviation of α_o	0.1**
Particle density (kg/m^3)	2,600**
Particle contact friction coefficient	0.7**

*adopted from the results of back analysis carried out by Xing et al. (2014).

**in case history studies, there are considered as a constant value since these values will not change a lot.

7.4.3. Simulation results

7.4.3.1 Velocity and run-out distance

Figure 7-4 shows the velocities and runout distance of the NRA. There is a high initial acceleration followed by the deceleration of frontal slice after few seconds until it reaches the location with a steep slope and it accelerates again to the maximum velocity, 54 m/s. After that the velocity decreases until it stops at a total run-out distance of 2,940 m. The entire simulation lasts about 150 s, but the front of the debris almost comes to a stop at around 94 s. In the remaining time, at least one slice is still moving with a velocity larger than the velocity threshold, 0.001 m/s. The profiles of the debris at various time are shown in Figure 7-5. The

shape of debris almost has no change after around 100 seconds except some adjustment in the debris. The elevation of the channel bed almost has not changed after that time as well.

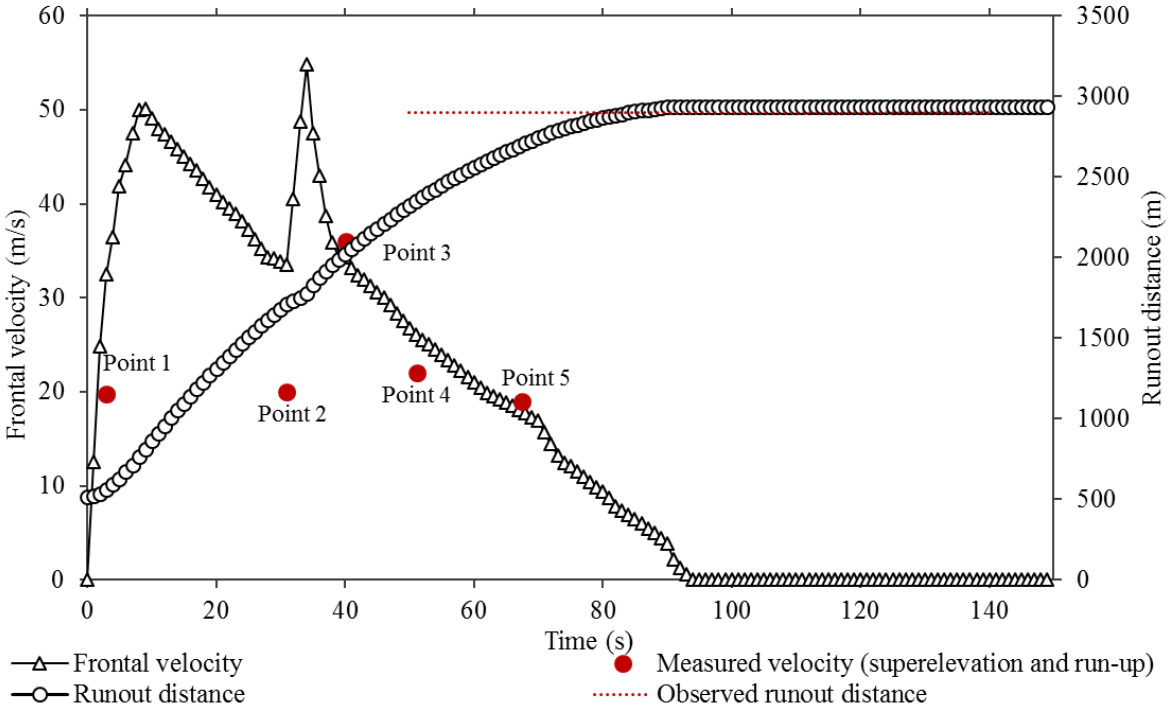

Figure 7-4: Change of frontal velocity and run-out distance during simulation

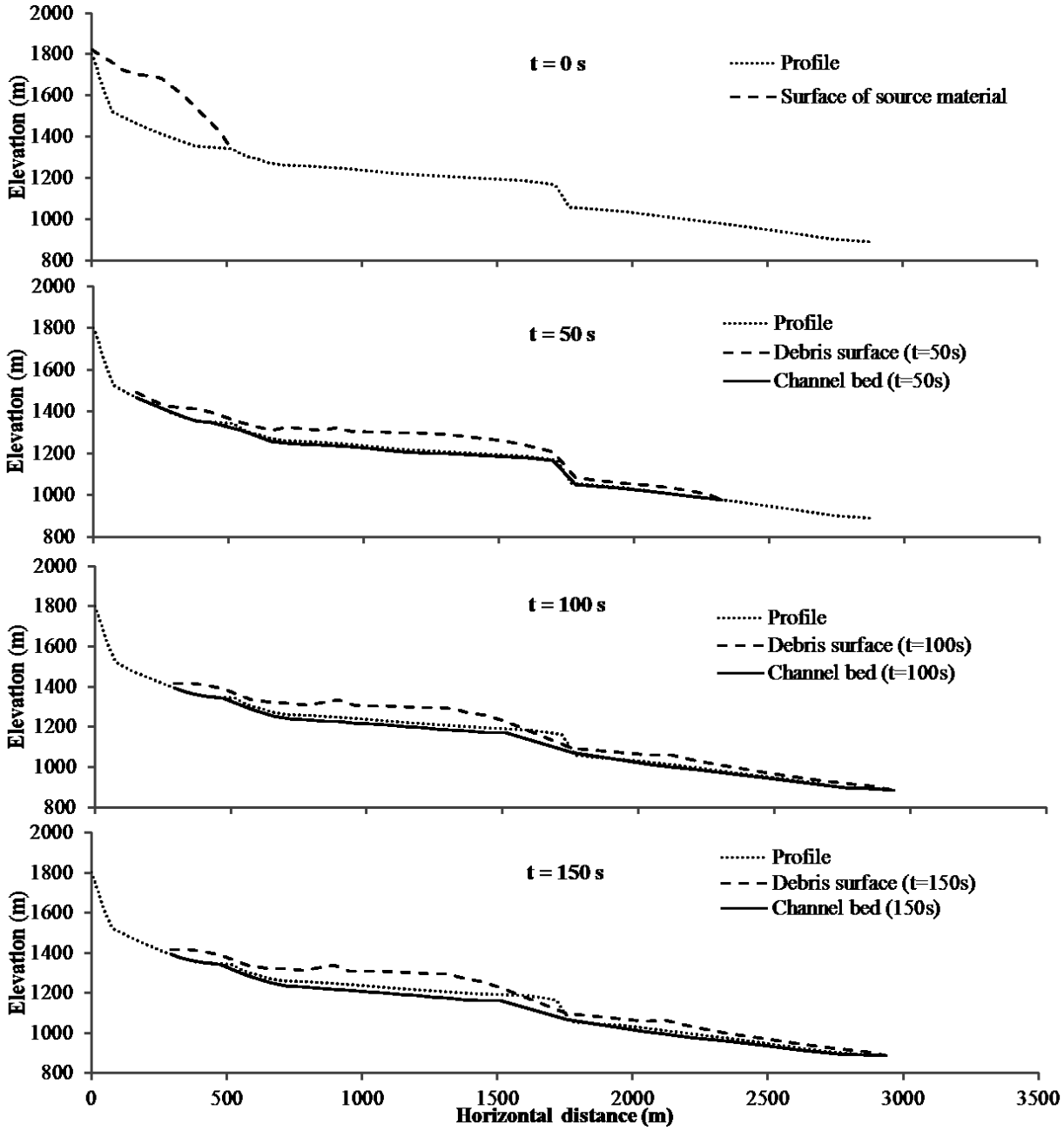

Figure 7-5: Variation of profile of debris and channel bed of NRA at each 50 seconds

7.4.3.2 Accumulated volume and entrainment rate

When soil material is being excavated or eroded, its volume increase known as bulking. Bulking is the loosening of the material during an excavation process. Usually bulking increase the volume by 20 to 30% with proportional decrease in density of the material. Therefore when

material is eroded from the channel bed and incorporated in the debris, the volume of the material will be increase while preserve the total mass of entrainment. In Figure 7-6, the abscissa axis shows calculation time. It can be seen that at the end of the simulation, the entrainment volume decreases but total volume increases rapidly resulting from the entrainment of the slices behind the first slice. The maximum entrainment rate is equal to 26.7×10^3 m^3/s and the final total volume is 7.42×10^6 m^3. When the front of the debris passes the location between x = 2,000 m and 2,500 m, the entrainment rate decreases and then increases. Therefore, the variation of the entrainment rate at this location is possibly contributed from the volume change of all the slices some of which probably reach relatively flat area leading to a decrease of entrained volume.

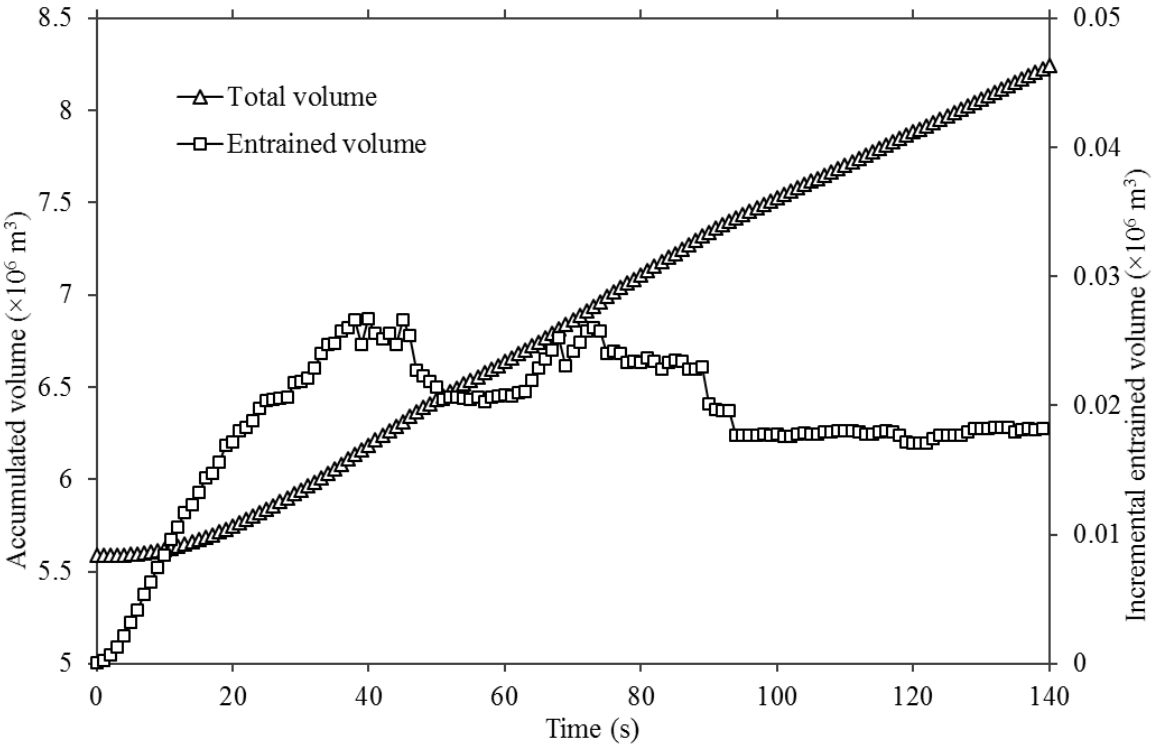

Figure 7-6: Calculated total entrainment and entrainment rate with time

7.4.3.3 Entrainment rate and maximum height

The rate of erosion for each slice at different time stage is shown in Figure 7-7. The rate of erosion at the tail of debris is very small since the slices in front of it block the movement of slice behind it. The debris can be divided into two parts: the first part is the slices that has passed the steep slope and the second part is behind the steep slope. The rate of erosion of slices at second part is higher than that of the first part since shear stress applied on the channel bed is impacted by the flow height. The maximum height and entrainment rate during the simulation is shown in Figure 7-8. The maximum entrainment rate, 0.67 m/s, appears after 22 seconds when the first slice moves around 1,400m. Most of time, the entrainment rate is around 0.4 m/s. Maximum height of the slices is 261 m when the rock avalanche starts to move. Sudden increases of maximum height and entrainment rate are detected when the rock avalanche reaches the section with a very steep slope located at around x = 1,700m. At the end of simulation, maximum flow height increases slightly and finally approaches to 135 m. If the lateral spreading of the rock avalanche is considered, this height could be reduced significantly. The depth of erosion along the channel is shown in Figure 7-9. The maximum depth of erosion is 25 m which is located at x = 940 m, that is around the position with very steep slope.

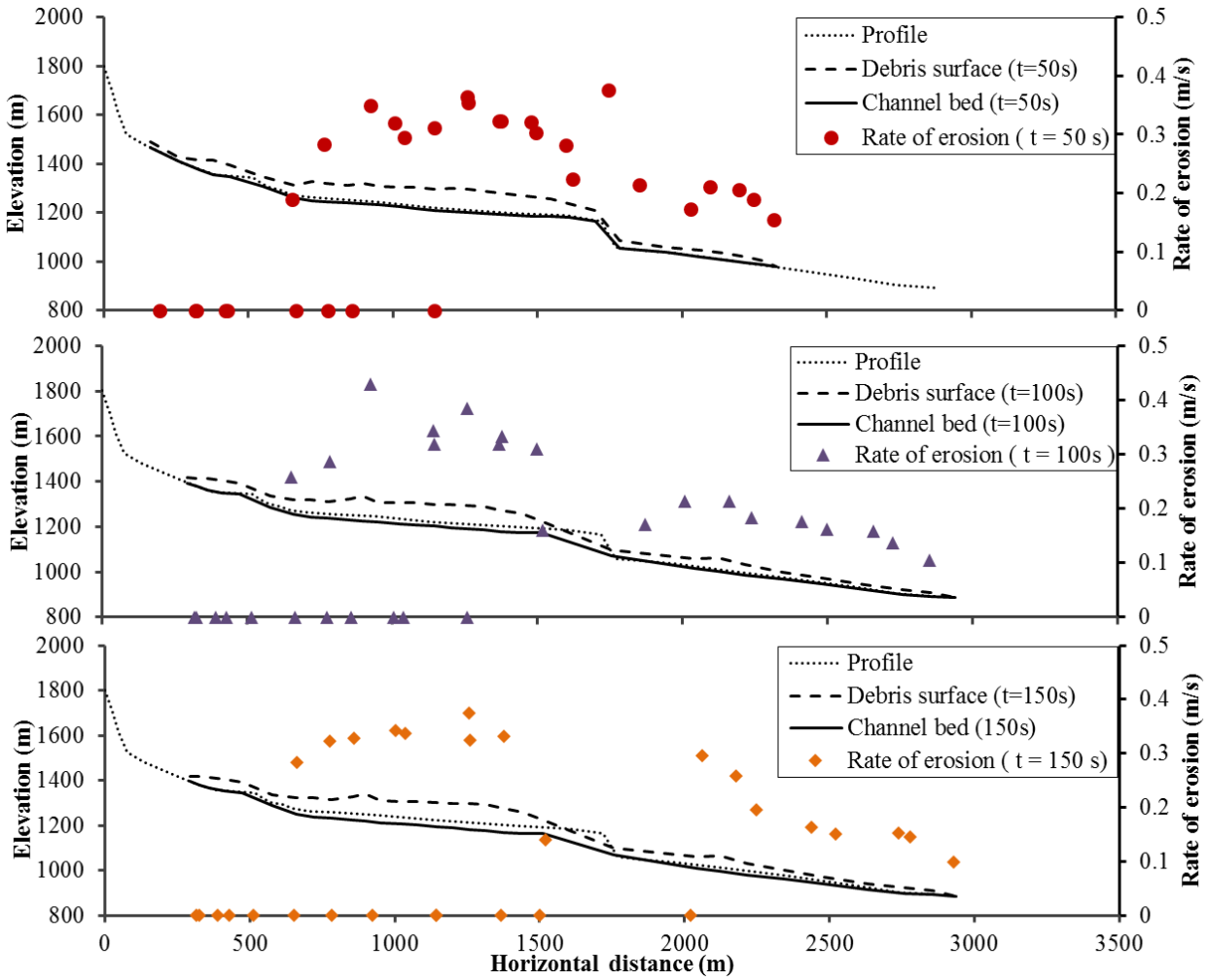

Figure 7-7: Entrainment rate of each slice at different time stage

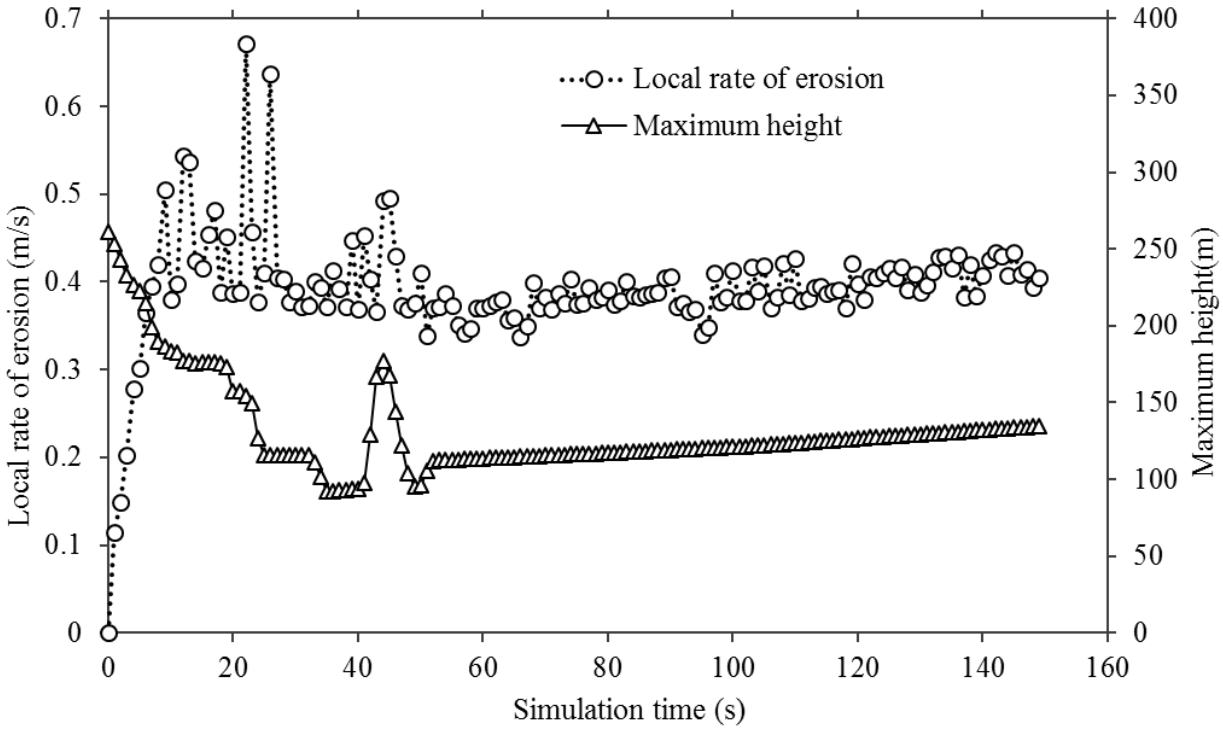

Figure 7-8: Maximum flow height and rate of erosion of NRA during simulation

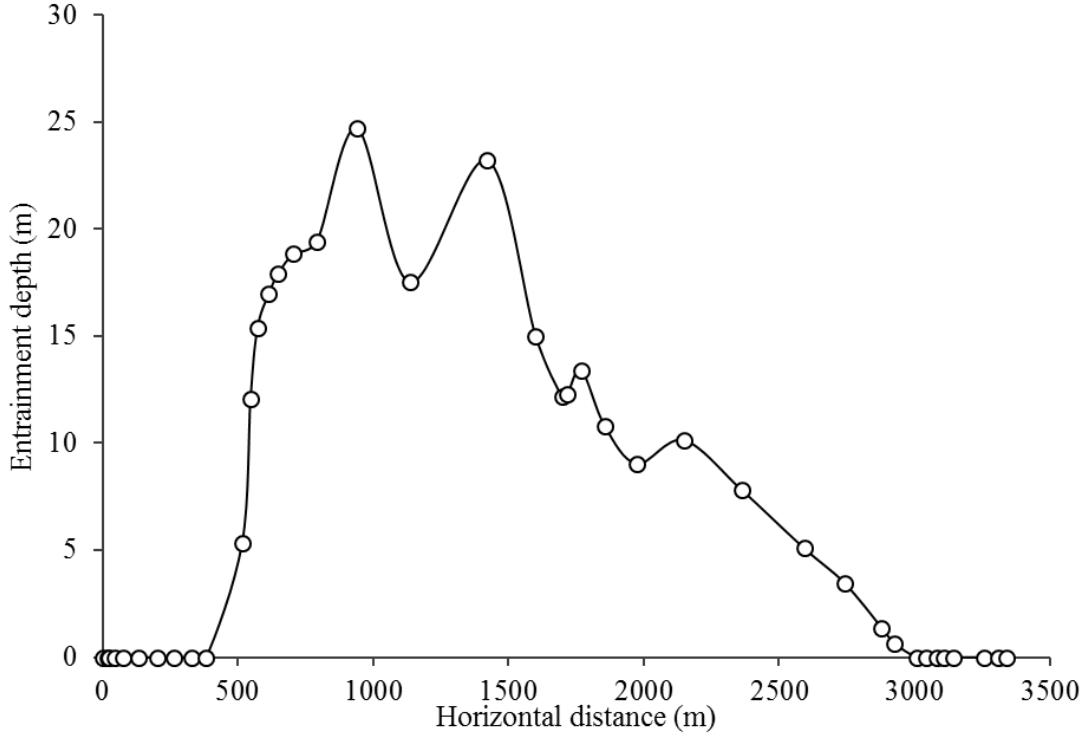

Figure 7-9: The simulated depth of erosion along the channel

7.4.4. Evaluation of the simulation results

The observed flow velocity and height of the debris at the depositional fan are used to compare the simulation results. It is indicated that the calculated velocities match the observed velocities at points 3, 4, 5 in Figure 7-4. Although the velocity at point 2 reduces to 33 m/s, it is still larger than estimated velocity using the superelevation method. The estimated total volume is larger than that estimated value by Xing et al. (2014), since the eroded material at the depositional area is also included. The run-out distance is around 2,940 m, 200 m away from the Min River, which agrees reasonably well with the description reported by Zhang (2013).

Since there is a section with a very steep slope located in the middle of the flow path, it can impact the velocities and deposition of the debris. Therefore, only the height of deposition after passing this section is used to evaluate the simulated shape of deposit as shown in Figure 7-10. The debris that has passed the steep slope is divided into two parts also. The part close to the front of debris is named first half. Another part is called second half. It seems that calculated flow height at first half is close to that observed. However, the flow height calculated at second half is smaller than that observed which is probably due to distance from the steep slope.

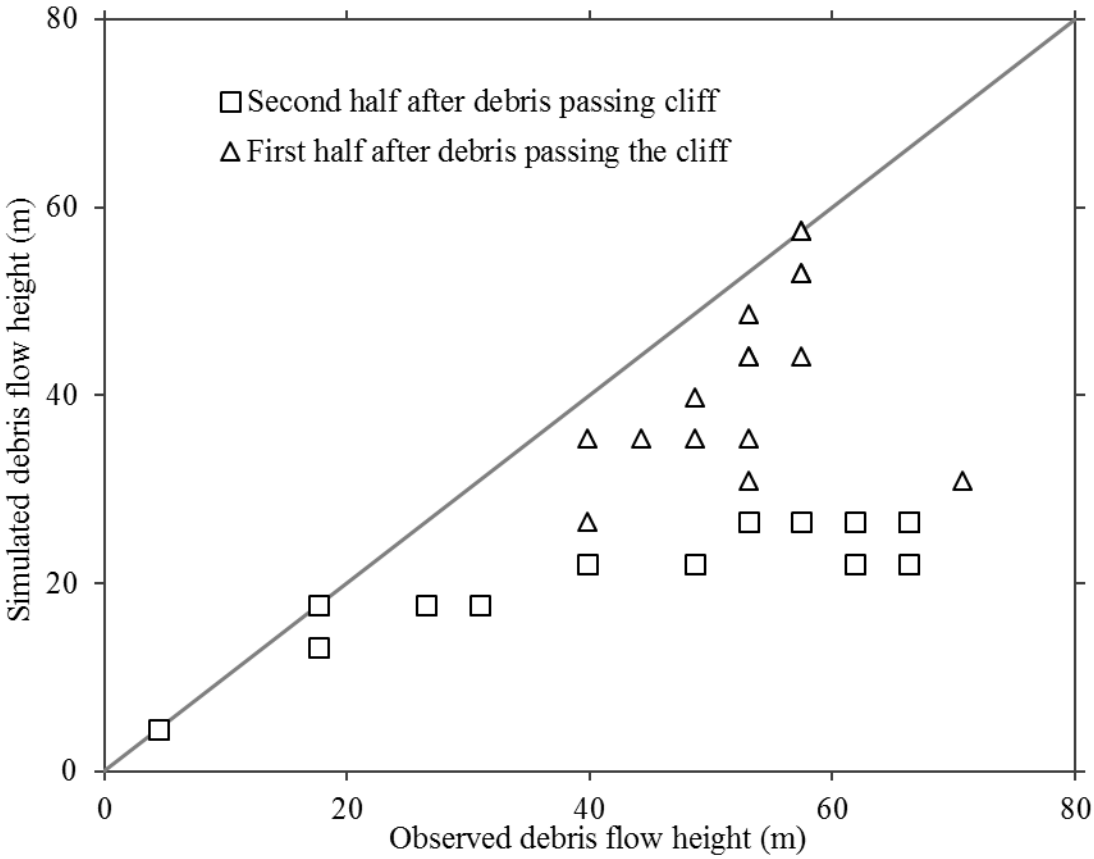

Figure 7-10: Comparison of observed and calculated height of debris behind x = 940 m

7.5. Fjærland debris flow

7.5.1. Description of Fjærland debris flow

Fjærland is located in the western part of Norway, in a tributary fjord to Sognefjord (Figure 7-11 (a)). The debris flow, triggered by a failure of a mountainous glacial moraine ridge, occurred on May 8, 2004. The flow started in a flat area and then passed a precipice of 300 m height drop. After that, it flowed with significant entrainment. The movement ended in a fan with huge boulders where Tverrdalen meets the flat floor of the main valley at around 20 m.a.s.l (Figure 7-11, (b)). The total height of drop and the run-out distance were around 1,000 m and 3,000 m,

respectively. Since the debris flow developed between the winter and summer seasons, fortunately, no casualties were reported in this hiking area (Breien et al., 2008; Breien, 2005).

Till is characterised by poor sorting and composed of fragments of all sizes from clay to boulders. The till cover is thin and discontinuous over large area of Norway, especially in the western part due to glacial net erosion in the steep terrain (Breien, 2005). Till in Norway is normally coarse grained tills where clay constitutes less than 10% of fine material and gravel between 2 to 16 mm makes up 20 – 40 %. The boulder fraction is between 30% and 70 % of the total till. The Fjærland debris flow channel is mainly covered by poor sorted till which include a very large amount of boulders (Figure 7-11, (c)). The largest one is around 3 m located 50 m away from the main fan.

The velocity when glacial moraine failed was not monitored, but according to witness, when the debris reached the deposition fan area, the debris flowed with an estimated velocity of around 50 km /h (Breien et al. 2008). This agreed with back analysis of the ejected stone found 20 m outside of the main track before entering the fan. The maximum velocity calculated using Bingham model, neglecting entrainment, was around 60 m/s (Breien, 2005).

The volume of the moraine breach in Fjærland was considered to be small compared to the volume of the depositional fan. The debris flow started with 25,000 m^3 and had almost no entrainment at the initial 1000 m. Entrainment started from the beneath of precipice to the start of fan and resulted in the total volume of 240,000 m^3. It was estimated that the average vertical erosion was 3.5 m assuming that the total volume eroded over the areas beneath the cliffs was evenly distributed. The deepest scour, up to 8 m, appeared in the lower parts of the track after passing the exit of a smaller tributary stream. The maximum measured width of the V-shaped scar at the west end of the lake was 35 m. The deposition fan was teardrop shaped, 420 m long

and 300 m maximum width, with an area of around 80,000 m^2. The thickness of the deposit in this area varied with the steepness of the terrain and altitude. The depth of the depositional fan seemed to vary from 0.5 m to approximately 5 m.

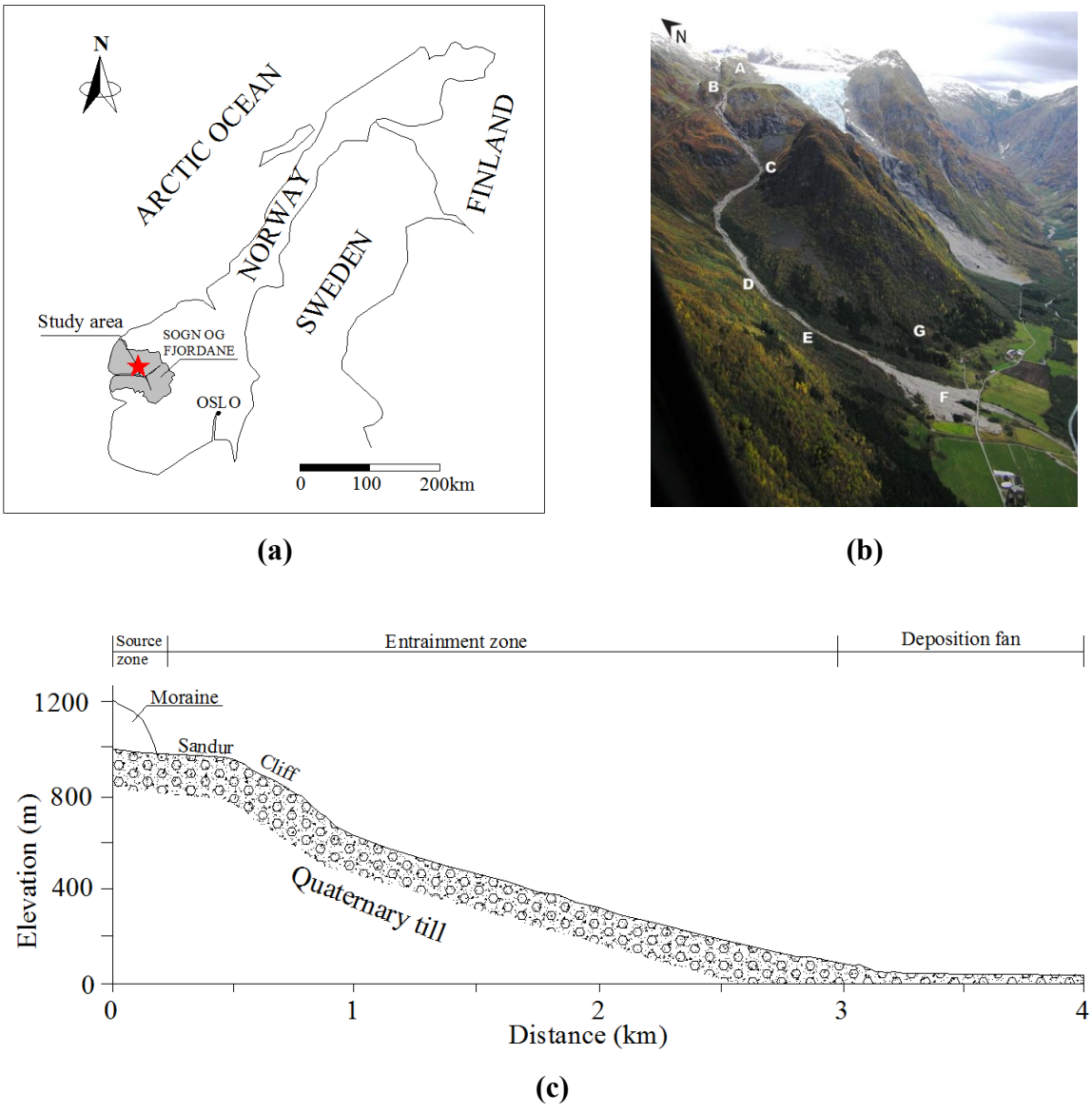

Figure 7-11: Geographical and geological condition of Fjærland debris flow (a) Geographical location of Fjærland debris flow, Western Norway, May 8, 2004; (b) Oblique aerial view of Fjærland debris flow (Breien et al., 2008); (c) Longitudinal profile of the channel of Fjærland debris flow.

7.5.2. Parameter selection

The properties of the Fjærland debris flow is dominated by the debris at source area and the erodible material lying on the channel bed. An estimation of the total volume of sediment and water gives a unit weight of 18.5 kN/m^3. Since 60 to 70 % of particles along the material lying on the channel composed of boulders, conservatively, a mean particles size equal to 300 mm is used in the simulation. The density of solid particles lying on the channel bed is 2,600 kg/m^3 in the model. Since the average slope at deposition fan is around 8-10º which can be considered as the repose angle of this material mainly eroded along flow path, basal friction angle therefore is considered as 9º. An internal friction angle close to the slope angle at deposition fan is first used. It then is calibrated during matching flow velocity and entrained volume. Turbulent coefficient is first determined by the suggestion from Luna et al. (2012). It is also calibrated in matching runout distance and entrainment volume. Selection of mean value of α_0 also considers the average slope angle, the pivoting angle and shape factor of particles. Finally, 10º is used as the mean value. All the parameters used in the simulation are summarized in Table 7-2.

Table 7-2: Parameters in the study of Fjærland debris flow

Parameters	Values
Unit weight (kN/m^3)	18.5*
Internal friction angle (º)	14
Basal friction angle (º)	9
Turbulent coefficient (m/s^2)	300
Particle size d_{50} (mm)	300*
Mean value of α_o (º)	10
Standard deviation of α_o	0.1**
Particle density (kg/m^3)	2,600**
Particle contact friction coefficient	0.7**

*adopted from the results of back analysis carried out by Breien, (2005).

**in case history studies, there are considered as a constant value since these values will not change a lot.

7.5.3. Simulation results

7.5.3.1 Velocity and run-out distance

Due to the flat area next to the source area, debris flow moves slowly until it reaches middle zone with steep slope. The velocity increases rapidly from 12 m/s to 42 m/s. After that, the velocity decreases gradually to zero after the simulation lasts 171 seconds (Figure 7-12). Figure 7-13 shows the variation of the shape of debris flow. Most of the travelling distance is completed in 150 seconds. The tail of debris moves out of source zone and travels together with the front of debris instead of staying at the source zone. The entire debris finally deposits at the toe of slope.

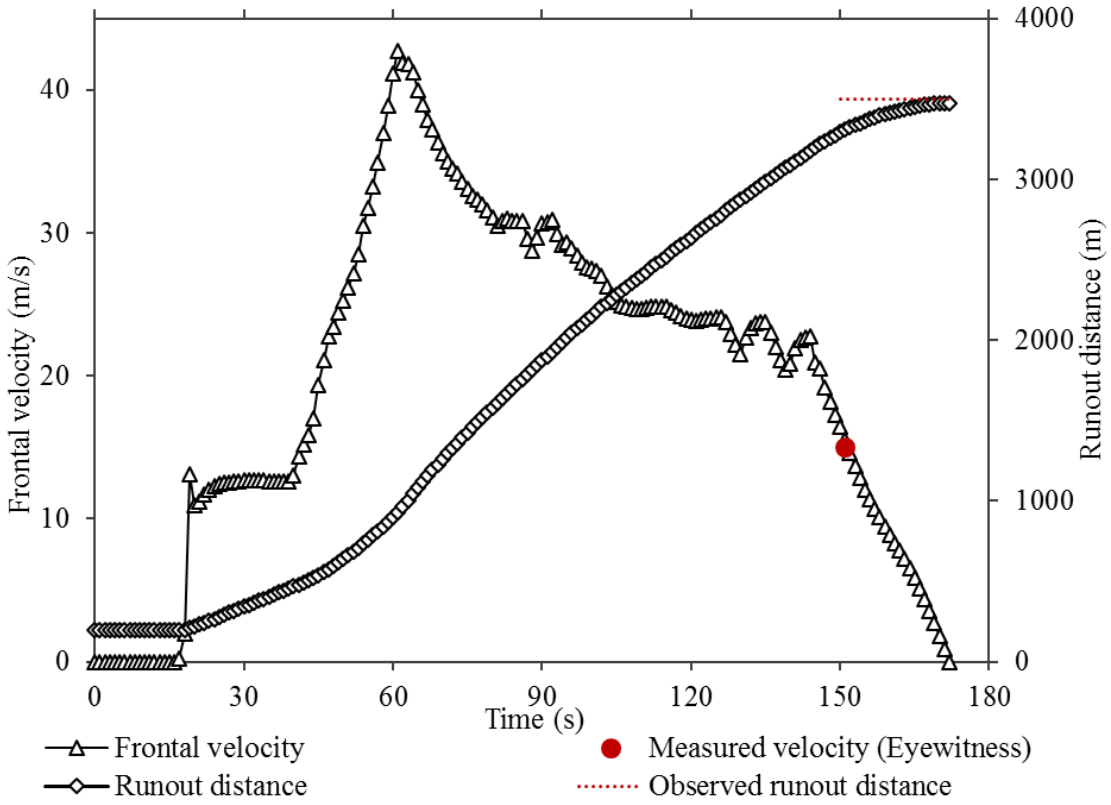

Figure 7-12: Simulated run-out distance and frontal velocity of Fjærland debris flow

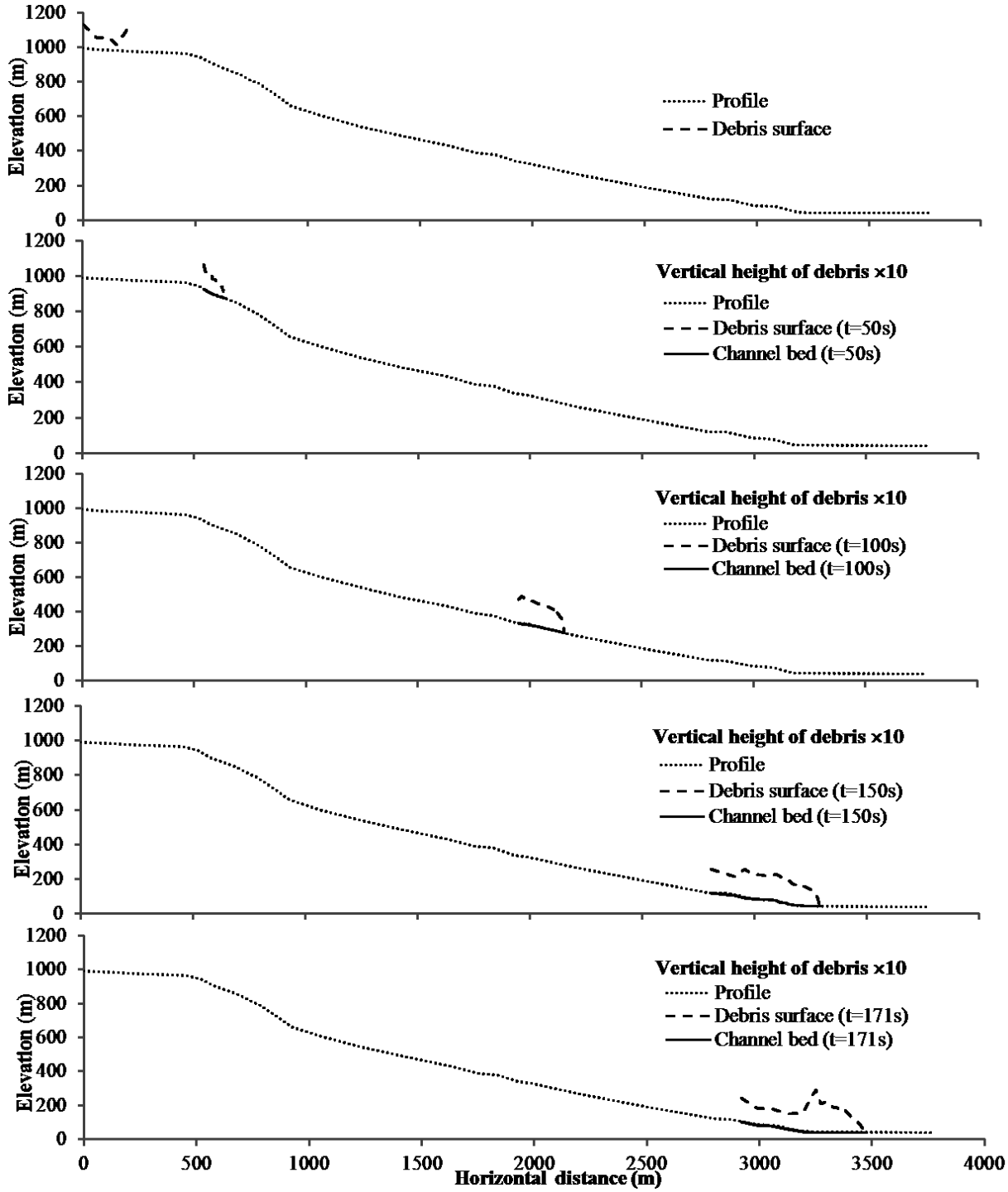

Figure 7-13: Fjærland debris flow shape at different time stage

7.5.3.2 Accumulated volume and entrainment rate

The rate of entrained volume change varies a lot from zero at the start of simulation to around 2.55×10^3 m^3 after 171 seconds. Figure 7-14 shows the simulated total volume at deposition fan which is 261×10^3 m^3, about 10 times greater than its initial volume. The variation of entrainment rate is mainly caused by the change of channel elevation. Total volume of the debris flow increases a lot. The calculated total volume at deposition fan is close to than measured in field.

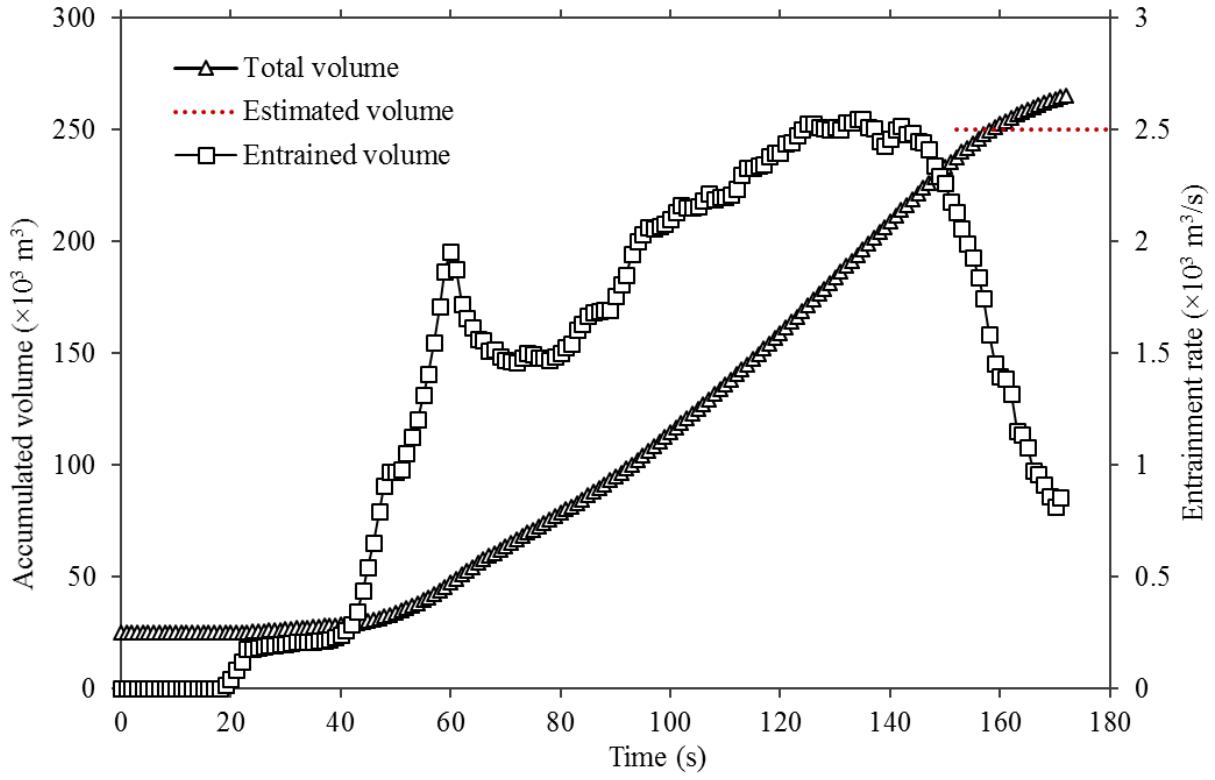

Figure 7-14: Increment on total volume and entrainment volume during debris flow movement

7.5.3.3 Entrainment rate and maximum flow height

Rate of erosion is around 0.3 m/s in the whole simulation process except when the slices moves to the cliff zone at which entrainment rate rapidly increases to 1.57 m/s (Figure 7-15). Mean height of all the slices is about 20 m. It is interesting that these undulations of maximum height of slices echo that of entrainment rate, except regions where slope changes suddenly since variation of slope angle leads to the change of driving force in entrainment calculation.

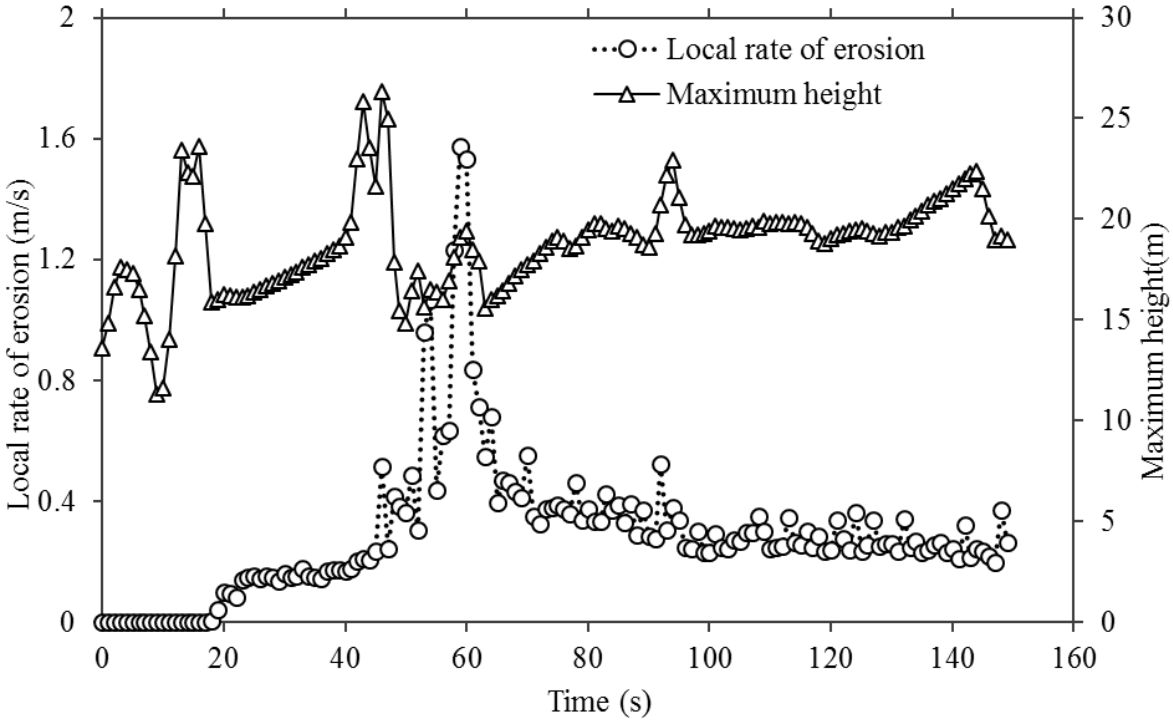

Figure 7-15: Maximum entrainment rate and maximum height of all slices in the simulation

Figure 7-16 shows entrainment rates of each slice at different time stage. The entrainment rates of most of slices are ranging from 0.07 m/s to 0.3 m/s. The depth of erosion along the channel is shown in Figure 7-17 indicating that the depth of erosion varies a lot on this case. The maximum depth of erosion is 21 m at x = 3,258 m which should be smaller if lateral spreading effect is

considered since this could lead to a lower shear stress treated as the primary driving stress for erodible material. The average depth of erosion measured is about 4 m. Most of measured entrainment depth is larger than that calculated using the entrainment model (Figure 7-17). In the runout model, since basal shear stress is calculated based on Mohr-Coulomb frictional model, large flow height could be expected which could result in high shear stress leading to a large entrainment rate.

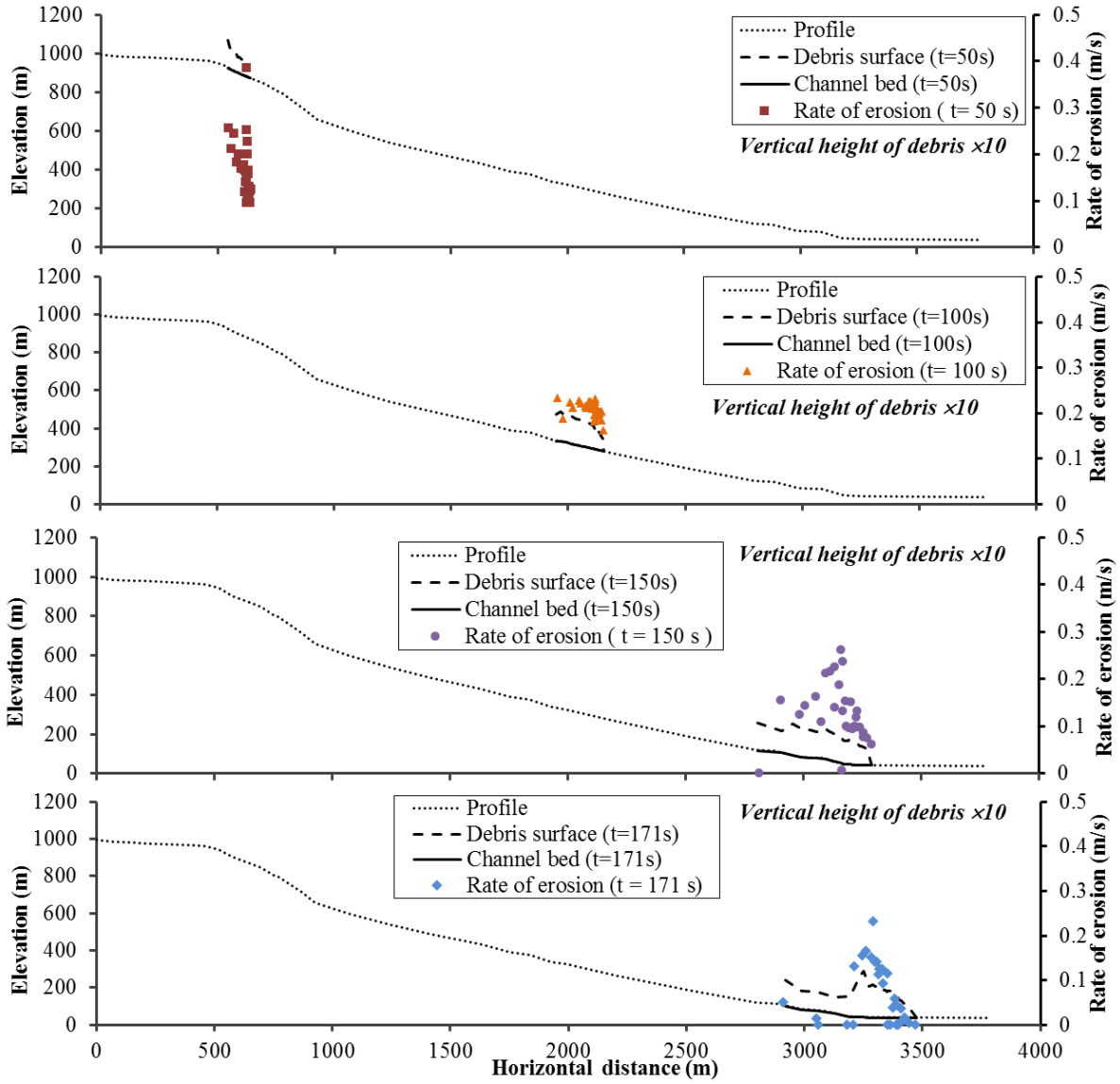

Figure 7-16: Entrainment rate of each slice at different time stage

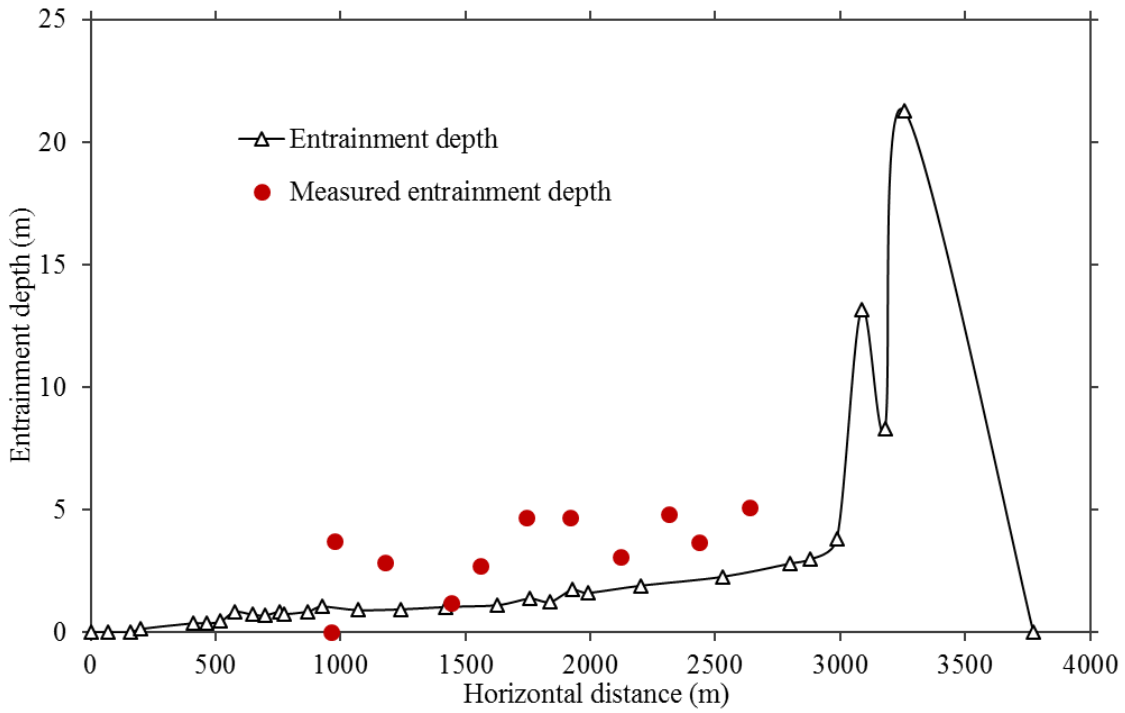

Figure 7-17: The simulated depth of erosion along the channel

7.5.4. Evaluation of simulation results

Criteria used to evaluate the simulation include estimated velocity, run-out distance, deposition volume, and the depth of erosion. Simulated velocity and run-out distance agree with the observed value very well. Simulated volume is 261×10^3 m^3, a little bit larger than that measured. Measured entrainment depth is also used to verify the calculation results. The observed entrainment depth varies along the flow path (De Blasio et al., 2011), the simulated entrainment depth changes gradually at entrainment zone.

7.6. 2003 Faucon torrent debris flow

7.6.1. Description of 2003 Faucon torrent debris flow

The Faucon torrent catchment is located in the Barcelonnette basin, a steep mountainous region in southern France (Figure 7-18, (a)). Elevation of this torrent ranges from 1,177 m to 2,984 m.

The total channel length is about 5,775 m with a surface area of 10.4 km^2 (Remaître et al., 2009; Remaître et al., 2005). The incised channel has an average slope of about 20º, ranging from 35º in the headwater basin to 3º on the alluvial fan.

Since 1850, fourteen major debris flows have occurred in the Faucon torrent (Remaître et al., 2008). The last major events occurred in 1996 (Remaître et al., 2005) and 2003 (Remaître et al., 2009). The 2003 Faucon torrent debris flow is considered to be back analyzed because of its significant entrainment and detailed information available.

The 2003 Faucon torrent debris flow occurred in the early evening of 5 August 2003 at two specified spots: the Trois Hommes area and the upper part of the Champerousse torrent. In Trois Hommes area, the depth of the incision was around 2 m. The width of the debris flow track ranged from 2 m at the headscarp to 5 m to confluence with Faucon torrent. In the Champerousse torrent, the depth of the incision varied from 2 m in the upper part to 1 m in the lower part. Mean width of debris path was 3 m (Remaître et al., 2009).

The entire area is heavily glaciated during the Pleistocene, leaving thick glacial deposits as tills, kame terraces and moraines. The highest parts of massif consist of two thrust sheets of faulted sandstones and calcareous sandstones (Figure 7-18, (c)). The lower slopes consist of Callovo-Oxfordian black marls, covered by various Quaternary deposits including boulders up to 1 – 2 m in size and 3 – 15 m in thickness (Remaître et al., 2008).

Back analysis of the velocity at points A and B in Figure 7-18(b) was performed using the run-up equation and the vortex equation respectively (Remaître et al., 2008). Velocities calculated using the run-up equation and the vortex equation at points A and B were 6.4 m/s and 7.8 m/s, and 7.1 m/s and 8.9 m/s. The debris flow occurred in five to six surges over a time interval between 2

and 5 minutes. Eyewitness revealed that the debris flow height of the last surge reached 5 to 6 m (Remaitre et al., 2011).

Observations at the Trois Hommes slope and the Champerousse torrent indicated that the source volume ranges from 7,500 m^3 to 9,500 m^3 suggesting a value of 8,500 m^3. The channel scour was responsible for the difference between the source volume and the total volume of debris deposition fan, 60,000 m^3 (Remaître et al., 2009). The total length of the debris flow track was around 3,500 m. The scour depth obtained from field investigation ranges from 0.5 m to 4 m.

The deposition material consists mostly of clast-rich, slightly bouldery, muddy grave; with clast-rich and coarse fractions of the depositions. The maximum thickness of small lobate deposits is around 1.5 m. Lateral and channel bed deposition forms discontinuous narrow levees, 1-3 m above surrounding ground.

(a)

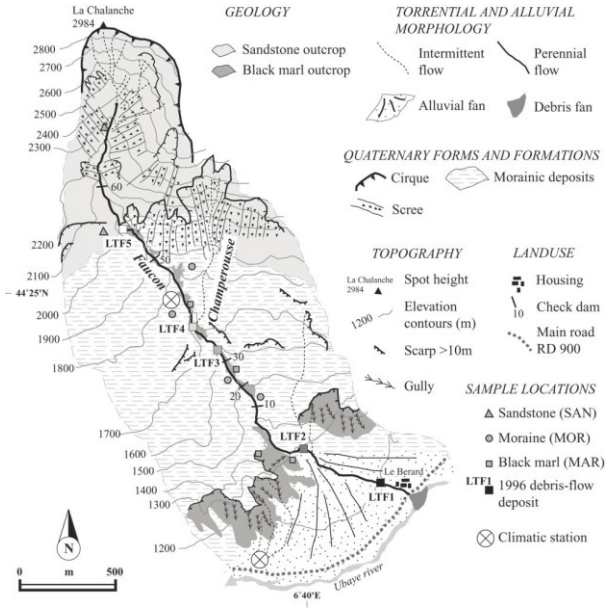

(b)

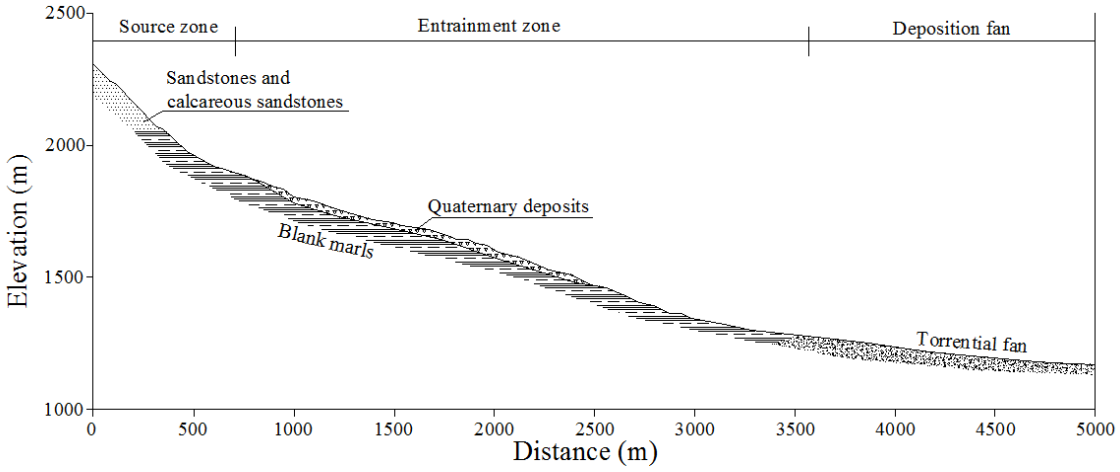

(c)

Figure 7-18: (a) Location map of 2003 debris flow at Faucon torrent; (b) Location of 2003 debris flow deposits samples at Faucon torrent (Remaître et al., 2005); (c) Longitudinal profile of 2003 debris flow channel at Faucon torrent

7.6.2. Parameter selection

Material sampled at 20 cm to 50 cm depth ranging from 20 to 0.05 mm was oven dried and sieved (Remaître et al., 2005). This part of particles accounted for 55 – 80% of total weight of samples. In this simulation, a mean particle size of 10 mm is used. Selection of unit weight and particles density are referred to the previous simulation results (Hussin et al., 2012; Remaître et al., 2005). Since most slopes are covered by Quaternary deposits having a sandy-silt matrix and deposition fan has a slope gradient ranging from 4º to 9º which can be considered as the repose angle of entrained material. Therefore, 5º is adopted as the basal friction angle in the calculation. Selection of internal friction angle refers to the average slope angle before the event. Mean value of α_0 is first determined through the relationship between α_0 and pivoting angle, which can be determined using empirical relationship between pivoting angle and average particle diameter.

Turbulent coefficient initially uses the value suggested for granular particle which is around 500 m/s^2. After that, parameters are calibrated by matching velocity at specified locations, total and entrainment volume and maximum erosion depth, successively. All the parameters used in the calculation are summarized in Table 7-3.

Table 7-3: Model Parameters for Faucon torrent debris flow

Parameters	Values
Unit weight (kN/m^3)	20*
Internal friction angle (º)	20
Basal friction angle (º)	5
Turbulent coefficient (m/s^2)	250
Particle size d_{50} (mm)	10*
Mean value of α_o (º)	14
Standard deviation of α_o	0.1**
Particle density (kg/m^3)	2,600**
Particle contact friction coefficient	0.7**

*adopted from the results of back analysis carried out by Remaître et al., (2005), Remaître et al., (2009) and Hussin et al., (2012).

**in case history studies, there are considered as a constant value since these values will not change a lot.

7.6.3. Simulation results

7.6.3.1 Velocity and run-out distance

Figure 7-19 shows the simulated velocity and run-out distance. Measure velocities according to superelevation and runup of debris at specified location are also labeled. Maximum velocity is 18.8 m/s occurred at t = 39s and t = 59s. The decrease of frontal velocity after around 45 seconds is caused mainly by the change of slope gradient. The velocities calculated agree well with that measured. Final run-out distance is 4,740 m, around 300 m smaller than observed runout

distance. Simulated positions of the debris flow at different time stage are shown in Figure 7-20. The tail of debris stops moving after 300 seconds, but the front of debris keeps moving until t = 460s.

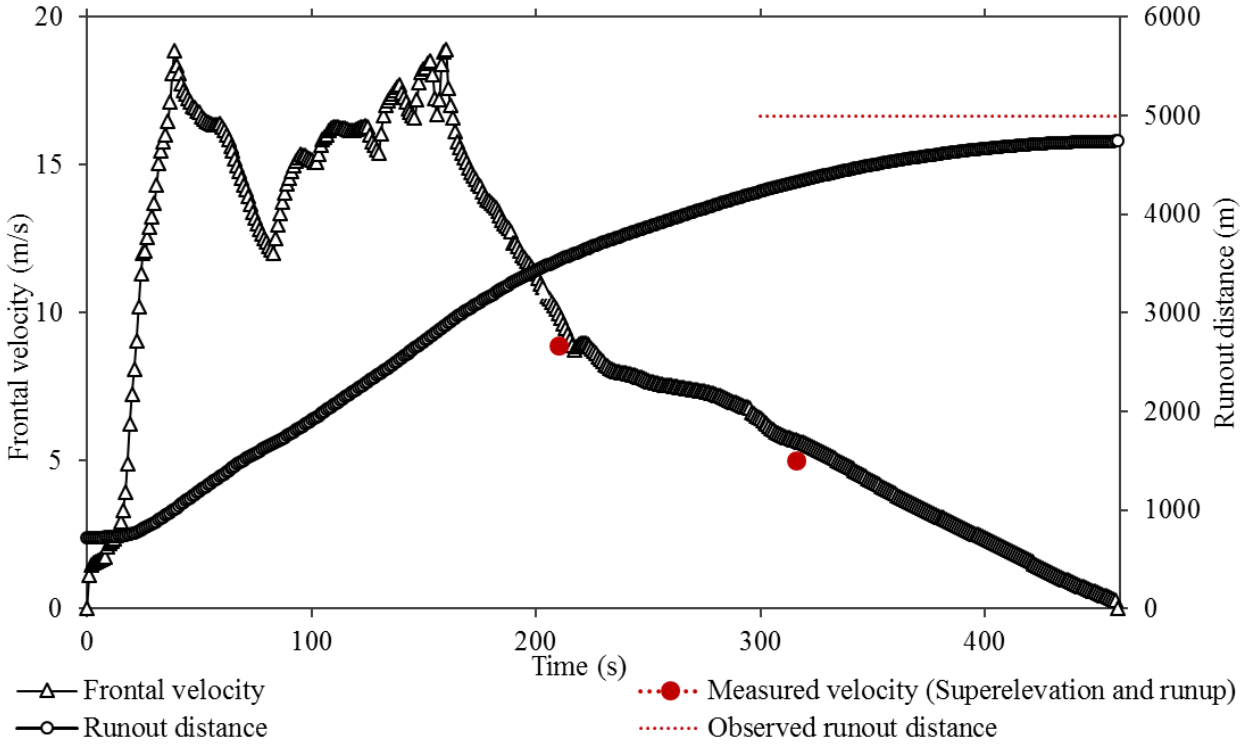

Figure 7-19: Calculated frontal velocity and run-out distance of Faucon debris flow (2003)

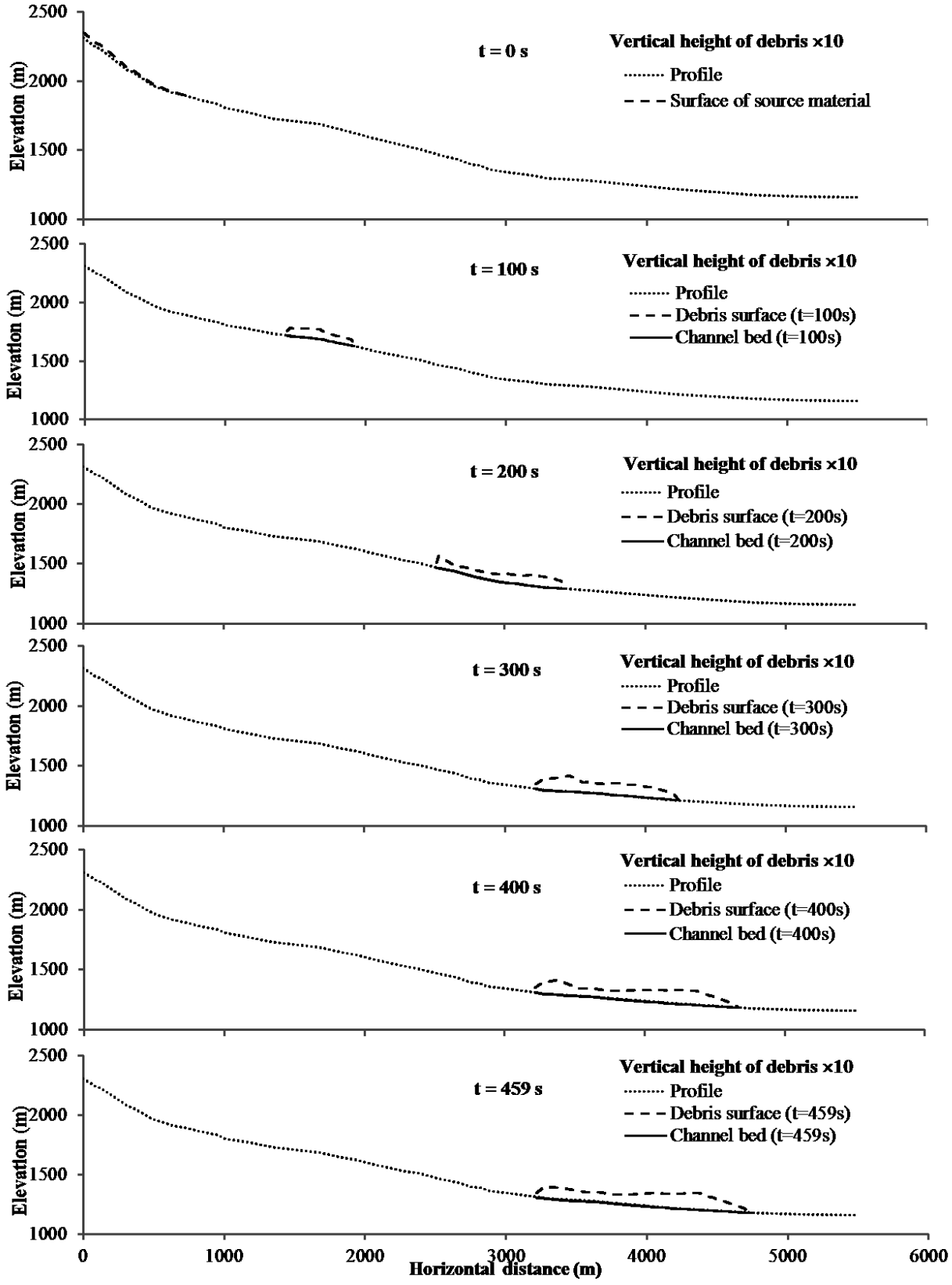

Figure 7-20: Simulated Faucon debris flow position at different time stage

7.6.3.2 Accumulated volume and entrained rate

In the simulation, a 4.6 m flow channel is assumed. Entrained volume increases suddenly and then varies along the flow path. Final volume is 67 × 10^3 m^3 larger than that estimated total volume according to the investigation. The rate of maximum entrained volume is 175 m^3/s. Maximum value of entrained value is detected when the first slice reached 2,950 m (Figure 7-21).

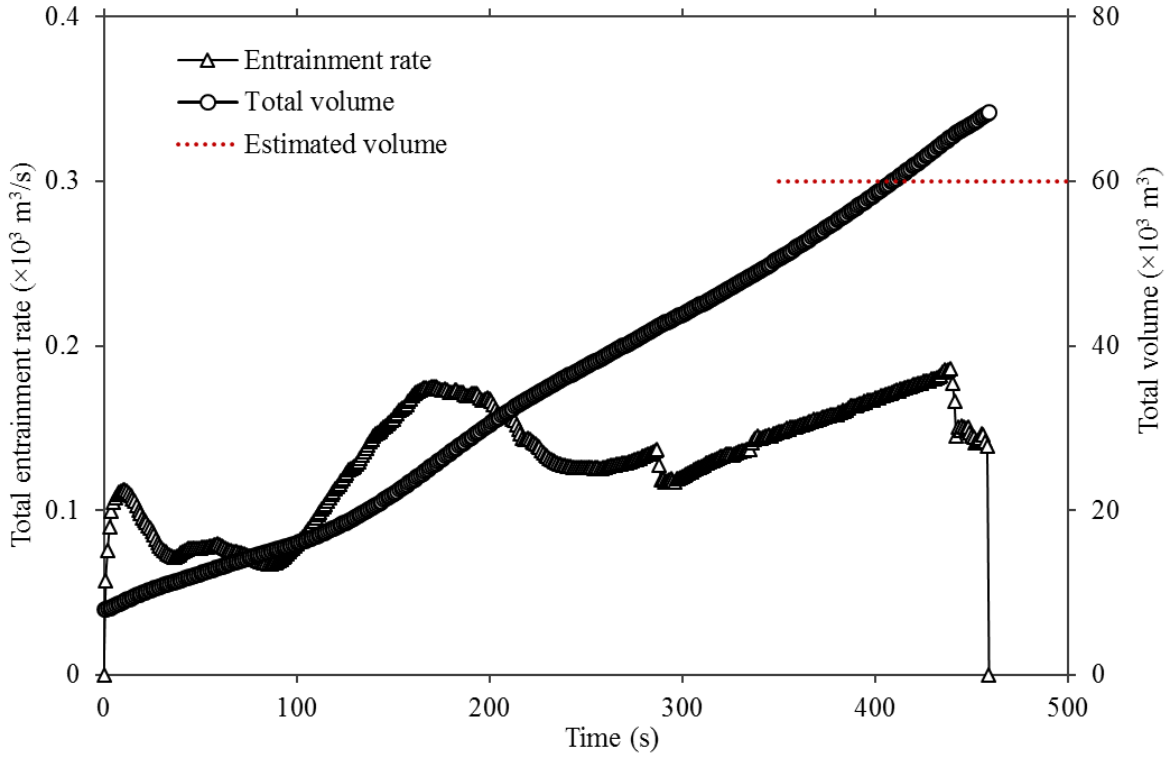

Figure 7-21: Simulated entrainment volume and total volume of Faucon debris flow (2003)

7.6.3.3 Entrainment rate and maximum flow height

Entrainment rate of the debris flow dramatically increases to 0.046 m/s and reaches its maximum value when simulation lasts around 50 s. Entrainment rate mainly is mainly ranging from 0.3 m/s

to 0.4 m/s. Flow height gradually increases and stops at 17.6 m which is caused by the ignorance of lateral spreading (Figure 7-22).

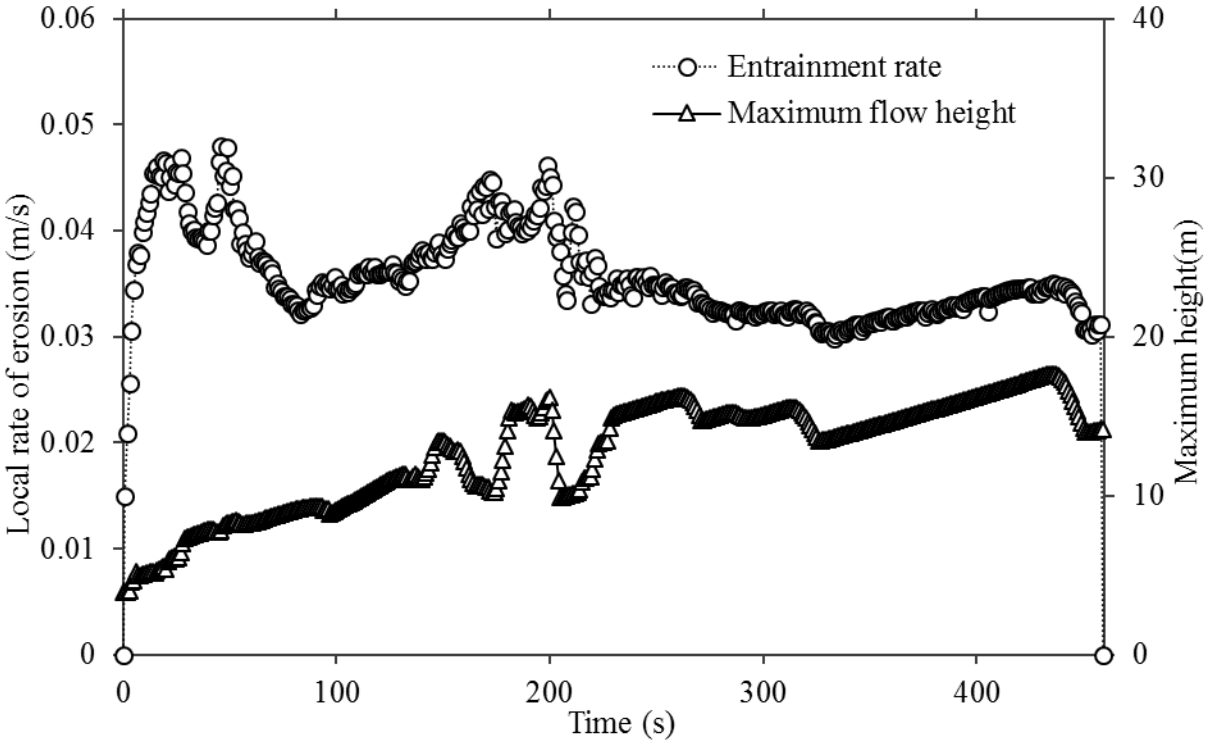

Figure 7-22: Simulated entrainment rate and maximum flow height of Faucon debris flow (2003)

Figure 7-23 shows rate of erosion at different time when the debris travels along the flow path. Entrainment develops with the movement of the debris. The location of maximum entrainment rate changes to downstream of flow path. However, the maximum entrainment rate does not vary a lot. The depth of erosion for the first half is less than 2 m, but after that, it starts to rise (Figure 7-24). The maximum depth of erosion in the calculation is 4.6 m.

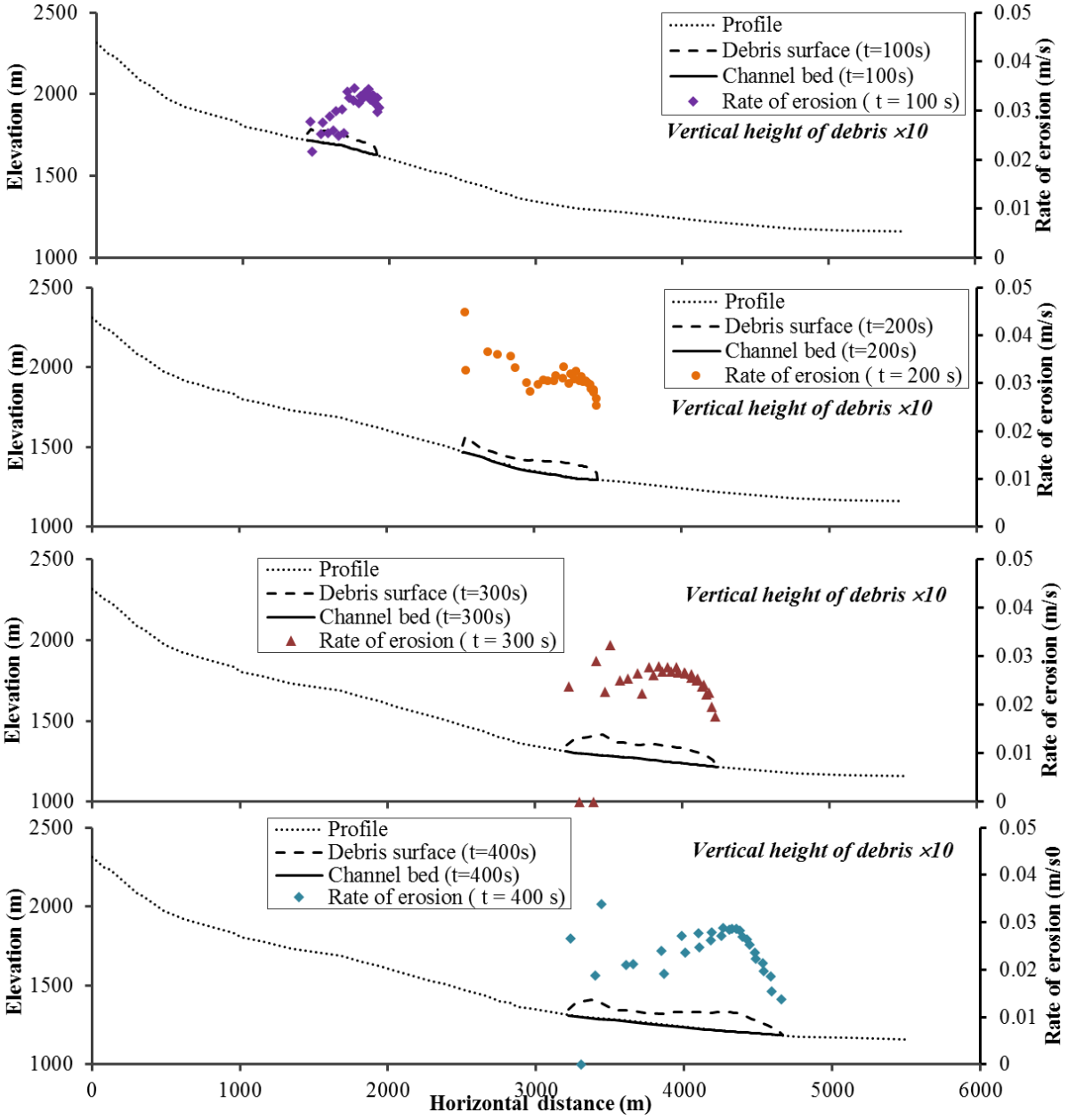

Figure 7-23: Simulated entrainment rate of each slice at different time stage

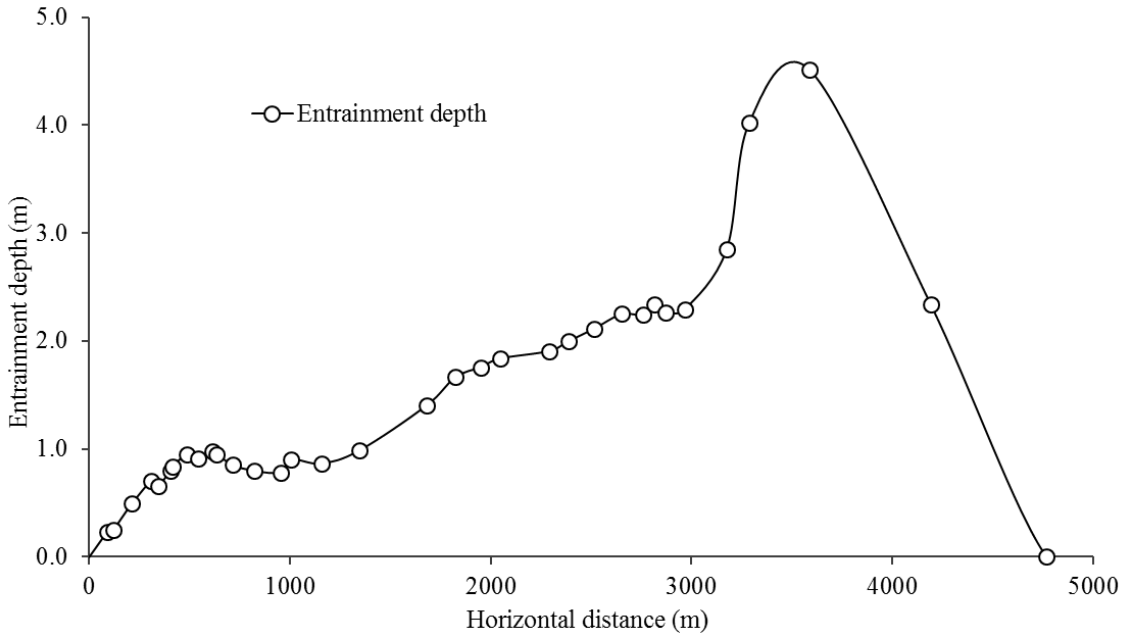

Figure 7-24: The simulated depth of erosion of Faucon debris flow along the channel

7.6.4. Evaluation of simulation results

Velocities, total volume and the maximum depth of erosion are selected as the criteria to verify the simulation results. Figure 7-19 shows the estimated velocities at two spots on site (Hussin et al., 2012). As a whole, simulated velocities agree with estimated values. The calculated volume and the maximum depth of erosion are larger than that observed, but difference is not large.

7.7. Zymoetz River rock avalanche (ZRRA)

7.7.1. Description of Zymoetz River rock avalanche

The Zymoetz River is located near Terrace in west central British Columbia, Canada, approximately 65 km east of Prince Rupert. On June 8, 2000 (see Figure 7-25 (a)), a large debris flow avalanche occurred at the left side of Zymoetz River and severed the Pacific Northern Gas pipeline with geographical coordinates 54º 26′ N, 128º 18′ W. The total economic losses associated with the landslide exceeded CDN $30 million, including the direct costs of repairing

the pipeline as well as lost timber and forestry access time (Schwab et al. 2003). The ZRRA initiated with 0.9×10^6 m^3 block of bedrock from cirque basin at the head of the valley (Figure 7-25, (b)) and finally stopped after it blocked the river with 1.4×10^6 m^3, but it was overtopped quickly (McDougall et al (2006)) (Figure 7-25, (c)). The variation of the elevation of the source material was around 1,245 m, from elevation 1,390 m to elevation 145 m, over a horizontal distance of 3.5 km, and a path length of 4.2 km (Boultbee, 2005).

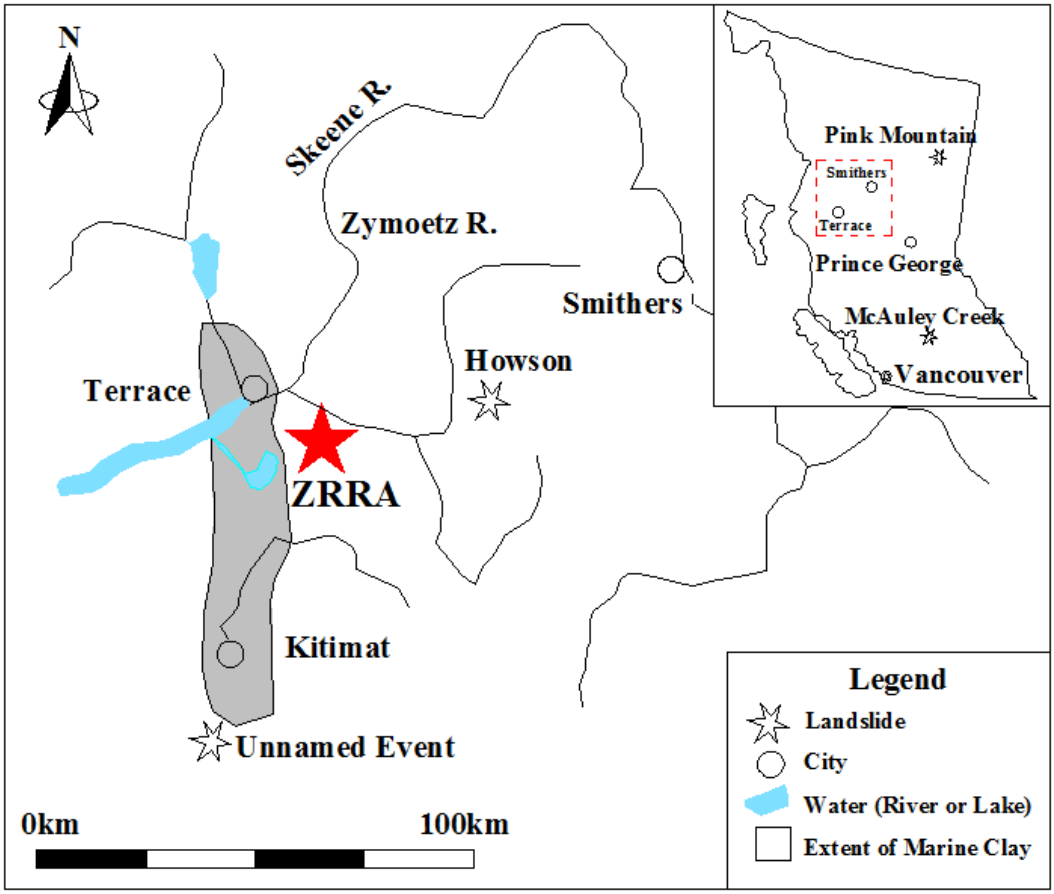

(a)

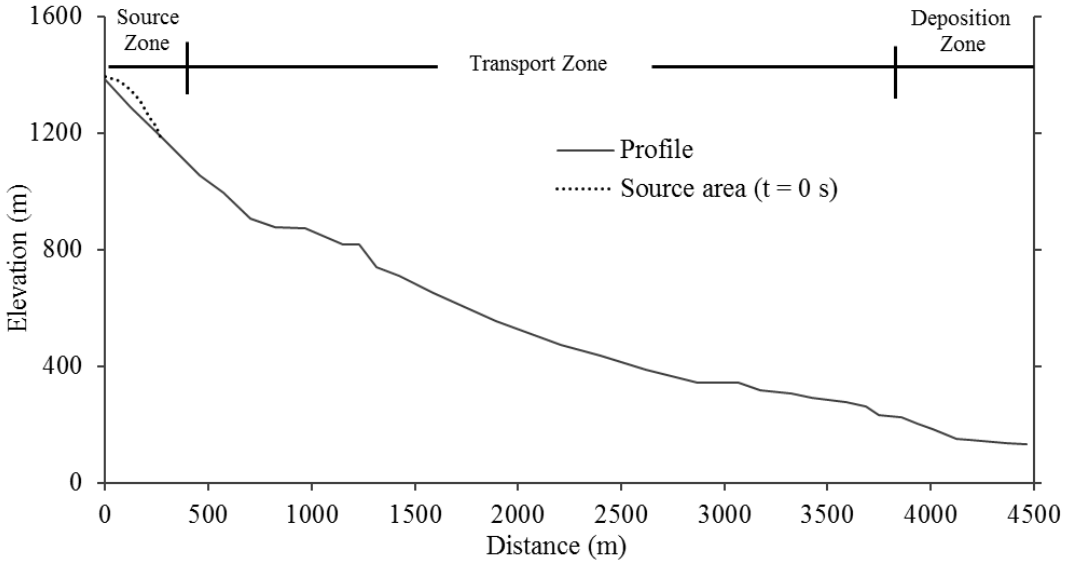

(b)

(c)

Figure 7-25: Geographical location and deposition fan of ZRRA (a) Geographical location, (b) longitudinal profile and (c) deposition fan of ZRRA (Boultbee et al. 2006)

No seismic activity was observed according to the investigation for the possible triggers of the landslide, but significant precipitation was observed two weeks prior to the event (Figure 7-26). The days before the event were cool with snow at higher elevations. Therefore, it was deducted that failure was probably triggered by progressive, long-term degradation of the tectonically deformed and altered volcaniclastic rock mass. Freeze-thaw activity and change in pore water pressure also impacted the change of shear strength of the failure surface (Boultbee et al. 2006).

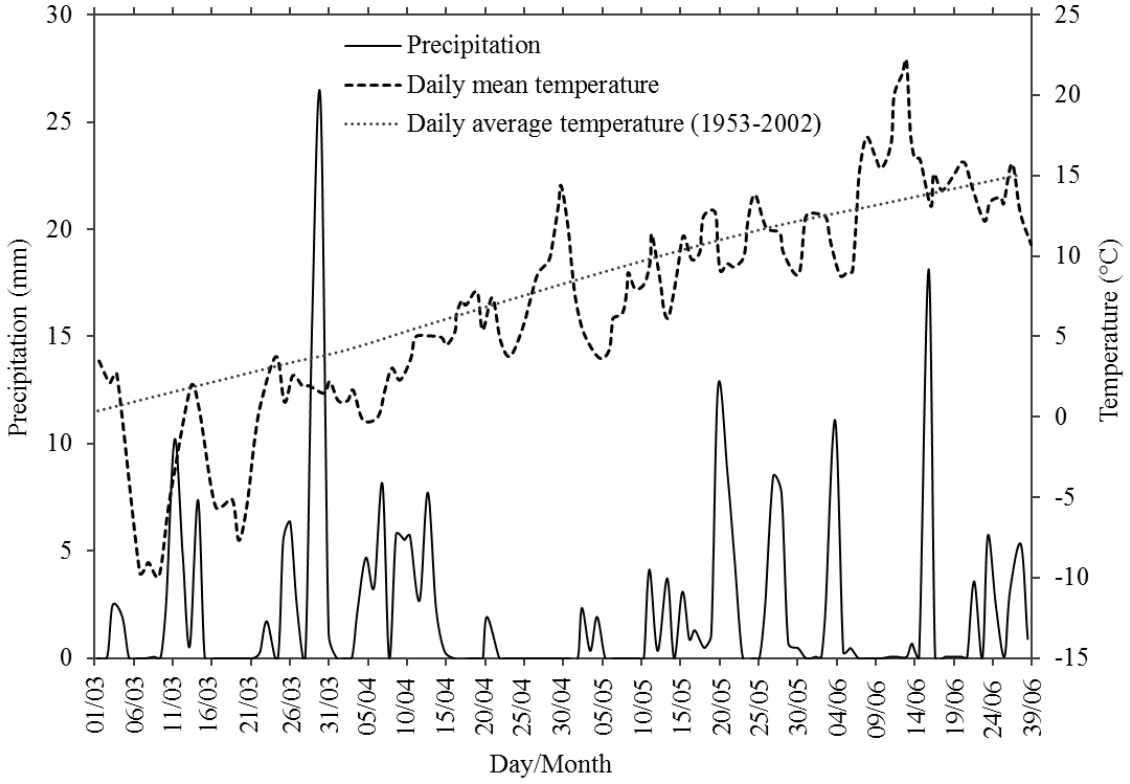

Figure 7-26: Precipitation and temperature before and after ZRRA

(adopted from Boultbee et al, 2006)

Surficial materials in this area are mainly composed of till, colluvium and exposed bedrock on hillslopes with waterlain deposits such as glaciomarine and fluvial and glaciofluvial sediments in

valleys. Kame terraces, and glaciolacustrine sediments are also found in this area (Boultbee et al, 2006).

Superelevation method was used to estimate the flow velocity at some of cross sections in Figure 7-28, using equation $v_c = \gamma_c\, g\, tan\theta\, cos\alpha$ (Method 1) and $v^2 = (\gamma_c\, g\, h)\, /b$ (Method 2) in which γ_c is the radius of curvature, θ is transverse slope, α is the longitudinal slope and b is the channel width. High kinetic energy caused up to 40 m superelevations along the length of channel. The estimated velocities are shown in Table 7-4. The most possible velocity of debris flow ranges from 15 m/s to 25 m/s although the velocity of debris avalanche varies within transport zone.

Table 7-4: Velocities estimated using superelevation methods (Boultbee et al, 2006)

Location	Velocity (m/s)	
	Method 1	Method 2
C-S 2	14	19
C-S 3	16	19
C-S 7	21	26
C-S 8	15	24
C-S 9	20	24

A 3m thick of snow remained under the debris after the event indicated that there was little entrainment of snow and no entrainment of debris at the far south end of the basin. As the debris moved along the channel, saturated sediment would have been entrained started from the north side of forested island. The entrained material was mainly the surficial soil cover. The estimated entrainment volume was around 0.6×10^6 m^3 (McDougall et al., 2006).

Deposition depth in the valley ranged from very thin layer to 4 m deep with an average depth of approximately 1.5 m. From the contour lines based on the digital elevation model taken 4 days after the event, it was estimated that the material deposited in the channel is approximately 200,000 m^3 (Figure 7-27). Based on field measurements, another 500,000 m^3 to 600,000 m^3 of coarse rock slide debris, averaging about 3 m thick, came to rest in the upper part of the cirque

basin immediately below the source area. Interpretation of air photo at the debris fan provided a volume of material deposited in the fan of approximately 625,000 m^3. The depth of the fan was difficult to estimate, but may be up to 10-12 m in places. It was deducted that total volume of 1.4×10^6 m^3 was mobilized and 500,000 m^3 of that was entrained along the path (McDougall et al., 2006).

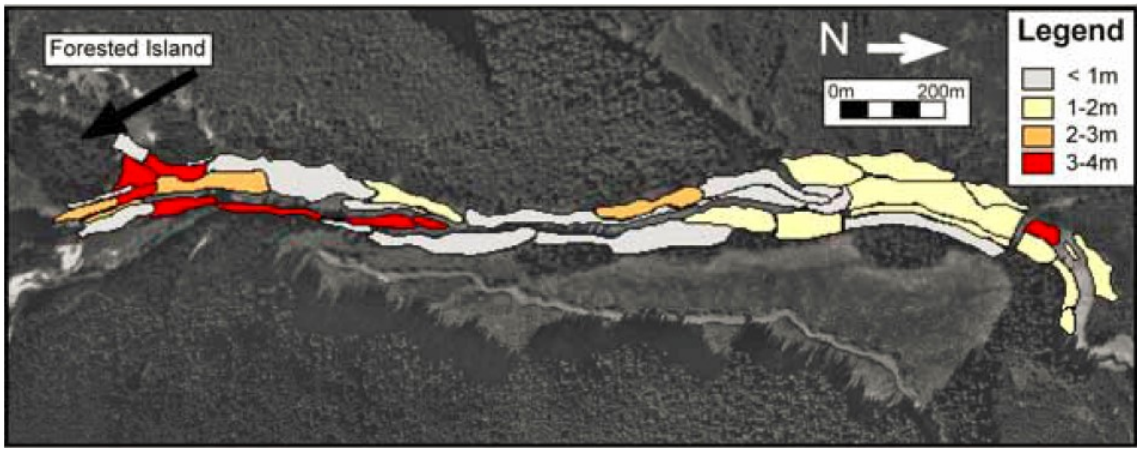

Figure 7-27: Thickness of deposition along the path of ZRRA from the forested island to the start of the canyon (Boultbee et al. 2006)

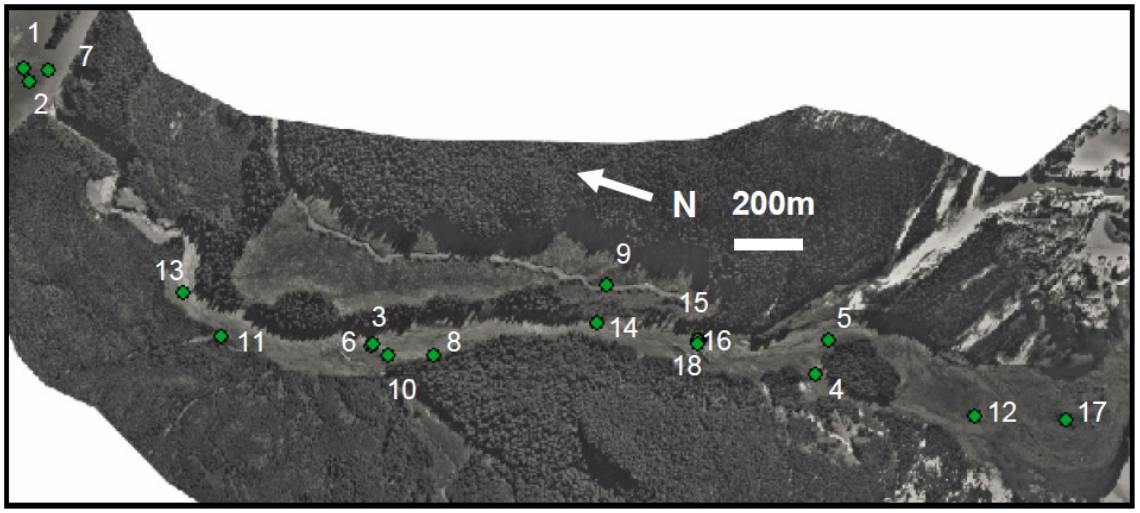

Figure 7-28: Location of sampling points of ZRRA (Boultbee et al. 2006)

Particle size analysis was carried out on the soil sampled from the sites in Figure 7-28 (Boultbee et al. 2006). D_{50} for particles lying on channel bed from forested island to deposition fan is around *10mm*.

Though landslides dams on the Zymoetz River was quickly overtopped, recording data from the Water Survey of Canada (WSC) station (Station No.08EF005), 3 km downstream on the Zymoetz River, still revealed that the turbidity spikes are correlated to a suspended sediment load of approximately 3,600mg/L to 12,000 mg/L (Boultbee et al. 2006).

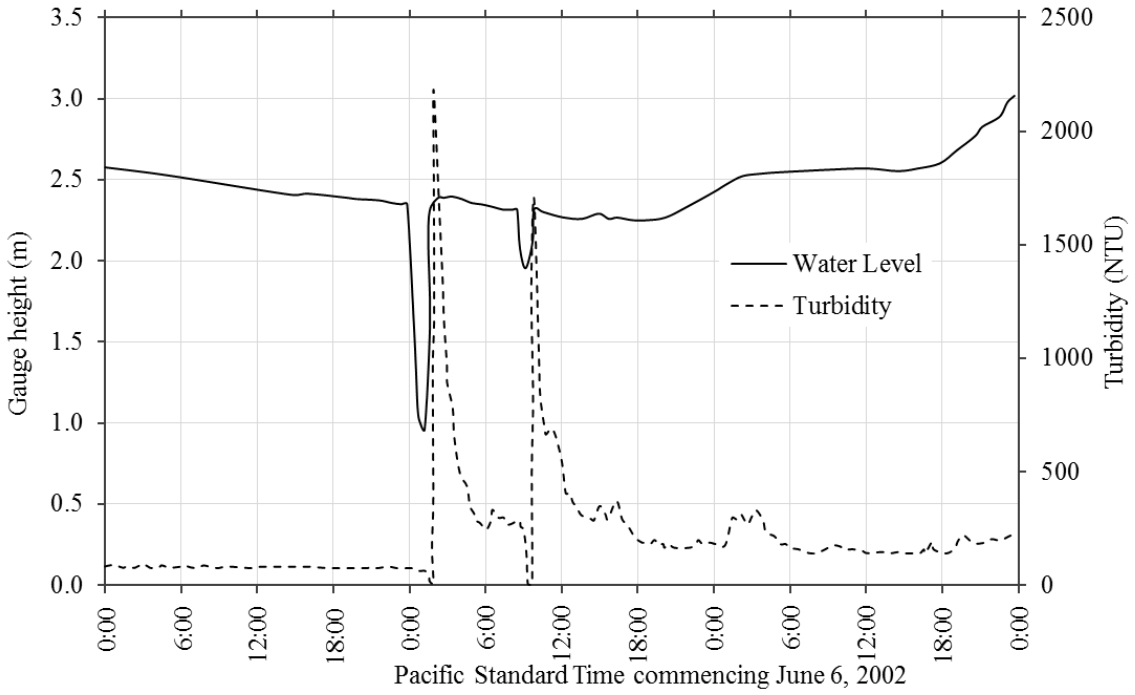

Figure 7-29: Impact of ZRRA on water level and turbidity monitored at water Survey of Canada Station No. 08EF005 (Schwab et al., 2003).

7.7.2. Parameter selection

Since snow is involved in the entrainment in ZRRA, the basal friction angle should be lower. Evidences from field investigation indicate that almost no material is eroded before the rock

avalanche reached the forested island. Therefore it is set in the model that entrainment starts below the forested island. Soil properties used in the simulation are mainly based on the measurements obtained from site investigation conducted by Boultbee et al. (2006). Since loose saturated soil is involved in this case, Boultbee et al. (2006) suggested that the basal friction coefficient of 0.1 can be used in the simulation, which is corresponding to about 5º. Internal friction angle is initially set as 18º. Other parameters used in the simulation are selected in reasonable range according to the case description by McDougall et al. (2006). Internal friction angle is then calibrated together with turbulent coefficient, mean value of α_o by matching velocity, deposition height and total volume. All the parameters used in the simulation are summarized in Table 7-5.

Table 7-5: Model Parameters for Zymoetz River rock avalanche

Parameters	Values
Unit weight (kN/m^3)	20*
Internal friction angle (º)	15
Basal friction angle (º)	5*
Turbulent coefficient (m/s^2)	300
Particle size d_{50} (mm)	100*
Mean value of α_o (º)	4
Standard deviation of α_o	0.1**
Particle density (kg/m^3)	2,600**
Particle contact friction coefficient	0.7**

*adopted from the results of back analysis carried out Boultbee et al. (2006) and McDougall et al., (2006).

**in case history studies, there are considered as a constant value since these values do not vary a lot.

7.7.3. Simulation results

7.7.3.1 Velocity and runout distance

Figure 7-30 indicates frontal velocities of ZRRA along flow path. Maximum flow velocity, 53 m/s, appears few seconds after rock block failed, which corresponds to 651m in horizontal displacements. The velocity drops to about 40 m/s when it meets flat area in Figure 7-25. Then the velocity continuously decreases until the debris stops except for some small variation at 135 s and 230 s. Figure 7-31 show the shapes of ZRRA at different time stage. After about 100 s, the tail of the debris does not vary a lot. However, the location of debris flow front significantly changes before the simulation is finished.

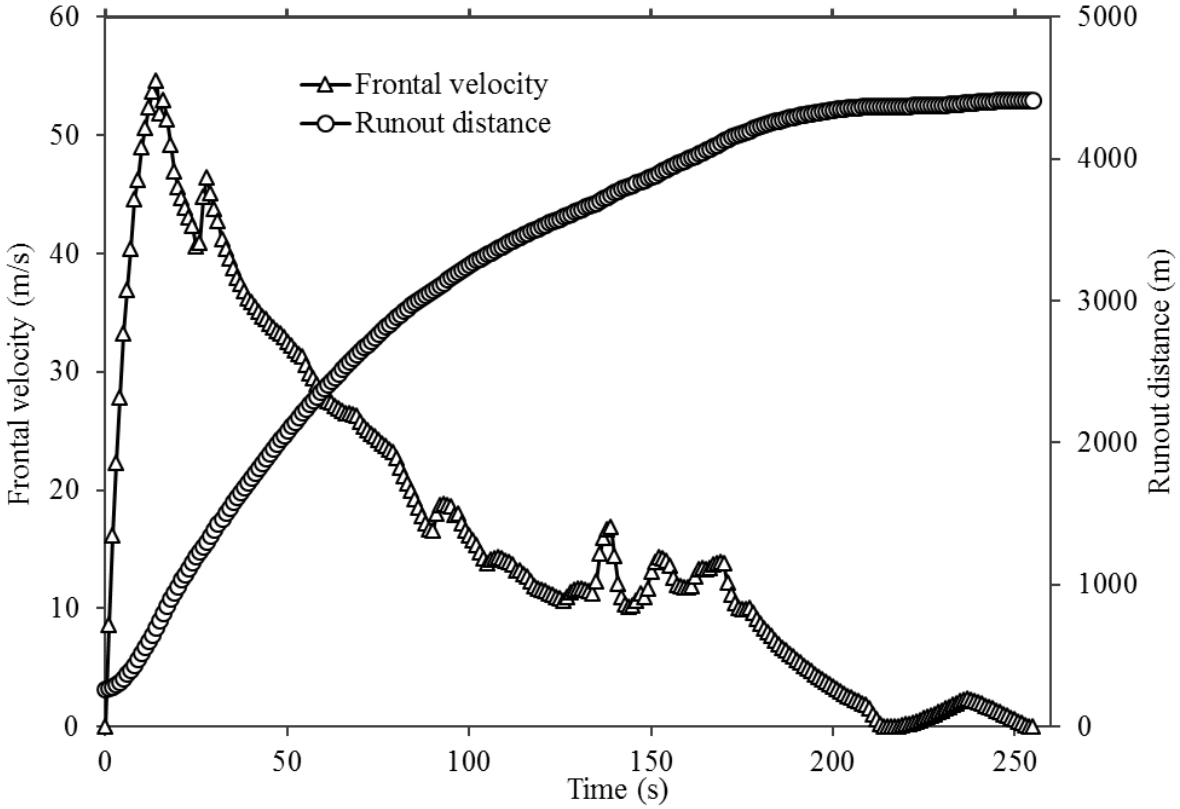

Figure 7-30: Calculated frontal velocity and run-out distance along the path of Zymoetz River Rock Avalanche (2002)

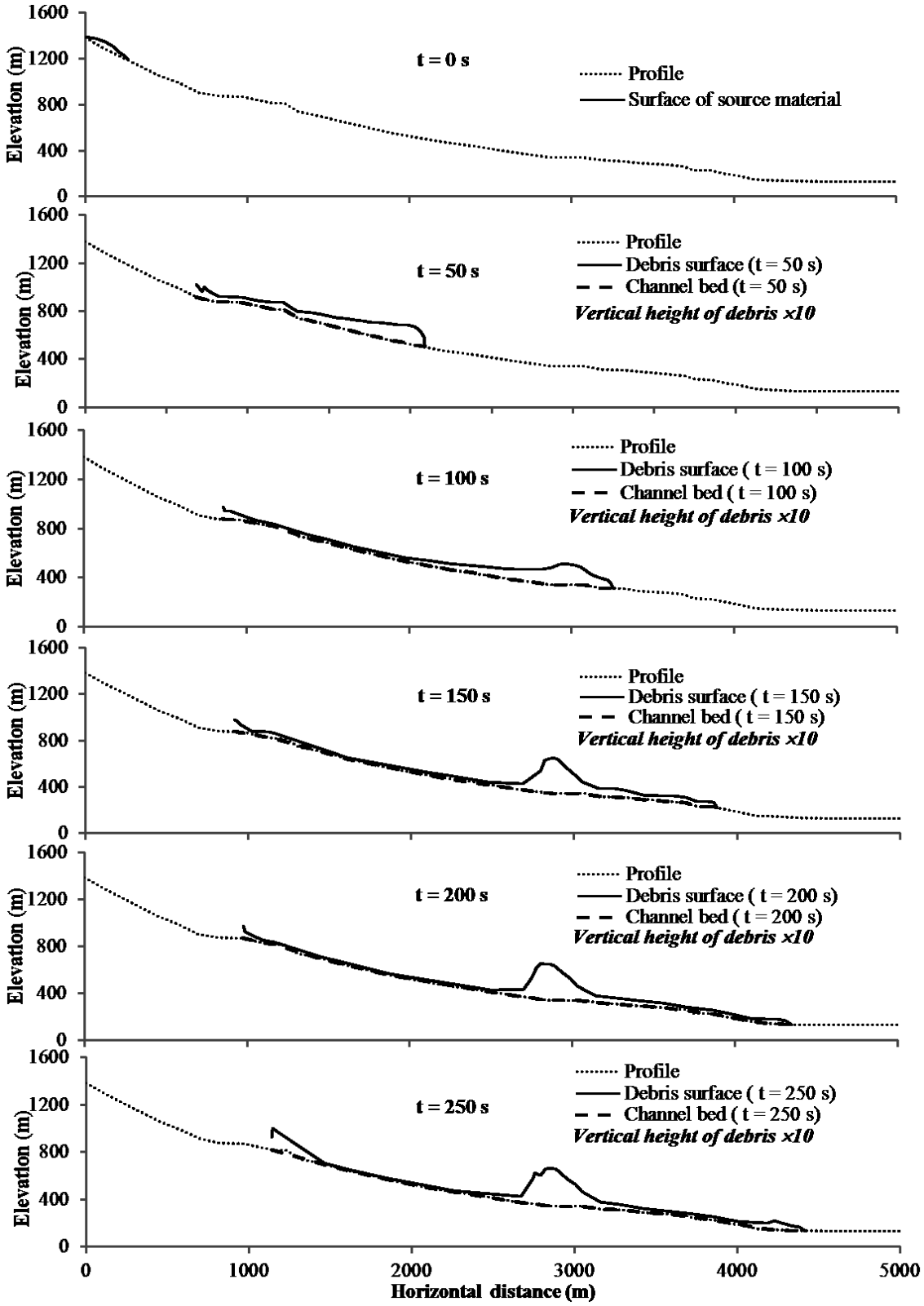

Figure 7-31: Shape of ZRRA at different time stage along flow path

7.7.3.2 Accumulated volume and entrainment rate

ZRRA starts with around 0.9×10^6 m^3 and no entrainment occurred until it reaches north side of forested island (McDougall et al (2006)). Figure 7-32 indicates that entrainment starts after the debris moves around 30 s. The maximum entrained volume, 5.3×10^6 m^3, appears when the front of debris moves around 60 s. Then it gradually decreases to zero when it arrives river channel where a deposition fan is formed.

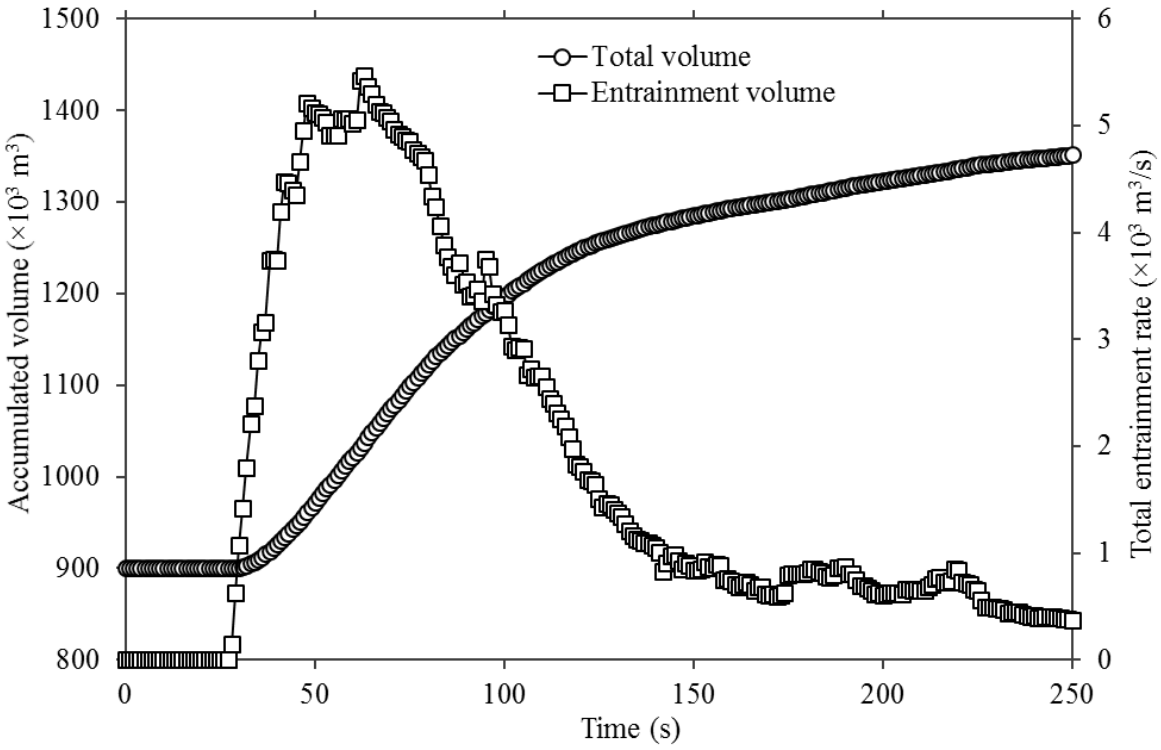

Figure 7-32: Variation of total volume and entrained volume along path of ZRRA

7.7.3.3 Entrainment rate and flow height

Flow height decreases rapidly at initial stage, but it vibrates after 20 s later. Maximum height is around 57 m found at t = 0s. Maximum height when it stops is about 33m. Actual height would be smaller if lateral spreading effect is considered. Maximum entrainment rate, 0.12 m/s, occurs

at the initial stage of entrainment (Figure 7-33). Entrainment rate of all the slices at different time stage is shown in Figure 7-34. It is interesting that maximum entrainment rate moves to downstream of flow path accompanying a decrease in the peak value. The maximum depth of erosion is around 3m between 1,500 m to 2,500 m in the simulation (Figure 7-35).

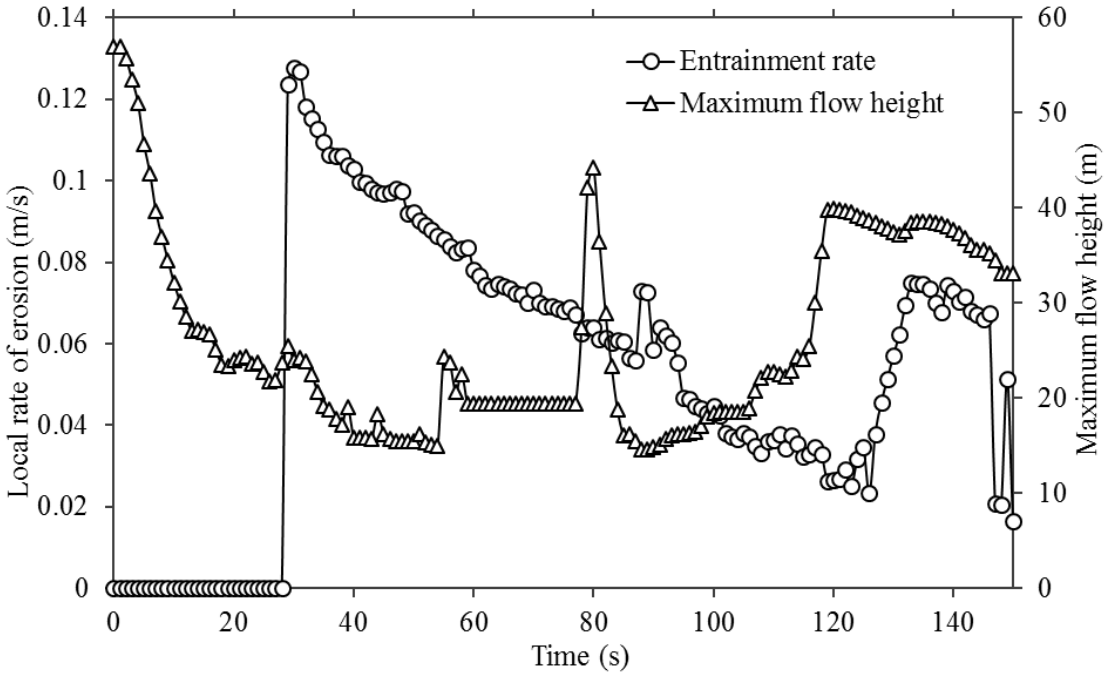

Figure 7-33: Entrainment height and maximum flow height along flow channel of ZRRA

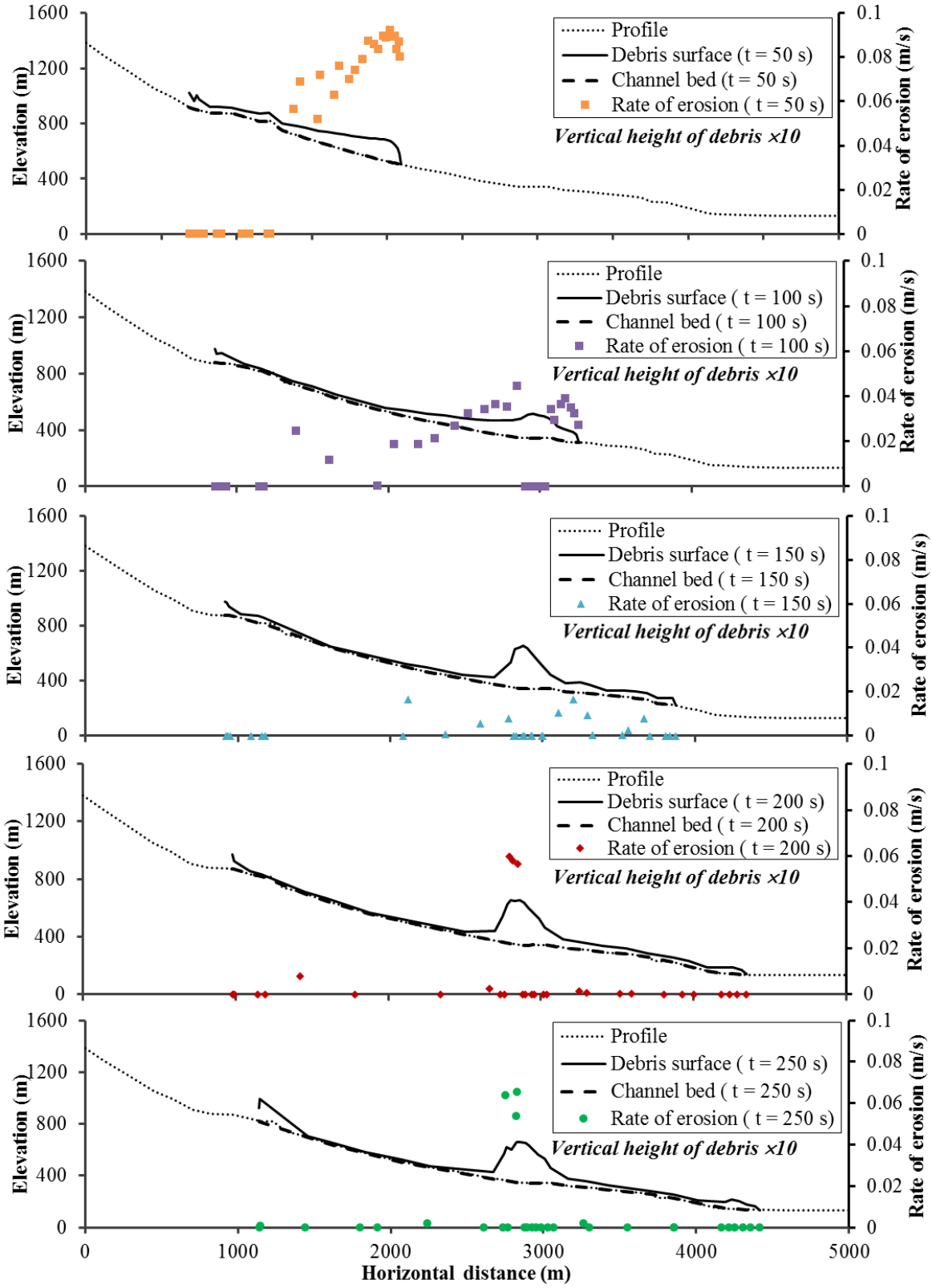

Figure 7-34: Entrainment rate of all the slices at different time stage

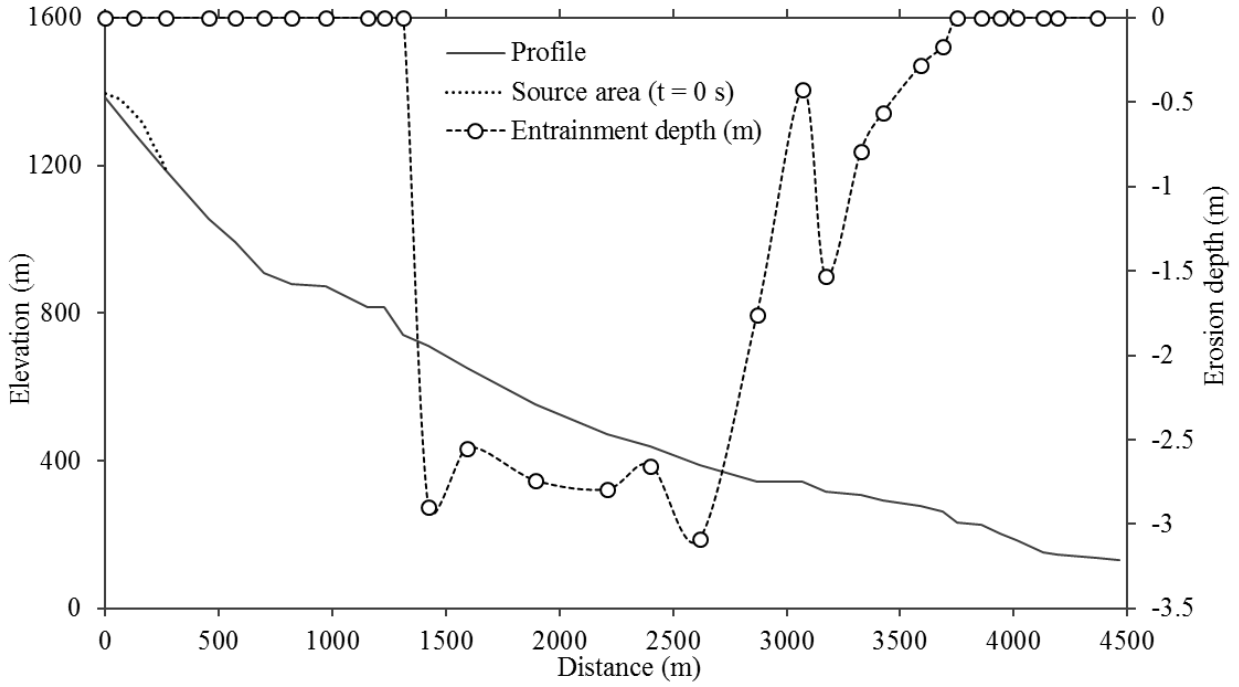

Figure 7-35: The depth of erosion along the path of ZRRA

7.7.4. Evaluation of simulation results

To evaluate the results of simulation, deposition height, velocity obtained using superelevation methods, final total volume and runout distance are used as criteria. Simulated deposition height and estimated average height are shown in Figure 7-36. Height of simulated debris deposition varies a lot at around 3,200m. The simulated height at deposition fan is smaller than that investigated. This is mainly caused by low precision of longitudinal profile at debris fan section extracted from published papers (Boultbee et al. 2006). Velocities at different time stage and that observed are shown in Figure 7-37. It seems that calculated velocities agree well with that observed.

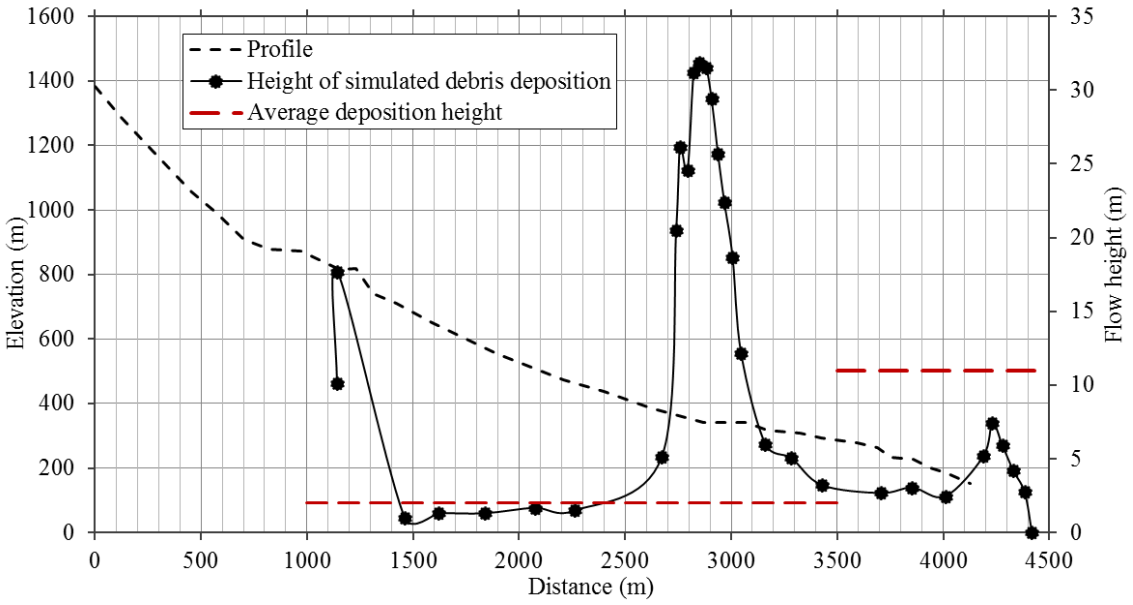

Figure 7-36: Height of debris deposition and estimated average height according to the investigation

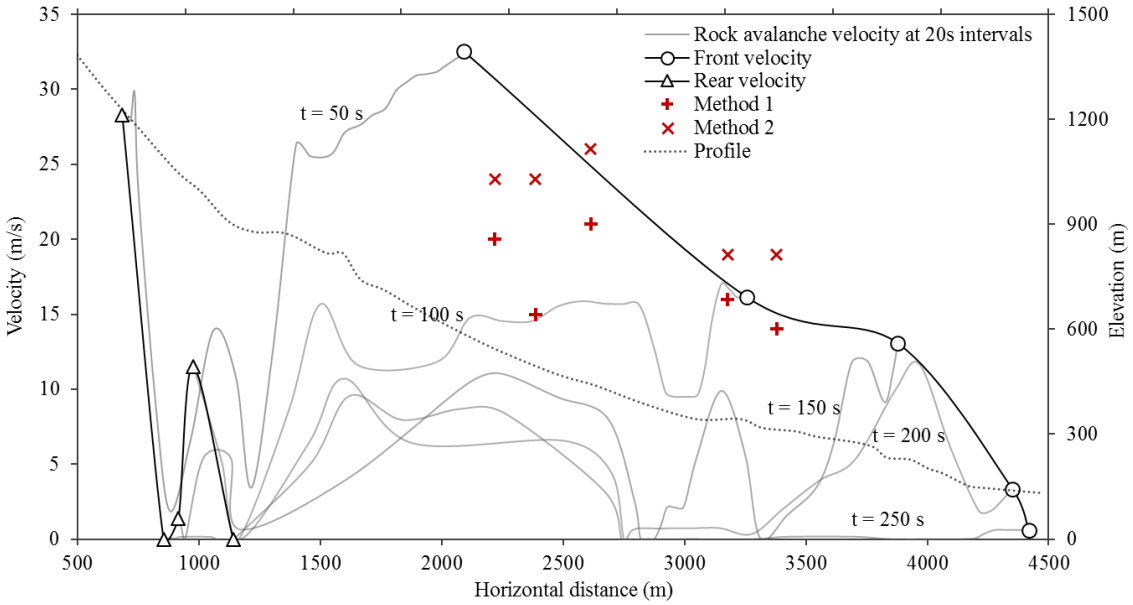

Figure 7-37: Velocity at different time stage and investigated velocities obtained using superelevation methods

7.8. Comparison of dynamic entrainment model and the new analytical model

7.8.1. Comparison results

To verify the hypothesis that it is easier for particles to be eroded by rolling motion rather than shear failure, a recent rock avalanche that occurred in Niumian (China), which more information is now available, is back analyzed using dynamic entrainment model. Velocity, final volume and entrainment rate estimated from the dynamic entrainment model and the new entrainment model are compared. In the calculation, the same parameters are adopted for both of models. Internal and basal friction angle are set as same value here.

Velocities estimated using the energy based runout model into which the dynamic and new entrainment model are incorporated separately, are identical except small gap at the end of simulation (Figure 7-38). Estimated velocities at specified locations from field measurement are also plotted in Figure 7-38. Deviations of both simulated velocities are almost same.

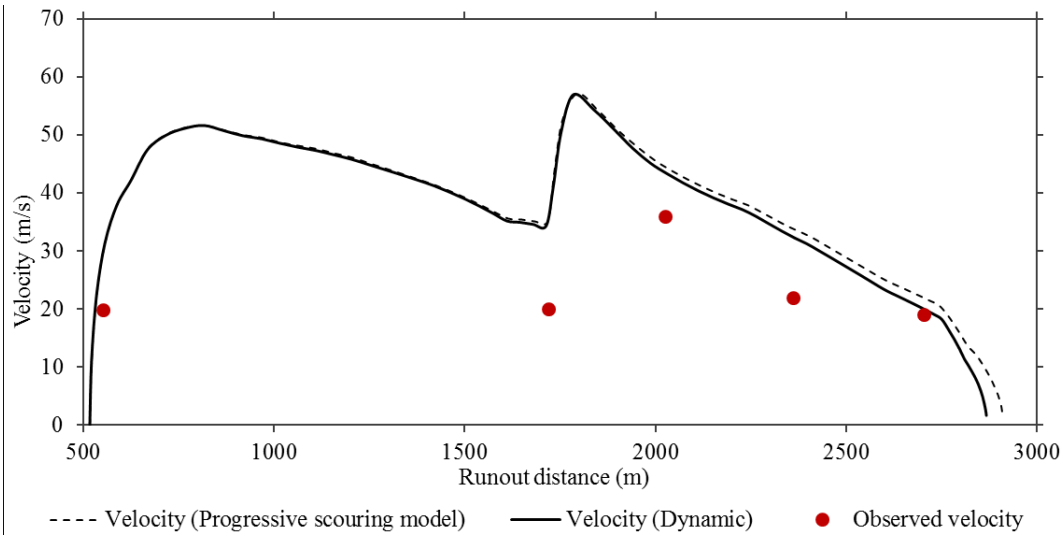

Figure 7-38: Estimated front velocities of Niumian rock avalanche

In order to compare the capabilities of those two model to simulate the entrainment, variation of total volume and entrainment rate along the flow channel are plotted in Figure 7-39 and Figure 7-40, respectively. It is obvious that total volume calculated using the new entrainment model is

larger than that simulated using dynamic entrainment model and is closer to the volume estimated on site (Xing et al. 2014). Entrainment rate estimated using the new entrainment model is also larger than that estimated using dynamic model. The maximum value from the new entrainment model is around 0.67 m/s larger than that from the dynamic model, 0.25 m/s.

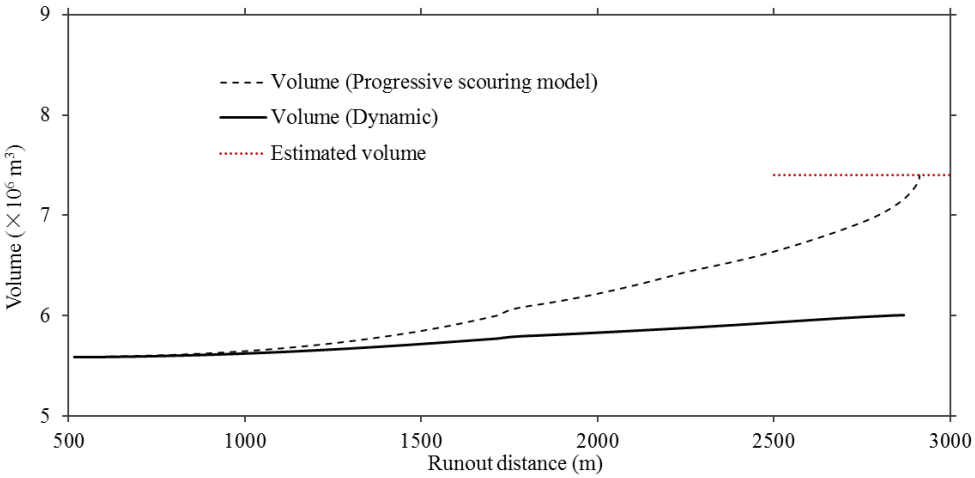

Figure 7-39: Variation of total volume of Niumian rock avalanche using new entrainment model and dynamic entrainment model

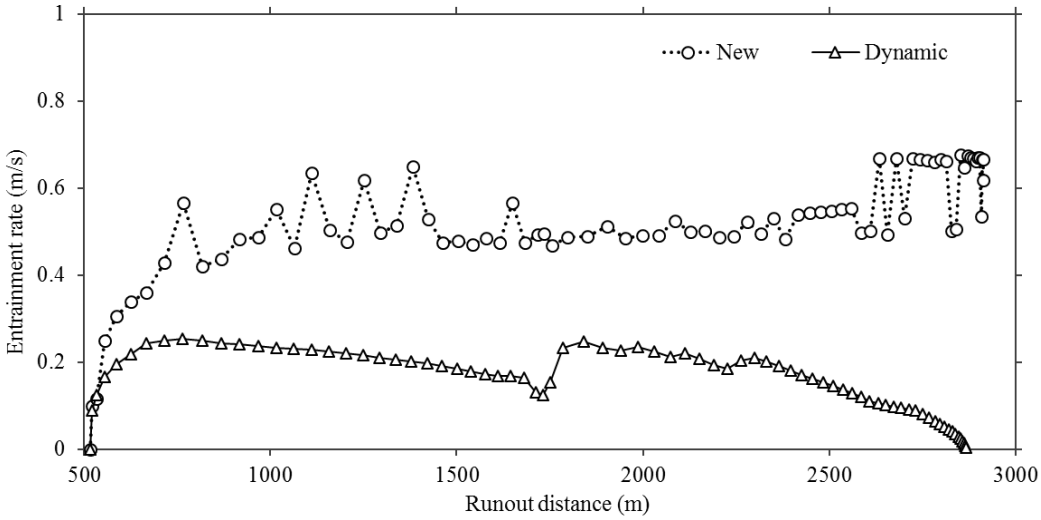

Figure 7-40: Estimated entrainment rate of Niumian rock avalanche along flow channel using new entrainment model and dynamic entrainment model

7.8.2. Sensitivity analysis of dynamic entrainment model

To clearly understand the reason of those differences in the results estimated using dynamic entrainment model, a sensitivity analysis is performed to clearly assess the impact of changes of the inputted parameters on the dynamic entrainment model outputs. The objective of the sensitivity analysis is to recognize which parameter impacts the output of dynamic model primarily. Parameters set in the initial stage are shown in Table 7-6. All initial parameters keep constant expect the parameters chosen for sensitivity analysis.

Table 7-6: Parameters adopted in sensitivity analysis

Parameters	ϕ_i (º)	ϕ_b (º)	c (kPa)	ρ (kg/m^3)	g (m/s^2)	h (m)	V (m/s)	θ (º)
Value	14	11	0	2,000	9.81	50	20	20

ϕ_i - internal friction angle; ϕ_b - basal friction angle; c - cohesion; g - gravity acceleration; ρ - density; h - flow height; V- flow velocity; θ - slope angle;

The sensitivity is quantified as the percentage of change in the outputs subjected to a constant variation in the input parameters (Figure 7-41). Since no entrainment occurs, if same friction angles for flowing mass and bed material are used, the variation of entrainment rate is only plotted when basal friction angle decreases and internal friction angle increases. It is indicated that flow velocity and friction angle (basal and internal) mainly affect the rate of erosion. The relationships between variation of friction angles and variation of entrainment rates are linear. For flow velocity, increasing the velocity could cause the entrainment rate decrease exponentially.

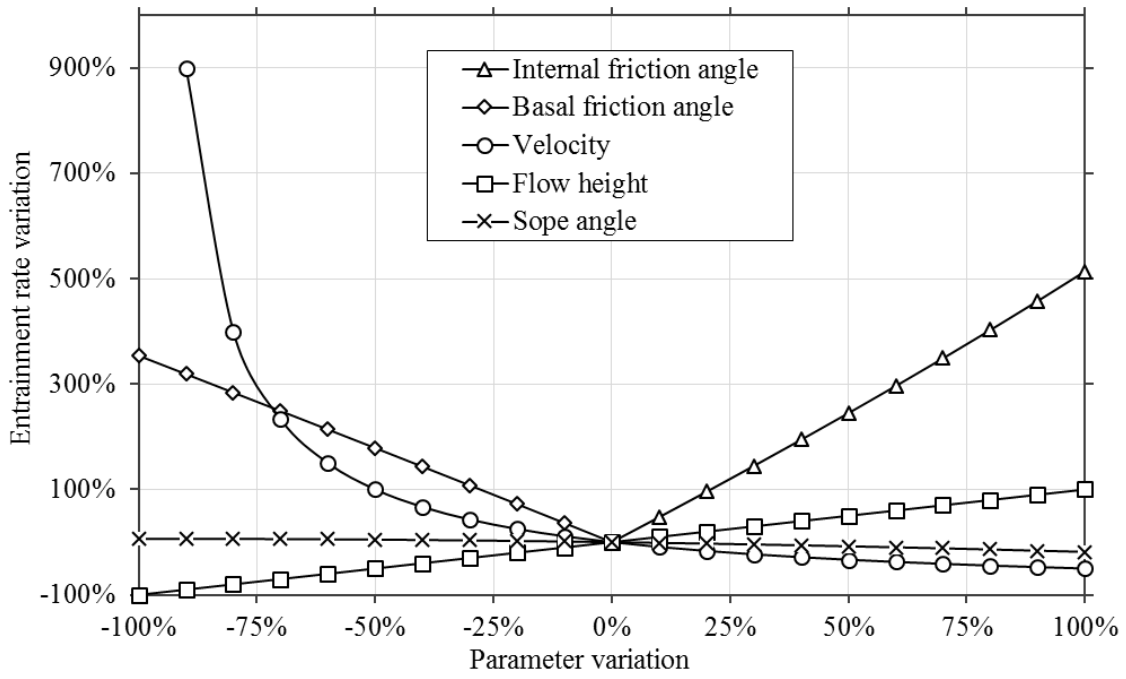

Figure 7-41: Variation percentage of the entrainment rate in regard to the change of most sensitive parameters

7.9. Discussion and conclusion

7.9.1. Simulation results

It is apparent that calculated run-out distance and maximum velocity or velocities at specified locations, agree with the estimated value very well. Meanwhile, simulated volume can approach the total volume at deposition fan which is estimated by subtracting the post-event digital elevation model from pre-event digital elevation model. The depth of erosion or the height of debris is not easy to match for channel which width varies a lot. This is a common problem for *2D* or *1D* simulation which is mainly caused by the ignorance of lateral spreading effect in the simulation which could lead to change of flow height. Moreover, it could cause the change of shear stress applied on channel bed, therefore the flow depth and entrainment rate also change.

Besides, assuming that the properties of particles lying on channel is identical could increase the gap between simulated results and observed values.

Maximum entrainment rate with respect to simulation time and entrainment rate of each slice at different time stage is plotted in previous section. It seems that although maximum entrainment rate undulates during the simulation, the variation is not large except when the slice reaches the region at which slope gradient changes a lot. No obvious regulations are observed for the entrainment of each slices at different time stage. This is caused by the rate of erosion not only depending on terrain and also relying on the properties of erodible materials lying on channel bed and in the flow. These factors make the estimation of the rate of erosion cannot be performed by simply using very few parameters.

Apparently, in the new entrainment model, the rate of erosion is considered. This is more reasonable in simulating progressive scouring process in which particles are eroded progressively. Therefore, it can be used to simulate the entrainment of channel eroded by flow during different time length. Additionally, channel bed elevation is adjusted after each time step rather than using same profile in the whole simulation that is not true in real cases. Though it probably cannot influence a lot on long channel with low entrainment rate, it affects a lot on short channels with large entrainment rate, notably on regions at which terrain is suddenly changed. This model not only incorporates the rolling motion of entrainment, it also considers the sliding motion of particle that is only motion considered for most of entrainment models. Therefore, considering the rolling motion in the estimation of debris flow entrainment logically replenishes the theory of entrainment estimation of granular particles.

7.9.2. Determination of α_0

As particle in field is not a sphere and particle size varies a lot in one case, particle protrusion relative to adjacent particles is difficult to measure. Therefore, particle properties are not easy to be represented using only one PDF. To find the correlation between soil properties and mean value of α_0, after analysis, correlations between part of soil properties and best matched mean value of α_0 used in the simulation are shown in Figure 7-42. It is indicated that correlation coefficient between mean value of α_0 and the difference between internal and basal friction angle is smaller than that between mean value of α_0 and internal friction angle. Besides, correlations between mean value of α_0 and slope angles are also shown in Figure 7-43. Obviously, maximum correlation coefficient of three groups' points is less than 0.6.

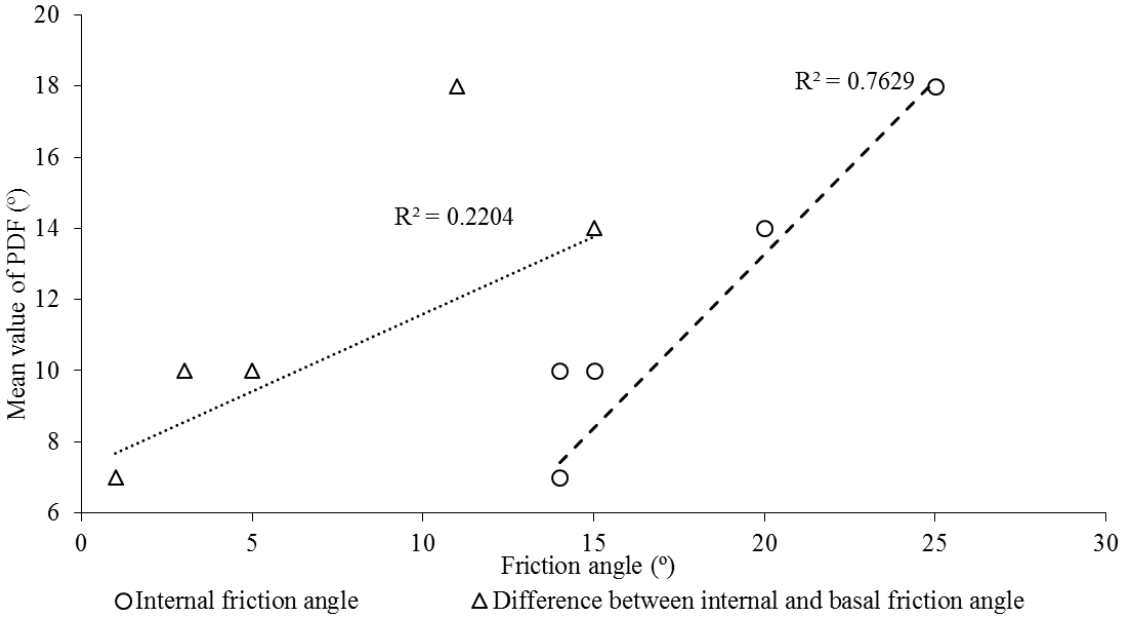

Figure 7-42: Correlation between mean of PDF and friction angles

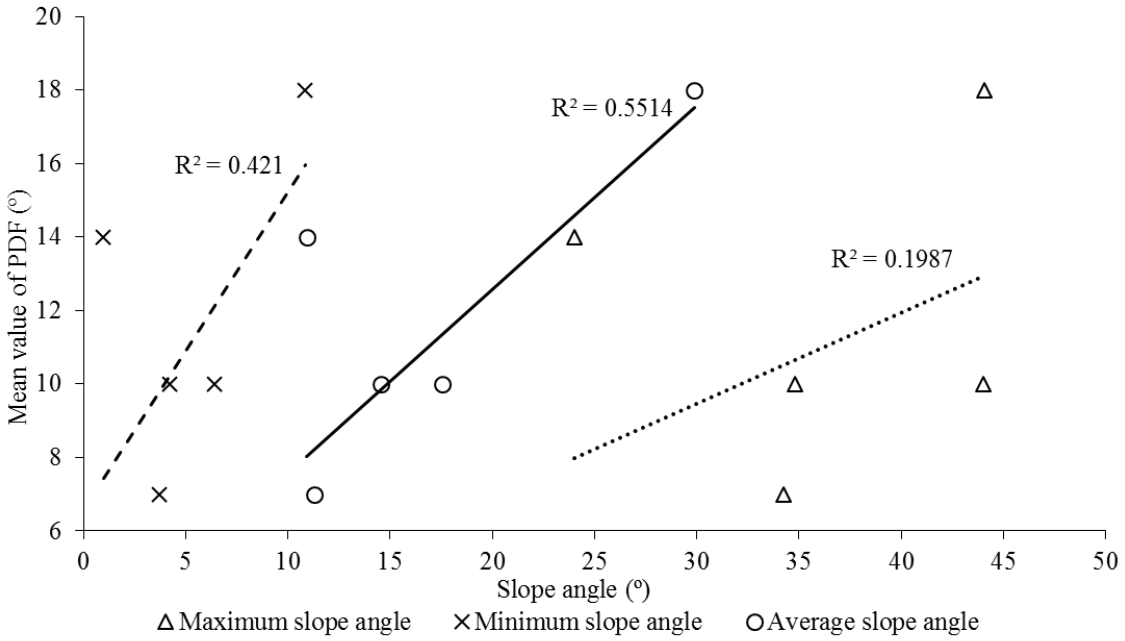

Figure 7-43: Correlation between mean of PDF and slope angles

Wiberg and Smith (1987) and Eagleson and Dean (1961) theoretically derived the equation for obtaining the pivoting angle which is $(\pi/2 - \theta - \phi)$ (Figure 7-44, (a)). Li and Komar (1986) empirically plotted the relationship between pivoting angle and D_i/D_{50} in which D_i is the particle size and D_{50} is the mean diameter of particles (Figure 7-44, (b)). Therefore, it means that α_0 can be estimated from the pivoting angle.

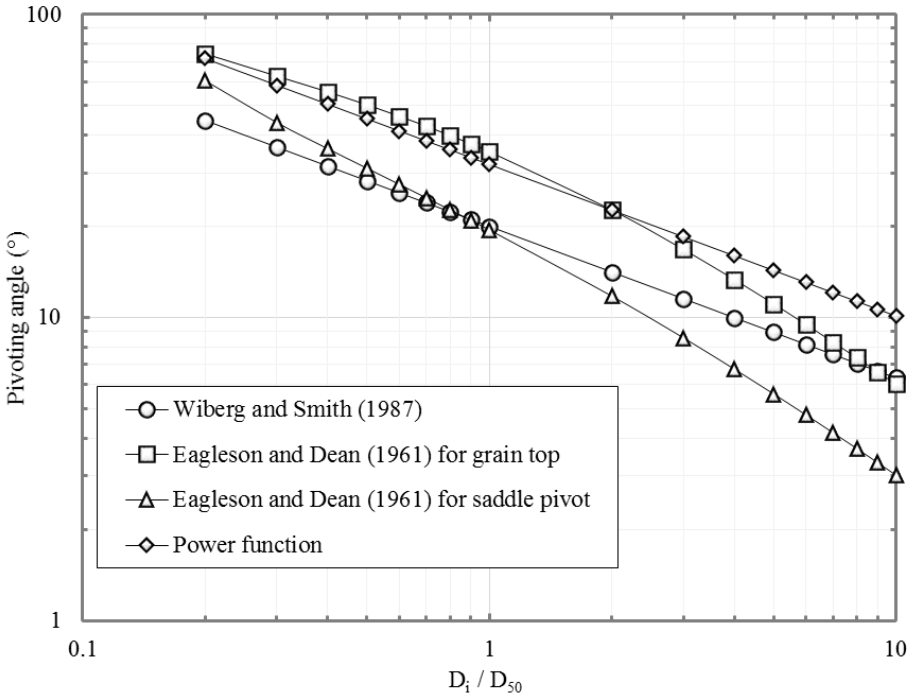

(a)

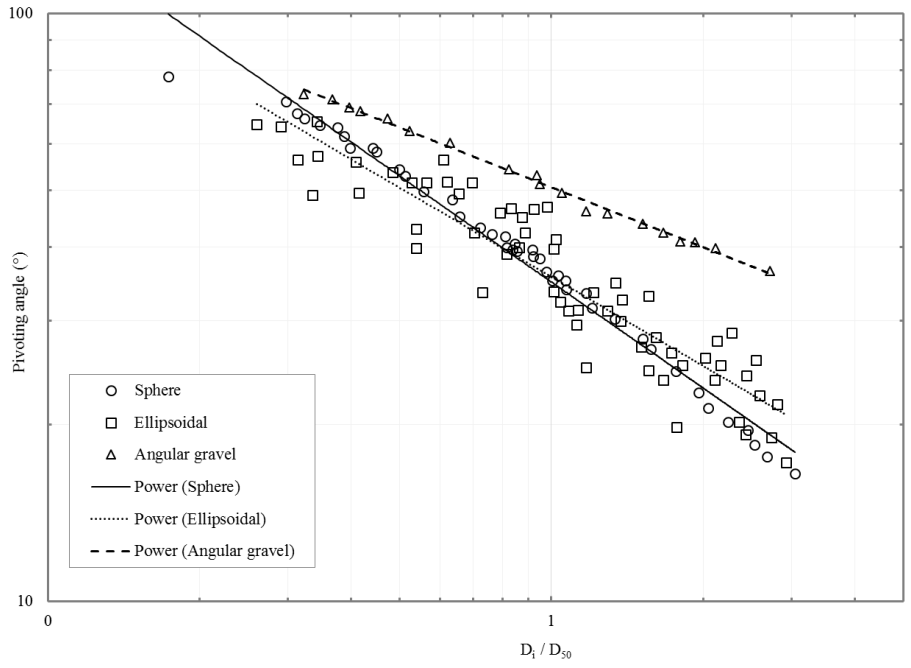

(b)

Figure 7-44: Pivoting angle equations determined (a) theoretically and (b) empirically.

(Wiberg and Smith (1987) is plotted based on the equation $\phi_p = e\ (D_i/D_{50})^{-f}$. Eagleson and Dean (1961) equation is $\tan \phi_p = \gamma / ((D_i/D_{50})^2 + 2\ (D_i/D_{50}) - 1/3)^{1/2}$, where $\gamma = 2/\sqrt{3}$ is for grain top and $\gamma = 1/\sqrt{3}$ is for saddle pivot. Power function is $\phi_p = 32\ (D_i/D_{50})^{-0.5}$ (Li and Komar, 1986))

7.9.3. Comparison of models

Comparison results indicate that entrained volume of debris flow estimated using dynamic entrainment model is fewer than that simulated using the new entrainment model. By comparing the simulation results with the measured data on site, it is found that the new entrainment model is more reasonable in estimating the rate of erosion in debris flow. Results of sensitivity analysis of the dynamic entrainment model indicate that flow velocity and friction angle mainly impact the simulation results a lot. Therefore, simulated entrainment rate could vary a lot if flow height and velocity change greatly during its movement.

7.9.4. Results explanations

According to Lambe (1973), "Predictions have always played a significant role in nearly every aspects of man's life." He stated that for geotechnical engineering, it is really difficult to accurately determine the field situation and mechanism, and to select the appropriate parameters in the simulation. The predictions can be classified into 5 types according to the relationship between prediction time and occurrence time of the case, and the availability of data for results verification. In most cases, type C and C1 predictions, performed after the event, are used to evaluate the validity of the model. Type C1 prediction, for which the results are available for the analysis, can be used to demonstrate the effectiveness of the technique or model.

The statement made by Lambe (1973) that "Type C predictions are autopsies…. One must be suspicious when an author uses Type C1 predictions to 'prove' that any prediction technique is

correct." is theoretically true. Generally, it is expected that precise data could be combined with scientifically derived methods to obtain precise predictions. However, soil behaviour is complex and soil properties are dependent on many variables, which contributes to the discrepancies between prediction and observations.

The development of the analytical entrainment model is based on the physics of entrainment for granular particles. Back analysis instead of prediction is carried out for several debris flow cases to calibrate the model. In the simulations, input parameters are mostly based on the published information or field investigations. Since the results are known in advance of the simulation, simulation results are matched with that observed by varying the parameters within reasonable ranges.

The entrainment model considers both rolling and sliding motions of moving particles. However, pore water pressure is not included in the current study. Moreover, erosion from the bank of the channel is also neglected in the 2D model. Besides, lateral spreading is not considered in the simulation which will improve the calculation and the flow height will change leading the variation of shear stress exerting on the channel bed.

In summary, the proposed analytical model adopts the conventional theory of rolling and sliding motions of particles. Simplifications of the field conditions together with reasonable adjustments of material parameters are used in the simulation and evaluation of the model. The model can be improved by including water and entrainment from the sides of the channel. Improvements in the determination of material parameters will also provide less variations and uncertainties of model parameters in the calibration process.

Reference

Boultbee N. (2005). Characterization of the Zymoetz River rock avalanche (Master's thesis), Simon Fraser University, Vancouver, Canada.

Boultbee N., Stead D., Schwab J., and Geertsema M. (2006). The Zymoetz River rock avalanche, June 2002, British Columbia, Canada, Engineering Geology, 83(1), 76–93.

Breien, H. (2005). On the dynamics of debris flows Case study Fjærland, Western Norway-a debris flow triggered by a natural dam breach (Master's thesis), University of Oslo, Oslo, Norway.

Breien, H., De Blasio, F.V., Elverhøi, A., and Høeg, K. (2008). Erosion and morphology of a debris flow caused by a glacial lake outburst flood, Western Norway, Landslides, 5(3), 271-280.

Cheng, N. S., Law, A. W. K., and Lim, S. Y. (2003). Probability distribution of bed particle instability, Advances in Water Resources, 26(4), 427-433.

De Blasio, F. V., Breien, H., and Elverhoi, A. (2011). Modelling a cohesive-frictional debris flow: an experimental, theoretical, and field-based study, Earth Surface Processes and Landforms, 36(6), 753-766.

Eagleson, P. S., and Dean, R. G. (1961). Wave-induced motion of bottom sediment particles, Transactions of the American Society of Civil Engineers, 126(1), 1162-1185.

Egashira, S., Honda, N., and Itoh, T. (2001). Experimental study on the entrainment of bed material into debris flow, Physics and Chemistry of the Earth, Part C: Solar, Terrestrial & Planetary Science, 26(9), 645-650.

Fenton, J. D., and Abbott, J. E. (1977). Initial Movement of Grains on a Stream Bed: The Effect of Relative Protrusion, Proceedings of the Royal Society of London Series a-Mathematical Physical and Engineering Sciences, 352(1671), 523-537.

Fraccarollo, L., and Capart, H. (2002). Riemann wave description of erosional dam-break flows, Journal of Fluid Mechanics, 461, 183-228.

Hussin, H. Y., Luna, B. Q., van Westen, C. J., Christen, M., Malet, J. P., and van Asch, T. W. J. (2012). Parameterization of a numerical 2-D debris flow model with entrainment: a case study of the Faucon catchment, Southern French Alps, Natural Hazards and Earth System Sciences, 12(10), 3075-3090.

Iverson, R. M. (1997). The physics of debris flows, Reviews of Geophysics, 35(3), 245-296.

Iverson, R. M., and Denlinger, R. P. (2001). Flow of variably fluidized granular masses across three-dimensional terrain 1. Coulomb mixture theory, Journal of Geophysical Research-Solid Earth, 106, 537-552.

Iverson, R. M., Logan, M., and Denlinger, R. P. (2004). Granular avalanches across irregular three-dimensional terrain: 2. Experimental tests, Journal of Geophysical Research, 109, F01015, doi:10.1029/2003JF000084.

Iverson, R. M., Reid, M. E., Logan, M., LaHusen, R. G., Godt, J. W., and Griswold, J. P. (2011). Positive feedback and momentum growth during debris-flow entrainment of wet bed sediment, Nature Geoscience, 4(2), 116-121.

Iverson, R. M. (2012). Elementary theory of bed-sediment entrainment by debris flows and avalanches. Journal of Geophysical Research, 117, F03006, doi:10.1029/2011JF002189.

Lambe, T. W. (1973). 13th Rankine lecture: Predictions in Civil Engineering. Géotechnique 23, No. 2, 149-202.

Li Z. L., and Komar, P.D. (1986). Laboratory measurements of pivoting angles for applications to selective entrainment of gravel in a current, Sedimentology, 33(3), 413-423.

Luna, B. Q., Remaitre, A., Van Asch, T. W. J., Malet, J. P., and van Westen, C. J. (2012). Analysis of debris flow behavior with a one dimensional run-out model incorporating entrainment, Engineering Geology, 128, 63-75.

Mangeney, A., Roche, O., Hungr, O., Mangold, N., Faccanoni, G., and Lucas, A. (2010). Erosion and mobility in granular collapse over sloping beds, Journal of Geophysical Research, 115, F03040, doi:10.1029/2009JF001462.

McCoy, S. W, Kean, J. W, Coe, J. A, Tucker, G. E, Staley, D. M., and Wasklewicz, T. A. (2012). Sediment entrainment by debris flow: In situ measurements from the headwaters of a steep catchment. Journal of Geophysical Research, 117, F03016, doi:10.1002/jgrf.20041.

McDougall, S., Boultbee, N., Hungr, O., Stead, D., and Schwab, J. W. (2006). The Zymoetz River landslide, British Columbia, Canada: description and dynamic analysis of a rock slide-debris flow, Landslides, 3, 195–204.

Medina, V., Bateman, A., and Hurlimann, M. (2008a). A 2D finite volume model for bebris flow and its application to events occurred in the Eastern Pyrenees, International Journal of Sediment Research, 23 (4), 348-360.

Medina, V., Hürlimann, M., and Bateman, A. (2008b). Application of FLATModel, a 2D finite volume code, to debris flows in the northeastern part of the Iberian Peninsula, Landslides, 5(1), 127-142.

Okada, Y., and Ochiai, H. (2007). Coupling pore-water pressure with distinct element method and steady state strengths in numerical triaxial compression tests under undrained conditions, Landslides, 4(4), 357-369.

Remaître, A, Malet, J. P., and Maquaire, O. (2005). Morphology and sedimentology of a complex debris flow in a clay-shale basin, Earth Surface Processes and Landforms, 30(3), 339-348.

Remaître, A, Van Asch, T. W., Malet, J. P., and Maquaire, O. (2008). Influence of check dams on debris-flow run-out intensity, Natural Hazards and Earth System Science, 8(6), 1403-1416.

Remaître, A., Malet, J. P., and Maquaire, O. (2009). Sediment budget and morphology of the 2003 Faucon debris flow (South French Alps): scouring and channel-shaping processes. Proceedings of the International Conference 'Landslide Processes': from geomorphological mapping to dynamic modelling, Editors: Malet, J.P., Remaître, A., and Bogaard, T., Strasbourg, France, February, 6-7, 2009, CERG Editions, Strasbourg, 75-80.

Remaitre, A., Malet, J. P., and Maquaire, O. (2011). Geomorphology and kinematics of debris flows with high entrainment rates: A case study in the South French Alps, Comptes Rendus Geoscience, 343(11), 777-794.

Schwab, J.W., Geertsema, M., and Evans, S.G., (2003). Catastrophic rock avalanches, West-Central British Columbia, Proceedings of the 3rd Canadian Conference on Geotechnique

and Natural Hazards, Editors: Anonymous, Edmonton, Alberta. June 9-10, 2003, Canadian Geotechnical Society, Edmonton, 252-259

Shodja, H. M., and Nezami, E. G. (2003). A micromechanical study of rolling and sliding contacts in assemblies of oval granules, International Journal for Numerical and Analytical Methods in Geomechanics, 27(5), 403-424.

Skempton, A.W. (1954). The pore-pressure coefficients A and B, Géotechnique, 4(4), 143-147.

Takahashi, T. (1991). Debris flow. Rotterdam: Balkema.

Tang, C., Van Asch, T. W. J., Chang, M., Chen, G. Q., Zhao, X. H., and Huang, X. C. (2012). Catastrophic debris flows on 13 August 2010 in the Qingping area, southwestern China: The combined effects of a strong earthquake and subsequent rainstorms, Geomorphology, 139, 559-576.

van Asch, T. W. J., Malet, J. P., Remaître, A., and Maquaire, O. (2004). Numerical modelling of the run-out of a muddy debris flow, The effect of rheology on velocity and deposit thickness along the run-out track, Proceedings of the 9th International Symposium on Landslides, Editors: Lacerda,W.A., Ehrlich, M., Fontoura, S.A.B. and Sayao, A.F.S.J., Rio de Janeiro, Brazil, June 28 - July 2, 2004, Taylor and Francis Group, London, 1, 1433-1438.

Wang, X. B. (2008). Geotechnical analysis of flow slides, debris flows, and related phenomena (Doctoral dissertation). University of Alberta, Edmonton, Canada.

Wiberg, P. L., and Smith, J. D. (1987). Calculations of the critical shear stress for motion of uniform and heterogeneous sediments, Water resources research, 23(8), 1471-1480.

Xing, A. G. , Xu, Q., and Gan, J. J. (2014). On characteristics and dynamic analysis of the Niumian valley rock avalanche triggered by the 2008 Wenchuan earthquake, Sichuan, China, Environmental Earth Sciences, 1-15.

Zhang, Y. J. (2013). Study on dynamic characteristics of typical rock avalanches on canyon area (Master's thesis), Shanghai Jiaotong University, Shanghai, China. (In Chinese).

8. SUMMARY, CONCLUSIONS AND RECOMMENDATIONS

8.1. Summary

This thesis focuses on the development and verification of a new analytical entrainment model in which progressive scouring entrainment process is considered. Sensitivity of the new model is tested by varying the parameters in the model. To clearly understand the entrainment process inside granular flow and verify the new entrainment model, numerical experiments have been carried out using DEM. Entrainment rates at specific cross sections of the erodible bed calculated using analytical model are compared with that calculated from the numerical experiment. This model is then used in studying different case histories for which field data is available.

Chapter 2 describes different approaches that have been developed for debris flow runout simulation. Constitutive models for estimating the shear stress underneath the debris are listed. The models developed for calculating the amount of entrainment in debris flow are classified according to the mechanisms used in the model. Methods adopted and apparatus used in the experiments are also described. The amount of materials in sourced zone and erodible zone are compared for each test. This chapter also describe the entrainment study in river.

Chapter 3 shows the development process of the new entrainment model in detail. The new model takes both rolling and sliding motions into consideration rather than simply considering shear failure in most existing approaches. The model is also evaluated by comparing the calculated entrainment rates with that estimated from flume experiments.

Numerical experiment is conducted to understand the entrainment process in Chapter 4. Flume with erodible bed is modelled using PFC2D. Shear stresses are calculated at specific cross

sections using measurement circles in PFC modeling. Average entrainment rates are also determined and compared with that calculated using the analytical model.

The process of incorporating the new entrainment model into an energy based runout model is presented in Chapter 5. Sensitivity analysis of the model has been carried out. Tsing Shan debris flow (1990) is a case with considerable entrainment. The case has been studied here and the simulated results are also evaluated by comparing them with field measurements.

The new model is applied to study the case histories in Chapters 6 and 7. In chapter 6, an extremely large rock avalanche is studied. Four typical cases with significant entrainment are presented in Chapter 7. The results are also verified by field measurements such as the depth of erosion, maximum velocity, runout distance and estimated volume of debris flow fan.

8.2. Conclusions

The outcome of this study provides a new particle scale entrainment model which can be used to incorporate entrainment into debris flow runout analysis. Development process of the entrainment model, numerical experiment used to experimentally verify the model, incorporating the model in runout analysis, and study of case histories are all included in this thesis. Therefore, based on the study of debris flow entrainment, following contents can be concluded.

Entrainment is important to study the kinematic characteristics of debris flow which involves erosion of material from channel bed/bank and inclusion of entrained material into flowing debris. The rate of erosion is generally defined as entrainment rate which can indicate the change of the channel bed downward (perpendicular to the slope surface). This process could impact the kinematic characteristics of the debris, since the incorporation process could increase potential energy of debris. Therefore, flow characteristics including velocity, flow height, basal shear

stress, etc. which are important in the estimation of kinematic energy of debris along the flowing channel are changed. For inclusion process, once the material lying on channel bed is eroded, it is generally considered as part of debris.

In granular material, erosion of material lying on channel bed due to rolling motion is easier than shear failure mechanism that is primarily considered in current entrainment analysis. This has been verified by PFC experiment in which a flume is formed with erodible material lying on downstream part of channel bed. When erosion starts, the eroded particles will rotate clockwisely or counterclockwisely. The rate of erosion is also calculated using the new entrainment model and a dynamic entrainment model in which only shear failure mechanism is considered. The results demonstrate that the new entrainment model in which rolling motion is considered can calculate an erosion depth closer to measured eroded depth than dynamic entrainment model.

The new entrainment model is sensitive to the mean value of α_0 in PDF which is related to pivoting angle of granular particle. Since it is not possible to measure the pivoting angle, a statistical correlation can be used to relate the pivoting angle to mean diameter of erodible granular particles which is easier to estimate. This has been verified in the study of historical cases.

PFC2D is useful in studying the characteristics of granular flow. It not only can capture the kinematic characteristics of moving particles, but also it can used to obtain the "micro" features of granular particles such as shear stress and normal stress applied on each particle which is not easy to measure in laboratory experiment or field experiment through current technology.

The simulation results from 6 debris flow cases, in which significant entrainment is involved, provide evidences that the runout model with the new entrainment model incorporated can capture the kinematic characteristics of debris flow. Therefore, it is possible to use the new

entrainment model which takes both rolling and sliding motions into account to calculate the rate of erosion of granular particles.

8.3. Recommendations for future research

To complement the new analytical entrainment model, the following work should be carried out in future.

8.3.1. Water

The pressure generated by water could affect the effective normal stress and then influence shear resistance. These forces can lead to the decrease of resistance for rolling motion as well. In this study, when water or precipitation is involved, it is considered that water only provide buoyancy for the particles. This assumption maybe is right for coarse particles. However, for fine particles, pore water pressure is not easy to be dissipated. Therefore, this assumption should be made with caution.

8.3.2. Normal stress in model derivation

Based on the experiments from Fraccarollo and Capart (2002), it is obvious that the vectors representing the velocity of flow "particles" are almost parallel to the channel bed. Therefore, in the derivation of the equation, it is assumed that the forces acting on the particle are based on particle movement parallel to the sliding surface. Therefore, normal force from debris flow is not considered. This assumption is right for the debris with high velocity, but for debris moving with a low velocity, it is still debatable. In addition, normal stress could probably limit the rolling motion. Therefore, normal stress should be considered when necessary.

8.3.3. Mean value of α_0 in PDF

The selection of the mean value of α_0 in PDF is suggested to refer to pivoting angle which can be obtained by an empirical relationship between pivoting angles and mean diameter of granular particles. In future, this approach should be tested and verified by studying more cases.

8.3.4. Deposition in flowing process

As another primary characteristic, deposition process is also significant in debris flow simulation since it could vary the potential energy of debris flow body. In flowing process, kinematic energy is dissipated by resistant force acting on the debris flow body. When all the kinematic energy is fully dissipated, debris is deposited on site. The amount of this part is dependent on properties of the slope and debris. Therefore, before incorporating this part into debris flow simulation, mechanism of deposition should be carefully studied and corresponding parameters should be included in the deposition model.

8.3.5. 3D effect

Since the erosion mechanism of channel bank is different from that assumed here, a new assumption has to be made to incorporate the erosion under 3D conditions. It is suggested that if the material of channel bed is uniform and loosely packed, channel bed is always adjust to a constant slope with the toe of slope contact the channel bed. Erosion mechanism of particles lying on the channel bed is same as that assumed. Or a coefficient can be introduced to take 3D effect into consideration."

Appendix A – Derivation of the governing equations in progressive souring model of erosion

The progressive scouring mode shown below is developed based on the rolling motion and shear failure. In the derivation, it is assumed that there is no cohesion between particles for granular sediment. It is also considered that the particles are uniform circles (2D).

Case 1: Rolling motion without sliding

Based on the forces applied on a rolling particle (Figure 3-1), the equation of rotational motion at a state of impending motion is given by:

$$\sum M_0 = T\,R\,\sin\alpha_t - m\,g\,R\,\cos(\alpha_t+\theta) = I\frac{d^2\alpha_t}{dt^2} + m\,\bar{a}\,R \qquad \text{[A - 1]}$$

where T is the shear force applied on the particle. It is assumed that T is applied at the center of the particle and parallel to the channel slope and R is the radius of the rolling particle. For material with different sizes, $d_{50}/2$ can be used. The angle between the channel bed and the connection line of centres of those two particles is denoted as α_t and m is the weight of the particle. For 2D analysis, $m=\pi R^2\rho$, ρ is the density of bed material, g is gravity acceleration, θ is the slope angle, and I is moment inertial which is equal to $m\,(3R^2+L^2)/12$, $L=1m$ for 2D, $d^2\alpha_t/dt^2$— angular acceleration, $\bar{a}$ is the resultant acceleration along the direction of motion.

$$\sum F_x = mgsin\theta + T - Ncosa_t + Fsina_t = ma_x \qquad \text{[A - 2]}$$

in which a_x is acceleration along the x-axis, N is the reaction force, F is the friction between particles:

$$\sum F_y = Nsina_t - mgcos\theta + Fcosa_t = ma_y \qquad \text{[A - 3]}$$

where a_y is the acceleration along y-axis:

$$a_x = \bar{a}\ sina_t \qquad \text{[A - 4]}$$

$$a_y = \bar{a}\ cosa_t \qquad \text{[A - 5]}$$

$$\bar{a} = R\frac{d^2\alpha_t}{dt^2} \text{ (For "pure" rolling motion only)} \qquad \text{[A - 6]}$$

To solve for $d^2\alpha_t/dt^2$, substituting [16] into [11] yields:

$$T\,R\,\sin\alpha_t - mgR\cos(\alpha_t + \theta) = I\frac{d^2\alpha_t}{dt^2} + m\,R^2\frac{d^2\alpha_t}{dt^2} \qquad \text{[A - 7]}$$

$$T\,R\sin\alpha_t - mgR\,\cos(\alpha_t + \theta) = (I + m\,R^2)\frac{d^2\alpha_t}{dt^2} \qquad \text{[A - 8]}$$

$$\frac{T\,R}{(I+mR^2)}\sin\alpha_t - \frac{m\,g\,R}{(I+mR^2)}\cos(\alpha_t + \theta) = \frac{d^2\alpha_t}{dt^2} \qquad \text{[A - 9]}$$

Equation [A- 9] is the governing equation for particle rolling.

To solve for *F*, substituting [A - 4] into [A - 2] yields:

$$\sum F_x = mgsin\theta + T - Ncosa_t + Fsina_t = m\bar{a}sina_t \qquad \text{[A - 10]}$$

Similarly, [A - 5] into [A - 3]

$$\sum F_y = Nsina_t - mgcos\theta + Fcosa_t = m\bar{a}cosa_t \qquad \text{[A - 11]}$$

Solving [A - 10] and [A - 11] simultaneously to obtain the expression for *N* and *F*:

From [A - 10],

$$N = (mgsin\theta + T + Fsina_t - m\bar{a}sina_t)/cosa_t \qquad \text{[A - 12]}$$

From [A -11],

$$N = (m\bar{a}cosa_t + mgcos\theta - Fcosa_t) / sina_t \quad \text{[A - 13]}$$

Combining [A - 12] and [A - 13],

$$(mgsin\theta + T + Fsina_t - m\bar{a}sina_t) / cosa_t = (m\bar{a}cosa_t + mgcos\theta - Fcosa_t) / sina_t \quad \text{[A - 14]}$$

$$F = m\bar{a} + mgcos(a_t + \theta) - Tsina_t \quad \text{[A - 15]}$$

Similarly solve for *N*:

$$N = mgsin(a_t + q) + Tcosa_t \quad \text{[A - 16]}$$

The minimum frictional coefficient to keep the rolling motion without sliding is equal to:

$$\mu_{\min} = \frac{F}{N} = \frac{m\bar{a} + mg\cos(\alpha_t + \theta) - T\sin\alpha_t}{mg\sin(\alpha_t + \theta) + T\cos\alpha_t} \quad \text{[A - 17]}$$

Case 2: Rolling motion with sliding:

If $\mu < \mu_{min}$, it means that the required friction is larger than maximum friction between two particles (F′). And $\bar{a} \neq R\, d^2\alpha_t/dt^2$

Substituting [A - 4] into [A - 2] and [A - 5] into [A - 3] changing the direction of the friction yield

$$\bar{a} = \frac{1}{m\cos\alpha_t}(N\sin\alpha_t - mg\cos\theta + F'\cos\alpha_t) \quad \text{[A - 18]}$$

Subsequently substitute [A - 18] into [A - 11] to solve for $\frac{d^2\alpha_t}{dt^2}$.

Appendix B – The permissions of citation